

AD-A139 624

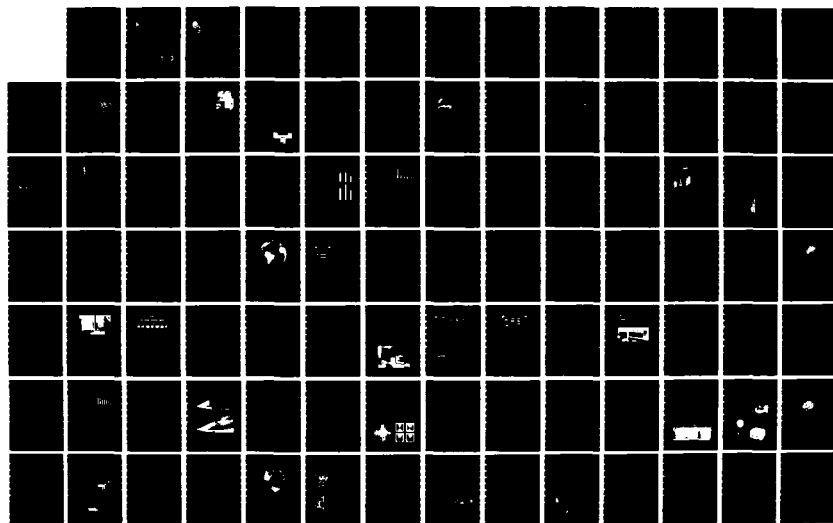
DEVELOPMENTS IN SCIENCE AND TECHNOLOGY(U) JOHNS HOPKINS  
UNIV LAUREL MD APPLIED PHYSICS LAB 1982 JHU/RPL/DST-10  
N00024-83-C-5301

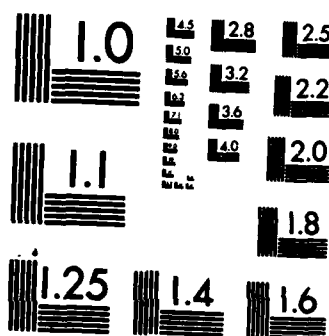
1/3

UNCLASSIFIED

F/G 14/2

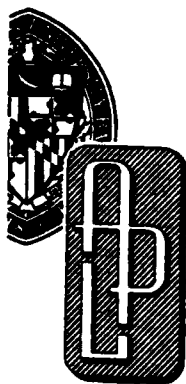
NL





MICROCOPY RESOLUTION TEST CHART  
NATIONAL BUREAU OF STANDARDS-1963-A

AD A139624



APPLIED PHYSICS LABORATORY

# DEVELOPMENTS IN SCIENCE AND TECHNOLOGY

DTIC FILE COPY

Approved for public release; distribution unlimited.

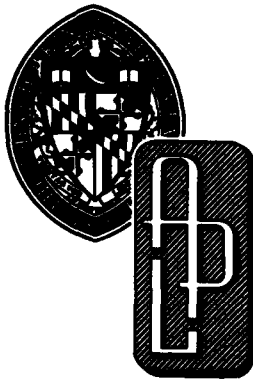
DTIC  
ELECTE  
MAR 3 0 1984  
S D  
E

THE JOHNS HOPKINS UNIVERSITY • APPLIED PHYSICS LABORATORY  
Johns Hopkins Road, Laurel, Maryland 20707

Operating under Contract N00024-83-C-5301 with the Department of the Navy

84 03 30 016

JHU/APL DST-10  
FISCAL YEAR 1982



APPLIED PHYSICS LABORATORY

# DEVELOPMENTS IN SCIENCE AND TECHNOLOGY

Approved for public release; distribution unlimited.



Accession For	
NTIS GRA&I	<input checked="checked" type="checkbox"/>
DTIC TAB	<input type="checkbox"/>
Unannounced	<input type="checkbox"/>
Justification	
By	
Distribution/	
Availability Codes	
Dist	Avail and/or Special
A-1	

THE JOHNS HOPKINS UNIVERSITY • APPLIED PHYSICS LABORATORY

Johns Hopkins Road, Laurel, Maryland 20707

Operating under Contract N00024-83-C-5301 with the Department of the Navy

*Technical Coordinators*

**Chairman, R. C. Morton**  
**C. B. Barger**  
**J. R. Champion**  
**H. K. Charles**  
**A. E. Davidoff**  
**M. Gussow**  
**R. H. Peery**  
**W. J. Roessler**  
**W. P. Willis**

*Managing Editor*

**M. B. Gilbert**

*Associate Editor*

**A. L. Machurek**

*Staff Artist*

**D. L. George**

## FOREWORD

The Applied Physics Laboratory (APL), a division of The Johns Hopkins University, is located in Howard County, Maryland, midway between Baltimore and Washington. Its work is carried out under contractual agreements between the University and the federal, state, and local governments. APL employs a staff of more than 2600 including 1430 professional scientists and engineers, of whom more than half have advanced degrees. Their ideas are implemented and extended through several field activities and a network of associate contractors and collaborators from coast to coast.

The primary mission of APL is to enhance national security by applying advanced science and technology to the solution of problems important to national objectives. The Laboratory conducts programs in fundamental and applied research, exploratory and advanced development, component engineering, systems engineering and integration, and test and evaluation of operational systems. Approximately 85% of the Laboratory's effort is for the Department of Defense (76% for the Navy and 9% for other DoD agencies). The remaining 15% is devoted to nondefense areas, including space research.

The current programs at APL cover a wide range of activities. Many are broad in scope, long term, or highly classified, and therefore not reportable herein. The articles for this document are solicited annually from the whole Laboratory. The writers are individuals or small groups who have been personally involved in particular efforts and are motivated to report to a wider audience than they usually communicate with. For these reasons, this publication does not necessarily represent all the accomplishments of APL during fiscal year 1982 (1 October 1981 through 30 September 1982).

APL was organized in 1942 under the auspices of the Office of Scientific Research and Development to develop a proximity (VT) fuze for antiaircraft defense; that was the principal effort during World War II. The era of emerging guided-missile technology extended from about 1944 to 1956. During that time, APL concentrated on providing better air defense for the Fleet by developing a family of shipborne surface-to-air missiles. The Navy-sponsored "Bumblebee" program pioneered many basic guided-missile technologies later used in other air, surface, and submarine missile programs.

The era of weapons systems engineering began in 1956 with the commissioning of the first guided-missile cruiser. The experience gained during that period has found application in many systems of interest to the Navy in various warfare areas and to other branches of the government. Significant activities are proceeding in areas of special APL competence, including advanced radar techniques, missile propulsion, missile guidance, countermeasures, and combat systems integration.

Of the newer weapon system programs, the Aegis Shipbuilding Project is of major importance. USS *Ticonderoga* (CG-47), commissioned in January 1983, is the first ship in a new class of multimission guided missile cruisers that will carry the Aegis surface-to-air weapon system. The Laboratory is Technical Advisor to the Navy in the design and development of the Aegis system. APL

now has the broader challenge of integrating the system into the operations of the battle group. This effort, for which APL is Technical Direction Agent, includes the design and development of the Battle Group Anti-Air Warfare Coordination System exploiting the operation of Aegis cruisers with other ships and aircraft of the battle group. Other areas of tactical systems support involve aviation countermeasures as well as the improved effectiveness of Tomahawk and Harpoon cruise missiles. APL has a major role in the conceptualization of future command, control, and communications (C<sup>3</sup>) systems to facilitate the operation of Naval forces. Both strategic and tactical aspects of the C<sup>3</sup> process are being examined. An important increasing effort at APL involves assessing the integrated performance of all the above systems.

The Laboratory continues to provide technical evaluation of the operational Fleet Ballistic Missile (FBM) System. Quantitative test and evaluation procedures are applied to every newly commissioned ballistic missile submarine. Similarly, APL currently provides precise evaluation of the Army's Pershing Missile programs. Significant programs are also under way for Naval strategic communications and tactical targeting. Since 1970, APL has had the responsibility for planning and conducting a significant technical program to ensure the security of the FBM submarine fleet against possible technological or tactical countermeasures. The approach is to quantify all physical and tactical means that might be developed to detect, identify, and track our submarines and to propose and evaluate suitable countermeasures and tactics.

APL has a significant space program. It started with the Navy Navigation Satellite System, originally known as Transit, one of the Laboratory's most important accomplishments since the wartime proximity fuze and the surface-to-air missile program. APL invented the concept, designed and built the initial satellite constellation, and set up and operated a worldwide satellite tracking network. The APL Space Program has greatly expanded and is now applied to the design and construction of a broad range of scientific satellites and spaceborne scientific experiments for NASA and the DoD.

With the encouragement of the DoD, APL is applying its talent and the experience developed in DoD programs to a number of government-sponsored civil programs. Some examples of the areas to which attention has been devoted in recent years are biomedical research and engineering; transportation; fire research; reduction of pollution of the biosphere; ocean thermal, geothermal, and flywheel energy systems; air traffic control; leak detection in natural-gas distribution lines; and advanced education.

By the extensive and intensive use of integrated circuits and microprocessor logic in satellites, in radar and other naval systems, and in biomedical engineering and other civil areas, APL has become a recognized leader in the area of computer technology. Furthermore, it continues to pioneer in innovative applications of computers of all sizes to problems of national importance. This trend is underscored throughout the document by the frequent references to computing as an integral part of most of the accomplishments reported herein.

To support its R&D activities through knowledge and experience in advanced research, the Laboratory performs fundamental research in biological, chemical, mathematical, and physical sciences related to its various missions. Through unique applications of system engineering, science, and technology to the needs of society, APL has enhanced the University's tradition of excellence while gaining worldwide recognition of its own.

## CONTENTS

### WEAPON SYSTEMS DEVELOPMENT

Introduction	12
Switch-Tube Modulator for the Aegis Crossed-Field Amplifier <i>R. E. Rouse</i>	14
Radar Electromagnetic Environment Simulator <i>C. Philippides</i>	17
A High-Fidelity Digital Computer Model of the Standard Missile Dither-Adaptive Autopilot <i>R. T. Reichert</i>	19
Simulation of SM-2(ER) Block II Terrier System <i>B. W. Woodford</i>	23
An Analysis of Aerodynamic Requirements for Coordinated Bank-to-Turn Autopilots <i>A. Arrow and L. L. Cronvich</i>	26
Comparison of Discriminant Sets for Autonomous Ship Classification <i>R. W. Riedel</i>	31
Graphite Ablation Measurements <i>R. W. Newman, C. H. Hoshall, and R. C. Benson</i>	34
System Data Recorder for the Pershing II Weapon System <i>C. C. Rodeffer and D. B. Kratz</i>	37
Requirements Study for a Trident II Accuracy Evaluation System <i>L. J. Levy</i>	40
Evaluation of UNITAS XXII HF Communications <i>G. R. Preziotti</i>	44

### NAVAL WARFARE ANALYSIS

Introduction	48
Harpoon Survivability Assessment Program M-on-N Model <i>L. D. Peck</i>	50
SMITE: A Simple Model for Investigating Tactical Environments <i>L. B. Carpenter</i>	52
A Software Architecture for a Multiple-Player War Game <i>R. R. Guenther, N. K. Brown, and J. F. Stader</i>	55

### COMPUTER TECHNOLOGY

Introduction	60
Array Processor Application to Emulation of the Terrier CWAT Radar <i>T. R. Hocker</i>	62

A New Hydrodynamic Computational Facility <i>T. D. Taylor</i>	65
A Hospital Information Distribution System <i>S. P. Yanek, J. A. Frantz, G. P. Gafke, D. M. Sunday, and J. C. Woodyard</i>	67
Evaluation of Computer Fault Detectors <i>M. E. Schmid, R. L. Trapp, and A. E. Davidoff (APL) and G. M. Masson (JHU)</i>	69
Simulation of Anomalous Electromagnetic Propagation with the EMPE Code <i>H. W. Ko, J. W. Sari, and J. P. Skura</i>	72
Iterative Solution of a Partial Differential Equation on an Image Processing System <i>C. A. Waters</i>	75

## SPACE SCIENCE AND TECHNOLOGY

Introduction	80
Completion of a Magnetometer for the Swedish VIKING Satellite <i>F. F. Mobley, K. J. Heffernan, and T. A. Potemra</i>	82
Reentry Thermal Design of a Lightweight Radioisotope Heater Unit <i>D. W. Conn, L. L. Perini, K. R. Waeber, and J. C. Hagan</i>	85
Search and Rescue Satellite Program <i>A. Eisner and J. B. Moffett</i>	88
The Satellite Missile Tracking Program <i>T. Thompson and C. W. Meyrick</i>	92

## OCEAN SCIENCE AND TECHNOLOGY

Introduction	99
Miniature Oceanographic Fluorometer <i>A. B. Fraser and R. P. H. Lee</i>	100
A Helicopter-Deployable Instrumented Spar Buoy for Ocean Heat Flux Measurements <i>C. V. Nelson and R. G. Chappell</i>	102
A Shipboard Real-Time Data Acquisition and Display System for Oceanographic Measurements <i>R. E. Ball, J. E. Coolahan, V. Vigliotti, and R. F. Cohn</i>	106
A PDP-11 Based Oceanographic Data Acquisition System <i>R. B. Harris III (Sachs/Freeman Assoc., Inc.) and S. J. Bockstahler-Brandt (APL)</i>	110
A Distributed, Intelligent Oceanographic Data Acquisition System for Towed Sensor Arrays <i>D. A. Kitchin, A. B. Fraser, L. E. Karner, R. P. H. Lee, and C. S. Best</i>	112

An Oceanographic Data Analysis System <i>B. E. Raff</i>	114
The Characterization of Mesoscale Oceanographic Features <i>J. J. Ousborne</i>	118
Aid Control and Monitor System <i>T. H. Man, E. E. Mengel, and C. A. Twigg</i>	121

## BIOMEDICAL SCIENCE AND ENGINEERING

Introduction	127
Possible Geometric Risk Factors for Arteriosclerosis <i>M. H. Friedman, O. J. Deters, F. F. Mark, and C. B. Barger (APL) and G. M. Hutchins (JHMI)</i>	128
A Microwave-Related Corneal Effect <i>H. A. Kues (APL) and L. W. Hirst, S. A. D'Anna, and G. Dunkelberger (JHMI)</i>	131
Robotic Arm to Provide Manipulative Capability to the Disabled Person <i>W. Schneider, J. H. Loveless, and W. Seamone</i>	134
Use of a Programmable Implantable Medication System to Control Plasma Glucose Levels in Diabetic Dogs <i>R. E. Fischell and W. E. Radford (APL), C. D. Saudek (JHH), and J. R. Champion (APL)</i>	137
Technical Support in Information Systems <i>B. I. Blum</i>	140

## ENERGY, ENGINEERING, AND CIVILIAN TECHNOLOGY

Introduction	147
The Development of Geothermal Energy in the Eastern United States <i>F. C. Paddison and A. M. Stone</i>	148
Application Design, Implementation, and Reliability Testing of the Ceramic Chip Carrier <i>H. K. Charles, Jr., G. D. Wagner, B. M. Romenesko, and R. E. Hicks</i>	152
Nondestructive Pull Testing of Hybrid Microelectronics <i>H. K. Charles, Jr., G. D. Wagner, and B. M. Romenesko</i>	156
Vehicle-Follower Controller Designs for Off-Line Automated Guideway Transit Vehicles <i>H. Y. Chiu</i>	159
Control System for a Magnetically Suspended Transit Vehicle <i>S. J. Brown</i>	162

## **FUNDAMENTAL RESEARCH**

Introduction	167
Optical Switching in Semiconductor Organic Thin Films <i>R. S. Potember, T. O. Poehler, and R. C. Benson</i>	168
A Simple Model for Flames with Complex Chemistry <i>R. M. Fristrom</i>	170
Discovery of a New Low-Energy Electron Diffraction Phenomenon <i>C. B. Barger, A. N. Jette, and B. H. Nall</i>	174
Optical Monitoring of Energy Transfer Processes Accompanying Pulsed Laser Excitation of Photosensitive Dyes in Condensed Media <i>J. G. Parker and W. D. Stanbro</i>	178
The Structure of Amorphous Iron-Boron Alloys from the Analysis of Magnetic Hyperfine Fields <i>N. A. Blum and K. Moorjani</i>	181

<b>PATENTS</b>	<b>186</b>
----------------	------------

<b>PUBLICATIONS AND PRESENTATIONS</b>	<b>190</b>
---------------------------------------	------------

<b>AUTHOR INDEX</b>	<b>198</b>
---------------------	------------

## **WEAPON SYSTEMS DEVELOPMENT**

## INTRODUCTION

During the initial development of the antiaircraft guided missile and its early introduction for service use, the APL staff worked with the Navy's equipment contractors to acquaint them with the characteristics of these new weapons. The role of the Laboratory necessarily expanded with the assumption of responsibility for technical direction of the Navy's anti-air-warfare guided missile systems in the late 1950's and for the evaluation of the strategic missile systems in the 1960's.

The challenge to the Fleet posed by manned supersonic bombers and their air-to-surface missiles attacking en masse under the cover of electronic countermeasures requires a radical departure from the relatively primitive, human-intensive control procedures that grew out of World War II.

Working first with analog and then with digital electronic computational techniques, the Navy has produced tactical data and weapon systems that relieve weapons personnel of much of the routine associated with a fighting ship. APL has made and continues to make important contributions in this evolution. In addition to its characteristic drive to discover and apply the basic principles underlying a problem, the Laboratory has brought to the Navy weapon community an understanding of the potential capabilities of the emerging world of electronic computation and automation.

APL has contributed to defining the basic structure of shipboard combat systems and to allocating functions consistently among the sensor, command, support, and weapon elements of these very complex systems. Such consistency of structure has aided technical interchange among major developments in which APL has played a role, including the Aegis Weapon System, Terrier and Tartar New Threat Upgrades, and, most recently, the new multimission DDG-51 Combat System.

Anticipating the potential threat of antishipping missiles, the Laboratory has focused its recent efforts on the definition and development of techniques that allow weapon systems to respond to a threat in minimum time while providing the requisite control capability for the several levels of tactical command. Integral to Laboratory efforts in this and other areas of weapon control is the identification of data processing and distribution approaches that allow the implementation of practical and economical designs — designs that provide requisite hardness to equipment casualty or battle damage.

The main thrust of the Laboratory's work in the strategic systems area was in developing and assisting in the conduct of an independent evaluation program for the Navy's Fleet Ballistic Missile (FBM) Weapon System that featured combined technical and operational testing that is continuous throughout the life of the weapon system. That program has continued and expanded to the current evaluation of the performance of the Navy's operational submarine launched ballistic missile weapon systems: Poseidon, Trident I, and Trident II. For those systems, quantified estimates of performance under operational conditions are derived, sources of system inaccuracy and unreliability are identified for corrective action or future improvement, and weapon system readiness for operational deployment is assessed.

In the mid-1960's, the Laboratory was requested by the U.S. Army to expand its strategic evaluation effort to develop and conduct an evaluation program for the Pershing Weapon System in its strategic role in Europe. The program, which was to be modeled as closely as possible after the evaluation program for the Navy's FBM Weapon System, continues today with the data collected and analyzed from test exercises performed on "alert" sites in Europe and from Operational Tests conducted in the United States.

## SWITCH-TUBE MODULATOR FOR THE AEGIS CROSSED-FIELD AMPLIFIER

R. E. Rouse

*A brassboard switch-tube modulator that uses a new long-life switch tube and can operate at twice the duty factor of the AN/SPY-1A radar has been developed. The modulator can be retrofitted into the SPY-1A radar or used in advanced Aegis systems.*

### BACKGROUND

The transmitter in the Aegis SPY-1A radar has 78 crossed-field amplifier (CFA) tubes, each of which is individually cathode pulsed by a Y-633 switch tube that has demonstrated less than desired reliability. A new switch tube, the Y-633A, was developed to correct the problem, but it requires an additional 200 W of filament power and is not a direct replacement. Furthermore, most of the radar system upgrades that have evolved require that the modulator be operated at higher power levels. Consequently, to incorporate the Y-633A and those upgrades into the SPY-1A radar, the switch-tube modulator had to be modified. There was concern whether a modulator using the Y-633A switch tube and demonstrating the upgraded performance could be built in the same size package as the present modulator. To prove the feasibility of such a modulator, APL designed and built a brassboard suitable for retrofit into the driver stage of the SPY-1A radar.

### DISCUSSION

Figure 1 is a diagram of the driver CFA stage of the transmitter. The modulator chassis is mounted on insulators and is connected to the -18 kV output of the high-voltage power supply. Prime power and triggers are brought to the chassis through high-voltage isolation transformers mounted on the chassis. The modulator chassis operates two CFA's and contains two switch tubes. The grid driver circuits in the present SPY-1A modulator use two 4CPX250 tetrode tubes in a bootstrap circuit to generate a 1 kV grid pulse and two 4CPX250 tubes as a "tailbiter." The grid drive circuit dissipates about 200 W and requires a fan to cool the tubes. The modulator power supplies are simple, unregulated transformer-rectifier circuits.

The new modulator had to satisfy the following requirements:

1. Have the same size and shape as the present modulator to ensure retrofit into the SPY-1A radar;

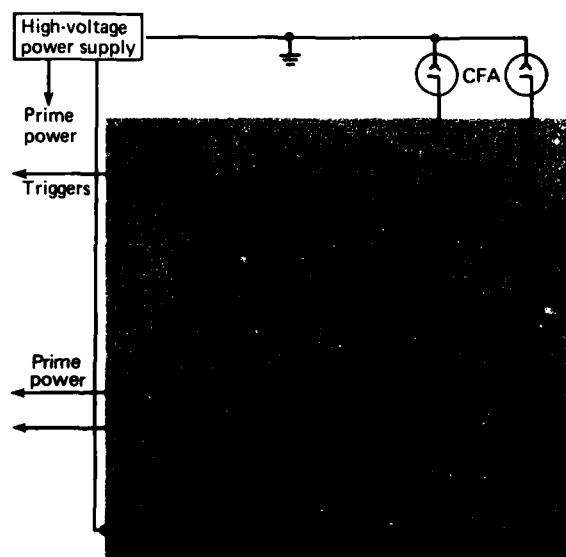


Figure 1 — The basic CFA stage of the transmitter.

2. Have the same system interface connections;
3. Provide about 40% more power to the switch-tube filaments;
4. Operate at twice the duty factor of the present modulator;
5. Provide twice the peak grid current to the switch tube (four times the average power);
6. Operate with pulse widths to 100  $\mu$ s; and
7. Provide a switch-tube grid pulse of 1 kV and 1.5 A, with 0.1  $\mu$ s rise and fall times.

The requirements for the pulse width and rise time are more stringent than are presently needed, but the extra performance provides a margin to accommodate possible new waveforms.

To handle the modulator's increased power capability in the same size package without incurring thermal problems, the redesign effort concentrated on reducing the amount of power dissipated in the modulator chassis. The major design areas were the power-isolation transformer, the grid-drive circuits, and the modulator power supply system.

## Transformer Design

Attempts to build commercially a transformer of the required power capability and size were unsuccessful; therefore, APL designed and built the power-isolation transformer. It is rated for three phase, 400 Hz operation at 2.2 kW and 20 kV isolation between the primary and secondary windings. The power dissipated in the transformer results from core losses and resistive losses in the windings. To minimize the core losses, cut C-cores fabricated from 2-mil-thick Permalloy-80 tape are used. The winding losses are minimized by having the lowest possible winding resistance consistent with the available space. Most of the power is in the windings that supply the switch-tube filaments (7.5 V, 100 A per tube). The windings were machined from 1/4 in. copper plates to provide the maximum winding cross section. The winding supports were designed to allow the free flow of oil between the windings for efficient cooling.

The transformer was built and successfully tested at high potential to 20 kV. The rise in temperature of the case and the oil was measured while operating into a full 2.2 kW resistive load. The temperatures required about 8 h to stabilize. The case temperature rose 45°C and the oil 55°C.

## Grid-Drive Circuit

To provide the extra grid-drive power and to reduce the power dissipated in the modulator, APL used power-switching transistors instead of tubes. The power switching rate had to be greater than 15 kW/ $\mu$ s to obtain a 0.1  $\mu$ s rise time. Power field-effect transistors (FET's) were chosen because they best met the switching-speed requirement. The maximum voltage rating of the FET was 500 V.

To provide a 1 kV grid pulse and to limit the energy transferred to the transistor in the event of a high-voltage arc in the switch tube, APL used a voltage step-up pulse transformer between the FET and the switch-tube grid. Attempts to purchase or build a pulse transformer that could pass a 0.1  $\mu$ s rise, 100  $\mu$ s wide pulse were unsuccessful; therefore, APL developed a circuit (Fig. 2) to synthesize the desired grid pulse from three pulses. A 5- $\mu$ s-long pulse provides the 0.1  $\mu$ s leading edge, and a 95  $\mu$ s pulse with about a 2  $\mu$ s rise and fall time supplies the mid part of the pulse. The third is a 5  $\mu$ s negative pulse that functions as a tailbiter. The three pulses are combined in a diode-resistor network to give the desired grid pulse. The amplitude of the grid pulse is clamped by a diode to the clamp-voltage power supply. Because of the action of the clamp, the amplitude and timing match of the three pulses are not critical. The final design of the grid-drive circuit produces a 1 kV,

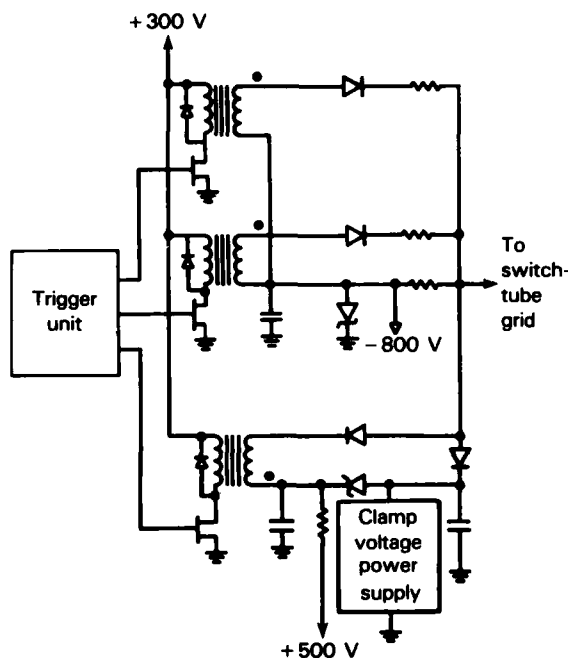


Figure 2 — The basic grid-drive circuit.

1.7 A, 100  $\mu$ s pulse with a 0.09  $\mu$ s rise time and a 0.15  $\mu$ s fall time. Separate drive circuits are used for each switch tube.

## Modulator Power Supply

Power supply voltages to the grid-drive circuits are regulated to minimize the operating dynamic range of the FET and the power dissipated in the grid-drive circuits. A high-frequency flyback-type power supply provides four independent regulated voltages from a single driver-regulator circuit. Figure 3, a basic schematic of the power supply, shows how the secondary voltage from the power isolation transformer is directly rectified to DC. An FET generates a pulse on the transformer primary to establish a magnetic field in the transformer's core. When the primary pulse ends, the energy stored in the core produces flyback voltages in the secondary windings, which in turn are rectified to DC output voltages. The energy stored in the core is controlled by the width of the FET pulse, thereby determining the output voltage. The pulse frequency is about 20 kHz. The transformer uses a Ferroxcube EC70-3C8 core. A similar power supply provides the screen voltage for the switch tube. Screen voltage must not be applied to the switch tube before the grid bias is applied. The delay is achieved by inhibiting pulsing of the FET in the screen power supply until the grid bias is

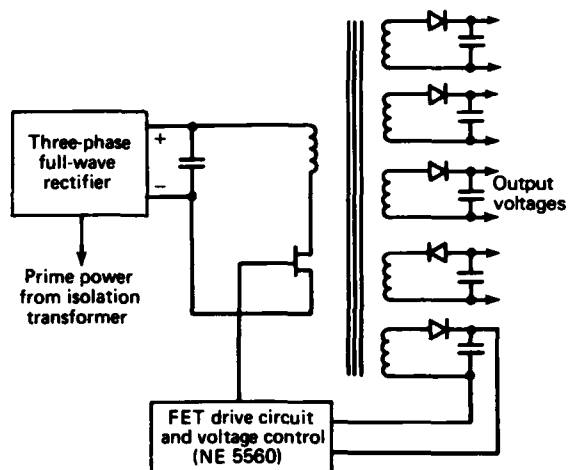


Figure 3 — The basic modulator power supply.

established. The overall efficiency of the power supply is about 80%.

The complete modulator has been assembled and tested successfully at low voltage. Figure 4 is a photograph of the modulator. Results to date verify that a modulator with the increased performance capability in the same size package as the SPY-1A modulator is feasible. An existing APL radar transmitter is being adapted for modulator operation and testing at high voltage.

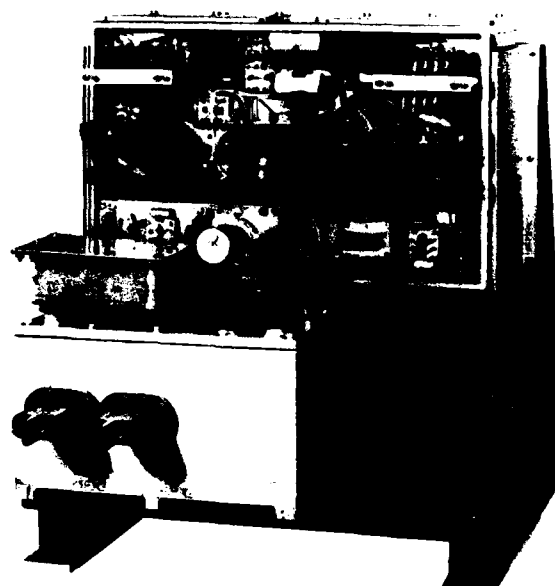


Figure 4 — The switch-tube modulator.

#### ACKNOWLEDGMENTS

T. F. Paraska detailed, constructed, and tested most of the electrical design. W. T. Howarth did the mechanical design.

This work was supported by NAVSEASYSOM, PMS-400B.

# RADAR ELECTROMAGNETIC ENVIRONMENT SIMULATOR

### C. Philippides

*APL provided technical guidance and assistance in the development and testing of the Radar Electromagnetic Environment Simulator Model 201 (REES-201) in conjunction with Development Testing of the New Threat Upgrade (NTU) Combat System (CS). The RF simulator provides accurately modeled RF signals in real time simulating targets, IFF responses, sea clutter, rain, chaff, and coherent and noncoherent jamming for injection into the CS AN/SPS-49(U) 5 two-dimensional and AN/SPS-48E three-dimensional search radars and accompanying AIMS Mk XII IFF systems. The RF simulator may be operated with or without radar transmitter radiation, and RF signals generated by the simulator may be combined with real radar returns. During the NTU CS Technical Evaluation, the RF simulator provided precise and repeatable radar stimulation, allowing the data that were needed to characterize and assess radar performance to be collected systematically, without the expense and operational difficulties inherent in using manned aircraft. In addition, the simulator provided threat-representative high-performance targets that could not be simulated by manned aircraft. The RF simulator was also used throughout the NTU CS Technical Evaluation for the rehearsal of missile-firing exercises and for crew training when aircraft and electronic countermeasure services were not available.*

## BACKGROUND

During the Technical Evaluation of the CG/SM-2 Combat System in 1978, the standard VS 441 Video Signal Simulator was modified for compatibility with the CS three dimensional (3D) search radar and was used extensively for crew training and the rehearsal of missile-firing exercises. Experience gained with that unit, which provided target video at the IF level, highlighted the need for a simulator that would provide realistic simulation at the RF level (to exercise the radar receiver) and that would simulate environmental effects and jamming in addition to targets. To support NTU CS Development Testing, the simulator would also be required to stimulate simultaneously both CS search radars and their accompanying IFF systems. In 1980, representatives from APL attended a demonstration of an RF simulator developed to support testing of a two-dimensional (2D) radar at the Rome Air Development Center. Discussions with the manufacturer of that simulator, Republic Electronics, Inc., indicated that the technology could be modified to stimulate the CS 3D search radar and appropriate IFF responses, and that it could be expanded to provide simultaneous stimulation

of both the radars, their IFF systems, and the desired environmental effects and jamming. Development of this enhanced simulator, the REES-201, was begun by Republic Electronics under APL contract in late 1980. It was delivered to USS *Mahan* (DDG-42) for use in NTU CS Development Testing in late 1981.

## DISCUSSION

## System Description

The RF simulator consists of a video display terminal (VDT), a controller, and three RF processors (RFP's), one for each of the radars and one for the IFF systems (Fig. 1). Figure 2 is a functional block diagram showing the main internal simulator connections and its interface with the NTU CS. Target, environmental, and jammer parameters are entered or altered at the VDT keyboard, and their status is shown on the VDT display. Data entered at the keyboard are transferred to the controller and stored in a common memory for use by the master and slave central processing units in producing command updates for the three RFP's. Those updates are input by each RFP for radar status, antenna, timing, and frequency from the radar and are translated by the RFP into instructions for the modulation or generation of RF by an RFP channel for output to the radar. A typical RFP channel (Fig. 3) provides for distribution of RF, pulse compression, Doppler shift, RF amplitude, and insertion at the proper delay and antenna position under control of the digital processor. The model used by the digital processor in modulating the RF adjusts for target noise, antenna motion, transmitter/frequency source phase errors, antenna pattern scan modulation effects, target radar cross section, and

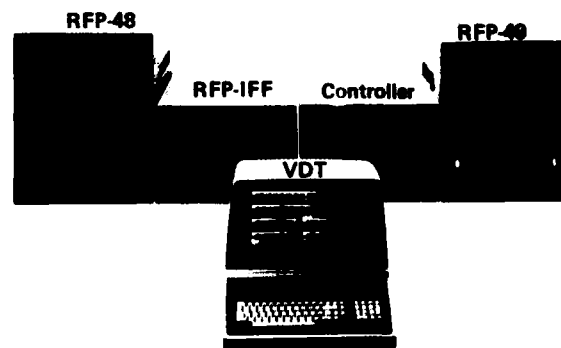


**Figure 1 — The REES-201.**

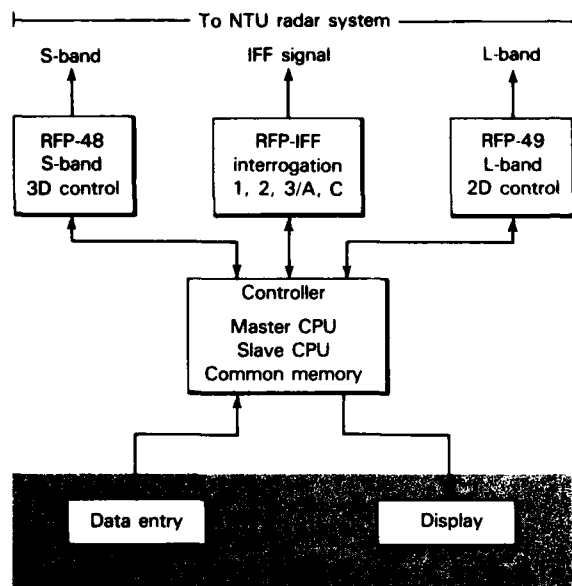


**Figure 2** — The interface of the REES-201 with the NTU radar.

multipath and slant range effects. Each radar RFP has two coherent RFP channels to provide at least two simulated targets simultaneously; the channels also provide for the generation of coherent jamming. The radar RFP's also have multiple noncoherent RFP channels

to provide barrage noise and deception jamming. Those channels have separate RF sources (voltage controlled oscillators), but processing and control of the RF is the same as that for the coherent channels. Each radar RFP also has an environmental channel that provides coherent returns for extended targets such as chaff, rain, and sea clutter. The model for that channel considers the additive effects of many RF scatterers, air mass motion, Doppler frequency effects (including Doppler noise), and amplitude noise modulation resulting from fluctuations in the radar cross section. The RF signals output by the channels are then inserted into the radar by a directional coupler for processing by the radar receiver.

The RF simulator provides 36 maneuverable targets and six fixed targets. Target course, speed, vertical velocity, and radar cross section may be changed in real time. The simulator provides targets with radar cross sections from 0.1 to 1000 m<sup>2</sup>, at ranges from 3 to 500 mi and altitudes from the surface to 100,000 ft through a full 360° azimuth. Up to six chaff events may be provided in point, medium, and large form. They are stationary but show four levels of spreading in azimuth and elevation. Rain of varying intensity is provided in the form of a shower, a storm, or a squall. Sea clutter is variable in both direction and intensity, simulating the effects of wind speed and sea state. The simulator also provides up to six jammers for range deception (with cover pulse), inverse gain, and synchronous, asynchro-

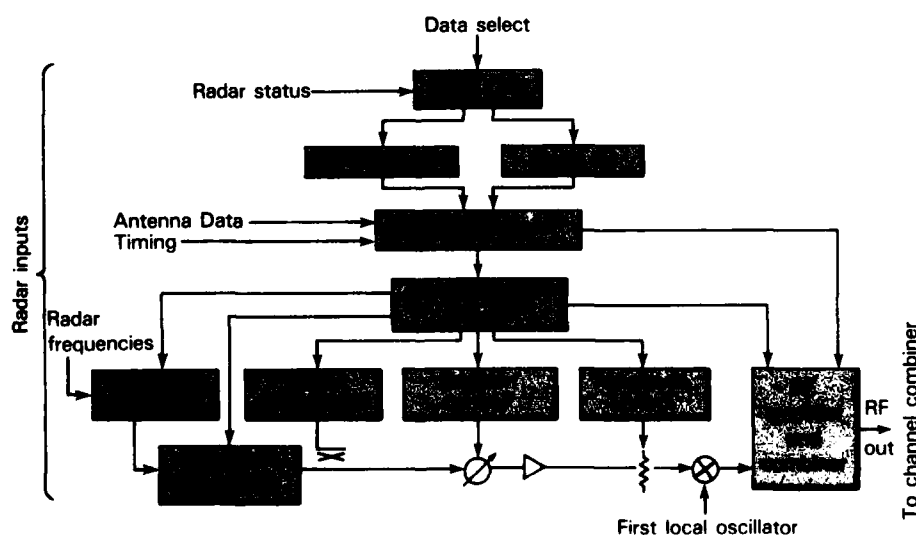


**Figure 3** — A typical RF processor channel.

nous, and barrage noise jamming at strengths from 10 to 4000 W/MHz.

## RESULTS

To deliver the simulator in time to support NTU CS testing in USS *Mahan*, APL formed an accelerated development program that provided for delivery, installation, checkout, and integration of the unit in less than a year. The effort included development of specifications for the simulator and the simulator interfaces<sup>1</sup> with the two radars and their IFF systems and additional technical guidance during design and fabrication. APL representatives directed factory acceptance testing and integration of the unit aboard USS *Mahan*. The simulator supported NTU CS testing during Phases 1 and 2 and was invaluable in providing precise, repeatable radar stimulation for radar testing and scenarios for crew training, CS team integration, and the rehearsal of missile-firing exercises. It was used daily to

allow testing or training to continue when emission was prohibited or aircraft and electronic countermeasures services were unavailable. In addition, it provided threat-representative targets that could not be simulated by manned aircraft, as well as chaff and jamming in areas where they could not actually be used. The simulator presents a picture of the RF environment that is real enough for the simulated training and test exercises to be meaningful and to prepare the operator for actual operations.

## REFERENCE

<sup>1</sup>Interface Specification for New Threat Upgrade Radar Electromagnetic Environment Simulator (NTU-REES), Naval Sea Systems Command WS-21131 (1 Aug 1981).

This work was supported by NAVSEASYSKOM, SEA-06A1.

## A HIGH-FIDELITY DIGITAL COMPUTER MODEL OF THE STANDARD MISSILE DITHER-ADAPTIVE AUTOPILOT

R. T. Reichert

*A cost-efficient digital computer model of the dither-adaptive autopilot for Standard Missile has been developed. The model accurately represents the autopilot characteristics over a frequency range of 0 to 30 Hz and also simulates the highly nonlinear effects of dither interruption, dither capture by the autopilot steering channels, and bistable tail actuator mismatch. It was used to assess proposed design modifications and the results of preflight and postflight test programs as well as to estimate high-fidelity system performance.*

## BACKGROUND

Standard Missile is a family of ship-launched surface-to-air interceptors that represents the culmination of design efforts spanning four decades (Fig. 1). Among the attributes that make this advanced tactical weapon so successful is the common autopilot and tail control configuration. In order to schedule feedback gains and guidance filtering levels that vary with a

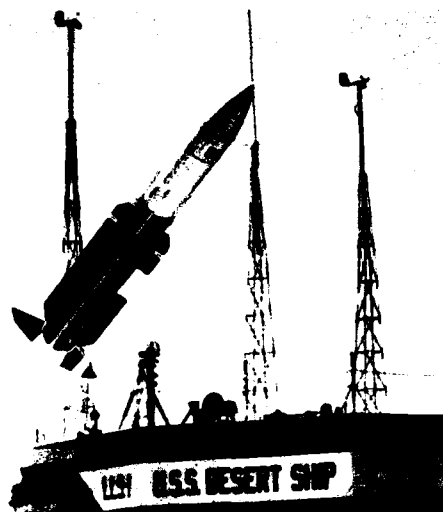


**Figure 1** — Launch of a medium-range SM-2 flight test round at White Sands Missile Range.

changing flight environment, the system uses a dither (limit cycle oscillation) adaptive control technique<sup>1</sup> that APL helped conceive and develop. The complex scheduling ensures maximum responsiveness and maneuverability during an engagement. The dither oscillation is established by the autopilot roll channel shortly after launch and continues uninterrupted under nonstringent environmental conditions throughout missile flight. However, under certain stringent conditions, the dither process may be disrupted. Heavy electronic countermeasures, instabilities induced by excessive aerodynamic cross coupling, and radome boresight errors can create such stringent conditions. Excessive dither interruption degrades the adaptability of the control system and may adversely influence system performance.

Because the dither process is complex, previous simulation models of the adaptive autopilot assumed that it continued uninterrupted throughout flight. That assumption can lead to overly optimistic estimates of system performance. An all-digital dithering simulation model was developed to overcome the uncertainty with respect to the actual performance of the autopilot.

## DISCUSSION

### Autopilot Function

The principal function of a missile autopilot is to develop the control surface deflections needed to produce controlled responsiveness in order to achieve commanded maneuvers while maintaining stability of the airframe. The form of the commanded maneuver is de-

termined by the steering policy. Skid-to-turn systems like that in Standard Missile operate with a fixed airframe roll attitude, and the maneuver is specified by a set of Cartesian or orthogonal acceleration commands.

The Standard Missile autopilot may be separated functionally into three channels: one roll control channel and two identical lateral channels for steering. Each steering channel develops a control surface deflection by processing the commanded acceleration input and the accelerometer and rate-gyro feedback signals. The roll autopilot channel maintains a fixed spatial roll orientation and attempts to maintain a sustained limit cycle oscillation.

The limit cycle (or roll dither) oscillation provides a way to estimate dynamic pressure. The estimate can be deduced from the amplitude ratio of the achieved roll angular rotation rate and roll tail deflection at the dither frequency. Given the dynamic pressure and speed of the missile (which can be derived from an on-board inertial reference unit), one can accurately estimate the altitude of the vehicle. With this information, one can automatically adjust autopilot feedback gains and guidance filtering levels, which are functions of dynamic pressure and altitude, to the changing flight environment.

Four independently controlled tails are located symmetrically about the aft end of the airframe. Each tail is deflected by a special-purpose bistable rate actuator. The composite motion of all four tails represents the required response to the combination of roll and steering deflections. The allowable control authority associated with each tail is thus shared among the three autopilot channels.

Situations that require large tail deflections to satisfy the requirements of the autopilot steering channel effectively reduce the response of the roll channel and may suppress it intermittently. That condition is called dither interruption. Momentary disruption of the dither oscillation can be tolerated without significant detriment to the system. However, with longer periods of disruption, the dynamic pressure estimation technique can break down, large roll moments may develop when the bistable actuators are mismatched in rate capability, and the steering channels may occasionally capture the dither process. All of these conditions are highly nonlinear and require a complex model to characterize the effects accurately.

### Implementation

Figure 2 is a functional block diagram of the computer model. The individual roll and steering chan-

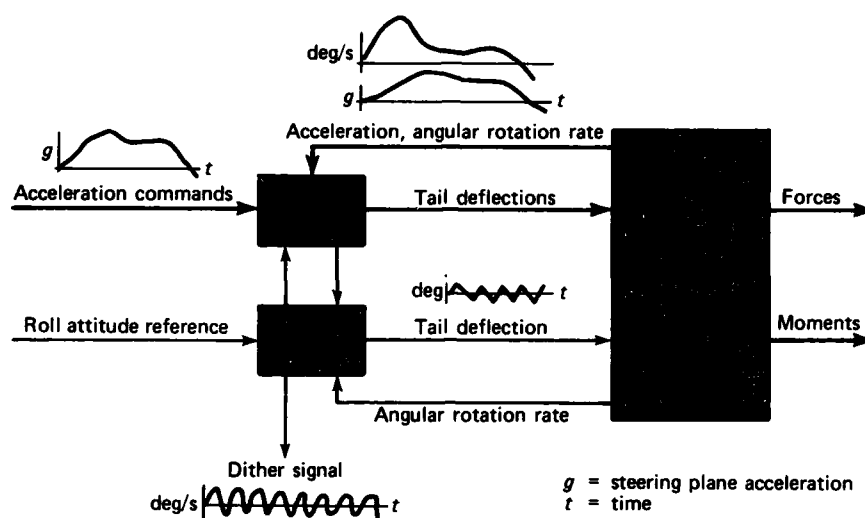


Figure 2 — Functional block diagram of the Standard Missile autopilot.

nel models replicate the phase and gain characteristics of the design specifications over a frequency range of 0 to 60 Hz and 0 to 30 Hz, respectively. The airframe is assumed to be a rigid body and is modeled by a lookup table technique, with force and moment coefficients specified as functions of tail deflection, angle of attack, Mach number, center-of-gravity location, and aerodynamic roll angle.

The nonlinear differential equations that describe the model are integrated using a modified fourth-order Runge-Kutta numerical method. A minimum fixed integration time step of 0.5 ms is required to observe capture of the dither process by the autopilot steering channels. However, a fixed integration time step of 2 ms is sufficient to represent the characteristics of the autopilot under less stringent dynamic operating conditions. To minimize the expense of simulation execution, APL developed a variable-step-size integration procedure. The nominal integration step size is 2 ms. However, when a bistable actuator switches state, thus introducing a discontinuity into the differential equations, the nominal step size is reduced. Figure 3 is a flow diagram of this cost-saving numerical integration process.

### Applications

The model was used to verify performance estimates of the proposed control test vehicle (CTV) for the medium-range Standard Missile-2 (SM-2) Block II design. In preflight investigations, APL compared the predicted flight trajectories and maneuver responses with similar predictions made by the design contractor.

For each CTV flight, preprogrammed maneuver sequences guide the missile from launch to impact, exercising the control capabilities of the autopilot over a widely varying flight environment. Figure 4, which was derived from an APL dithering-autopilot simulation, illustrates the response of the dithering autopilot during a segment of a proposed flight test. During the maneuver sequence, the vehicle enters a region of excessive aerodynamic cross coupling; the result is large-amplitude oscillations and extensive dither interruption. The simulated response illustrates the ability of the Standard Missile autopilot to operate satisfactorily under difficult and varying conditions.

A launch-to-intercept simulation of the extended-range SM-2 Block II system has recently been modified to incorporate the dithering-autopilot model. The modified system-level simulation has been used to predict potential system performance improvements associated with autopilot design modifications under consideration. It was also used for preflight analysis and for the evaluation of postflight results that exhibited anomalous behavior.

At the present time, a launch-to-intercept simulation of the vertically launched medium-range SM-2 Block II system is being similarly modified to incorporate the dithering-autopilot representation. A simulation of the vertical launcher system will be used to study the effect of high-angle-of-attack maneuvers at low speed on the autopilot control system.

In summary, the simulation model of the high-fidelity dithering autopilot has been used extensively to support analyses of Standard Missile performance in re-

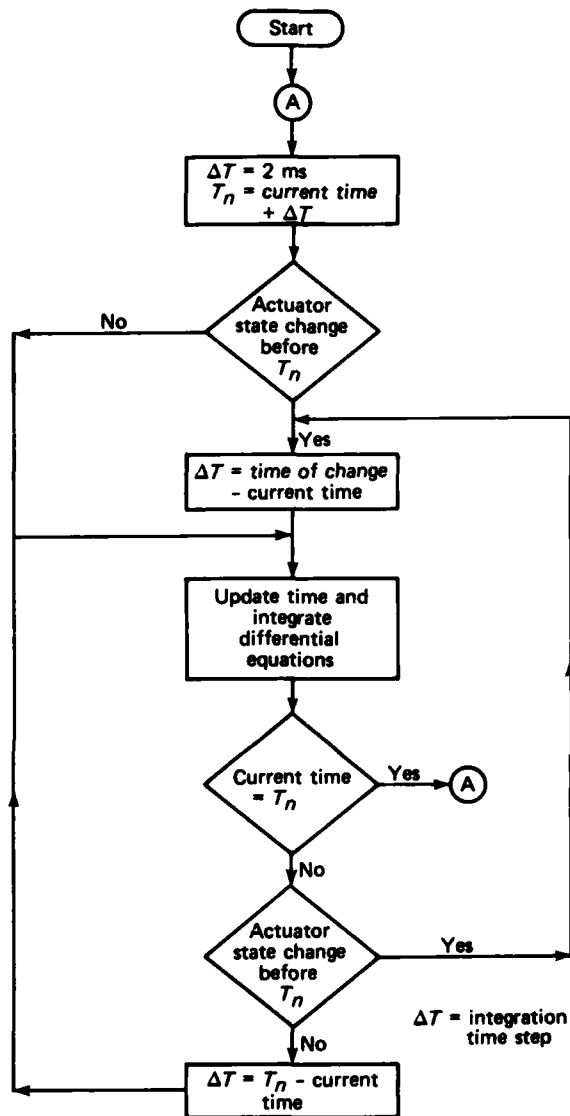


**Figure 3** — Flow chart of the variable-time-step numerical integration process.

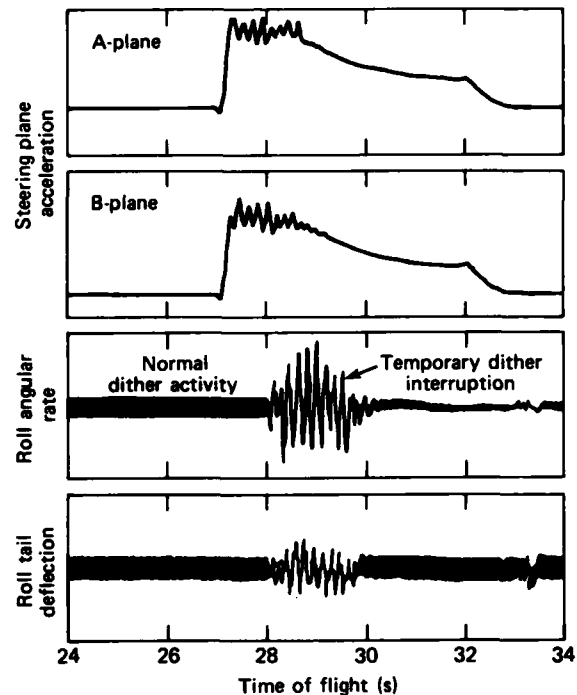


**Figure 4** — Representative simulation response during an oscillation induced by excessive aerodynamic cross coupling.

gions where previous simulation models left some uncertainty with respect to its actual performance. The model provides a valuable, affordable, and necessary capability to support the development of Standard Missile.

## REFERENCE

- <sup>1</sup> B. E. Amsler and R. E. Gorozdos, "Analysis of Bistable Control Systems," National Automatic Control Conf., Dallas (5 Nov 1959).

This work was supported by NAVSEASYSKOM, PMS-400M.

# SIMULATION OF SM-2(ER) BLOCK II TERRIER SYSTEM

B. W. Woodford

*APL has developed a three-dimensional, six degree-of-freedom, launch-to-intercept digital simulation model of the Extended Range Standard Missile-2 (SM-2(ER)) Block II missile used with the Terrier Weapon System. The simulation accurately models missile response in stringent operational environments, including target maneuvers and countermeasures. It is primarily used to estimate system performance in those environments and to aid in system design.*

## BACKGROUND

The increasingly stringent operational environment faced by defensive missile systems (Fig. 1) requires that more attention be given to realistic test and evaluation. Because actual missile firings on instrumented ranges are too expensive for use in more than spot checks against performance requirements, simulation has become a primary way to assess missile system performance. This article discusses the features of a digital simulation used as an analytical tool to evaluate the performance of the SM-2(ER)/Terrier Weapon System in specific countermeasures environments, particularly against standoff jammers (SOJ's). A previous article<sup>1</sup> discussed testing in the APL Guidance System Evaluation Laboratory, where simulation is combined with missile guidance hardware.

## DISCUSSION

### Simulation Overview

As indicated in Fig. 2, a missile flight has five distinct phases (initialization, boost, midcourse, homing, and endgame), four of which are represented in the simulation.

During the initialization phase, the ship system tracks the target and develops a fire control solution.

During the boost phase, the missile flies ballistically while the booster accelerates it to a high speed. The missile trajectory is not simulated during this phase because the missile is unguided. Instead, end-of-boost flight conditions obtained from tables are used to initialize the missile at the beginning of the next phase.

(These conditions are obtained from a separate boost-phase flight simulation.)

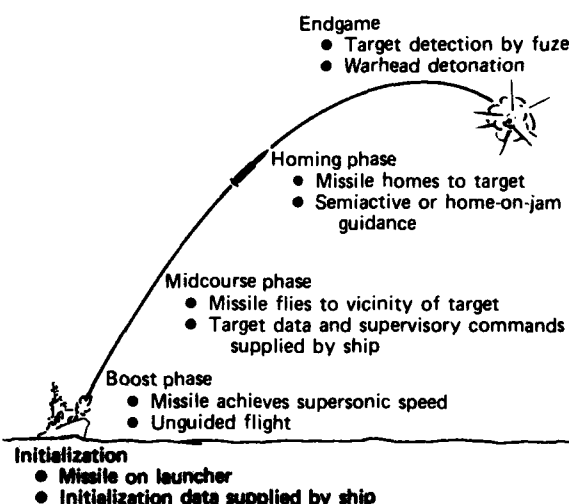


Figure 2 — The Terrier/Standard Missile-2 operational sequence.

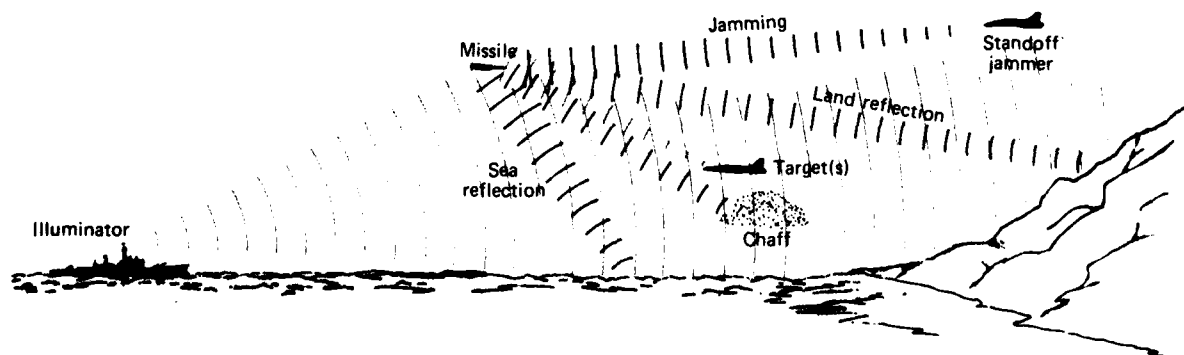


Figure 1 — The operational environment of a missile.

During the midcourse phase, missile guidance is based on target position and velocity data sent to it via an uplink (a ship-to-missile radio-frequency communication channel). Target data are obtained from the ship system, as in the initialization phase. Acceleration commands are computed by the missile guidance computer in accordance with the target data and are sent to the autopilot, which determines the tail deflection rates required to execute the commands. The tail deflections cause the missile to accelerate in the desired direction according to the missile's aerodynamic characteristics. The resulting trajectory positions the missile for initiation of the homing phase, which begins while the missile is still some distance from the target.

During the homing phase, an on-board seeker determines target location and guides the missile to intercept. During the acquisition portion of the homing phase, the seeker is pointed toward the expected target location on the basis of data derived from the ship system. After the receiver has acquired the target and the seeker tracking loop is closed, data from the seeker are used to generate acceleration commands in the guidance computer. The commands are operated on by the autopilot and aerodynamics, as indicated previously, and cause the missile to close on the target.

During the endgame phase in which the missile's fuzing system detects the presence of the target, the warhead is detonated and the target destroyed. This phase is represented in a separate simulation model, the APL endgame simulation.

The SM-2(ER) Block II/Terrier simulation is composed of functional blocks corresponding to subsystems of the overall Terrier Weapon System (Fig. 3). The features of each functional block are discussed be-

low; particular emphasis is placed on modeling the effects of countermeasures on the seeker.

### Target Representation

The simulation has a sophisticated and flexible capability for target trajectory generation that allows it to represent three-dimensional (3D) target motion and specify target speed and course. It can also simulate realistic lateral maneuvers, represent the effects of target-control-system time constants, and specify axial decelerations. Preprogrammed maneuver sequences represent the characteristics of typical threat targets. In addition, target glint characteristics related to the orientation of the target body may be simulated.

### Ship System Representation

To represent a ship system tracking a target, the simulation uses a representation of the SPS-48E search radar and the AN/SYS-2 tracker, or a simplified representation of the AN/SPG-55B tracking radar, as appropriate. Timing functions critical to missile operation (such as illuminator assignment) are also simulated, as is the generation of the uplinked target position and velocity data.

### Missile Representation

In Fig. 3, each indicated subsystem of the SM-2(ER) Block II missile is represented in considerable detail. For example, the seeker subsystem (shown in more

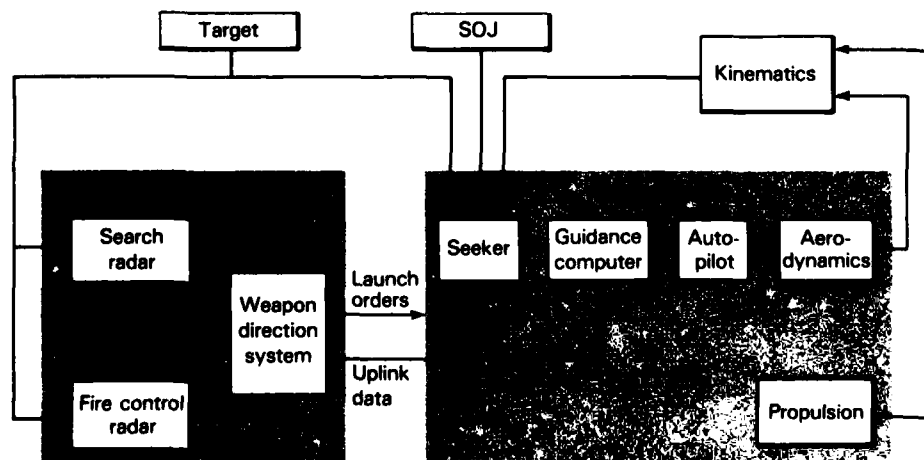


Figure 3 — Simulation of the overall Terrier Weapon System.

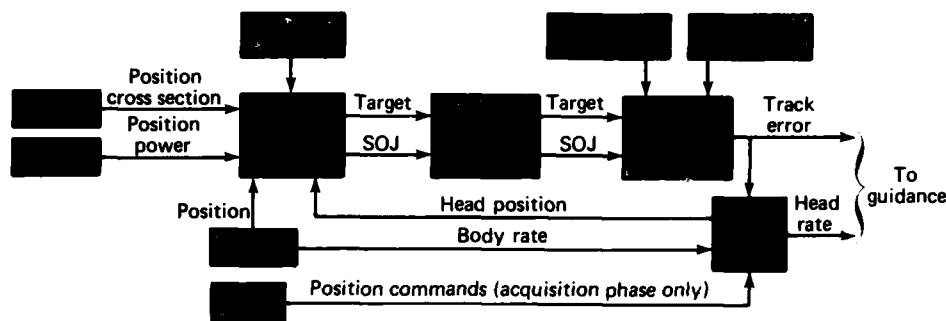


Figure 4 — Simulation of the seeker subsystem.

detail in Fig. 4) includes (a) a detailed representation of the target-missile-SOJ-illuminator geometry; (b) a 3D model of radome errors; (c) 3D representations of the antenna sum pattern, the azimuth and elevation difference patterns, and the ancillary pattern; (d) relative power levels of the signal returned from the target and the SOJ and thermal noise signals; (e) a representation of receiver signal processing; and (f) a simplified representation of the seeker servo track loops. This portion of the simulation executes at the actual receiver sampling rate. It provides a way to assess the effects of thermal and SOJ-induced noise on missile performance.

The guidance simulation represents both the midcourse guidance equations and the adaptive terminal guidance filters, using the actual iteration rate of the hardware. Radome compensation feedback, acceleration command limits, antigravity bias, and burnout compensation are also included.

The representation of the missile autopilot has been simplified by eliminating body mode and other high-frequency filtering, thus permitting more economical simulation runs. Enough detail has been maintained to represent autopilot response to about 3 Hz, which is sufficient to assess the effect of radome errors and aerodynamic roll-yaw-pitch coupling on guidance performance.

The simulation has a very detailed 3D representation of the SM-2(ER) missile aerodynamics, including normal force, axial force, moment, and cross-coupling coefficients that are functions of Mach number, aerodynamic roll angle, angle of attack, and tail deflections. This representation is based on extensive wind-tunnel testing that encompasses the range of conditions expected during missile flight.

The representation of the missile propulsion includes modeling of rocket motor thrust and of missile

weight and center of gravity as a function of time from ignition.

### Implementation and Application

The simulation is resident in the Laboratory's IBM 3033 computer system, where it executes approximately two times faster than real time. The basic cycle rate of the simulation through midcourse phase is 20 Hz; i.e., computations are performed every 50 ms of simulated flight. At the start of the homing phase while the seeker is attempting to acquire, the cycle rate is increased to the computation rate of the actual receiver. After the start of homing guidance, the computation rate is doubled to better represent the effects of noise in the autopilot and aerodynamics portions of the simulation.

This simulation has been used in a number of studies to determine the effectiveness of the SM-2(ER)/Terrier system in stressful operating environments, including combinations of high target speeds, high intercept altitudes, maneuvers, and SOJ's. In a typical simulation study, an intercept point is chosen and nominal runs are made (without noise or tolerance effects). The simulation automatically stores the conditions that exist at the start of the homing phase on a disk file for use as initial conditions in sets of Monte Carlo runs. In the Monte Carlo runs, the principal stochastic errors affecting guidance are introduced, including midcourse guidance errors (missile inertial reference unit initialization and drift error, obtained using a covariance propagation procedure, and target track error), head rate gyro bias, thermal and SOJ-induced noise, and target glint and fading. Ensembles of 20 to 50 Monte Carlo runs are used to estimate the distribution of miss distances that would occur in the chosen environment. Ordnance effectiveness estimates also can be provided by means of an interface to the aforementioned APL endgame simulation.

## ACKNOWLEDGMENTS

The simulation represents the joint effort of many contributors at APL. Those most directly involved were A. Chang, E. T. Federighi, D. R. Fenner, S. F. Haase, M. Hydock, L. E. Klein, B. E. Kuehne, R. T. Reichert, D. D. Richards, R. A. Slaven, and L. E. Tisserand.

## REFERENCE

- <sup>1</sup>K. E. Barnes and R. W. Witte, "SM-2 Block 11 Guidance Section Evaluation in GSEL" (U) (Confidential), in *APL Accomplishments, Fiscal Year 1981* (U) (Confidential), pp. 83-86.

This work was supported by NAVSEASYSKOM, PMS-400.

## AN ANALYSIS OF AERODYNAMIC REQUIREMENTS FOR COORDINATED BANK-TO-TURN AUTOPILOTS

A. Arrow and L. L. Cronvich

*Desirable aerodynamic properties were evaluated for an airframe that is to be controlled using bank-to-turn (BTT) steering. Both aerodynamic and autopilot design goals were considered. The evaluation was performed by comparing two planar missile airframes that have the potential for improved BTT control but have different aerodynamic properties. The comparison was made with advanced level autopilots using both linear and nonlinear three-dimensional aerodynamic models to obtain realistic missile body angular rates and control surface incidence. Critical cross-coupling effects were identified, and desirable aerodynamics were recommended for improved coordinated BTT (CBTT) performance. In addition, design and analysis techniques were recommended for developing autopilot control laws that can provide improved CBTT performance.*

## BACKGROUND

Although it has long been understood that BTT controlled missiles have the potential for better maneuverability and drag reduction than conventional cruciform, roll-stabilized, skid-to-turn controlled missiles, limitations in interrelated subsystem technology have delayed the development of BTT control systems. Major technological advances during the past decade (e.g., the availability of advanced on-board digital computers) have made BTT control feasible in spite of the added complexity of the control laws of the autopilot. Many programs<sup>1</sup> were initiated during the past decade to improve a missile's capability by means of BTT control. As pointed out in Ref. 1, those studies uncovered several areas where potential problems may

arise with BTT control. One area is missile guidance instability arising from a critical coupling loop formed by the BTT roll angle command. To reduce the gain in this loop and thus increase stability, the seeker must improve the decoupling of missile roll rate from the guidance signal. Radome aberration errors at radio frequencies and antenna stabilization errors are major sources of coupling. The problem is now under study. Meanwhile, simplified guidance studies<sup>2</sup> that neglect radome effects and assume coordinated missile motion have shown that CBTT can provide acceptable homing performance with roll rates that are not excessive for autopilot control.

The objective of this investigation was to determine what types of aerodynamic properties are desirable for an efficient CBTT autopilot (which implies small control surface effort, small sideslip, and high relative stability for a required acceleration response in the desired maneuver plane). Two planar airframes (Fig. 1) that have potential for CBTT control and have sufficiently different aerodynamic properties<sup>1</sup> were selected for study.

## DISCUSSION

### Airframe Configurations

The two airframes shown in Fig. 1 were sized to provide the realistic mass properties needed for the study. The weights and moments of inertia differ only slightly for the two configurations, except for the mass moment of inertia in roll of the elliptical configuration,

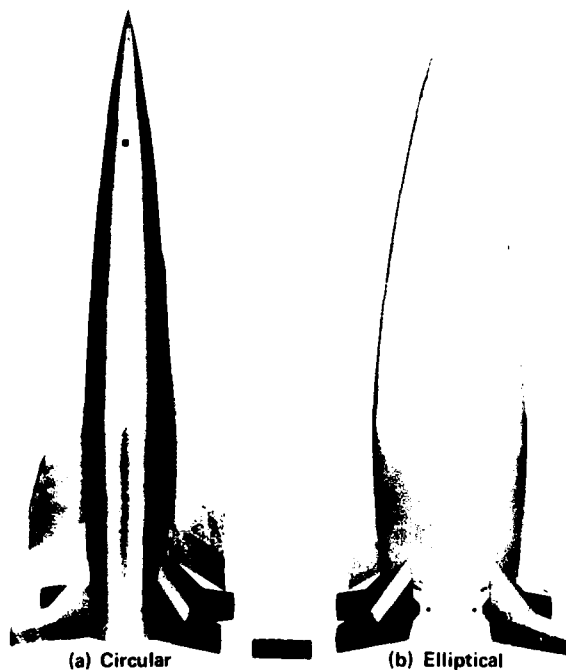


Figure 1 — Models of missiles having potential for improved BTT control.

which is nearly three times larger than that of the circular configuration.

On the other hand, the aerodynamic properties are quite different (Table 1). The circular configuration is stable in pitch and roll but unstable in yaw, whereas

the elliptical configuration is stable in yaw and roll but nearly neutrally stable in pitch. The elliptical configuration can generate a given maneuver in pitch at a lower angle of attack than can the circular, but it needs a higher angle of sideslip than does the circular to generate a maneuver in yaw. The control authority (control moment per degree incidence) of the elliptical configuration is somewhat smaller because of the requirement for a skewed hinge line. Both have control coupling moments that approach the control authority at very high angles of attack.

The performance comparison of these two airframes using CBTT control was made for a flight condition of Mach 3.95 at 60,000 ft altitude, with missile maneuvers requiring large enough angles of attack to exercise sideslip control.

### Bank-to-Turn Autopilot

Missiles with only one plane of symmetry should use an autopilot that forces the missile to bank in order to turn, similar to an aircraft, so that the steering maneuver occurs with the airframe oriented in a specified or preferred maneuver direction with respect to the incoming airstream. BTT control may also be used to enhance the performance of cruciform airframes.

CBTT is missile motion that is coordinated so as to minimize sideslip or yaw acceleration. An autopilot suitable for CBTT control is shown in Fig. 2. Inertial acceleration commands are applied in polar coordinates; i.e., the magnitude of the command,  $\eta_c$ , is applied to the pitch autopilot, and the direction,  $\phi_c$ , is ap-

Table 1 — Comparison of aerodynamic characteristics of circular and elliptical airframes.

Characteristic	Pitch Channel		Yaw Channel		Roll Channel	
	Circular	Elliptical	Circular	Elliptical	Circular	Elliptical
Stability	Stable	Nearly neutral	Unstable	Stable	Stable	More stable than circular
Force per unit angle of attack/sideslip	Moderate	Larger than circular	Larger than elliptical	Small		
Control authority	Larger than elliptical	Moderate	Larger than elliptical	Moderate	Larger than elliptical	Moderate
Ratio of control coupling to control authority	Neglected		Roll to yaw ( $C_{n_{\delta_R}}/C_{n_{\delta_Y}}$ ) small at low $\alpha$ , approaches unity at very high $\alpha$		Yaw to roll ( $C_{l_{\delta_Y}}/C_{l_{\delta_R}}$ ) small at low $\alpha$ , approaches unity at very high $\alpha$	

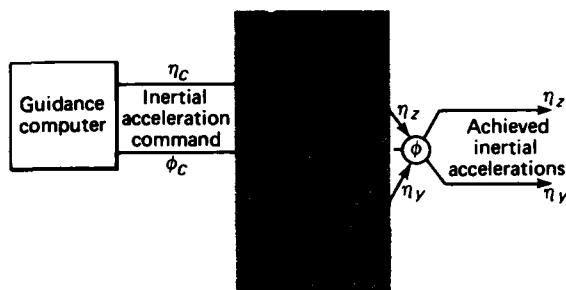


Figure 2 — CBTT control concept.

plied to the roll autopilot. The yaw autopilot is slaved to the roll autopilot to minimize sideslip angle by coordinating the missile yaw and roll motion. The achieved maneuver plane or inertial acceleration in rectangular coordinates ( $\eta_z$  and  $\eta_y$ ) is determined by resolving achieved body-fixed accelerations ( $\eta_z$  and  $\eta_y$ ) through the missile roll angle,  $\phi$ .

The CBTT steering policy for the autopilots of the circular and elliptical airframes was chosen to achieve maximum maneuverability from the airframes. Because the magnitude of the polar inertial command is applied to the pitch autopilot, only positive angles of attack are commanded. Therefore, the missile is forced to roll about its velocity vector to change maneuver direction, and roll attitude changes of  $180^\circ$  can occur. Coordinated motion or zero sideslip angle is achieved by directing the body-fixed pitch axis of the missile at the missile velocity vector so that there is no component of missile velocity along the body-fixed yaw axis. When an upward maneuver is commanded (i.e.,  $\phi = 0$ ), the missile body moves upward with its pitch axis directed at the velocity vector until it reaches the desired maneuver level or angle of attack. No roll motion is required to maintain coordination for this maneuver.

As was noted earlier, a fixed flight condition (i.e., constant altitude, Mach number, missile weight, and moments of inertia) was selected for these preliminary performance studies of circular and elliptical airframes. Fixed flight conditions are typically used in preliminary autopilot designs to identify and address critical areas of concern. When the autopilot requirements are satisfied at fixed flight conditions, areas of concern introduced by time-varying flight conditions are then addressed. A series of acceleration commands was applied to reveal the critical problem areas for CBTT control. In particular, the first command (a climb) was applied to cause the missile to increase angle of attack without a corresponding roll maneuver (i.e., to pull an upward maneuver from a trimmed cruise attitude). The second command (a dive) forced the missile to roll about its velocity vector while at an angle

of attack that would require sideslip control and could result in kinematic and inertial coupling problems.

The first phase of the design approach for the CBTT autopilot was to design each channel independently with all coupling between channels removed. This approach reduced the problem to the well-established linear and nonlinear design techniques of roll-stabilized, skid-to-turn missile autopilots. Sufficient high-frequency attenuation was added for actuator and missile elastic mode frequencies so that the resulting missile body angular rates and control surface motion represented a practical missile design. A relationship was established among the relative speeds of response of the uncoupled channels in order to meet CBTT requirements. The acceleration response of the pitch channel must be the same as the required response in the desired maneuver plane to satisfy a climb maneuver when the roll and yaw channels are not required. The roll channel must have an attitude response that is at least as fast as that of the pitch channel so that the missile may be rolled around the velocity vector fast enough to achieve the required maneuver plane response. To coordinate missile motion or to minimize sideslip, the response of the yaw channel must be faster than that of the roll channel to which it is slaved.

The second phase of the design approach for the CBTT autopilot was to use a linear design and analysis technique to predict (and adjust when necessary) the stability of the coupled autopilot and the quality of sideslip control. In addition, the influence of cross-coupling (aerodynamic, kinematic, and inertial) was isolated in order to reveal ideal airframe characteristics for CBTT. The combination of linear analysis and nonlinear 3D analysis identified the limitations of CBTT control of the circular and elliptical airframes investigated and the importance of the various aerodynamic parameters in establishing satisfactory CBTT control.

### Critical Coupling for CBTT Control

Critical coupling paths have been identified that may limit the performance of a missile using CBTT control. These paths are illustrated in Fig. 3. The autopilot in Fig. 2 is shown in more detail in Fig. 3. Pitch, roll, and yaw dynamics are controlled through the motion of tails driven by servos. Pitch and roll tail servo commands are determined by comparing the inertial acceleration command from the guidance computer with sensor measurements from the missile dynamics. The coordination command to the yaw channel is compared with the yaw sensors to command the yaw tail servos to minimize sideslip.

The roll and yaw dynamics are shown coupled in Fig. 3 by control coupling moments and yaw-induced

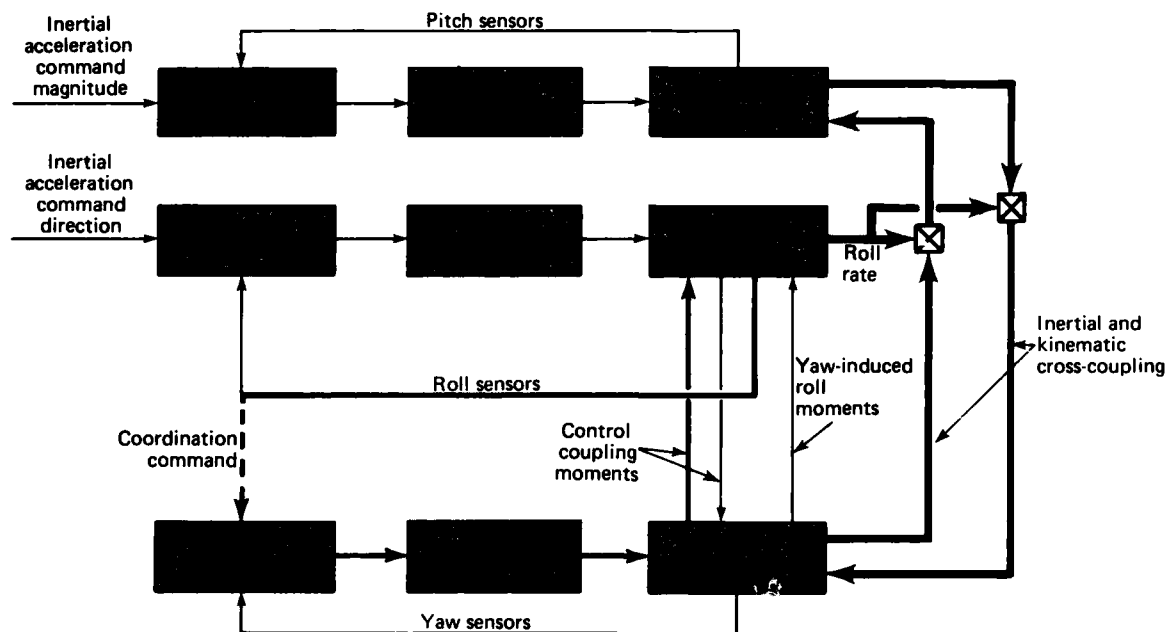


Figure 3 — Critical coupling paths for CBTT control concept.

roll moments. This aerodynamic cross-coupling, which also exists in roll-stabilized missiles, becomes more severe with high angles of attack and may reach a condition for which the control capabilities are exceeded and the missile becomes uncontrollable. The critical coupling path at high angles of attack for roll-stabilized missiles (formed through yaw-induced roll moments and the kinematic cross-coupling of roll rate into yaw dynamics) is not critical for CBTT because the yaw-induced roll moment is now stabilizing, as is shown by the roll stability in Table 1. However, the kinematic cross-coupling of roll rate into yaw dynamics is critical in CBTT because it produces large sideslip, which is counteracted by the coordination command. The coordination command, which forces the missile yaw angular rate to counteract the effects of the kinematic coupling on sideslip, forms the critical coupling path shown by the heavy black lines in Fig. 3. This coupling path was identified in linear analysis and verified by nonlinear 3D simulation studies. It influences the relative stability in the coordination command branch that, in turn, determines the quality of sideslip control. Reduction of the ratio of control coupling (yaw to roll) to control authority alleviates this problem (Table 2).

Another critical coupling path formed by BTT control that was not critical in roll-stabilized missiles is inertial and kinematic cross-coupling between pitch and yaw dynamics, shown by the heavy gray line in Fig. 3. This coupling is more severe with increasing missile roll rate. Identified by means of nonlinear 3D simulation

studies, it causes transients in the form of overshoots and undershoots in the maneuver plane acceleration response. The transients may also result in a slower maneuver plane acceleration response.

## RESULTS

The performance of CBTT autopilots was found to be limited by aerodynamic, kinematic, and inertial cross-coupling. The desired aerodynamic characteristics that would alleviate these limitations are outlined in Table 2. Some of the significant findings were the unexpectedly small effect of yaw stability on controlling sideslip, the importance of induced rolling moment resulting from yaw control ( $C_{l_{\delta_Y}}$ ) on autopilot stability, and the probable need of some pitch stability to lessen the effect of the pitching moments from kinematic and inertial coupling from the yaw channel into the pitch channel.

The yaw stability of the elliptical airframe was not sufficient to influence significantly the sideslip control; therefore, the required yaw stability is still an issue. The control cross-coupling  $C_{l_{\delta_Y}}$  tended to degrade autopilot stability, while the cross-coupling  $C_{n_{\delta_R}}$  (induced yawing moment resulting from roll control) had little effect for the condition studied. Therefore,  $C_{l_{\delta_Y}}$  should be kept small relative to control authority,  $C_{l_{\delta_R}}$  (see Table 2), in order to reduce its influence. As noted in Table 1, this requirement may be met at low to

Table 2 — Desired aerodynamic characteristics for CBTT control.

Type	Pitch Channel	Yaw Channel	Roll Channel
Stability	Neutral or stable still an issue ( $C_{m_\alpha} \leq 0$ )	Stable or neutral still an issue ( $C_{n_\beta} \geq 0$ )	Moderate ( $C_{l_\beta} < 0$ )
Force per unit angle of attack/sideslip	Large ( $C_{N_\alpha} > 0, C_{Y_\beta} < 0$ )		
Control authority	Large to minimize control effort ( $C_{m_{\delta_P}}, C_{n_{\delta_Y}}, C_{l_{\delta_R}} > 0$ )		
Ratio of control coupling to control authority		Not yet determined ( $C_{n_{\delta_R}}$ )	Minimize ( $C_{l_{\delta_Y}} < C_{l_{\delta_R}}$ )

moderate angles of attack but may be difficult to meet at high angles of attack. Moderate roll stability is desirable because it reduces the transients in the maneuver plane acceleration response resulting from kinematic and inertial cross-coupling between pitch and yaw channels through roll rate and is not critical for autopilot stability. Too much roll stability might require excessive roll control to carry out the roll needed to place the missile in the correct attitude for the pitch maneuver.

The pitch stability of the circular airframe was not sufficient to influence significantly the pitching moments from kinematic and inertial coupling from the yaw channel. An increase in pitch stability, however, will require increased pitch control to achieve a given maneuver. On the other hand, nearly neutral stability minimizes the control requirement but offers no resistance to the coupling from the yaw channel. The desired pitch stability for CBTT control is another issue to be resolved.

Because the elliptical airframe achieved the desired performance at the selected flight condition with less autopilot complexity than did the circular airframe, it merits further CBTT investigation. Additional studies

should include a range of dynamic pressures (a function of Mach number and altitude) and possibly higher called-for accelerations before one can safely conclude that the aerodynamic characteristics of such an airframe are those desired for CBTT control.

More details may be found in Ref. 4.

## REFERENCES

- <sup>1</sup>F. W. Riedel, *Bank-to-Turn Control Technology Survey for Homing Missiles*, NASA CR-3325 (Sep 1980).
- <sup>2</sup>R. T. Reichert, *Homing Performance Comparison of Selected Airframe Configurations Using Skid-to-Turn and Bank-to-Turn Steering Policies*, NASA CR-3420 (May 1981). See also R. T. Reichert, "Bank-to-Turn Missile Guidance Performance," in *APL Developments in Science and Technology, Fiscal Year 1980*, JHU/APL DST-8.
- <sup>3</sup>E. B. Graves, *Aerodynamic Characteristics of a Monoplane Missile Concept with Bodies of Circular and Elliptical Cross Sections*, NASA TM 74079 (Dec 1977).
- <sup>4</sup>A. Arrow, *An Analysis of Aerodynamic Requirements for Coordinated Bank-to-Turn Autopilots*, NASA CR-3644 (Nov 1982).

This work was supported by the NASA Langley Research Center.

## COMPARISON OF DISCRIMINANT SETS FOR AUTONOMOUS SHIP CLASSIFICATION

F. W. Riedel

*The autonomous classification of ship targets by a cruise missile is based on features or image discriminants that characterize the ship classes of interest. Three different types of discriminant sets have been compared to determine their ability to classify and distinguish idealized ship images.*

### BACKGROUND

Long-range, low-flying antiship missiles require a classification capability in order to reject noncombatant and friendly ships and to select high-priority targets from an enemy battle group. Because data links at long ranges are impractical, the missile must operate autonomously (i.e., without human intervention). The resolution needed for classification and the small size of a missile-compatible sensor suggest the use of an imaging infrared seeker. One approach to the problem of identifying and classifying a ship is to use pattern recognition methods on infrared images. However, no recognition algorithm will perform better than the information input to it. It is therefore critical to identify a set of discriminants (image descriptors) that can distinguish various ship images.

An important characteristic of discriminants is invariance. To minimize computer storage requirements and to ease the burden on the classification algorithm, the discriminants should be independent of changes in uncontrollable variables such as weather and diurnal effects. They should also be unaffected by ship operation (i.e., at full steam or at anchor) and immune to countermeasures. To reduce sensitivity to these effects, the discrimination procedure does not use infrared intensity. Rather, the procedure converts infrared images into one-bit silhouettes, thereby retaining only geometric shape information. The problem is thus reduced to a determination of discriminants that characterize ship shapes.

Target ship range and aspect angle are also important considerations. Because range information is not available from a passive sensor, the discriminants should be independent of it. Also, because a missile might locate a ship at any aspect, the discriminants should be able to characterize the ship at all aspect angles.

### DISCUSSION

The approach used to compare the discriminants is to perform recognition experiments using each type.

Any investigation of pattern classification methods requires data. Because the usefulness of a particular type of discriminant may vary with the particular patterns to be classified, only ship images — not contrived shapes (crosses, squares, circles, etc.) — should be used. It is desirable to have ship image data that are noise-free and undistorted. Tolerance to noise and distortion will be evaluated after the initial discriminant comparison. Infrared images have intensity variations that depend on the temperature of the target and the background, and on atmospheric attenuation. These intensity variations are greatly influenced by the relative orientations of the sun, the target, and the sensor; cloud cover for the previous several hours; weather; diurnal variations; etc. In addition, they can be altered intentionally. For these reasons, infrared intensity variations probably are not good features for recognition. It is desirable to have basic characteristics that are less sensitive to uncontrolled variables.

The geometric shape of the ship is invariant to such changes. Also, the shape can be measured using optical wavelengths. Therefore, data were generated at APL by digitizing television images of 1:1250-scale ship models. The data base consists of 315 images of five ship classes, i.e., the aircraft carrier *Kiev*, the cruisers *Kresta II* and *Kashin*, the destroyer *Krivak*, and a West German tanker. Data from all aspect angles are not required for this comparison, although they would be when designing a complete system. Images were taken at 21 aspect angles ranging from 10° port to 100° starboard, and at three simulated ranges. The depression angle was approximately 2°, simulating the view from a low-altitude missile. The data are well calibrated, of high resolution, and noise-free. The results of this comparison are thus independent of the characteristics of any particular sensor. Only minimal processing was required to convert the data to one-bit silhouettes.

The 1-nearest-neighbor classification algorithm was selected for these experiments. This classifier is well documented in the literature and has analytical justification, at least in the limit of a large number of samples. A typical recognition experiment would proceed as follows.

Certain images are selected as known prototypes. For this study, the prototypes are usually the 5 nmi data, with aspect angles equal to integral multiples of 10°. The discriminants are calculated and stored as vectors. The remaining images are the unknown samples to be classified. The discriminants are

calculated for each of these unknown samples, and the distance (according to some metric or distance measure) is measured from an unknown sample to each of the prototype discriminant vectors. Various metrics and weightings are examined; however, all the results presented here use the metric induced by the  $L_1$  (absolute value) norm. The 1-nearest-neighbor algorithm assigns the unknown image to the class of the nearest prototype.

## RESULTS

The first type of discriminant investigated was moment invariants. First proposed by Hu<sup>1</sup> and later extended by Dudani et al.,<sup>2</sup> moment invariants are a set of seven combinations of central moments that are invariant under translation within the field of view, rotation within the field of view, and reflection. Range (scale) invariance can also be imposed at the expense of reducing the set from seven to six. The seven moment invariants were computed for both the silhouette images and for images consisting of only the border or the boundary of the ship. When combined, the set contained 14 discriminants (12 if range invariance is imposed).

Figure 1a shows the percent of misclassifications when the range to the unknown ship being classified is assumed to be known. The fact that the result for the combined silhouette and border is better than either taken individually indicates that there is independent information in the combination. The dependence on range seems erratic, although the 2.5 nmi unknowns are always classified most accurately.

For the next recognition experiment, range was assumed to be unknown (i.e., range invariance was imposed). The results are shown in Fig. 1b. Notice that the classification performance degrades significantly. Again, performance for the combined data is better overall but only slightly better than for the silhouette-only data; also, range dependence is erratic.

Aspect dependence was also investigated.<sup>3</sup> Although most misclassifications occurred for near bow aspect angles, the misclassification rate for near quartering and near broadside aspects was approximately 12%.

The second type of discriminant investigated was a set of two-dimensional orthogonal transform coefficients. The Walsh-Hadamard (W-H) transform<sup>4</sup> was selected because its basis functions consist of square waves with values of +1 and -1. As such, this transform is natural to use with one-bit ship silhouettes. Fast transform algorithms are also available.

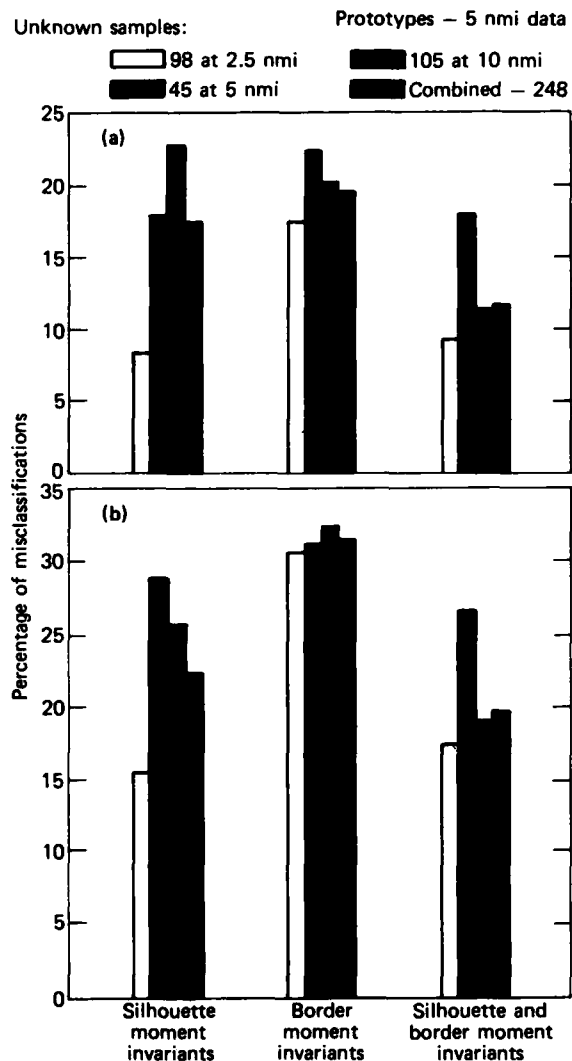


Figure 1 — The percentage of misclassifications and range dependence; (a) range is assumed to be known; (b) range is assumed to be unknown.

The W-H transform does not exhibit the desired invariant properties. A method was devised to provide invariance to translation within the field of view and to scale changes. Extensions of the method could also provide invariance to rotation within the field of view. The method consists of first finding the smallest rectangular box containing the ship, regardless of its location within the field of view, and then dividing the box into  $N$  by  $M$  elements, where  $N$  and  $M$  are fixed regardless of box size and width-to-height ratio ( $N = 16$  and  $M = 64$  were used). The new  $N$  by  $M$  array is resampled and transformed using the W-H algorithm.

The transform coefficients are elements of the discriminant vector.

The normalization procedure described above suggests another type of feature, i.e., the  $N$  by  $M$  binary-valued elements of the resampled array. The number of elements in an unknown image that have the same values as corresponding elements in a prototype image is a measure of image similarity. This measure is a binary correlation.

Figure 2 illustrates the results for the W-H transform and the binary correlation method. The number of W-H coefficients used is a parameter in the figure. The misclassification rate is about 4 to 5% for the W-H method and 3% for the binary correlation method.

The misclassification rate as a function of aspect angle was also examined. For combined near quartering and near broadside aspects, the misclassification rate for the W-H method (36 coefficients) was less than 5% and for the binary correlation method, less than 4%. The normalization procedure described above resamples bow aspect views at a higher sampling rate than for quartering or broadside aspects. This higher sampling rate resulted in very good classification performance at near bow aspects for the ideal, noise-free images used in this study. These results suggest refinements to the procedure that are discussed further in Ref. 3.

## CONCLUSIONS

This paper presents early results from an investigation to identify discriminants that are well suited for autonomous ship classification. It was concluded that both the W-H method and the correlation method perform better than the moment-invariant method. Moreover, techniques to improve both methods have been identified.<sup>3</sup>

Autonomous ship classification is a complex task in which environmental effects, sensor parameters, image processing, and classification algorithms as well as discriminants must be examined. Results from this discriminant comparison provide valuable insights into

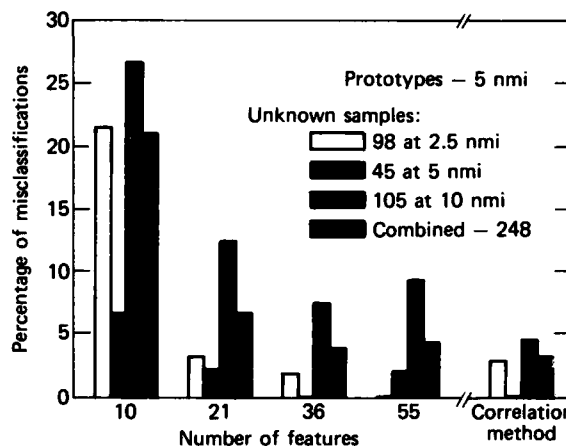


Figure 2 — The percentage of misclassifications and range dependence using the Walsh-Hadamard transform coefficients and the correlation method.

the design of a complete classification system for long-range, low-flying antiship missiles.

## ACKNOWLEDGMENT

The author wishes to acknowledge the support of D. K. White, who programmed and produced the results from the moment-invariant method.

## REFERENCES

- 1 M-K. Hu, "Visual Pattern Recognition by Moment Invariants," *IRE Trans. Info. Theory* (Feb 1962).
- 2 S. A. Dudani, K. J. Breeding, and R. B. McGhee "Aircraft Identification by Moment Invariants," *IEEE Trans. Comp.* (Jan 1977).
- 3 F. W. Riedel, "Comparison of Discriminant Sets for Autonomous Ship Classification," in *Proc. Tri-Service Workshop on Missile Ship Targeting*, Naval Research Laboratory, Washington (10-12 Aug 1982).
- 4 W. K. Pratt, J. Kane, and H. C. Andrews, "Hadamard Transform Image Coding," in *Proc. IEEE* (Jan 1969).

This work was supported by Independent R&D.

# GRAPHITE ABLATION MEASUREMENTS

R. W. Newman, C. H. Hoshall, and R. C. Benson

*A test apparatus has been developed to measure graphite ablation rates. Mass loss measurements were made on ATJ graphite samples in CO, CO<sub>2</sub>, argon-H<sub>2</sub>O, air-H<sub>2</sub>, O<sub>2</sub>, and simulated Shelldyne-air environments. The results have been used to improve our analytical model of graphite ablation in supersonic ramjet combustors.*

## BACKGROUND

The diffuser, combustor, and nozzle components of ramjet and supersonic-combustion ramjet (scramjet) engines have internal gas flows that are highly oxidizing and structural temperatures that exceed the melting points of most metals. Carbon and graphite materials can be used, but they ablate. For satisfactory scramjet engine performance and durability, the amount of ablation must not exceed prescribed limits; therefore, analytical methods must be available for predicting the amount of ablation.

Computer codes have been developed for predicting the rate of ablation; however, the necessary kinetic data relating mass loss rate to pressure, temperature, surface material, and environmental gas species are not usually available. Consequently, experimental data taken under controlled, well-defined environmental conditions are needed to enhance the theoretical prediction of carbon/graphite ablation.

## DISCUSSION

### Analytical Model

The ablation of graphite in a scramjet combustor environment is a complex process in which the combustor liner is heated by the hot combustion gases to a temperature at which the graphite reacts with some of the combustion gases. This reaction either absorbs or liberates heat, raising or lowering the surface temperature in turn. The process is currently being modeled using an APL version of the Charring Materials Ablation (CMA) computer code.<sup>1</sup> Values of mass loss parameter ( $\beta'$ ) are input to CMA, assuming the reacting products at the surface are in chemical equilibrium (not necessarily true). A test apparatus has been developed to measure ablation mass loss rates from ATJ graphite,<sup>2,3</sup> and the results have been used to refine our analytical model.<sup>4-6</sup> In addition, an analytical procedure is being developed to convert the subsonic flow conditions

of the test model to the supersonic conditions of the combustor environment.

### Apparatus and Test Procedure

Figure 1 is a simplified block diagram of the test apparatus. The graphite specimens are pellets machined from ATJ graphite and placed in close-fitting rings made of the same material. The rings shield the sides of each pellet and prevent rounding of the edges by the reactive gases. This technique provides an effective yet easily implemented simulation of a continuous surface. In this series of tests, a shield made of the same material was used in addition to the pellet and ring. Typical dimensions of the pellets were a diameter of 3.3 mm (0.13 in.) and a length of 1.78 mm (0.07 in.); the typical weight was approximately 23 mg. The outside diameter of the rings was typically 5.6 mm (0.22 in.).

The specimen, ring, and shield were heated by placing them on an electric heater (insert, Fig. 1), which was also made of ATJ graphite. Heating was accomplished by radiative and conductive transfer from the heater. To measure the recession rate, the test chamber was purged with argon, and then the specimen was raised to operating temperature. Reagent gases metered through choking orifices and controlled by solenoid valves were turned on manually; the gases passed through the nozzle onto the specimen until the gas flow and the heater power were turned off automatically by a preset timer.

Recession rates were determined by weighing the part of the specimen remaining at the conclusion of the test, thereby determining weight loss. The specimens were also measured with a micrometer for comparison with the initial dimensions. The amplitudes of critical variables indicated in Fig. 1 were recorded with a Visicorder during each test.

## TEST RESULTS

The measured ablation rates from 40 tests (Table 1) have given us a better picture of the ablation process at the surface of ATJ graphite. When comparable data are available in the literature, they are in good agreement with our test data.<sup>7,8</sup> The results for simulated Shelldyne-air mixtures (Fig. 2) indicate that at 3500°F, CO<sub>2</sub> and O<sub>2</sub> react with the ATJ graphite at the diffusion limit to form CO. At 2000°F, they react at about half the diffusion-limited rate. If a water vapor reaction

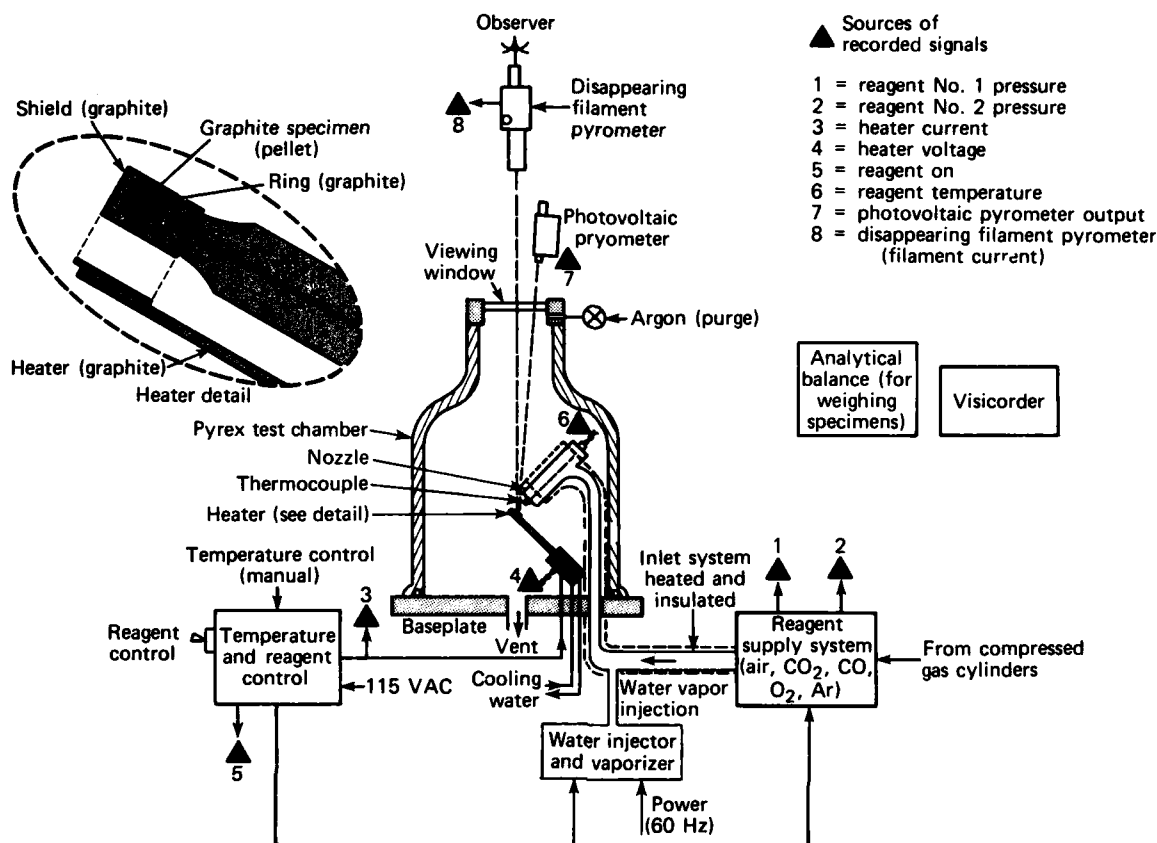


Figure 1 — The test apparatus for graphite ablation measurements.

$\text{H}_2\text{O} + \text{C} \rightarrow \text{H}_2 + \text{CO}$  is assumed, the measurements show that only half the water reacts in this manner.

Recession rate data taken at various gas velocities correlate well with the theory that, in the diffusion limit, the ablation rate is directly proportional to the enthalpy-based heat transfer coefficient ( $h_i$ ). An important finding of this test program is that at 3500°F,  $\text{CO}_2$  and  $\text{H}_2\text{O}$  both react with ATJ graphite. Even at temperatures as low as 2000°F,  $\text{CO}_2$  reacts with the surface. This finding is especially important for high equivalence ratio (ER) gas flows, for which little  $\text{O}_2$  is available but for which there is an abundance of  $\text{CO}_2$  and  $\text{H}_2\text{O}$ . Previous thermal analyses of materials under these conditions will be reanalyzed using a reacting  $\text{CO}_2$  and  $\text{H}_2\text{O}$  chemical model.

#### Extrapolation of Test Data to Flight Conditions

An analytical procedure<sup>9</sup> has been developed and is currently being evaluated. The evaluation will take ablation rates measured under subsonic and perpendicular flow conditions and transform them into

supersonic ramjet combustor flight conditions where the flow is supersonic and parallel to the surface. The transformation between flow conditions is made by plotting

$$\log \left( \frac{\dot{m}}{\rho} \left( \frac{1 + \beta}{\beta_d - \beta} \right) \right)$$

against  $1/T$ , where

- $\dot{m}$  = measured ablation mass loss rate,
- $\rho$  = density of ablator,
- $\beta = \dot{m}/h_i$ ,
- $\beta_d$  = same as  $\beta$  except that  $\dot{m}$  is replaced by a calculated diffusion-limited mass loss rate ( $\dot{m}_d$ ).

The curve is independent of flow because the flow conditions are accounted for by  $h_i$ .

#### Reaction Gas Products Measurements

One limitation of the current test procedure is that while the amount of carbon mass loss is known, the

Table 1 — Test conditions (identified by run number).

	Sample Temperature (°F)									
	2000		2500	3000	3500			4000		4500
	1*	16.6	1	1	1	16.6	20	1	10	1
Air										
<400 ppm H <sub>2</sub> O	4				3	16,17		5,8	1,2	
4.5% H <sub>2</sub> O		21				20				
6.5% H <sub>2</sub> O	12		13	14	11	18,19		9,10		15
Simulated Shelldyne-air										
ER = 0.3	24				25,26		22,23			
ER = 0.6	27				28,29					
ER = 1.0	30				31,39			40		
O <sub>2</sub>										
6.5% H <sub>2</sub> O					36					
CO <sub>2</sub>										
<400 ppm H <sub>2</sub> O					34					
6.5% H <sub>2</sub> O	33				32					
CO										
6.5% H <sub>2</sub> O					35					38
Argon										
6.5% H <sub>2</sub> O					37					

\*Nominal velocity (m/s) of gas based on room-temperature gas exiting from nozzle.

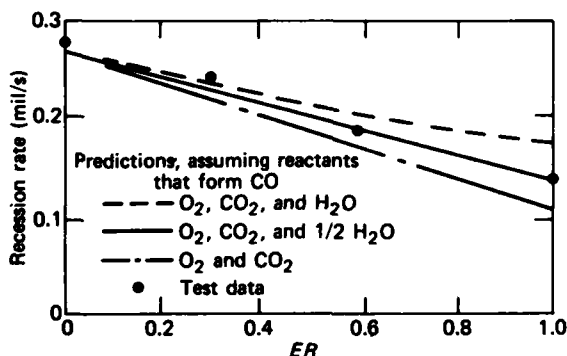


Figure 2 — The recession of carbon in Shelldyne-air mixtures; surface temperature = 3500°F; flow is normal to the surface at 1 m/s.

chemical reactions that take place are not. An improved test procedure is being developed to solve this problem by measuring the reaction product concentrations at the surface using a Raman scattering technique.

Following the preliminary bench checkout of the coherent anti-Stokes Raman scattering (CARS) apparatus, a test was made using the ablation apparatus. The broadband dye laser spectrum was adjusted so that CO and N<sub>2</sub> were detected simultaneously. Several ablation

runs were made with the carbon temperature at about 3000°F and the airflow at approximately 1 m/s. The CO and N<sub>2</sub> CARS signals were compared with their corresponding calibration signals. The results were encouraging; however, modifications of the ablation apparatus and improvements to the CARS system will be required before accurate measurements can be made of CO gas concentrations as a function of distance above the ablating surface.

## ACKNOWLEDGMENT

The authors wish to acknowledge the contributions of L. W. Hunter, L. B. Weckesser, and H. Y. Chiu.

## REFERENCES

- <sup>1</sup>D. R. Cruise, "Notes on the Rapid Computation of Chemical Equilibria," *J. Phys. Chem.* **68**, 3797-3802 (Dec 1964).
- <sup>2</sup>H. Hoshall, *Graphite Ablation Tests*, JHU/APL CFP-80-003 (15 Jan 1980).
- <sup>3</sup>R. W. Newman, *Test Plan to Measure High Temperature Graphite Ablation Rate*, JHU/APL BBE/EM-4999 (Jun 1981).
- <sup>4</sup>C. H. Hoshall, *ATJ Graphite Ablation Tests, 1981 Series*, JHU/APL BBE/EM-5044 (17 May 1982).
- <sup>5</sup>R. W. Newman, *Ablation Rate Test Results for ATJ-Graphite Surfaces Exposed to High Temperatures and Various Reacting Gas Mixtures*, JHU/APL BBE/EM-5040 (29 Apr 1982).

<sup>6</sup>R. W. Newman and C. H. Hoshall, *Graphite Ablation in Several Gas Environments*, JHU/APL TG 1336 (Jan 1983).

<sup>7</sup>E. S. Golovina and G. P. Khaustovich, "The Interaction of Carbon with Carbon Dioxide and Oxygen at Temperatures up to 3000°K," *Eighth Symposium on Combustion*, Williams and Wilkins (1962).

<sup>8</sup>K. Matsui et al., "Fluid-Mechanical Effects on the Combustion Rate of Solid Carbon," *Combust. Flame* 25, 57-66 (1975).

<sup>9</sup>L. W. Hunter, "A New Approach to Correlating Carbon Ablation Data in an Oxidizing Gas" (to be published).

---

This work was supported by Independent R&D.

## SYSTEM DATA RECORDER FOR THE PERSHING II WEAPON SYSTEM

C. C. Rodeffer and D. B. Kratz

*An instrumentation set has been built to be deployed tactically with the Pershing II weapon system. It is transparent to the tactical system, can be built for a relatively low cost per unit, and has a menu of instrumented parameters that can be changed as the need arises by firmware changes in the instrumentation equipment.*

### BACKGROUND

Currently, Pershing 1a missiles are on Quick Reaction Alert (QRA) status in West Germany. The Laboratory serves as an independent evaluator of the Pershing weapon system and prepares an annual evaluation report for the Commander in Chief, U.S. European Forces, for submission to the Joint Chiefs of Staff. The same function will be performed for the Pershing II weapon system after deployment.

The principal responsibilities of APL center around determining realistic measures of performance, including weapon system reliability, weapon system accuracy, communications reliability, and reaction time. In order to fulfill this responsibility, an independent, separate record of events surrounding those elements of the Pershing force on QRA status must be obtained. APL uses dedicated data collectors and ground instrumentation to acquire such a record for the currently deployed Pershing 1a system.

A new configuration for the ground instrumentation had to be developed for the Pershing II weapon

system. The instrumentation used with the deployed Pershing 1a system had proved valuable in gathering data not only for the annual evaluation report but also for supporting the Army's Pershing Project Manager and the prime contractor, Martin Marietta, in locating system problems. Experience also confirmed that if the inventory of instrumented parameters could be varied readily, the instrumentation set would be even more valuable in locating postdeployment problems. Furthermore, if such an instrumentation concept were integrated into the weapon system at an early stage in its design, a more powerful instrumentation capability could be achieved with little increase in cost.

A plan was approved in 1978 by the Pershing Project Manager for the Laboratory to work with the weapon system's prime contractor in developing a low-cost System Data Recorder (SDR) that would be integrated with the tactical system and would be able to change the inventory of recorded parameters by changing only the firmware in the SDR.

### DISCUSSION

#### Physical Description

Figure 1 shows the SDR with its front cover opened. A combination mounting/carrying handle is bolted to its top. The configuration weighs 63 lb and requires less than 80 W of the single-phase, 60-Hz power used by the weapon system. The two cartridge drive

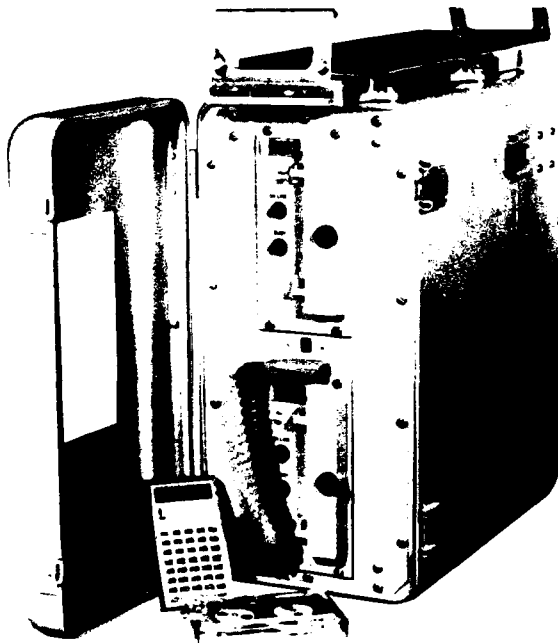


Figure 1 — The System Data Recorder.

units use an industry standard 3M four-track cartridge; each cartridge can hold at least  $1 \times 10^6$  words of 16 bits each. When one cartridge is full, the SDR automatically switches to the next cartridge drive unit. The control and primary display for the SDR are afforded by the pocket terminal shown in Fig. 1. The operator carries the pocket terminal with him; thus, there does not have to be a terminal for each SDR, saving space and weight for an equivalent keyboard and display.

The philosophy followed to minimize the cost of the SDR is to use off-the-shelf components with as little modification as possible. In addition, virtually no modification to the tactical weapon system is required; only minimal provisions were made to acquire the necessary signals. The SDR comes complete with its own weather-proof enclosure; cables for signal, power, and grounding; and a combination mounting/carrying handle to suspend the SDR from a catwalk on the erector/launcher.

The equipment has been designed to meet the weather conditions expected in Europe and the United States and to meet the full electromagnetic pulse/radio frequency interference specifications for the tactical equipment. In effect, the design makes the SDR a part of the weapon system's Faraday cage.

The SDR is buffered directly in parallel to the 16-bit input/output (I/O) bus of the tactical launch

computer. The data pulses on the bus are only about 110 ns long, and the time between words on the bus can be as little as  $1.7 \mu\text{s}$ . The most reliable and conventional way to transmit such data would be to use dual differential line drivers and to match the lines all the way to the SDR, with the SDR placed as close as possible to the launch computer. However, for economy, only a single-ended line-driver scheme was made available to the SDR, and the SDR had to be mounted approximately 10 ft from the tactical connector to the launch computer. In order to improve the signal-to-noise ratio to the SDR and to further isolate it from possible interference with the launch computer, an active buffer and transmission line matcher were designed to be part of the signal cable. Those circuits were miniaturized and incorporated in an elongated backshell right at the signal cable connector that mates with the tactical connector to the launch computer.

### Functional Description

Functionally, the SDR is connected to the I/O bus of the Pershing launch computer (PLC) and can record information going to or from it. The SDR is transparent to the PLC when connected to the I/O bus. The tactical software is not required to slow down to accommodate the presence of an SDR, and the PLC does not require a READY or ACKNOWLEDGE signal from the SDR. Therefore, the SDR is completely passive as far as the PLC is concerned, and the SDR is designed to send no signals back to the PLC.

The central processing unit (CPU) puts out alternate address words and 16-bit data words on the I/O bus. The address word is put out on the I/O bus, enabling the particular interface or data link for which the data that follow are intended (see Fig. 2). The CPU then loads the 16-bit data word on the I/O bus. All the various interface devices and data links see the data word, but only the one just addressed receives the data word and begins to condition and transmit it to the proper location. The interface or data link receiving data from the CPU will not be ready to receive additional data until its circuits are cleared and it has received an ACKNOWLEDGE signal from the receiving device. The CPU can service other interfaces or data links while a particular device is receiving and acknowledging a data word.

A 16-bit parallel interface is required in order for the SDR to be able to receive and interpret all the information on the I/O bus. The instrumentation interface (I/I) card in the PLC provides such an interface for the SDR. Another section of the I/I card does a parallel-to-serial conversion of the data; the output is planned for use only at firing ranges in the United States. The

tactical software in the PLC stores an inventory of data elements of an instrumentation nature that are addressed to the I/I card. The normal mode of the SDR is to receive only the data elements preprogrammed for the I/I card, but only a quick firmware change in the SDR is needed to add data elements for special purposes.

In Fig. 3, the parallel interface logic screens the data elements to be recorded. Much of the data appearing on the PLC I/O bus are repetitive; this is also true of the data addressed to the I/I card. A major task for the SDR thus becomes one of real-time data compression. The board 1 microprocessor stores the initial value of each data element and compares each subsequent transmission of that data element to the initial value. The initial value and any subsequent changed values are sent to the shared memory along with pertinent information as to the destination of the data element in the tactical system.

The shared memory is divided in half. Board 1 is filling one half at its own pace while board 2 is emptying the other half at an asynchronous pace. When board 2 has finished emptying its half, the microprocessors switch halves and the process continues. The logic on board 2 takes the data element and source information,

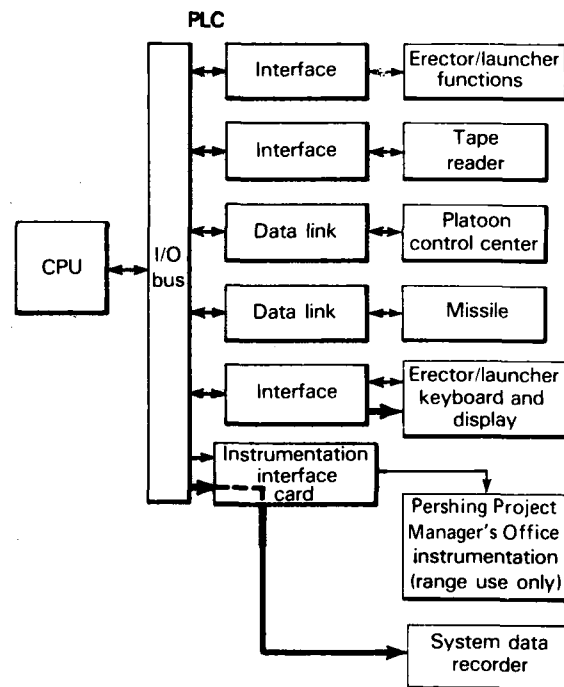


Figure 2 — Functional interfaces of the SDR.

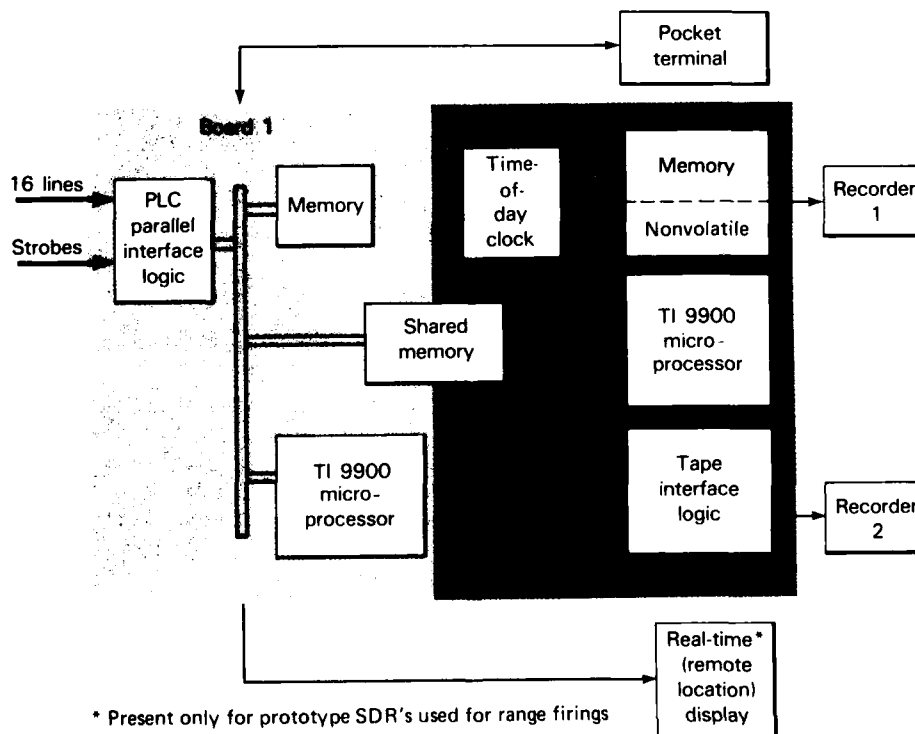


Figure 3— Functional block diagram of the SDR.

tags it with date and time-of-day information, and controls the recording of the data on the tape. Because the continuous flow of data to be recorded does not allow time for the cartridge to be rewound to start a new track, the data elements are recorded on the tapes in a "serpentine" fashion; that is, at the end of the tape, another recording head is selected, and the next track is recorded in the reverse direction.

A nonvolatile memory is needed to store recorder and track information when the power to the SDR is turned off. The time-of-day clock and the non-volatile memory are battery powered when the power is off.

Prototype SDR's have been used on three Pershing II engineering development firings to date. Their real-time display feature has been invaluable to the Test

Director for Range Safety. The feature of flexibility in the recorded parameters has been called for on two occasions, and the data elements recorded by the SDR have been used by the Pershing Project Manager and the prime contractor to help solve a weapon system problem. The drawings, parts lists, software listings, etc. will be delivered to the Pershing Project Manager in fiscal year 1983; an initial production contract for at least 20 units will be issued from that office. The production units will be deployed with the Pershing II units on alert status in the same way that the Pershing Ia system is now instrumented.

---

This work was supported by the U.S. Army Missile Command, Pershing Project Manager's Office.

## **REQUIREMENTS STUDY FOR A TRIDENT II ACCURACY EVALUATION SYSTEM**

**L. J. Levy**

*Fundamental approaches and quantified instrumentation requirements to evaluate the accuracy of an advanced SLBM weapon system were developed in the Accuracy Evaluation System study as part of the Improved Accuracy Program. This first attempt to determine the instrumentation requirements systematically prior to SLBM weapon system design provided the design foundation for the Trident II accuracy evaluation system currently being developed at APL.*

### **BACKGROUND**

Some of the IAP (definitions may be found in the glossary at the end of this article) objectives were to

provide a basis of understanding for developing accuracy evaluation tools for Trident II. Much experience with new data processing and instrumentation was gained in evaluating Trident I. Analytical studies provided additional candidates of advanced methodologies and instrumentation that would be desirable for Trident II. The purpose of the Accuracy Evaluation System (ACES) study was to integrate those insights into a comprehensive approach for Trident II accuracy evaluation that would satisfy quantified requirements. The associated analysis tools would then allow systematic trade-offs in test planning and instrumentation design as the weapon system was being designed and developed.

## DISCUSSION

The approach used was first to determine the accuracy evaluation capability that was to be required from an ACES. Next, the accomplishments and problem areas of other IAP tasks were examined to provide insight into what instrumentation and methodologies were needed. As they were examined, appropriate software was developed to relate their characteristics with the ACES performance. The more promising approaches were examined iteratively to arrive at a selected configuration of methodology and instrumentation. The associated error models used in the selected configuration served as the desired instrumentation requirements.

### Objectives and Requirements

The major objective of an ACES for a high-accuracy missile is to confirm (by system testing) the attainment of the weapon system's tactical accuracy goal and to understand quickly the demonstrated weapon system model for problem resolution. The confirmation of a tactical accuracy goal required that test data be projected into tactical accuracy estimates (i.e., CEP) with "small enough" confidence intervals. (Confident problem resolution dictated that the subsystems' contribution to tactical accuracy be estimated with small enough confidence intervals.) The isolation of outliers from the cumulative data base required that each test's contributions to system miss distance be estimated with a small uncertainty.

### Concepts and Methodologies

In order to estimate tactical accuracy, test data had to be extrapolated to untested tactical conditions. Also, it was mandatory, for statistical "leverage," that test data from many different scenarios be combined. This is possible theoretically if the weapon system error model is a known structure (of the particular scenario) propagating fundamental error sources (error sources independent of the scenario, e.g., gyro drift error parameters). Estimates of the fundamental error sources from each test can be accumulated across all the tests to estimate the statistical model parameters (usually means and covariances) of the fundamental error sources. The estimated model can then be projected by means of the tactical scenario structure (a statistical simulation) into target accuracy (CEP). The uncertainties in estimating the error sources for each test (along with the number of tests) determine the uncertainty in estimating the fundamental statistical model parameters. They, in

turn, project into a confidence interval about the estimated CEP.

A Kalman filter usually was assumed to estimate error sources on a per test basis by deducing the causes of the divergence of data between the weapon system and the independent instrumentation. Only a minimum amount of prior knowledge of the weapon system's statistical model was assumed in order to obtain data-driven estimates.

On a cumulative basis, maximum likelihood techniques were assumed to estimate the statistical model parameters from the accumulated test data. Those techniques also provided explicit estimates of the uncertainty in determining the statistical model parameters, enabling confidence intervals to be calculated.

For practical convenience, each phase (e.g., pre-launch) or subsystem of the weapon system can be processed independently and in parallel, to be combined later in an optimal overall estimate of all the error sources, taking into account the interphase instrumentation and weapon system correlations.

### Instrumentation Trade-Offs and Recommendations

In order to conduct trade-offs, software was needed to relate instrumentation and methodology models with ACES performance (confidence intervals etc.). The capability analysis software (Fig. 1) statistically modeled the assumed characteristics of the instrumentation, weapon system, and data-processing software. Many instrumentation options were analyzed in order to derive the recommended configuration, shown in Table 1. Instrumentation above that needed for the IAP was recommended in order to satisfy the ACES requirements. The most novel and useful addition was the TAI, a strapdown inertial system fastened to the tactical guidance case. It would provide high quality "acceleration" data that would complement a dual-frequency SATRACK system with continuous ring antennas. ARA's, also strapdown inertial systems, would be used to transfer the reference velocity through the SSBN flexure environment. Independent gravity VD measurements would allow an independent assessment of the tactical VD model. The "Special NAV Test" provides the main source of tactically representative test statistics for the navigation subsystem. The Advanced Precision Instrumentation Package, a strapdown inertial system in the reentry body, provides the data to evaluate the reentry body deployment as well as the reentry phases.

A performance comparison of the recommended ACES instrumentation and the IAP instrumentation in

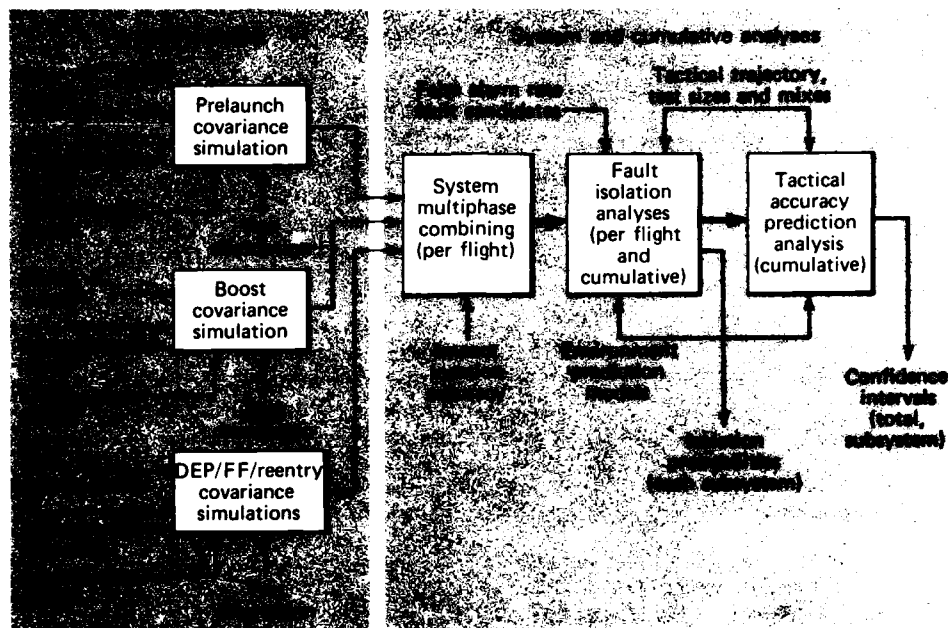


Figure 1 — Software for the ACES capability analysis.

Table 1 — Recommended instrumentation configuration.

	Test Program			
Subsystem	Development (X)	PEM/DASO	OT	Patrol
NAV	Pad surveys	GPS/ARA on TI mast and at ESGN Independent VD verification	VPRS/ARA at ESGN  Independent VD verification	Special NAV Test*  Independent VD measurement
FC		SATRACK heading estimate TAI at guidance		
GUID	Dual-frequency ring antenna SATRACK with TAI Launch area gravity surveys			
FF	GEOSAT survey results into gravity anomaly data base			
DEP, reentry	Advanced PIP on reentry body ( ≈ 1/flight)			

\*Short span of GPS high density data plus position fixes of opportunity.

predicting the Trident II tactical accuracy is shown in Fig. 2. The major advantage of the recommended ACES instrumentation is in its ability to evaluate parts of the weapon system confidently so that proper fault isolation can occur.

The ACES recommended instrumentation and processing methodology has been accepted by the Strategic Systems Projects Office as the basis upon which to budget, plan, and design the Trident II accuracy evaluation.

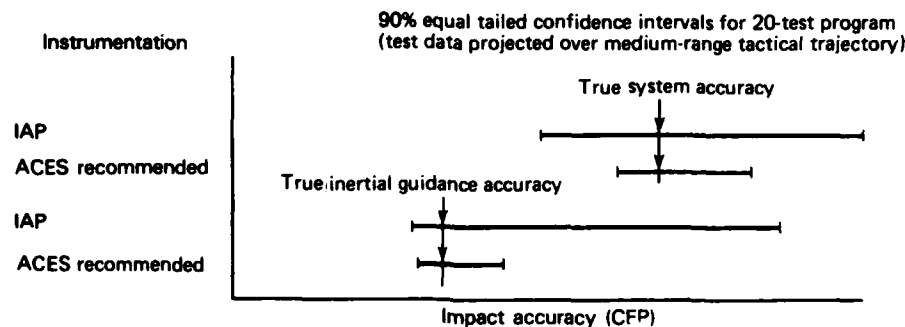


**Figure 2** — Comparison of IAP and ACES instrumentation applied to the Trident II accuracy prediction.

## GLOSSARY

ACES Accuracy Evaluation System  
 ARA attitude reference assembly  
 CEP circular error probable (radius of circle containing 50% of the impact errors)  
 DASO Demonstration and Shakedown Operation  
 DEP deployment  
 ESGN electrostatic gyro navigator  
 FC fire control  
 FF free fall  
 GEOSAT Geodesy Satellite  
 GPS Global Positioning System (satellite navigation system)  
 GUID guidance  
 IAP Improved Accuracy Program  
 IC initial conditions  
 NAV navigation  
 OT Operational Tests

PEM submarine-launched flight tests using production evaluation missile  
 PIP Precision Instrumentation Package  
 POS position  
 SLBM Submarine Launched Ballistic Missile  
 TAI three-axis instrumentation  
 TI test instrumentation (antenna mast for DASO's)  
 VD vertical deflection  
 VPRS Velocity/Position Reference System  
 X development flight tests from flat pad

This work was supported by the Strategic Systems Projects Office.

# EVALUATION OF UNITAS XXII HF COMMUNICATIONS

G. R. Preziotti

*At the direction of the chief of Naval Operations (CNO), APL tested and evaluated high-frequency (HF) surface communications from existing shore stations to the Atlantic and Pacific areas surrounding South America. The primary purpose of the test, conducted from July through December 1981, was to determine the ability of selected shore stations to support HF communications in the UNITAS operating areas and thereby allow the Navy to make decisions on future communications support.*

## BACKGROUND

Virtually no qualitative empirical data have been available for HF transmissions from existing shore stations to the Atlantic and Pacific areas surrounding South America. To determine the communications resources required to support future operations in those areas, CNO requested that APL evaluate HF communications during the UNITAS XXII exercise in 1981. (UNITAS is an annual exercise in which naval forces of the United States and of several South American countries conduct joint maneuvers.) APL prepared a test plan and acted as the evaluation agency. The following ground rules were observed:

1. Evaluate an individual station's performance, not multistation broadcasts. (No attempt was made to copy only the best available frequency.)
2. Use only authorized frequencies, not those presently assigned to other use. (The results indicate the HF propagation conditions present during the test, conditions that change seasonally and yearly.)
3. Present the results as daily averages, without accounting for diurnal variations in HF propagation conditions.

## DISCUSSION

### Test Methodology

To accomplish the test objective, APL adapted the procedure used in the Fleet Ballistic Missile Communications Continuing Evaluation Program (FBM COMM CEP). That procedure has been used since 1974 to determine the performance of the very-low-frequency, low-frequency, and HF broadcasts that carry messages to FBM submarines.

For UNITAS, throughout the test period, APL equipment activated a special HF broadcast (75 baud, with frequency shift keying), which participating Navy ships monitored with APL-supplied test equipment. This broadcast was a repetitive, 15-min test transmission that contained a 5 min test message and a 10 min tuning signal. The test message consisted of a series of 13 bit test sequences (Barker pattern), shown in Fig. 1, repeated to obtain the required length. This test sequence was selected because it enhances the probability that the code sequence will be recognized in the presence of errors and lessens the probability that some other sequence will be falsely recognized. The repetitive sequence allows a reasonable measurement of channel error rate without the need for an exorbitant amount of stored information in the test instrumentation processor.

Two transmitters were used to key the test transmissions from each participating shore station (Fig. 2, which also identifies the 11 operating areas for which results were reported). The transmission frequencies for the test were selected from the authorized frequency pool for each station; predictions from an HF propagation program were used for guidance. The UNITAS operating area was divided into seven zones to reflect the propagation characteristics of different geographic

Legend: 1 = mark	0 = space	Technical test message
Test sequence coding	1111000110101 0000011001010 1111100110101 0000011001010 1111100110101	
Corresponding Teletype character	K N S O H V B R T D X W Y	
	0000111001010 1111100110101 0000011001010 1111100110101 0000011001010	
	T W G U J E I Y K P L F N R	

Figure 1 — Barker sequence test pattern.

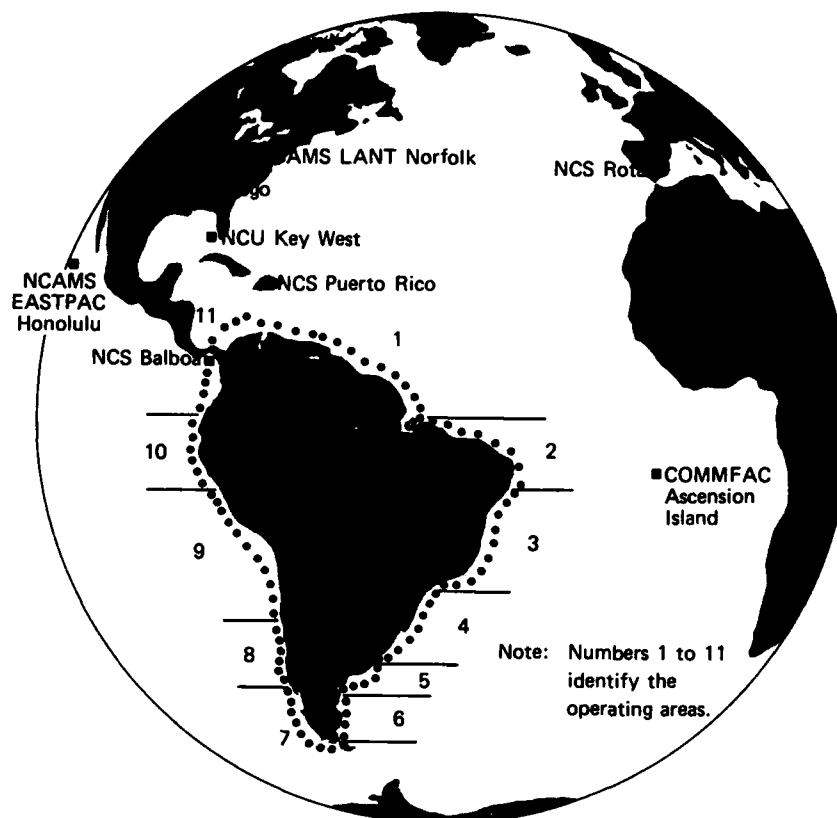


Figure 2 — UNITAS HF test stations and operating areas.

areas of South America, and frequencies were selected for each zone.

Two participating ships from the UNITAS task group monitored the test transmissions with three to seven receivers, depending on the number available. To sample each station equally, the ships switched the receivers every half hour to different transmission frequencies in accordance with a schedule that provided a nonbiased sampling of each station's performance without regard to signal quality.

The test messages automatically activated APL-developed Modular Data Collection and Recording (MDC&R) equipment on board the participating ships. This equipment recorded the time of message reception and the Teletype channel character error rate (CER), and the operator entered the receive frequency. The MDC&R equipment is shown in Fig. 3.

#### Data Analysis

After the test, APL evaluated the performance of all the shore transmitting stations and compared

them to determine their ability to support HF communications in the UNITAS operating area. Several sectors of the UNITAS operating area were examined, and the performance in each was identified.

To determine each station's effectiveness in supporting HF communications, APL calculated the availability and quality of the reception from each station. Availability was defined as:

$$\text{Availability} = \frac{\text{Number of received test messages}}{\text{Number of reception opportunities}}$$

This equation gave a fraction that indicates the percentage of time messages from a station could have been received. Quality was computed as:

$$\text{Quality} = \frac{\text{Number of received test messages with a CER} < 3 \times 10^{-2}}{\text{Number of received test messages}}$$

This equation gives the fraction of received test messages that were of usable quality. The CER value of  $3 \times 10^{-2}$  for the cutoff point of a message of usable quality was obtained from the North Atlantic Surface Communications Evaluation conducted by APL in 1976, which determined that messages with up to 3 er-

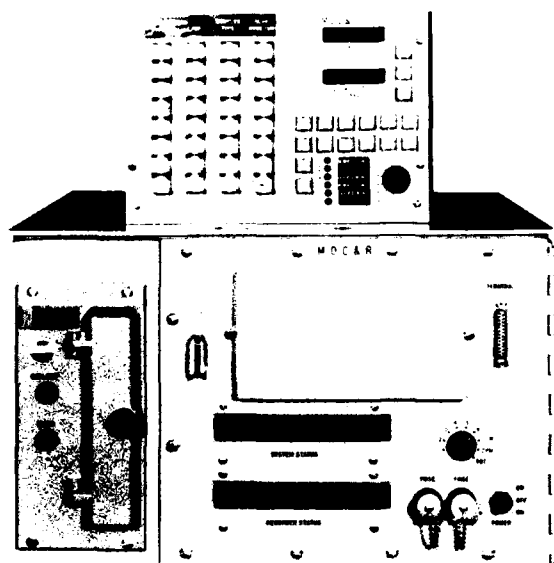


**Figure 3 — Modular Data Collection and Recording equipment developed by APL.**

ror characters in 100 were of usable quality for tactical operations.

The effectiveness of each station was defined as the fraction of time each station would have been received with usable quality by the UNITAS task group:

$$\text{Effectiveness} = \text{availability} \times \text{quality} .$$

## RESULTS

The UNITAS XXII HF communications evaluation shows each transmitting station's effectiveness in all 11 operating areas around South America (Fig. 2). The U.S. Navy used those results to determine the support required from the relevant communications facilities. The Navy was thus able to base decisions on measured communications performance data, where none had been available before. APL has been asked to conduct a similar evaluation of HF communications in the Indian Ocean.

## ACKNOWLEDGMENT

The following persons also contributed to this evaluation: M. D. Sullivan, J. S. Quinn, and R. W. Rowe.

---

This work was supported by the Chief of Naval Operations.

## **NAVAL WARFARE ANALYSIS**

## INTRODUCTION

Analysis of naval warfare was first performed by APL during World War II when the Laboratory addressed the optimum use and characteristics of fire control directors. Since then, APL has continued to be involved in the analysis or assessment of Navy combat systems. The role of analysis is to investigate objectively on a quantitative basis how well current and future Navy systems will perform in battle.

With the increasing threat to the survivability of our Naval forces and the expanding technology in warfare areas like computers, missilery, sensors, and electronic countermeasures, the tools for analysis and the nature of the combat systems analyzed are becoming more complex. Now an analyst can interact with a computer simulation program via a console and find out, for example, how well a Naval force can obtain and maintain track of strategic submarines. Where previously one could track friendly and enemy positions manually by means of calculations, charts, and nomograms, the analyst today has available a computer-based setup (APL's Warfare Analysis Laboratory) with a series of displays. With the computer and display capability, calculations are much faster and the bookkeeping of weapon and position information on all forces is current and accessible. By being able to program more functions and conditional "what if" statements, the analyst can gain more insight into the sensitivities of a problem and thus provide more operational options to the Navy. One recent use of this wargaming facility was the identification of key technical issues regarding hard kill and soft kill mechanisms. (An example of hard kill is the destruction of a target by hitting it with a projectile or guided missile; an example of soft kill is the decoying of an incoming target so that it misses the ship.)

To understand the broad range of analyses performed by the Laboratory, a succinct review of examples of past work is presented. During the late 1940's, APL analyzed warhead designs, prepared specifications for future guided missiles, compared Talos and Terrier for the defense of a cruiser, and defined expected air attacks on Naval forces. During that time, APL laid the groundwork for defining the anti-air-warfare (AAW) problem in terms of the types of threats expected and the methodology to analyze the defense of the Fleet with the introduction of guided missiles.

In the 1950's, studies were conducted on electronic jamming, cruise and ballistic missiles launched from submarines, and an improved methodology for determining warhead detonation and kill probability. Formulas and doctrines on missile-fire coordination were developed. Comparisons were made of the capability of interceptors, missiles, and guns for Fleet defense, and the nuclear Talos missile was compared to the Nike missile.

In the 1960's, the Air Battle Analyzer was developed and applied to Fleet air-defense problems. Natural environmental factors such as sea state, wind velocity, and atmospheric refractivity were investigated with respect to naval applications. APL engaged in studies on NATO air defense, the SOSUS system, point defenses of large ships, small-ship missile systems, and amphibious support weapons.

During the 1970's, APL became heavily involved in effectiveness studies for the Aegis Weapon System and the New Threat Upgrade (NTU) program for Terrier and Tartar ships. APL evaluated the Close-In Weapon System and other self-defense systems. Analyses were made of nuclear weapons, cruise missile survivability and attack on enemy ships, and the requirements for high-capability surface-to-air missile systems.

The trend in the 1980's is pointing toward the Navy's increased coordination of multiwarfare areas in spaceborne, airborne, surface, and subsurface systems. Toward that goal, the Warfare Analysis Laboratory, through a series of "open seminar" evaluations, has provided physical and tactical insight into hard kill/soft kill interactions and outer air battle operations. In the Battle Group AAW Coordination Program, requirements for communication links between ships and aircraft were developed. Operational tactics guidelines for the use of the EA-6B tactical electronic warfare aircraft were prepared and issued to the Fleet. Simulation models were developed that examined the survivability of Harpoon missiles against hostile fire and electronic countermeasures. Analytic support was given in developing combat system requirements for the new DDG-51 class of guided missile destroyers and for NTU guided missile cruisers, and in identifying and evaluating alternate AAW systems for the 1990's mid-life upgrading of the 50-ship FFG-7 class of frigates. A study was performed to define missile loadout options for a new Vertical Launching System in surface combatants. Various midcourse trajectories for a wide area defense missile as a function of target environment were examined to enhance the detection and intercept probability of the target. A computer model, SMITE, was developed as a missile target arrival distribution model to permit the analysis of battle effectiveness as a function of attack coordination; data results appeared in a *Surface Warfare Threat Handbook* prepared by the Laboratory. A Submarine Surveillance Model, an interactive model that simulates an enemy's antisubmarine warfare platforms and their detection mechanisms against a friendly nuclear attack submarine, was developed. Another interactive model was developed in which Red and Blue players perform the functions of opposing theatre commanders in a naval campaign in a multiwarfare environment.

This introduction attempts to summarize the scope of APL's programs in naval warfare analysis. The articles in this section are a few examples of these analyses.

## HARPOON SURVIVABILITY ASSESSMENT PROGRAM M-ON-N MODEL

L. D. Peck

*A large-scale, Monte Carlo, digital simulation of multiple air targets attacking a force with numerous anti-air-warfare defenses has been developed. The model was used to estimate the survival probability of attacks by many Harpoon anti-shiping missiles on a force of several ships defended by guns, surface-to-air missiles, and electronic warfare weapons. The estimates were used to evaluate and make recommendations regarding the configuration and tactics for the current versions of the Harpoon Weapon System and proposed changes thereto.*

### BACKGROUND

The Harpoon Anti-Ship Missile Survivability Assessment Program (ASM SAP) has the threefold objective of (a) evaluating the survivability of the current anti-ship missile against the current and future threat, (b) evaluating options for enhancing the survivability against the current and future threat, and (c) documenting results under the joint approval of the Anti-Ship Missile Project Office (PMA-258) and the Director of Naval Intelligence. One aspect of ASM SAP is to specify multiship scenarios where multiple (M) ASM's (Harpoons) attack a force with numerous (N) defenses. The second aspect is the threat element analysis to estimate the result of the encounter of one Harpoon and one defensive weapon or sensor and of one Harpoon and many defending electronic warfare weapons.<sup>1</sup> The information from the two parts is combined in the M-on-N model to estimate the results when a group of Harpoon missiles attacks a defended force.

The Harpoon SAP M-on-N model is a successor to the Force Mix Shipboard AAW Simulation,<sup>2</sup> which was designed to quantify the effectiveness of U.S. Navy defenses — in particular, multiunit AAW escort forces defending high value ships with area surface-to-air missile (SAM) batteries.

### DISCUSSION

The Harpoon SAP M-on-N model is a large-scale, Monte Carlo, digital simulation of the encounter between multiple air targets and numerous AAW defenses. When used for Harpoon studies, the air targets are missiles and the AAW defenses are in ships that make up a naval force.

The development of the M-on-N model concentrated on three areas: (a) the information flow and decision logic at a single air defense decision center (shipboard combat information center or battle information post), (b) the interaction among the different sensors and weapons at an AAW location (ship), and (c) the interactions among several different locations (ships). One modeling precept was that details treated in the one-on-one or one-on-many threat element analyses need not be included in the M-on-N model; one reason for this precept is to keep the M-on-N model as simple as possible so that it may be understood and may be used with enough Monte Carlo iterations to obtain adequate statistics. The results from the one-on-one and one-on-many analyses are included in the M-on-N data base, which is available at the start of simulation.

The M-on-N model is a discrete event/time model, where state changes occur only at the required simulated times. The model world view is as follows:

1. An air target starts at an initial point and flies to a terminal point.
2. The air target is "detected" by the defending sensors, and air defense system "tracks" are created for the target.
3. The tracks are evaluated for weapon engagement and assigned to a defending weapon.
4. The defending weapon engages the target.
5. The engagement ("kill") results are determined.
6. The air target reaches the terminal point and may kill the defenses.
7. Statistical results are collected.

The dynamic state of the model at any event (or time) within this world view is used to find the value (e.g., the SAM time of flight to intercept) for the interactions between an air target and the defenses. Each state parameter that is determined to be important (by means of the one-on-one and one-on-many threat element analyses) is modeled. The total instantaneous state vector is used to retrieve the interaction value from the model data base, where the complete set of interaction values determined by the threat element analyses is entered.

Only Harpoon missiles have been considered as air targets for the M-on-N model up to the present time. Some of the state parameters considered important for the missile are the flight geometry (e.g., the range from

a defending element or missile altitude) and the missile electromagnetic signal radiation status (a defending ship signal-intercept receiver cannot detect the Harpoon if the signal is not radiated).

The different types of defending elements that are modeled are listed in Table 1. The model and the data base structure allow for several kinds of defending elements of each type (e.g., several kinds of gun batteries or SAM systems) and include the requisite indexing functions, etc., to allow different ships (sites) to have different weapon suites while minimizing the size and amount of information that must be entered into the data base for any single defending element.

**Table 1** — Types of defending elements in the M-on-N model.

Search Sensors
Radar
Electronic support measures receiver
Weapons
Guns
Surface-to-air missiles
Electronic warfare
Chaff
Deceptive countermeasures
Noise jammers

The Monte Carlo (probabilistic) capabilities in the model include selecting from the uniform, Gaussian (or normal), lognormal, and Weibull (including exponential) continuous probability distributions, and from multiple-valued (or single-valued) discrete distributions. The pseudorandom numbers used in the model are managed to ensure sequence duplications from simulation case to case, thereby eliminating the extra variation in results that arises when different sequences are used for different simulation cases. The model elements to which a Monte Carlo method may be applied are given in Table 2.

The statistical data for model simulation runs are collected in the form of tables and distributions for the desired model elements; these data are available for use during model checkout and are saved (on microfiche) for each production case. A subset of these results is used to generate a standardized four page report for each case. The first page lists the geometric inputs for the defending force and the air target initial points, the second is a general summary of the results for the case, the third summarizes the results for the defense, and the fourth summarizes the results for the air target attack.

The model is written in modular form at several levels. A preprocessor is used to transform simulation

**Table 2** — M-on-N model elements to which a Monte Carlo method may be applied.

Air target variables
Launch time
Time of flight
Terminal point
Defending system variables
Weapon kill probability
Time delays
Recognition by sensors
Firm track by sensors
Track evaluation
Weapon assignment
Fire control radar acquisition
Electronic warfare weapon activation
Communication between sites (ships)

input data into the forms required for the model cases. The event store part of the model, including the data base and results collection routines, is written in a structured format in the General Purpose Simulation System language. A postprocessor operates on the subset of the results to prepare the case reports. Both the preprocessor and the postprocessor are written in PL/I programming language.

To date, the M-on-N model has been used to investigate a naval force defending itself against an attack with Harpoon missiles. The variations in the air attack have included all types of Harpoon launch platforms or launchers, changes in the total number of missiles in an attack iteration, the use of different initial points for the attack relative to the defended force (in terms of both range and relative bearing), and changes in the time delay between launches of successive air targets. The variations in the defending naval force have included changes in defending ship class (selected from 12 classes in the data base), defending force size (varied from a single ship to a group of six ships), defending force ship dispositions, and most of the defending system time delays listed in Table 2.

The M-on-N model is presently run on the IBM 3033 computer. The model uses an average of about 850 kilobytes of machine memory and requires about 200 seconds of machine time for one case with a total (summed over all iterations) of 200 air targets attacking a force of six ships, defended by a total of 14 gun batteries, 13 SAM batteries, and electronic warfare weapons.

## ACKNOWLEDGMENT

The PL/I programs for the preprocessors and postprocessors were written by B. Bundsen. The Force Mix model and the initial M-on-N modeling were written by E. A. Davis.

## REFERENCES

<sup>1</sup>K. T. Plesser and L. W. Wald, "A Digital Simulation for Missile System Survivability Analysis in a Multiple ECM Environment," *APL Developments in Science and Technology, Fiscal Year 1980*, JHU/APL DST-8.

<sup>2</sup>E. A. Davis and B. Bundsen, *The Force Mix Shipboard AAW Simulation*, JHU/APL CLA-1498 (revision) (Jan 1977).

This work was supported by NAVAIRSYSCOM, PMA-258.

## SMITE: A SIMPLE MODEL FOR INVESTIGATING TACTICAL ENVIRONMENTS

L. B. Carpenter

*A simple Monte Carlo simulation has been developed to model a multiraid attack on a multiship formation. The model provides a tool for analyzing the target arrival rates and crossing distances presented to individual ships in the formation.*

### BACKGROUND

In order to analyze the effectiveness of surface-to-air missile systems and command, control, and communications systems in a realistic multiattack multiship scenario, we need a way to determine the arrival-rate and crossing-distance distributions presented to individual ships. For any situation of realistic complexity, it is usually impossible to derive a closed-form mathematical solution to those distributions. One must resort to numerical simulation. The SMITE model was developed for that purpose.

### DESCRIPTION

Functionally, SMITE is composed of two essentially independent parts. The first, using the input descriptions of the raids and ships, generates a history table of all the antiship missiles (ASM's) fired (for all Monte Carlo replications). The second, in an interactive mode, allows the user to choose any ship, specify a radius of interest about it, and get a statistical summary of

the crossing distances and peak arrival rates seen by that ship (for all missiles entering the circle of interest). Subsequently, the user may request the picture seen by other ships and other radii of interest.

### Raids

In the model, a raid is a mechanism for generating ASM's. It does not necessarily correspond to physical platforms in the real world. To simplify the inputs, a raid is usually used to simulate a group of platforms launching several ASM's. The raid parameters are as follows:

1. Initial position (range and bearing, at begin-launch time,)
2. Course and speed,
3. A "box size" within which the launch positions for the ASM's are randomly dispersed,
4. The (maximum) number of ASM's the raid can fire,
5. A target list from which the raid chooses its targets,
6. A begin-launch time (which may be perturbed by a Gaussian random variable),
7. A "launch sequence" defining the time spacing of ASM launches, and
8. An average speed for the ASM's (which may be perturbed by a Rayleigh random variable).

## Ships

The ships are represented only by their positions (in range and bearing). Their relative importance is implied in the targeting lists for the enemy. They are stationary, and they are not damaged by the enemy attack.

There is no explicit simulation of defensive actions by the ships, such as SAM firings, electronic countermeasures, etc. However, input attrition factors may be applied to the ASM's to provide rough approximations of the effects of defensive actions.

## Outputs

The output from part 1 of the model is a set of tables depicting the characteristics and history of all the ASM's that were generated for all Monte Carlo replications. The tables may be saved for subsequent analysis or used immediately as the input to part 2. Table 1 is a sample of an ASM history table.

Part 2 provides several tabular and graphical outputs, samples of which are shown in Figs. 1 and 2. The most important output from part 2 is the distribution of peak arrivals as a function of the length of specified time windows. For each simulated attack (Monte Carlo iteration), the peak arrival for a given time window is the maximum number of targets arriving within any time interval of that length.

The counts (maximum arrivals versus window size) are stored for each iteration; at the end of the run, the data are tabulated to show the minimum, mean, and maximum observed for the various window sizes (see Fig. 2).

Figure 1 shows the tracks of all the ASM's that entered a circle of 20 nmi radius around ship 3. (In this example, there were nine ships and 11 raids; the average number of ASM's penetrating the circle was 120.) The crossing distances of the ASM's that penetrated the circle are shown in Table 2. Their peak arrival rates at the circle are plotted in Fig. 2.

Table 1 - Sample ASM history table.

Time of Launch (min)	Launch Point (°N)		Target Ship	Av. Speed (nmi/min)	Raid No.	Distance Flown (nmi)	Impact Time (min)
	Range	Bearing					
15.17	146	9	1	20.04	1	146	22.46
15.07	147	9	2	19.59	1	129	21.65
15.97	140	7	3	20.13	1	138	22.81
15.20	146	9	1	20.22	1	146	22.42
14.94	148	9	1	19.56	1	148	22.50
15.90	141	7	3	19.43	1	138	23.01
15.36	145	8	1	19.87	1	145	22.64
15.27	145	8	1	19.72	1	145	22.64
15.28	145	8	5	19.76	1	159	23.31
15.62	143	8	1	19.37	1	143	22.99
13.98	170	230	1	20.16	2	170	22.41
14.06	170	230	1	20.26	2	170	22.46
14.56	171	232	2	19.58	2	184	23.98
14.65	171	232	1	20.24	2	171	23.08
15.15	171	234	1	20.31	2	171	23.59
15.23	172	234	1	20.24	2	172	23.71
15.73	172	236	1	19.89	2	172	24.40
15.81	173	236	7	19.58	2	166	24.29
16.31	174	238	1	20.13	2	174	24.94
16.40	174	238	1	19.54	2	174	25.29
17.65	50	310	5	8.93	3	63	24.76
17.67	50	310	1	8.86	3	50	23.32
17.84	50	310	8	9.04	3	43	22.54
17.85	50	310	1	8.68	3	50	23.61
18.02	50	310	1	9.00	3	50	23.57
18.04	50	310	1	8.79	3	50	23.73
18.20	50	310	1	9.02	3	50	23.75
18.22	50	310	1	8.78	3	50	23.92
18.39	50	310	1	9.09	3	50	23.89
18.40	50	310	6	9.02	3	51	24.11

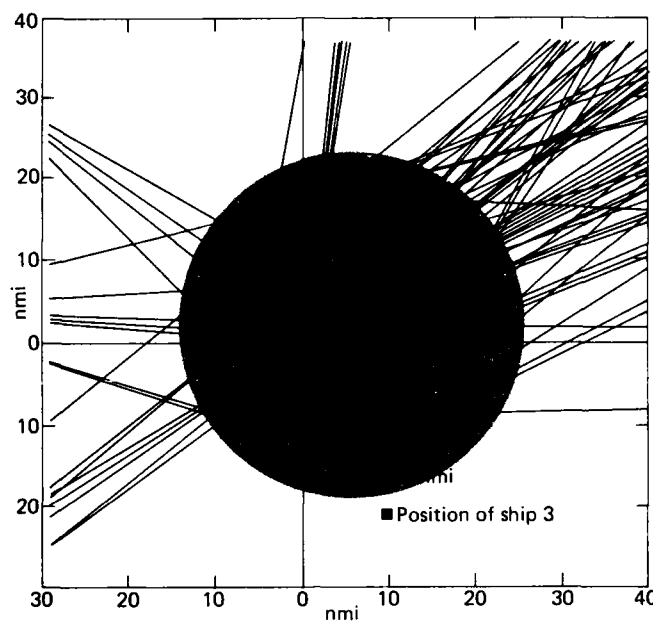


Figure 1 - Plot of ASM's seen by an individual ship.

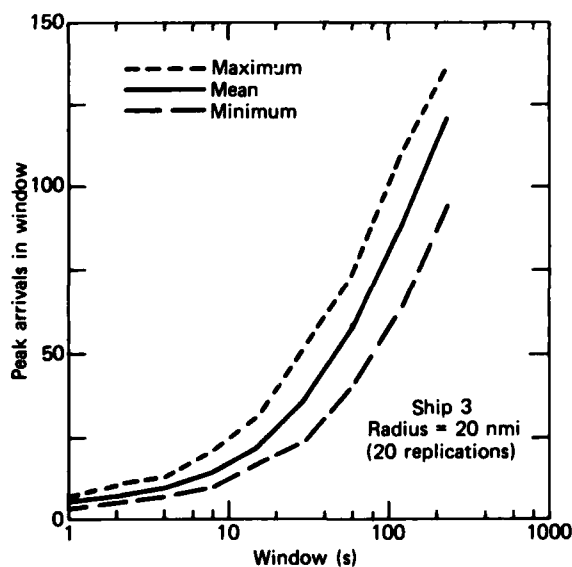


Figure 2 - Summary of peak arrival data.

### Applications

The model has been used extensively to generate battle overviews for the *Surface Warfare Threat Handbook*. It could also be used for approximate answers to the defensive coverage of various ship formations or the

Table 2 - Crossing distance statistics.

Distance	Mean	Std. Dev.	Min.	Max.
0.00 to 1.99	38.70	3.20	34	44
2.00 to 3.99	40.40	3.07	36	47
4.00 to 5.99	26.80	1.91	24	31
6.00 to 7.99	6.95	2.09	4	11
8.00 to 9.99	6.70	2.45	1	12
10.00 to 11.99	4.55	1.57	2	8
12.00 to 13.99	4.30	1.56	1	7
14.00 to 15.99	0.10	1.29	6	10
16.00 to 17.99	1.50	0.95	0	3
18.00 to 19.99	0.00	0.00	0	0

positioning of particular ship classes. It will be a useful tool for raid planning and coordination studies.

### ACKNOWLEDGMENTS

Significant contributions to the development of SMITE were made by W. P. Richardson, B. Bundsen, and L. D. Peck. Improvements and modifications to the original model were made by J. R. Moore and J. M. Giblin.

This work was supported by NAVSEASYS COM, PMS-400.

# A SOFTWARE ARCHITECTURE FOR A MULTIPLE-PLAYER WAR GAME

R. R. Guenther, N. K. Brown, and J. F. Stader

*A simulation model for the analysis of theater-level naval campaigns has been developed by APL. In the model, player support architecture manages the resources of a minicomputer system to form the interface between the model (which runs on APL's IBM-3033) and the teams of players at the Pentagon. This design for software architecture improves the facilities available to the player to support his command function and also enables fast and orderly additions to player functions in response to developments in the simulation itself.*

## BACKGROUND

The Naval Nuclear Warfare Simulation (NNWS) was developed by the APL Fleet Systems Department to provide the Chief of Naval Operations with a vehicle to study and analyze theater-level naval campaigns. The simulation is interactive: the opposing sides provide responses similar to those that would be generated at a theater command center. The players interact with the simulation through a minicomputer system located at the Pentagon and tied to the IBM-3033 computer system at APL.

A basic antisubmarine warfare (ASW) model was built and tested in 1980.<sup>1</sup> In the fall of 1980, APL initiated an effort to upgrade the satellite computer system at the Pentagon to expand the scope of player actions to include more than a single player role for each side and to support, in addition to ASW modeling, the full complement of naval operations associated with a campaign. In April 1982, the new interactive player system was incorporated into the NNWS.

## DISCUSSION

### Player Roles

The war game consists of two opposing sides, each having a set of players that directs its forces. Players may assume primary, secondary, or supporting player roles, which are defined by the scope of a player's command responsibility. Primary players perform functions similar to those of theater commanders. Secondary players perform functions similar to those of on-scene commanders, such as controlling force dispositions, planning air operations, or conducting ASW. Supporting players assume a theaterwide role, such as directing strategic submarine operations or allied naval

forces. An umpire may be present to manage the war game and possibly to provide external intelligence.

### Player Stations

A Digital Equipment Corp. (DEC) PDP-11/34 minicomputer located at the Pentagon serves as the satellite computer system that enables the players to interact with the simulation program residing on APL's IBM-3033. An alternate player facility using a PDP-11/60 is located at APL. Each satellite facility can support five player stations.

A player station consists of two display terminals (Fig. 1). A graphics terminal provides the geographic positions of both friendly forces and enemy contacts. An alphanumeric terminal provides textual information in the form of reports from friendly forces and summaries of data such as contacts and unit status. The players interact with the simulation through their alphanumeric terminals by issuing orders to their forces, directing such force actions as mission assignments, contact investigations, and defense condition changes. Several tactical decision aids have been implemented for both the graphics and the alphanumeric terminals.

The continued development of NNWS will create various new satellite computer system and player configurations. Some that are planned include:

1. One satellite computer, three player stations: Red and Blue primary players and an umpire.
2. One satellite computer, five player stations: Red and Blue primary players, two Blue secondary or supporting players, and an umpire.
3. Two satellite computers, up to ten player stations.

### Player System Software

A software architecture was designed to accommodate each player function with a single computer program or task. The architecture is realized within the context of the RSX-11M, the real-time operating system that DEC supports for PDP-11 computers. Real-time systems are often used for process control applications such as manufacturing or laboratory experiments. Viewing the player system as a real-time system was a unique approach that has one primary advantage: each player function can be implemented with a simple pro-



Figure 1 — An NNWS player station.

gram that requires only a few of the satellite computer's resources. The major obstacle in the design of real-time systems is overcoming the contention for the same resources by multiple tasks. Contention problems are minimized here because much of the time spent by the player is idle time for the computer. If contention for memory or a particular file arises, the delay in resolving that contention generally is not noticeable to the players.

The architecture for the NNWS player system is a three-level hierarchy (Fig. 2). The two higher levels consist of executive tasks that coordinate interaction among the third-level functions, the players, and the simulation model. In structural terms, the task pool at the third level consists of individual programs that perform, as nearly as possible, single functions within the system. Third-level tasks can also be categorized by the type of function they perform.

Data base maintenance tasks are generally initiated from the report-processing executive. Historical data such as contact history files and unit PIM's (position and intended movement) are maintained.

Picture creation tasks build graphics displays and save them in files on disk for recall on request. They are initiated in several ways. The pictures for the unit status and contact displays are initiated by the player's graphics executive after receipt of a new set of reports from the simulation model. If the player selects a different background map, new unit and contact pictures can also be generated. Background maps are initiated from the alphanumeric executive or are run in an

off-line mode when the other player system tasks are inactive. Other picture-building tasks such as ocean-depth contours, pack-ice boundaries, acoustic regions, air-fields, and ports are executed off-line with optional access through the graphics executive.

Picture display tasks load picture files into the player's graphics processor for display on the MEGATEK terminal. Those tasks operate only on displays that have already been generated by a picture creation task. Structuring the system so that the building and the displaying of pictures are separate resulted in a very flexible and responsive player graphics capability. The number of different graphics displays available at a player station was arbitrarily set to 45, three for each of the 15 special function keys on a MEGATEK keyboard.

The alphanumeric display tasks generate summaries from the player's data base and display them on the VT-100 terminal. Each alphanumeric task also creates a display file for an optional printed copy.

Order-generation tasks build the player's orders file for subsequent transmission to the simulation model. They are initiated by the alphanumeric executive in response to the player selecting the appropriate item from an orders menu. Some orders tasks check the orders files of allied players to prevent the generation of conflicting orders. All orders tasks have validity checks and help functions that guide the player through the orders composition process.

Tactical decision aids, which can be either graphics or alphanumeric displays, assist the player in mak-

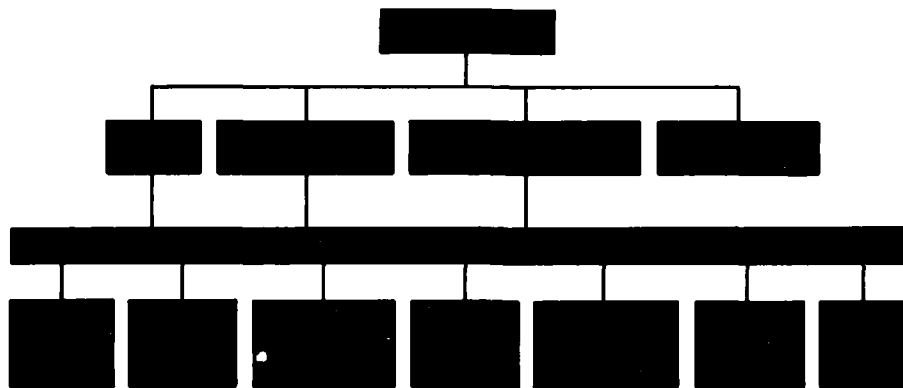


Figure 2 — Software architecture for the NNWS player system.

ing his decisions. Some examples are the display of a unit's PIM or the calculation of the probability of detection of a given sonobuoy pattern. Utility tasks are generally reserved for the umpire, enabling him to configure the display system, perform backup functions, and initiate or reestablish playing sessions.

#### Development Process

Because of the evolutionary nature of military systems and missions, NNWS is expected to require modification for an extended period of time, thus preserving its utility with respect to the world it simulates. Therefore, APL has established an NNWS system architectural philosophy and development process to support the incorporation of recurrent modifications to the simulation model and to the player facility in an orderly, efficient, and well-documented manner.

The development process is inherently related to the modularity of the system architecture and encompasses architectural specification, prototype building and evaluation, and implementation. Configuration control throughout development is maintained by means of progressive refinements in documentation associated with each phase.

The basic development document is the System Change Proposal (SCP). It is both a configuration control device and the source document for all permanent system documentation. When approved, it becomes the architectural specification for a structural module of

the system. Hence, each structural/functional module affected by the modification of a general NNWS system capability will require an SCP. The SCP governs development activities and is kept current so that it describes the operational system element accurately. Thus, the documentation generated by the development process is itself modular and is characterized by the accuracy and completeness required to support continued response to NNWS requirements. Adoption of this software architecture has provided a framework to the NNWS development process that enables APL to make incremental improvements while maintaining reliability and configuration control of an expanding complex system.

#### ACKNOWLEDGMENT

The authors wish to acknowledge software engineers H. E. Conn, S. K. Grasberger, and R. M. Conner of HADRON, Inc., who implemented the software architecture.

#### REFERENCE

- <sup>1</sup> L. R. Gieszl and J. W. Marrow, "Development of an Interactive Warfare Simulator," *Johns Hopkins APL Tech. Dig.* 1, 52-54 (1980).

This work was supported by the Office of the Chief of Naval Operations, OP-654.

## COMPUTER TECHNOLOGY

## INTRODUCTION

Computer technology at the Applied Physics Laboratory is an integral part of all technical, systems, and administrative functions. The computer so pervades scientific life at APL that the scope and magnitude of its contributions to space science, medicine, energy research, naval fleet defense, missile guidance, and other problems of national importance are often lost in the daily intensiveness of computer implementation activities. Yet the importance of the computer at APL with its myriad technologies and applications cannot be over-emphasized.

Extensive computational facilities maintained by the Laboratory for use by its scientists and engineers include: a major digital computer; an integrated computer-aided-design/computer-aided-manufacturing (CAD/CAM) system; analog/hybrid computer laboratories; a computer-based image processing system; rapid real-time data reduction systems; and hundreds of special-purpose computers, word processors, and computer-controlled data acquisition systems.

The central digital computer facility consists of an IBM 3033 multiprocessor with high-speed, large-scale dual data processors. The 3033 uses a virtual memory operating system that accesses a 16 million byte main memory and up to 115 billion bytes in auxiliary direct access storage (disk and mass). The central computer serves a wide variety of tasks, including large-scale simulations, complex analyses, and data processing and reduction. The 3033 and its associated computers in the linked APL computer network provide extensive facilities for interactive real-time processing, image processing, large data base transfers, advanced graphic processing, and resource sharing.

The Computervision CAD/CAM system has provided the Laboratory with a modern design, drafting, and manufacturing capability. It is a flexible system providing three-dimensional design capability for mechanical, electrical, and electronic systems. Output from the system, in addition to the normal hard copies, includes photoplotted master masks and numerically controlled machine tool tapes. Resident system software, along with data linking to larger computers, can provide design analyses including finite element modeling, logic simulation, and design rule checking.

The Laboratory also supports two analog/hybrid computer laboratories: the Interactive Simulation Laboratory with EAI 680 analog computers, and the Guidance System Evaluation Laboratory with the EAI Pacer 600 system. Analog and hybrid computations are essential to the solution of complex problems requiring the simultaneous solution of a large number of differential equations. The hybrid laboratories provide simulations for large physical systems and are particularly useful in the missile and missile guidance field.

Because computers and computer applications at APL are so interwoven with all Laboratory activities, it is impossible in a limited section to provide articles addressing all the yearly accomplishments in this field. The selected articles represent the generic type of activities that one may find in all parts of the Laboratory. They range from special-purpose processors, emulators, hardware, and data information facilities through standard modeling and simulation activities to specialized graphical outputs and even the solution of problems at the graphics level. This trend toward specialized computers, novel methodologies, and emphasis on graphical display and interaction is expected to continue.

## ARRAY PROCESSOR APPLICATION TO EMULATION OF THE TERRIER CWAT RADAR

T. R. Hocker

*A signal-processing emulator whose key element is an array processor has been developed to support the upgrading of the Terrier continuous-wave acquisition and track (CWAT) fire control radar. The emulator allows various digital signal-processing techniques to be evaluated for use in the CWAT system upgrade.*

### BACKGROUND

To reduce the vulnerability of the Terrier fire control radar to electronic countermeasures (ECM), the Navy undertook the development of a new, high-speed, digital signal processor for the CWAT radar. Because that development involved advanced technology and signal-processing algorithms for which experience was limited, there was a need for a signal-processing emulator to test proposed techniques before they were incorporated into the actual hardware. A CWAT signal-processing emulator whose key element is an array processor was developed at APL to meet that need (Fig. 1).

### DISCUSSION

#### Method of Emulation

Since the CWAT signal processor was the major unit to be modified, and digital signal-processing techniques were limited, a hybrid emulator concept was chosen for development. In addition to an array processor, the signal-processing emulator uses the AN/SPG-55B radar (Fig. 2) at the land-based test site at APL. The radar's CW transmitter, receiver, antenna, and synchros provide real target characteristics and ECM and also permit saving of time and money. For real-time operation with an actual system, the emulator must process large amounts of data and pass that information back to the radar many times a second. An array processor, which can process data a thousand times faster than a general-purpose computer, is the only programmable processor capable of performing that task.

Array processors are special-purpose devices that combine parallel and serial processing. This, together with a floating-point data format and preloaded

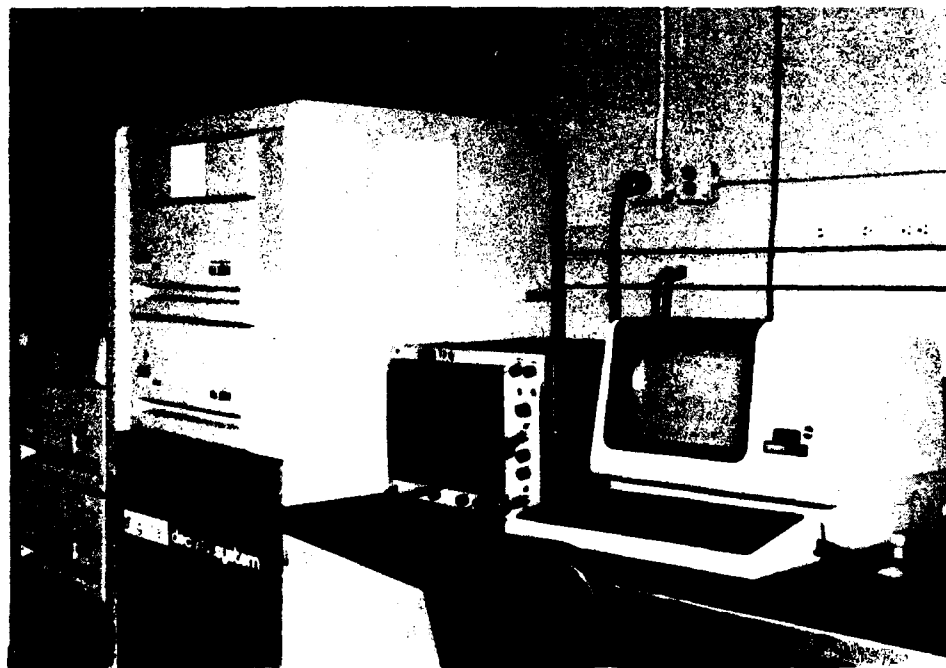


Figure 1 — The CWAT signal-processing emulator.



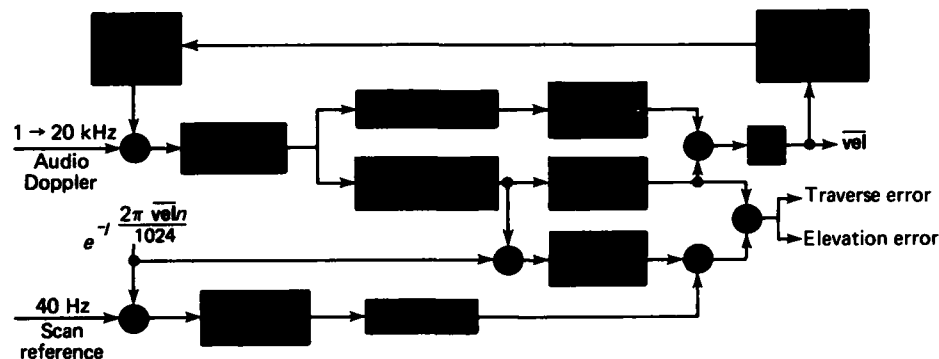


Figure 4 — The velocity- and angle-tracking system.

### Hardware Implementation

During construction of the emulator, it was necessary to fabricate certain hardware systems. An analog-to-digital (A/D) converter that digitizes not only radar Doppler data but also reference signals was needed for data input. The A/D conversion equipment is housed in two units, one located with the array processor and the other with the radar. A D/A converter was needed to feed the array processor output signals back to the radar. Monitoring, an essential function, was added as well. APL thus designed and built all the hardware needed to interface the array processor with the radar and to monitor the system during operation.

### APPLICATION

Preliminary results obtained for closed-loop velocity and angle tracking verify the fundamental design of the CWAT radar processor. However, the emulation uncovered three unexpected difficulties in the proposed design. First, the coefficients of the variable low-pass finite impulse response filter had to be modified to provide the necessary 90 dB out-of-band signal rejection. Second, the root-sum-square approximation algorithm originally proposed had to be modified by

adding a look-up table to provide the required 16 bit accuracy in the envelope detector. Finally, the period averaging interval had to be increased to allow for a full 25 ms period of the scanning modulation. These problems were detected and alternative methods were developed and evaluated quickly and conveniently by reprogramming the appropriate software modules for the array processor before the radar was built.

The continuing emulation process includes the evaluation of range tracking, target detection, and ECM susceptibility.

In summary, the primary value of the emulator system is that it allows APL to implement, test, and compare alternative systems at great savings compared to implementation in a hardware system.

### ACKNOWLEDGMENTS

W. E. Snelling and A. S. Hughes contributed significantly to this effort.

This work was supported by NAVSEASYSOM, SEA-62CM.

## A NEW HYDRODYNAMIC COMPUTATIONAL FACILITY

T. D. Taylor

*A new, limited use computational facility has been assembled that permits very complex hydrodynamic flows to be simulated economically. It consists of a Digital Equipment Corp. VAX Model 11/780 host computer and a large Floating Point Systems Model 164 array processor that provides 1.5 million 64-bit words of memory and can operate at about twice the speed of the Control Data Corp. Model 7600 computer. The system has 60 million dedicated words of disk memory. The array processor and disks cost about \$550,000.*

### BACKGROUND

Computer simulations of hydrodynamic flows, such as those in ocean waves, estuaries, and ship wakes as well as around submarines, require the solution of unsteady nonlinear flow equations in two and three dimensions. Simulations of this kind can use millions of words of computer memory and some problems may require days of computation, even using today's fastest computers; therefore, alternative computing approaches are needed for practical applications.

### DISCUSSION

#### The Issues

Improvements in computers and numerical methods in the last decade have made the large-scale simulation of hydrodynamic flows practical for Navy applications. Such advances have an effect on ship and submarine design. They also extend the understanding of oceanographic phenomena such as ocean surface wave interactions as they influence remote sensing techniques. In order to bring this technology to bear on practical problems, it is necessary to minimize the cost of simulations and maintain reasonable computer turn-around time. Persons experienced with large computers are well aware that those ends are difficult to attain if a large memory and lengthy calculations are required on a multiuser computer because of interference with other users. One can of course "buy" priority and avoid interference, but this can be an expensive option when very large problems are being addressed.

Until recently, no alternative to the use of a multipurpose computer center was available for large-scale simulations. The introduction of low-cost, high-speed array processors, such as the Floating Point Systems

(FPS) Model 120B and the CSP Inc. Model MAP 6400, suggested that large-scale calculations might be performed at a low cost. Table 1 gives comparative computer statistics to show the relative hardware costs. Studies by the author over a two-year period proved that such processors could yield an economical alternative to the large mainframe for solution of the partial differential equations of fluid flow. However, a problem was posed by the limited memory and short word length of the initial processors. This problem was pointed out by the author to personnel at Floating Point Systems, who decided to expand their Model 120B array processor to form the FPS 164. The latter has up to 7 million words of memory, uses 64-bit arithmetic, and can solve large-scale problems at low cost. The cost without disks is around \$400,000. Benchmarks show that its speed can reach one-third to one-half that of a CRAY for large simulations.

#### The Computational Facility

After careful examination of the issues and needs, it was decided that the FPS 164 array processor would be a practical computer for performing large-scale hydrodynamic simulations. The add-on array processor was purchased and attached to an existing VAX Model 11/780. Sixty million words of disk storage were added to the array processor to augment the 1.5 million words of core memory. A block diagram of the system is shown in Fig. 1; Fig. 2 is a photograph of the equipment.

Table 1 — Comparison of computer performance.

	MIPS	MFLOPS	MTTF	Approximate Relative Hardware Cost
FPS	36†	12 (6)**	125 days	0.03
Control Data 7600	40	40 (10)	days	1.00
CRAY*	80	80 (25)	7 h	0.60††

MIPS: million instructions per second.

MFLOPS: million floating-point operations per second.

MTTF: mean time to failure.

\*Taken from LASAL CRAY-1 evaluation.

†FPS instruction contains six independent operations: floating-point add, floating-point multiply, indexing, branching, register transfer, and memory transfer. The FPS-AP modular units may be configured into a larger system that can increase the throughput.

\*\* ( ) Typical and/or usually obtained speeds.

†† Without a system control computer.

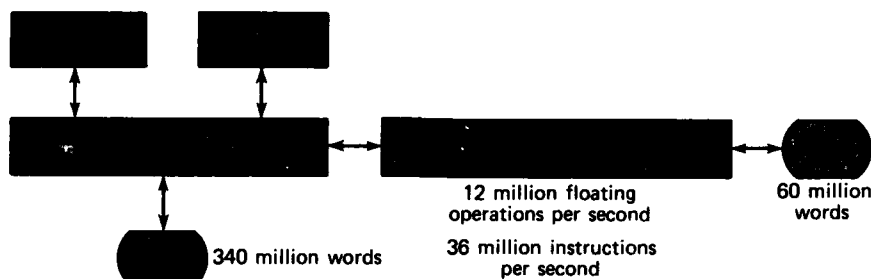


Figure 1 — Block diagram of the hydrodynamic computational facility.

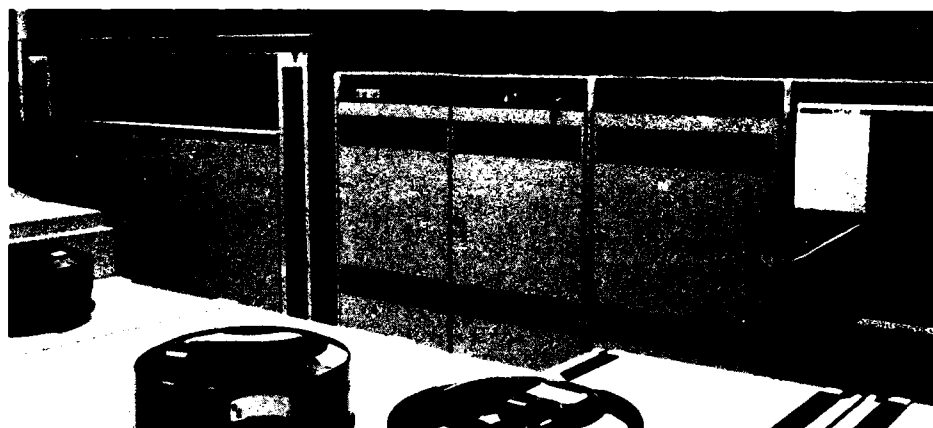


Figure 2 — The computational facility.

The use of the computer is straightforward in that a program is written in Fortran and compiled on the VAX, using Floating Point Systems preprogrammed subroutines when possible to increase the speed. The compiled program is then transferred to the FPS 164 array processor along with the input data. Thereafter, the program can be executed for as long as desired without affecting VAX operation. Upon completion of the program, the results are transferred to the VAX for listing.

The array processor is powerful because it makes use of parallel operations designed into the hardware by the manufacturer. Even without concern for optimization, the user gains about a factor of 10 in speed over the VAX 11/780. With some care, the speed can be increased by a factor of about 20 and, if one is extremely careful, by a factor of 30 to 40. At that level, one approaches the practical program execution speeds of the supercomputers.

The real advantage of the array processor for large simulations is that the capital cost is modest. It is important to note, however, that the array processor system described here is not a replacement for a supercomputer. Although it is ideal for the special purposes

of a few users with high computer central processing unit demands, it does not have the high-speed input/output or multiuser capabilities of a supercomputer. As a result, such a facility should be viewed as being complementary to a major computer installation.

### System Potential

The current array processor is constructed with 16,000 transistor-transistor logic chip technology and has a cycle time of about 200 ns for 64-bit floating-point operations. The 16,000 chips can be replaced by 64,000 chips, thereby increasing the memory in the FPS 164 to 7.2 million words. In addition, its computational speed could be increased by a factor of about 5 by introducing emitter-coupled logic chip technology. Processing speeds could be increased by a factor of 3 to 4 by adding small array processors to the FPS 164.

### REFERENCE

- <sup>1</sup>T. D. Taylor and G. Widhopf, "A Trend Towards Inexpensive Computer Simulations," *Aeronaut. Astronaut.*, 31-34 (Apr 1979).

This work was supported by the Strategic Systems Projects Office, SP-202.

## A HOSPITAL INFORMATION DISTRIBUTION SYSTEM

S. P. Yanek, J. A. Frantz, G. P. Gafke,  
D. M. Sunday, and J. C. Woodyard

*APL has developed a microcomputer-based Hospital Information Distribution System for Navy hospitals. The microcomputer controls data flow between two independent computer systems designed for two different hospital functions, i.e., patient administration and patient care. The system initiates and manages all transmission activities within a three-node network by performing line control, code translation, error detection, message formatting, management reporting, and terminal emulation functions.*

### BACKGROUND

The U.S. Navy directed APL to develop a prototype Hospital Information Distribution System (HIDS) to support the prerequisite function for patient care (i.e., registering for care) in large and medium sized Navy hospitals. The Navy uses several computer-based systems from several vendors to administer patient care in ancillary areas of the hospitals. Each patient care system requires a unique combination of identification and demographic data elements to establish a patient file, which represents the first step for access to patient care services in each system.

Although the ancillary computer systems require isomorphic or common data elements to establish patient files, no method existed by which an ancillary system could automatically transfer common data to another ancillary system. This meant that the sharing of common data required duplicative manual data entry.

Because as many as 500,000 persons are eligible to receive care at larger Navy medical treatment facilities, the amount of storage available for identification and demographic data for each ancillary system varied and was also a cause for concern. In addition, each ancillary system required the data to be in a unique format and sequence. The level of administrative staffing at the medical treatment facilities was inadequate to accommodate such database synchronization and data entry problems.

The Bethesda Naval Hospital, which was selected as the site of the prototype system, had been using a remote, time-shared service for its pharmacy and a local system for its laboratory. The laboratory system was also used to register inpatients and outpatients eligible for care. As part of the registration process, the

laboratory system produced embossed, encoded plastic cards that verified patient registration.

In developing the prototype system for data entry and database synchronization, APL was faced with a major constraint; that is, there was to be no alteration in the hardware or software configuration of the hospital's existing patient care systems. APL also had to resolve other issues before going ahead with design and development. Some of those issues were associated with Navy Medical Command directives for collecting, maintaining, and reporting data on patient registration, admission, disposition, and transfer (R/ADT). To comply with the Navy directives, it was necessary to collect 400 to 500 characters of data per patient. The laboratory system had been collecting approximately 100 characters of identification and demographic data, and its daily workload was about 150 patient admissions and registrations. The projected daily workloads were estimated to be approximately 300 new registrations or record edits and 50 inpatient admissions.

Both the laboratory and the pharmacy systems were to be replaced by systems authorized by the Tri-Service Medication Information Systems (TRIMIS) Program Office at the Department of Defense (DoD), the pharmacy system in December 1982 and the laboratory system during calendar year 1984. However, the Navy decided to include the laboratory system as an ancillary computer system to demonstrate the concept of a common registration system. The pharmacy system was excluded because of impending replacement. To establish database congruity, the Navy also decided that one system, dedicated to administrative functions, would be added and only that system would be able to add, edit, or delete data, in compliance with Navy Medical Command directives.

### DISCUSSION

A terminal emulation mode of operation was selected to transfer data to the ancillary system and to obtain information from the master system. However, terminal emulation software would not be developed or installed in the master R/ADT system or in the ancillary laboratory system. Thus, the architecture evolved toward a three-node network, i.e., a master R/ADT system, an ancillary system in terms of R/ADT data management, and a system to process communications between the two special-purpose systems.

### The Master R/ADT System

The Patient Administration (PAD) system developed under the TRIMIS Program was selected as the master R/ADT system. Two major functional modules of the PAD system are registration and inpatient admission. The registration function allows the hospital to collect and maintain identification and demographic data on individuals eligible for care at DoD medical treatment facilities. Under the inpatient admission function, the hospital collects and maintains data concerning an inpatient's admission, disposition, and transfer status during periods of hospitalization. The PAD system has features that ensure integrity of the database and accuracy of the data collected.

The original version of the PAD applications software had to be modified to accommodate differences in the plastic card embossing and encoding equipment, to comply with the data collection and reporting requirements of the Navy Medical Command, and to conform to the operational procedures of the Bethesda Naval Hospital.

### The Ancillary System

The clinical laboratory system at the Bethesda Naval Hospital is derived from the Pathlab system developed by the Medlab Co., a division of Control Data Corp. The version of Pathlab in operation at Bethesda is known as LABIS (for Laboratory Information System). The system was relieved of the registration and card embossing functions, which are now controlled by the PAD system.

### The Hospital Information Distribution System

The actual transfer of patient identification and demographic data between the PAD system and LABIS is totally controlled by HIDS, a terminal emulation and control software system designed and developed by APL. The interrelationship of the systems is illustrated in Fig. 1.

HIDS performs two major processing activities, the addition of missing data elements to incomplete LABIS registration records and the automatic transfer of complete records or relevant data from PAD to LABIS. Both functions start automatically and need no operator intervention, although the capability for operator control exists.

Appropriate data transferred to LABIS are the result of a new registration or admission or a change in an existing registration or admission record on the PAD system. However there are instances when a patient requires laboratory service but is not registered on

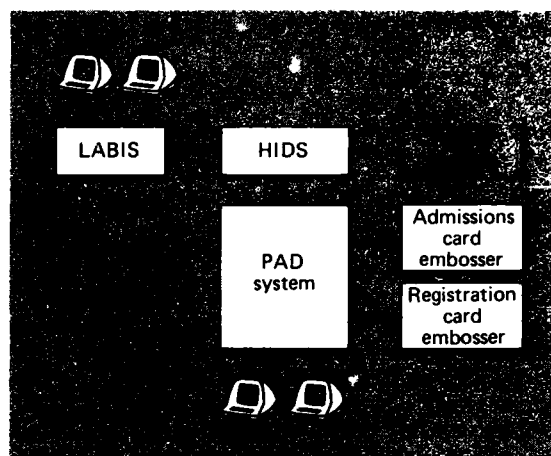


Figure 1 — The relationship of HIDS to the PAD system and LABIS.

LABIS. For emergency service, for example, a record may be established by a laboratory clerk supplying a minimum amount of information, i.e., patient identification number and name. This procedure allows immediate access to laboratory services but results in an incomplete registration record for which additional information will be needed. The complement of information is retrieved automatically from the PAD system and transferred to LABIS.

Management reports describing transactions handled by HIDS are available on hard copy at the end of the day or when requested.

HIDS consists of a 16-bit microcomputer system and associated peripherals selected by APL. The processor has less than a megabyte of random access memory, several serial input/output ports, Winchester disk drives, a floppy disk drive, a cartridge tape drive, a keyboard video display terminal, and a line printer. The total hardware costs were approximately \$30,000. Software for HIDS consists of a UNIX-based operating system and application programs developed in the C language.

### CONCLUSIONS

The HIDS installation at the Bethesda Naval Hospital brings several benefits. Information transferred to ancillary systems is likely to be more accurate and syntactically correct because the transfer procedure extracts and reformats the information from a highly controlled database before forwarding it. HIDS eliminates the need for manual data entry into an ancillary system, thereby reducing the work needed to achieve consistency among multiple databases.

The laboratory computer that had been supporting a multiple number of keyboard terminals and two embosser/encoders for administrative functions is now available for clinical laboratory functions, as had originally been intended.

HIDS operation has demonstrated that the transfer of identification and demographic data be-

tween independent machines in a terminal emulation mode is reliable, effective, and labor-saving—results that are particularly important in both military and civilian hospitals.

This work was supported by the Navy Medical Data Services Center.

## EVALUATION OF COMPUTER FAULT DETECTORS

M. E. Schmid, R. L. Trapp, and A. E. Davidoff (APL)  
and G. M. Masson (JHU)

*The use of simple monitors to detect computer faults has been explored as a technique for improved fault-tolerant computing. Candidate monitors were evaluated through extensive experimentation, and one particularly effective monitor that verifies program flow has undergone further development and evaluation.*

### BACKGROUND

The current evolutionary trend toward automation in military, industrial, and consumer products is creating an increasing dependency on computers. Our reliance on them is made evident by the significant disruptions that occur when they err or fail. Fault-tolerance, a way to improve a system's reliability, accepts the notion that faults may occur. Instead of trying to eliminate faults, it emphasizes design for continued correct operation when faults are encountered. Fault-tolerance usually is achieved by the synchronous operation of redundant systems that "vote" on all results. Thus, errors made by a single element are outweighed by the correct operation of other copies, and the fault is "masked" from affecting the system. However, this expensive technique is affordable only for the most critical applications.

Recently, attention has been given to an alternative to fault masking as described above. Called "external monitoring," the approach uses relatively simple monitoring devices to detect computer faults. Frequent-

ly, faults that occur are transient in nature, and the monitor need only return the computer to correct operation. Permanent faults may be handled by transferring the computing function to a spare system if one is available.

This article describes experiments conducted over the past two years to evaluate a number of proposed external monitors.

### DISCUSSION

#### Candidate Monitors

Seven characteristics of computer operation were identified as features that can be monitored to detect faults effectively:

1. Valid program flow — Monitor the sequence of instructions that the computer is executing to verify proper operation.
2. Valid opcode — Monitor the instruction being executed to determine if the instruction is among those used when the computer executes properly.
3. Valid opcode address — Monitor the location of instructions being fetched to ensure that they are valid.
4. Valid read address — Monitor all non-opcode read operations to verify the use of the proper addresses.

5. Valid write address — Monitor all write operations to verify the use of the proper addresses.
6. Valid memory — Monitor all memory accesses to ensure their occurrence in an acceptable region of the address space.
7. Valid and used memory — Monitor all memory accesses to verify their occurrence in a memory region that is actively used by the executing program.

Some of these characteristics are very similar to each other. In fact, they essentially can be grouped into three categories: program flow, memory access, and instruction repertoire. Five of the candidate monitors are memory access checkers. They vary in the type and precision of the address verification. Generally, greater precision has the associated penalty of increasing the monitor's implementation complexity.

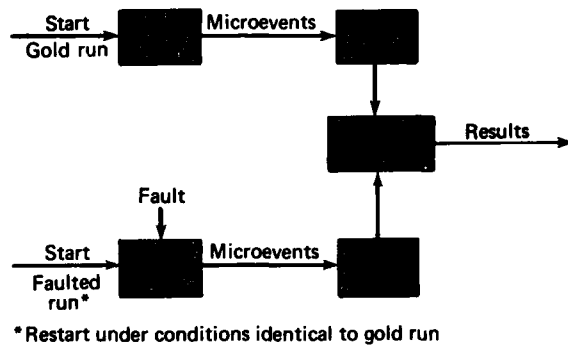


**Figure 1** — Basic experimental procedure to verify the effectiveness of the monitors in detecting faults.

The concept of monitoring program flow in systems with complex programs and many possible correct instruction sequences may not be readily apparent. Rather than periodically checking long sequences of instructions, the monitor verifies the transition between the previous instruction and the current instruction every time a new instruction is executed. This verification is possible because most operations have a limited number of valid successors.

## Experiments

The monitors were experimentally evaluated to determine their effectiveness in detecting faults. Figure 1 shows the basic experimental procedure. For each experiment, a baseline of information describing the computer's normal operation is obtained by making detailed time recordings of all signals connected to the processor. This recording is referred to as the "gold" run. A second recording is made under identical conditions, with the exception of a single precisely controlled fault that is injected shortly after recording begins. This recording is referred to as the "fault" run, and it provides a detailed account of the disruption caused by the particular fault that was injected.

During analysis, each time-step from the fault run containing abnormal activity (as determined by comparing the gold and the fault runs) is applied to models of the proposed monitors. Each model then has the opportunity to indicate that faulty operation has occurred. Figure 2 shows an analog signal into which a fault was injected. The heavy black line is the gold run; it shows normal execution. The gray trace shows the activity during the fault run. Note that although the fault itself was injected for a very short time (1  $\mu$ s), the rami-

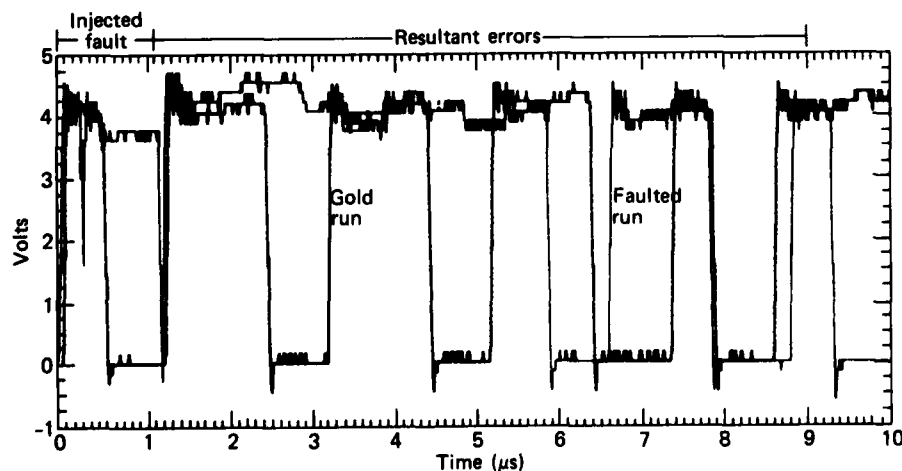


**Figure 2** — Sample recording of gold and fault runs.

fications of that fault continue past the end of the recording. Typically the fault itself is not detected by the monitors; instead, it is the continued propagation of the fault that is seen.

More than 1400 experiments were conducted over the past two years to evaluate the monitors over a wide range of injected fault conditions. The fault duration, target signal, instruction under execution, and software environment were varied throughout the series.

## RESULTS

The performance of the monitors is shown in Fig. 3 for two software environments. The primary criteria for evaluating such monitors are coverage (percent of fault injections detected) and latency (time from fault injection to detection). The best performance, both in terms of coverage and latency, was demonstrated by the program flow monitor. Further analysis indicates that multiple monitors may be used together to provide better performance than any one alone. The "all" plot indicates the performance attained by the combination of all seven monitors.

The effectiveness of the program flow monitor prompted further investigation. Detailed models of six versions of an easily implemented "compressed" program flow monitor were developed. The analysis was carried out on each of the models, with excellent results. One of the compressed models captured 95% of the original monitor's coverage, paving the way for a simple but effective implementation.

The project has clearly demonstrated that monitors can be effective in detecting computer faults and yet remain simple to implement. These attributes great-

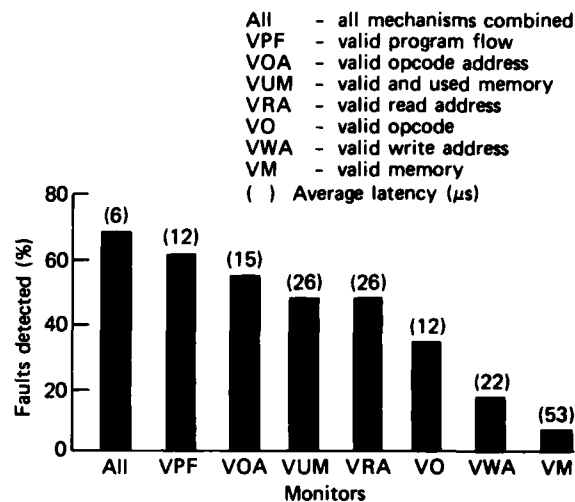


Figure 3 — Summary of monitor performance.

ly widen the range of applications that may benefit from fault-tolerant computing techniques.

## ACKNOWLEDGMENT

The authors would like to acknowledge the contributions of three individuals: R. Haddad and K. LaBel of The Johns Hopkins University, and C. Gira of Duke University. Their significant efforts have been a primary element in the success of this project.

This work was supported by Independent R&D.

# SIMULATION OF ANOMALOUS ELECTROMAGNETIC PROPAGATION WITH THE EMPE CODE

H. W. Ko, J. W. Sari, and J. P. Skura

*A computer program has been developed to aid in investigations of anomalous electromagnetic propagation. Called EMPE (for electromagnetic parabolic equation), it computes propagation loss in arbitrarily complex atmospheres for standard conditions or for conditions of anomalous propagation. Predictions for anomalous wave behavior have been made for frequencies from 100 MHz to 10 GHz. The results are thus relevant to a variety of microwave electromagnetic systems such as those used for communications, radar, and airplane instrument landings.*

## BACKGROUND

Most analyses of wave propagation by means of simple refractive changes in the atmosphere can be treated with geometrical ray tracing techniques based on Snell's law. However, ray tracing methods have certain general limitations: (a) the refractive index must not change appreciably in a distance comparable to a wavelength; (b) the spacing between neighboring rays must be small or else the results are questionable when rays diverge, converge, or cross; (c) constructive and destructive interference is difficult to evaluate for more than one reflection from a surface; (d) the distance a ray may travel is difficult to evaluate without a way to compute propagation loss; and (e) diffraction phenomena are not accounted for in homogeneous media. Therefore, a physical optics approach (such as that used by EMPE) that can account for propagation loss and diffraction is needed for most sophisticated problems. A special feature of the EMPE program is its ability to deal with inhomogeneous atmospheric changes in both the horizontal and the vertical directions. Spatial energy patterns and propagation loss can now be computed for antennas inside and outside anomalous regions such as ducts and subrefractive layers.

## DISCUSSION

### High-Elevation Ground-Based Antenna in an Elevated Duct Environment

In one simulation, an antenna designed for 1.2 GHz operation is placed at an elevation of 7000 ft, and a 0° elevation angle and a 4° vertical beamwidth are used. These conditions illustrate an application to a high-sited, air-search radar. In coastal environments, a

warped elevated duct of varying curvature may be present to alter normal or standard antenna coverage.

The anticipated diversion of rays from standard coverage leading to regions of reduced coverage (so-called holes or voids) is seen in Fig. 1, which gives the decibel loss relative to 1 m. The figure shows the vertical coverage of the antenna for propagation along the direction of maximum inhomogeneity. Several significant results appear that would not have emerged from the application of simple ray-tracing techniques. There are several regions (not just one) of reduced coverage; the loss is computed everywhere, including inside the trapping layer, the top of which is defined by the dashed line. In some cases (e.g., in the unshaded, 90 dB region), excessive energy is diverted down to the surface well beyond 120 nmi.

Along a direction of lesser inhomogeneity, different features are seen (Fig. 2). The elevated duct is less warped spatially. New voids at high altitude are seen because of the waves' inability to "burn through" the elevated duct. Also, waves are trapped and "guided" by the elevated duct and not diverted to the surface as in Fig. 1.

The detailed synoptic view of propagation loss can be important in the design and operation of high-elevation antennas used for communications, data telemetry, or (as above) radar surveillance systems. Note that for transmission between two points of high elevation, periodic path fading, similar to low-altitude multipath fading, is predicted in Fig. 2.

### Shipborne Antennas and the Evaporation Duct

Other products from the EMPE code can be used to examine the propagation loss structure in more detail. Figure 3 gives the transmission loss at 3 GHz in decibels relative to free space at selected ranges away from a shipborne antenna at a height of 100 ft. The antenna is above an inhomogeneous surface duct, the height of which varies from 50 ft at the antenna to 100 ft at 100 nmi downrange. Therefore, the antenna is placed above the duct. Enhanced over-the-horizon coverage is shown extending beyond 100 nmi. This downrange trapping is not ordinarily predicted by other techniques. Here, given vertical loss profiles can aid in quickly determining the altitude and depth of coverage voids. Figure 4 gives the transmission loss in decibels relative to 1 m at selected altitudes. Horizontal loss be-

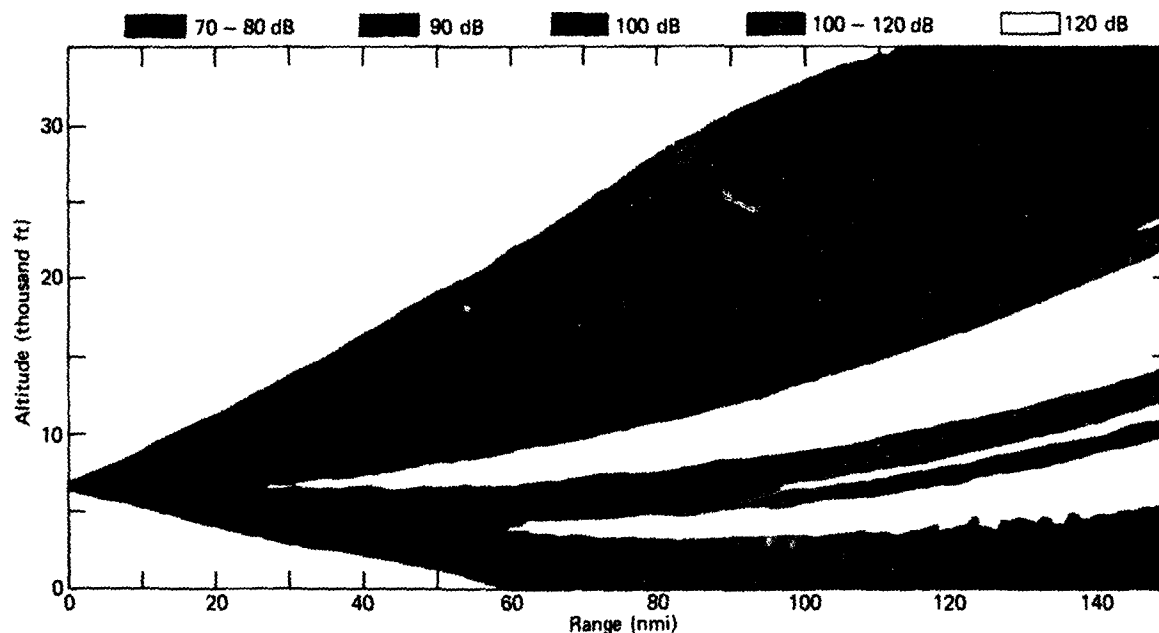


Figure 1 — Vertical coverage of the antenna for propagation along the direction of maximum inhomogeneity.

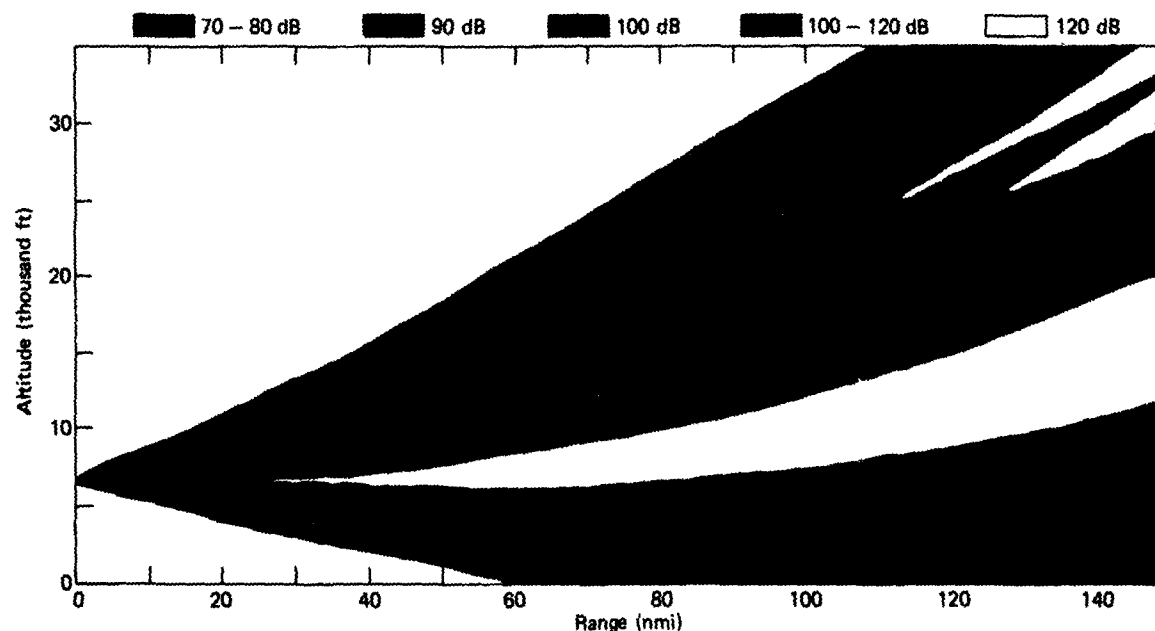


Figure 2 — Vertical coverage of the antenna for propagation along a direction of lesser inhomogeneity.

behavior is helpful in discerning path fading inside and above the surface duct.

#### Features of the EMPE Approach

The analytical approach followed in using the EMPE code is based on approximations to the propagation equation for inhomogeneous media that are com-

parable to those obtained by Leontovich and Fock.<sup>1</sup> The resultant propagation equation is of the parabolic type, which admits of a marching type of numerical solution in the horizontal direction called the split-step Fourier algorithm.<sup>2</sup> The advantage of this approach is that it allows for complex inhomogeneous profiles in the dielectric constant and yields accurate physical-op-

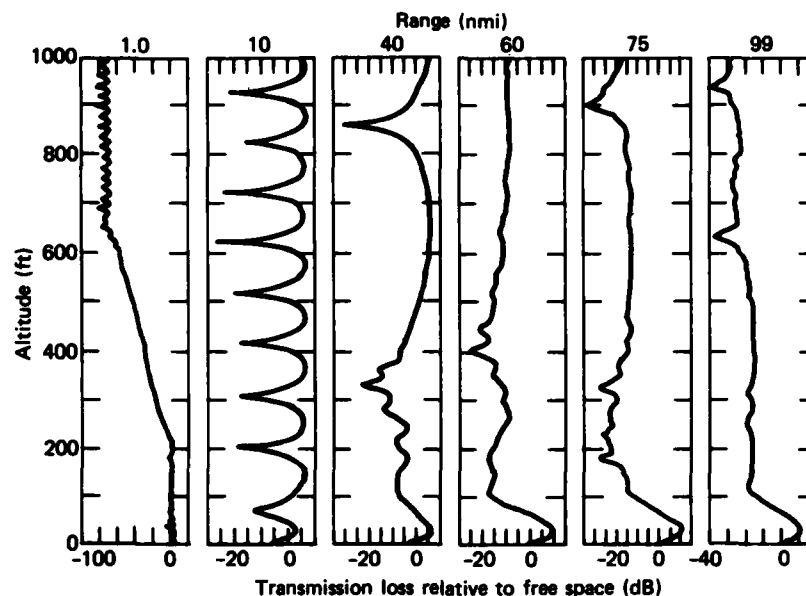


Figure 3 — One-way transmission loss in decibels relative to free space.

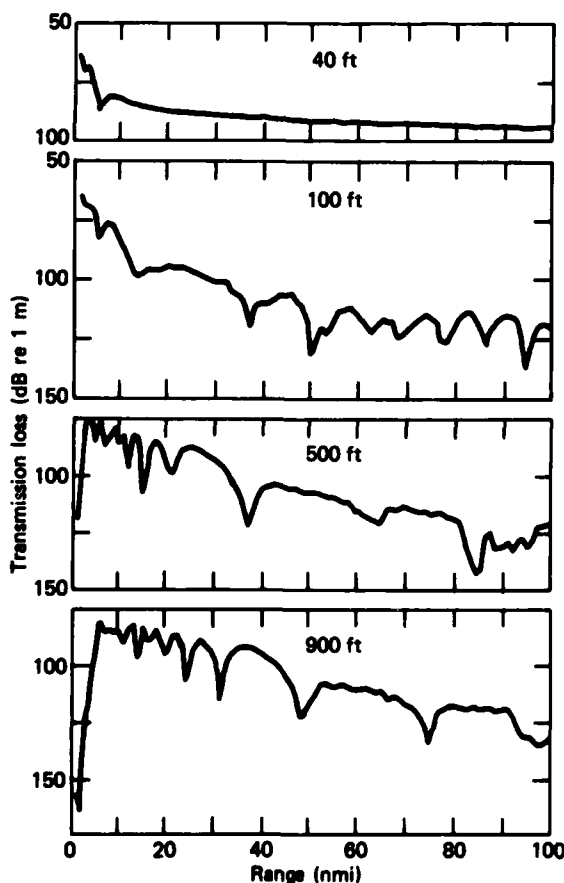


Figure 4 — One-way transmission loss in decibels relative to 1 m.

tics computations of transmission loss with computational efficiency. The limitations of this approach are generally avoided in cases of relatively oblique propagation in the troposphere.<sup>3</sup>

Several important aspects of wave behavior in the ducting environment are predicted and given in analyzable form by means of the EMPE approach:

1. Propagation loss is given everywhere, allowing range extension or compromise to be quantified.
2. Peculiar downrange behavior is allowed for horizontally inhomogeneous situations; for example, rays not initially trapped can be trapped downrange, energy can leak out of surface or elevated ducts, and initially trapped rays can burn out of a duct.
3. Excessive energy is observed to be diverted away from normal coverage areas, leading to coverage holes and excessive clutter with different azimuthal and range variations.
4. Situations can be analyzed for antennas within or distant from anomalous refractive layers.

## REFERENCES

- <sup>1</sup> M. A. Leontovich and V. A. Fock, "Solution of the Problem of Propagation of Electromagnetic Waves Along the Earth's Surface by the Method of Parabolic Equation," *J. Phys. Moscow* 10, 13 (1946).
- <sup>2</sup> R. H. Hardin and F. D. Tappert, "Applications of the Split-Step Fourier Method to the Numerical Solutions of Nonlinear and Variable Coefficient Wave Equations," *SIAM Rev.* 15, 423 (1973).
- <sup>3</sup> J. W. Sari, J. P. Skura, and R. I. Joseph, *Electromagnetic Propagation in an Inhomogeneous Stratified Atmosphere*, JHU/APL STD-R-612 (4 Mar 1982).

This work was supported by the U.S. Air Force.

# ITERATIVE SOLUTION OF A PARTIAL DIFFERENTIAL EQUATION ON AN IMAGE PROCESSING SYSTEM

C. A. Waters

*A digital image processing system has been used to generate approximate solutions for two-dimensional partial differential equations of the Laplace type. The computer program that implements the solution allows boundary values to be defined interactively through the time sharing facilities of the Laboratory's IBM 3033 computer. A color monitor that is part of the image processing system displays the progress of the iterations toward a solution.*

## BACKGROUND

Differential equations have extensive applications to virtually all areas of science and engineering. Much effort has gone into their study. Generally, solutions may be classified as analytic (derived along the lines of mathematical proofs) or numerical (resulting from approximate calculations). Since computers have become widely available, a great deal of time has been devoted to the development of programs that generate numerical solutions and to the interpretation of the results of those programs.

As computers and numerical methods become more powerful, problems of greater size may be addressed. However, this raises another difficulty because the researcher now has more data to interpret. Graphical display methods are invaluable because they condense numerical results into forms that are quickly understood. Contour plots are one example of a convenient display format for output from a numerical program.

An image processing system is a special-purpose computer that can process large quantities of data very quickly and display the data in graphical form. An example of such a system is the Grinnell image processing system attached to the Laboratory's IBM 3033 computer. The Grinnell system may be controlled interactively from a computer terminal. It was selected as a test system for a program that uses image processing hardware to both calculate and display solutions to partial differential equations.

## DISCUSSION

### Iterative Solution of a Partial Differential Equation

One of the most important of all the partial differential equations occurring in applied mathematics

is the Laplacian equation, which, in two dimensions, has the form

$$U_{xx} + U_{yy} = 0$$

where  $U = U(x, y)$  is a function of the two variables  $x$  and  $y$ , and subscripts indicate that partial derivatives have been taken. Because of its application to gravitational and electrostatic potential problems, it is often referred to as the potential equation. It has applications as well to steady-state problems involving heat conduction, to the flow of an incompressible fluid, and to certain elasticity problems.

As there is no time dependence in the Laplace equation, there are no initial conditions to be satisfied in its solution. Instead, certain boundary conditions are specified on the bounding curve of the region in which the equation is to be solved. Those conditions may involve values of the function  $U$  or of its derivatives. Only the first case is considered here; this special case is called the Dirichlet problem. (See Ref. 1 for a discussion of the Laplace and Dirichlet problems.)

In order to solve this equation using digital methods, it is necessary to recast the problem in discrete form. Cover the region of interest with a mesh, that is, with two perpendicular sets of equally spaced parallel lines. Restrict the function  $U$  to the points of intersection of the sets of lines, the mesh points. Under this interpretation, the boundary is a discrete set of points rather than a continuous curve. However, we still require that the boundary be closed.

Once the boundary conditions and the mesh have been selected, an approximate solution to Laplace's equation can be generated by iteration in the following way. First, initialize all interior mesh points. They may be set to zero or to any suitable values. Next, let  $P$  be any mesh point taken from the interior of the region, and let  $A$ ,  $B$ ,  $C$ , and  $D$  be the four neighbors of  $P$  in the mesh. Replace the value at  $P$  by the new value  $(A + B + C + D - 4P)/4$ . Do this for each mesh point in the interior to complete one iteration toward a solution. It may be necessary to repeat this step many times until the values on the boundary of the region can propagate throughout the interior and until the interior values reach a steady state. Techniques have been developed to accelerate the process so that fewer iterations are required but they will not be considered here. See Ref. 2 for further details on the techniques.

It is convenient to think of each step in the sequence as the application of a template (Fig. 1) to each interior mesh point. Place the template over a point, multiply the template values by the corresponding values at the mesh points, calculate the sum of the products, and place that value at the mesh point in the center of the template. This process is called template convolution; it can be implemented easily in an image processing system.

### Implementation of the Solution

The Grinnell GMR-270 image processing system, which was chosen for implementation of the method, is manufactured by the Grinnell Systems Corp. of San Jose, Calif. The system has four 512 by 512 resolution image memories, which can store 8-bit values. The individual picture elements, or pixels, in an image can be viewed as mesh points to which values in the range 0 to 255 correspond. If necessary, two memories can be processed together as a single memory containing 16-bit values. The arithmetic unit of the image processor accepts two 16-bit operands. Operations such as multiplication and division are simulated by means of look-up tables associated with the arithmetic unit.

Of particular usefulness is a feature of the image processor that allows two independent operations to be carried out on one image in a single pass through the processor, thereby allowing the function values on the boundary to be kept constant while the template is applied to all interior points.

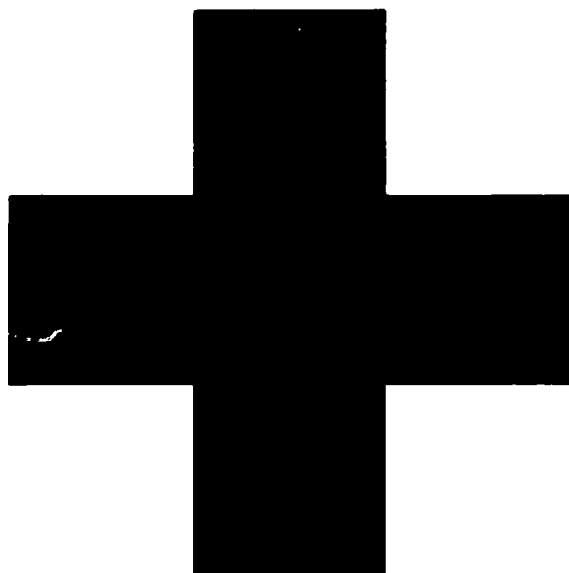


Figure 1 — A Laplacian template.

Figure 2 illustrates the solution of a steady-state heat flow problem using the image processing system. Graphics commands in the processor were used to define the boundary in one of the digital memories. Because 8 bits were used to represent function values, the range of temperature is 0 through 255. The interior of the region was approximately 256 by 256 pixels. Figure 2a shows the system before iterations were applied. The boundary contains two values: 255 in the white region and 0 in the gray region. There is also a small boundary region of intensity 0 near the upper right corner (not visible in the image).

Figure 2b and 2c show the system after 100 and 200 iterations, respectively. On the color monitor, a pseudo-coloring would be used to display the grayscale images. Here, certain intensity ranges have been highlighted to bring out their structure. The asymmetry in the images results from the boundary region of intensity 0 in the upper right. Figure 2d shows the system after 270 iterations, when it has reached a steady state. It takes about three minutes to generate this image.

### SUMMARY

An image processing system has proved to be well suited for the approximate solution and the display of problems involving partial differential equations. The array sizes can be larger than those ordinarily used in computer solutions (up to 512 by 512). The time for

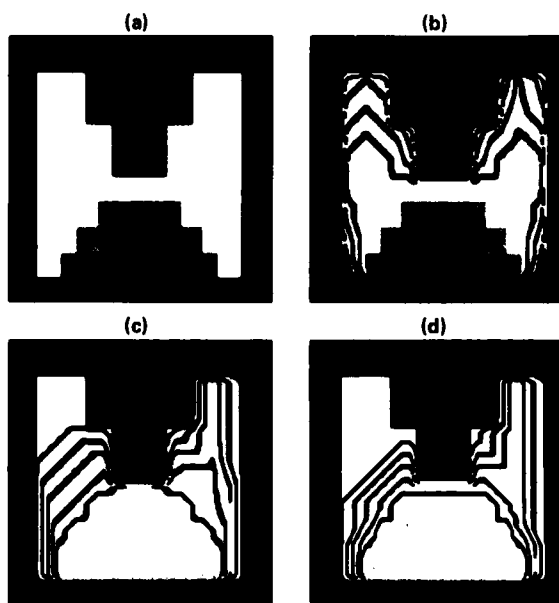


Figure 2 — The solution of a steady-state heat flow problem using the image processing system.

one iteration in the solution is independent of the array size although, of course, the time to reach a steady state does depend on the problem size. The display of the progress of the solution toward a steady state is particularly useful because it allows the researcher to experiment interactively with alternative boundaries and with pseudocolorings for the data in order to bring out details in the solutions. One device is used for both calculations and, therefore, the display results are immediately available in graphical form.

## REFERENCES

- <sup>1</sup>W. E. Boyce and R. C. DiPrima, *Elementary Differential Equations and Boundary Value Problems*, John Wiley and Sons, New York, pp. 470-476 (1969).
- <sup>2</sup>V. Vemuri, *Digital Computer Treatment of Partial Differential Equations*, Prentice-Hall, New York, p. 291 (1981).

---

This work was supported by NAVSEASYSKOM.

# **SPACE SCIENCE AND TECHNOLOGY**

## INTRODUCTION

The Laboratory's involvement in space programs began in the postwar years when Aerobee and captured V-2 rockets carried Geiger tubes, magnetometers, and optical spectrometers high above the earth's surface. The flights provided the first high-altitude measurements of cosmic rays, the geomagnetic field, and atmospheric constituents such as ozone, and were conducted by pioneers James A. Van Allen, John J. Hopfield, and S. Fred Singer (who were then APL staff members). In 1946, a V-2 rocket carried the first camera, installed by APL, to look at the earth from an altitude of 100 miles. From those beginnings, APL's record of accomplishments proceeds and includes the conception, design, and development of the Transit Navigation Satellite System and the SATRACK Missile Tracking System for the Navy.

Space activities at APL have been supported by an active program of basic research directed toward understanding the chemical and physical processes involved in the earth's atmosphere, ionosphere, and magnetosphere, and in interplanetary phenomena. Laboratory achievements include the first detection of solar cosmic rays with satellite-borne solid-state detectors, the design and construction of one of the longest lived scientific satellites ever launched (1963-38C), the first measurement of short-period magnetohydrodynamic waves near synchronous altitude, the discovery of heavy ions trapped in the earth's radiation belts, the experimental confirmation of large-scale field-aligned currents in the auroral regions, the demonstration of the effect of stratospheric pressure variations on the ionosphere, the discovery that Jupiter is a source of energetic particles in the earth's vicinity, and the development of radio astronomy techniques for predicting geomagnetic storms that can disturb terrestrial radio transmissions. Research activities have involved international collaborations with scientists from more than a dozen academic and defense organizations.

In addition to the work reported in this issue of the *APL Selected Accomplishments*, there are a number of space activities presently under way at the Laboratory. The following list is far from inclusive but is intended to provide examples of current efforts.

- APL is collaborating with the Max-Planck Institute on the Active Magnetospheric Particle Tracer Experiment (AMPTE). By creating and monitoring an artificial ion cloud within the distant magnetosphere, AMPTE will yield information on the mechanisms responsible for the formation of the Van Allen radiation belts.
- APL is supporting NASA in the design of spacecraft to simultaneously map the earth's gravitational and magnetic fields.
- The Laboratory is collaborating with the Jet Propulsion Laboratory and the Max-Planck Institute in the development of an energetic particle detector for the NASA Galileo mission. The instrument will be integrated into the Galileo spacecraft scheduled to orbit Jupiter in 1990.
- An APL-built instrument to measure the heliosphere will be aboard the Solar Polar spacecraft scheduled to pass over the sun's poles at the end of this decade.

- APL continues to participate in planning for the Voyager encounter with Uranus in 1986.

Four articles have been chosen for inclusion in this section of the *APL Selected Accomplishments*.

The first describes the magnetometer built by APL for the Swedish VIKING satellite. The instrument was delivered to the Swedish Space Corp. in August 1982.

Next, the development of a lightweight radioisotope heater unit is discussed. The unit, used to provide heat in spacecraft for temperature-sensitive equipment, had the conflicting design goals of a 30% weight reduction and improved reentry safety margins relative to its predecessor. APL developed the thermal design for the radioisotope heater unit, which is being manufactured by the Department of Energy for space missions and will be used for the Galileo mission to Jupiter.

The third article reports on an APL plan for an operational Search and Rescue Satellite (SARSAT) system to locate shipwreck and air-crash victims. The SARSAT system, as conceived by APL staff, would provide global coverage and a maximum "wait time" of two to four hours. NASA has asked the Laboratory to provide a detailed technical plan.

The fourth article describes the Satellite Missile Tracking (SATRACK) program developed by APL to support Trident missile flight tests. The SATRACK system allows missile trajectory determinations to be made by means of radio frequency measurements between the missile and satellites of the DoD Global Positioning System. SATRACK is now fully operational and is used routinely to evaluate missile accuracy.

## COMPLETION OF A MAGNETOMETER FOR THE SWEDISH VIKING SATELLITE

F. F. Mobley, K. J. Heffernan, and T. A. Potemra

*A three-axis vector magnetometer has been designed, built, and delivered by APL for the Swedish VIKING satellite, to be launched on the Ariane rocket in 1984. The magnetometer has four different ranges that are selected automatically to cover magnetic fields from  $\pm 64,000$  to  $\pm 1000$  gamma, with digital resolution from 16 to  $1/4$  gamma. The instrument will be used to collect scientific data on the magnetic fields in high-altitude auroral regions to further APL research on field-aligned current systems in the aurora.*

### BACKGROUND

APL has been active since 1963 in basic research on auroral phenomena, especially using satellites with vector magnetometers to measure the magnetic field in the aurora and other physical activity such as field-aligned currents. Data from the APL Triad satellite have been collected since 1972<sup>1</sup> in low-altitude auroral regions.

The VIKING satellite will be launched with the French SPOT satellite by the Ariane rocket in 1984. Viking is dedicated to scientific research at high altitude (15,000 km) in the northern auroral region. APL was invited to participate in this research effort by providing a three-axis vector magnetometer and sharing in the scientific investigation to follow.

### DISCUSSION

The magnetometer system was designed and fabricated in the period January to October 1981; testing of the electronics system then began. The electronics system consists of three circuit boards (Fig. 1): a DC/DC converter, an analog system, and a digital system.

The DC/DC converter takes the input DC voltage of  $28 \pm 4$  V and converts it to the required internal voltages of  $+12$  and  $-12$  V. The converter is synchronized to an external frequency source and runs at 27.3 kHz. It provides input current limiting, transient suppression, and automatic turnoff in case of excessive output load.

The analog system has a crystal oscillator at 3 MHz, which is counted down to 15 kHz to provide excitation for the three fluxgate sensors. The output of each sensor is analyzed by a detector circuit that rectifies the second harmonic (30 kHz) of the sensor output and produces a DC signal voltage proportional to the applied magnetic field component.

The three vector component signals then go to the digital board for analog-to-digital conversion to 12 bits plus sign and organization of the 39 bits of data plus 1 bit of parity information for transmission to the telemetry system. The sampling rate is 53 vector samples per second.

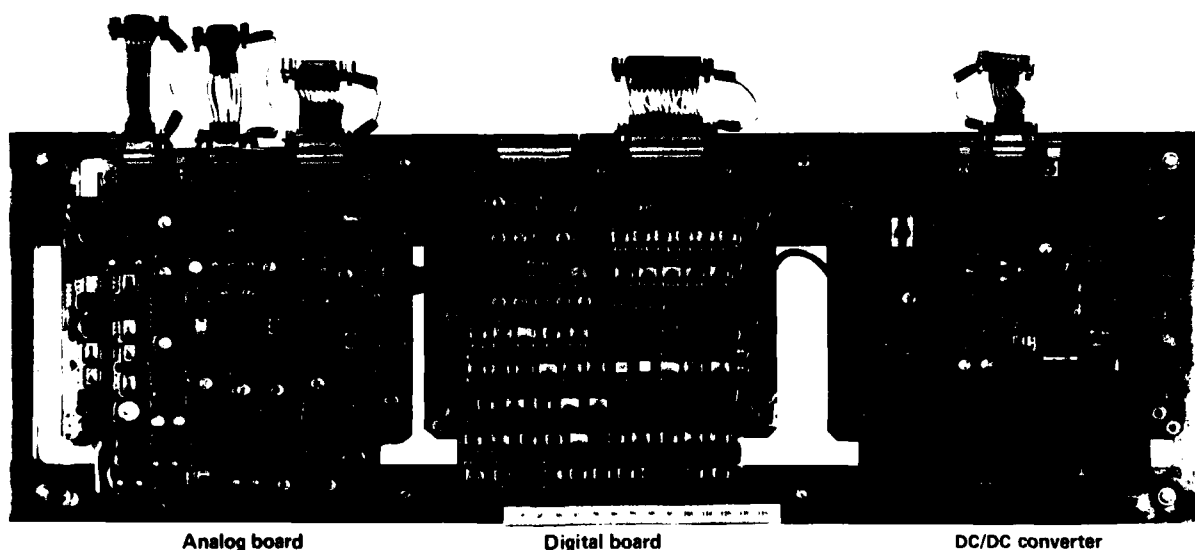


Figure 1 — Electronics boards for the Viking magnetometer.

Automatic range changing is determined by analysis of the amplitude of the digital data on the digital board. If all three signals are "low," the system shifts to a more sensitive range. If any signal is "high," it shifts to a less sensitive range. In this way, large changes in the field arising from the highly elliptical orbit of Viking will be compensated.

Figure 2 shows the three-axis sensor assembly. It contains three ring-core sensors of highly permeable 6-81 moly-permalloy. The excitation windings are toroidal, and the output windings are solenoidal. A DC feedback current in each output winding counteracts the external field and maintains a null condition within each sensor. The amplitude of the feedback current is a measure of the external field.

Figure 3 shows the magnetometer system, which consists of the electronics box and the sensor assembly with its spherical protective cover. The external paint and aluminized dots on the sensor produce a thermal environment of 20°C in full sunlight in orbit. The sensor will be mounted on the end of a boom about 2 m from the satellite body. The boom will be deployed in orbit.

Figure 4 shows the satellite assembly; the various scientific instruments are identified.

From October 1981 to July 1982, electrical performance, vibration, thermal-vacuum, alignment, and calibration tests were accomplished satisfactorily.<sup>2</sup>

The instrument was delivered to the Swedish Space Corp. in August 1982 and has been integrated with the other instruments in the Viking satellite by Saab-Scania, the Swedish contractor for spacecraft integration.

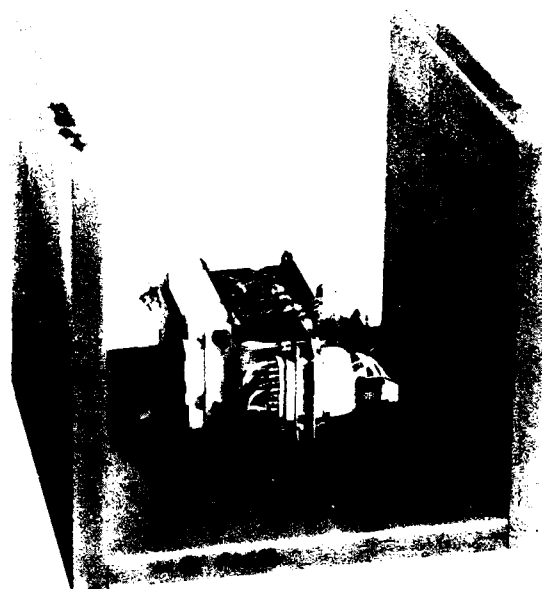


Figure 2 — The magnetometer sensor.

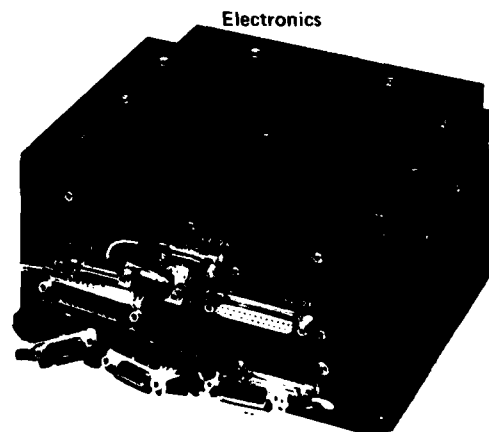
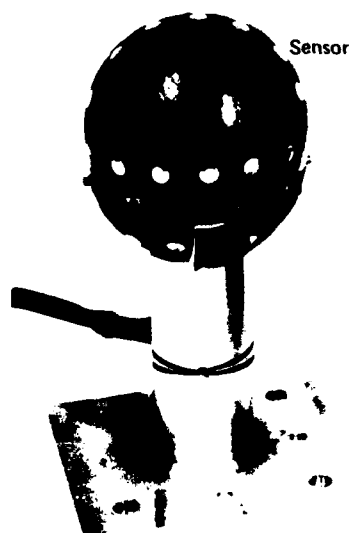


Figure 3 — The Viking magnetometer.

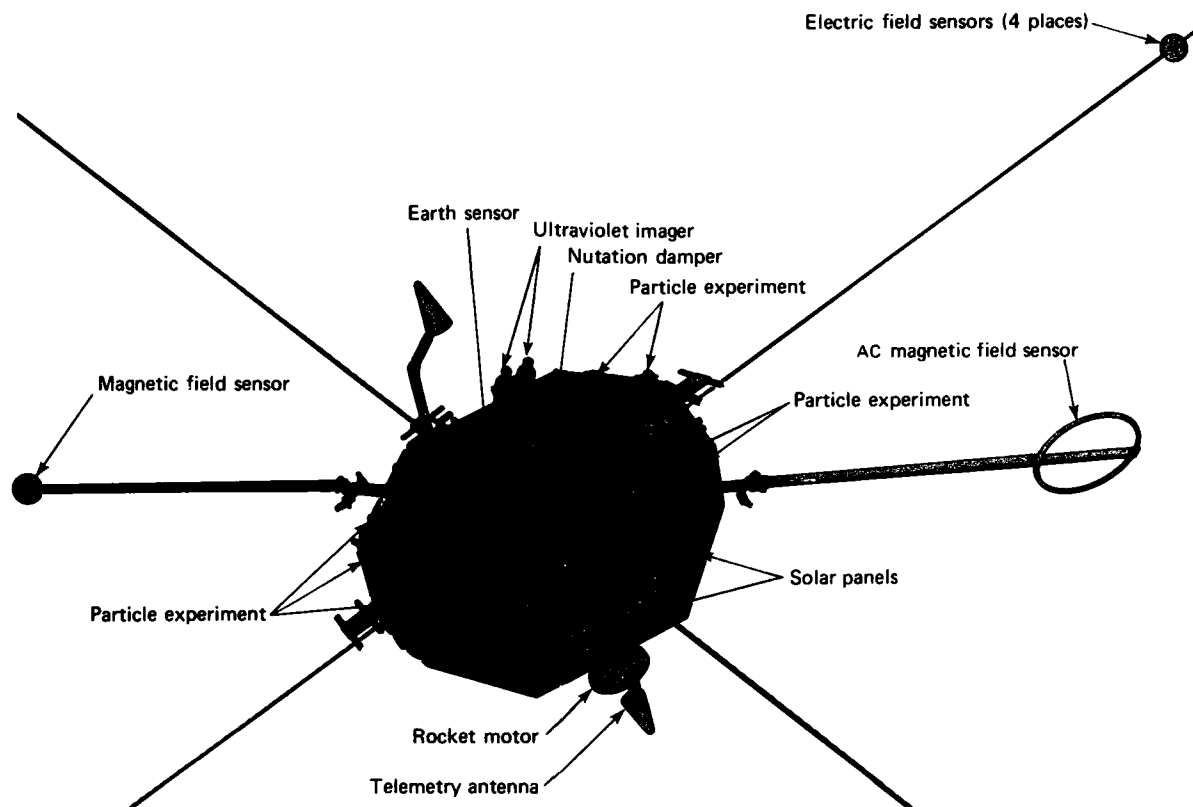


Figure 4 — The Viking satellite assembly.

## FUTURE PLANS

Saab-Scania will continue the testing and flight qualification of the assembled satellite. The magnetometer system will be calibrated in 1984 at the West German magnetic test facility near Munich. The satellite will be launched from the French facility in Kourou, French Guiana.

A VIKING 2 satellite is in the preliminary discussion phase.

## ACKNOWLEDGMENTS

Significant technical assistance in the magnetometer design has been provided by M. H. Acuna of the Goddard Space Flight Center. The magnetometer sensor is a result of Dr. Acuna's development efforts and is similar to that provided by him for the APL Magsat satellite, launched in 1979.<sup>3</sup> C. A. Wingate of APL

performed the thermal design and analysis for the sensor assembly. H. T. Henline of APL was responsible for a large portion of the electronic testing as well as integration testing in Sweden.

## REFERENCES

- <sup>1</sup>T. A. Potemra, "Large-Scale Characteristics of Field-Aligned Currents Determined from the Triad Magnetometer Experiment," presented at the NATO Advanced Study Institute on Dynamical and Chemical Coupling of Neutral and Ionized Atmosphere, Spind, Norway (Apr 1977).
- <sup>2</sup>K. J. Heffernan, *Pre-shipment Review of the Viking Magnetometer*, JHU/APL S4A-3-343 (6 Aug 1982).
- <sup>3</sup>M. H. Acuna, C. S. Scarce, J. B. Seek, and J. Scheifele, *The Magsat Vector Magnetometer — A Precision Fluxgate Magnetometer for the Measurement of the Geomagnetic Field*, NASA TM 79656 (Oct 1978).

This work was supported by the Naval Research Laboratory.

# REENTRY THERMAL DESIGN OF A LIGHTWEIGHT RADIOISOTOPE HEATER UNIT

D. W. Conn, L. L. Perini, K. R. Waeber, and J. C. Hagan

*A Lightweight Radioisotope Heater Unit has been developed and is being qualified for use in future space missions. It will be used to keep sensitive spacecraft equipment from freezing in the space environment.*

## BACKGROUND

Plutonium-fueled radioisotope heater units (RHU's) are sometimes used in spacecraft to thermally condition electronics, science experiments, and other temperature-sensitive equipment.

The potential health effects of the plutonium require that safety be a primary design consideration. To test the design, a safety evaluation of all credible accident scenarios associated with a mission is carried out, including in-flight accidents resulting in reentry of the earth's atmosphere. A design goal for an RHU is containment of the fuel with a high probability of success against the hostile thermal and structural environments associated with a variety of earth reentries. A Safety Analysis Report is prepared and reviewed by the Inter-agency Nuclear Safety Review Panel (INSRP). Then a Safety Evaluation Report is prepared by the INSRP to assess the occurrence probabilities and consequences of the various accident scenarios. The Safety Evaluation Report forms the basis for obtaining launch approval.

In 1979, the Office of Special Nuclear Projects of the Department of Energy (DOE) (then the Advanced Nuclear Systems and Projects Division) began a program to develop a second-generation Lightweight RHU (LWRHU) that would supply one thermal watt. The program had the competing goals of providing a 30% weight reduction but substantially improved safety margins compared to those of its predecessor. As part of a collaborative, multiorganizational effort, APL was requested by DOE to assist in developing the reentry thermostructural design for the LWRHU. This design effort included consideration of the thermal stress and ablation performance of the heat shield as well as control of the maximum in-flight temperature and impact temperature of the platinum alloy that was used to encase the plutonium.

The goal of the LWRHU program was to develop a standard heater unit, fully qualified for use in future space missions. The first uses of the unit will be on the Galileo mission to Jupiter.

## DISCUSSION

The reentry thermostructural design of the LWRHU or similar radioisotopic devices must account for four basic environmental conditions that could affect the containment of the radioactive fuel during flight and earth impact:

1. The ablation environment, in which there is loss of heat shield material as a result of sublimation and/or chemical reaction with the surrounding heated boundary layer, as well as mechanical removal resulting from aerodynamic and thermal stresses;
2. The heat shield stress that occurs because of a combination of (a) mechanical stresses resulting from aerodynamic and internal inertial loads, and (b) thermal stresses resulting from thermal gradient formation in response to the reentry heating environment;
3. The high temperature of the metallic alloy containment shell that occurs because of aerodynamic heating;
4. The impact of the LWRHU, as dictated by the kinetic energy of the heater unit and the mechanical response of the shell upon earth impact.

Early in the LWRHU design process, a restrictive design condition was imposed during a Galileo spacecraft design freeze. To permit packaging compatibility within the spacecraft, the volumetric envelope of the LWRHU was constrained to be a right circular cylinder with a length of 1.26 in. and a diameter of 1.02 in. This requirement had a broad effect on the design process for two reasons. First, the definition of the LWRHU's aerodynamic configuration, taken in combination with the DOE-specified mass goal of 40 g, predetermined the design environment from initial reentry to terrestrial impact. This early constraint on the envelope restricted the design process to that of judicious material selection and manipulation of the size of the LWRHU components within the envelope. Second, the length-to-diameter ratio of the cylinder was such that both an aerodynamically stabilized side-on and an end-on position had to be considered; therefore, the scope of developing and validating the LWRHU's reentry safety design was extended.

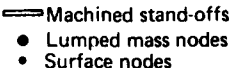
Under the program direction of DOE and the Los Alamos National Laboratories, collaborative analytical and test studies were conducted by Los Alamos, APL, Mound Laboratory, and Fairchild Industries to establish the LWRHU design. At APL alone, several hundred reentry simulations were conducted to track the evolving thermal design characteristics. The simulations included detailed modeling of the LWRHU structure, heat shield ablation mechanisms, and energy transport mechanisms such as convective and shock layer radiative heating. Figure 1 presents a plane section of a three-dimensional thermal model developed by APL to assess the thermal performance of the LWRHU for stabilized side-on reentries.

The final LWRHU design is shown schematically in Fig. 2. The objective of the reentry thermostructural design was to maintain an integral heat shield throughout the reentry flight and also to restrict heat flow into the platinum alloy containment shell during passage through the hypersonic heat pulse. With these objectives in mind, several important thermal design features may be noted from Fig. 2.

The heat shield, the component that provides ablation protection, also is the component that is subject to thermal stress. The concern about thermal stress was minimized by selecting a three-dimensional carbon-carbon material. Maximum thermal stresses typically are encountered during steep-angle reentries. The sharp temperature gradients associated with rapid heating of the LWRHU result in a differential expansion of the

heat shield that introduces intramaterial stresses and strains. A structural analysis of the LWRHU subject to a steep-angle reentry heat pulse was conducted to investigate the thermostructural response of the LWRHU under extreme heating conditions and to compare the structural response of the carbon-carbon material with that for a traditional bulk graphite heat shield material. Detailed thermostructural analyses, using a trajectory

Note: The model extends 0 to 180° in the circumferential direction



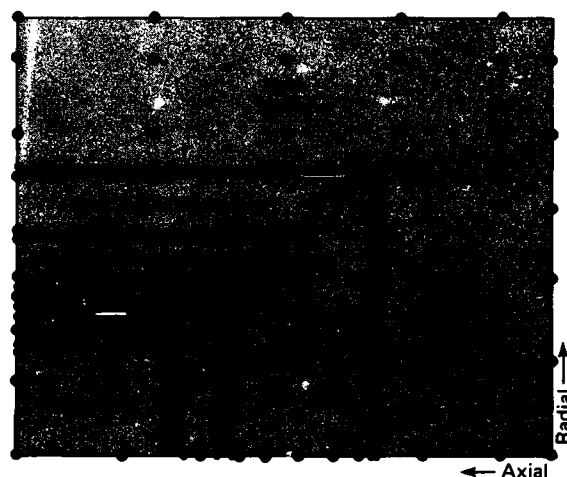
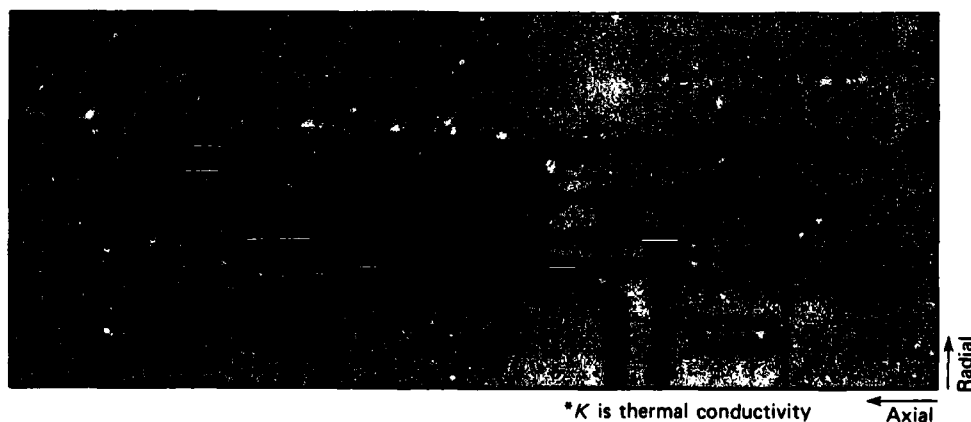


Figure 1 — A plane section of the side-stable three-dimensional thermal model of the LWRHU.

Component No.	Material
1	Fine Weave Pierced Fabric™, 3D carbon-carbon
2 and 3	Pyrolytic graphite
4	Pt 30 Rh alloy
5	Plutonium oxide


 Machined stand-offs



\*K is thermal conductivity

Figure 2 — Schematic of the LWRHU design.

that produced the most severe temperature gradients, showed that satisfactory stress margins are maintained in the heat shield.

The pyrolytic graphite sleeves are designed to provide thermal protection to the containment shell in the radial and axial directions. Because of the manufacturing process, its insulation effectiveness is highly directional; that fact must be accounted for in the insulator design. The 45° stepped interface between the sleeves and the end plugs accommodates the directional characteristic during either a side-on or an end-on reentry. The stepped interface also inhibits direct "radiation shine" onto the containment shell from the hot inner surface of the heat shield.

The containment shell is fabricated from the noble alloy, Pt20Rh, a material well suited for this purpose. Because of its high carbon eutectic temperature (3100°F) and heat capacity, Pt20Rh permits excellent accommodation for the portion of the reentry heat pulse that penetrates the insulation. Also, it has good ductility properties over a broad temperature range to permit quite large shell deformations at earth impact.

Figure 2 shows radial standoffs machined onto the outer surfaces of the containment shell and onto the insulation sleeves. Axial standoffs are located on the outer surfaces of the shell and the inner surfaces of the heat shield. By forcing gaps between the various internal components, these standoffs perform a vital function in the thermal design by further increasing the thermal resistance to heat flow into the shell (Fig. 3).

The increase in thermal resistance provided by the gaps is achieved because heat can cross a gap only by radiation. However, helium is generated continuously by the alpha decay of the  $^{238}\text{Pu}$  isotope, and under low-temperature storage or operating conditions, most of the helium is retained within the fuel lattice. Upon exposure to the reentry pulse, the stored helium is released from the fuel through the vent into the gaps. In addition, the Fine Weave Pierced Fabric<sup>TM</sup> aeroshell is a highly porous material that allows the passage of gases into and out of the gaps. To account for this gas flow, a computer program was developed to estimate the inventory of the gases in the gaps so that the gas thermal conductivity could be coupled with the thermal response code. An initial small amount of helium in the gaps is assumed. On the basis of experimental data that define the rates of helium release from the fuel, the procedure evaluates the rate at which the helium is released from the fuel lattice into the capsule. The release rate depends on the temperature of the fuel. The passage of air into the heat shield and the movement of the air/helium mix out of it were evaluated using experimental values for the porosity of the material, the local temperature, and the pressure gradient across the aeroshell. Tracking the flow of the gases in this manner allows the evaluation of the effective thermal conductivity of the gas in the gaps. The clad temperature history for the design reentry trajectory is shown in Fig. 3.

The primary purpose of this gas flow analysis was to estimate the LWRHU impact temperature in order to evaluate the impact test results. With this in

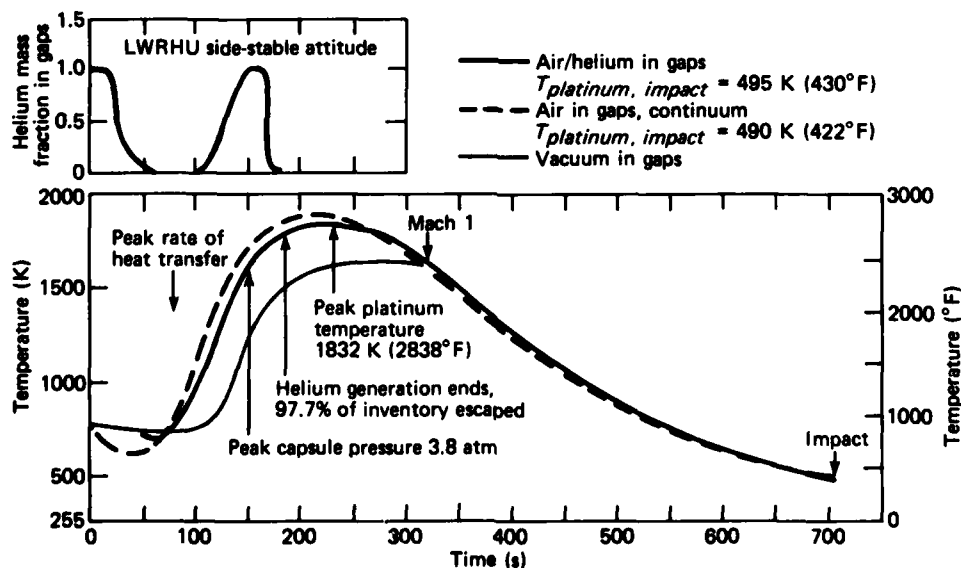


Figure 3 — The mass fraction of helium in gaps and the thermal response of the platinum container.

mind, the temperature results were derived using a two-dimensional thermal model of the LWRHU, rather than the three-dimensional model described in Fig. 1, to conserve computing costs. Impact tests at the predicted temperature indicated satisfactory performance.

The LWRHU developed under this program is now being fabricated by DOE for the Galileo mission to Jupiter, which will require more than 65 units.

---

This work was supported by the Department of Energy.

## SEARCH AND RESCUE SATELLITE PROGRAM

A. Eisner and J. B. Moffett

*APL has prepared a program plan for an operational Search and Rescue Satellite system to locate victims of shipwrecks and air crashes. Features of the system include long operational life (seven years), global coverage, and a maximum "wait time" of two to four hours.*

### BACKGROUND

Accident-activated rescue beacons have come into use over the past decade. In the United States alone there are 200,000 on aircraft and 6000 on ships. Those beacons, which transmit on a frequency of 121.5/243.0 MHz, originally had the dual function of alerting anyone who listened and of helping rescue forces locate the distress site. To expand the coverage of the beacon signals, an experimental, satellite-aided COSPAS-SARSAT project has been under development by the United States, Canada, France, and the U.S.S.R. for nearly a decade. (COSPAS stands for Cosmicheskaya System Poiska Avariynch Sudov, or space system for search of vessels in distress. SARSAT stands for Search and Rescue Satellite.) The project will demonstrate that the detection and location of the beacon distress signals can be enhanced greatly by a global monitoring system comprising low-altitude, near-polar-orbiting spacecraft. The project will use the American SARSAT (Tiros-N) and the Soviet COSPAS spacecraft. Each satellite will have SAR repeaters for relaying beacon distress signals to a ground-based station, or local user terminal, when the spacecraft is "in view" of both the beacon and the terminal. To demonstrate global capabilities (i.e., when the spacecraft is not in view of both the beacon and the terminal) the spacecraft will

carry a SAR processor/memory unit, which will receive, preprocess, digitize, and store signals from a more powerful, 406 MHz experimental rescue beacon for delayed transmission to a master control station.

The culmination of the COSPAS-SARSAT project will be the dedicated, fully operational SARSAT system. Under the sponsorship of NASA, the U.S. Coast Guard, and the U.S. Air Force, APL has prepared a program plan covering the analysis, configuration, specifications, cost, and implementation of the operational system.<sup>1</sup>

### DISCUSSION

#### The SARSAT Mission

The operational SARSAT system will more than satisfy the mission requirement<sup>2</sup> of alerting rescuers and estimating the location of activated rescue beacons in less than six hours. A constellation of four satellites (Fig. 1) is planned. They will be in circular orbits at about 1000 km altitude and inclined about 105°, with equally spaced nodal crossings. A network of terminals will support the constellation.

A four-satellite constellation ensures that the time required to locate the beacon signal will not be more than about four hours. The probability of being heard in less than two hours (one satellite revolution) will vary between 60% at the equator and 100% in the polar regions, if the beacon is in a region covered by a terminal. If it is not in such an area (e.g., it is in the broad oceans), data from the new (406 MHz) rescue beacons will be stored aboard a SARSAT for delayed

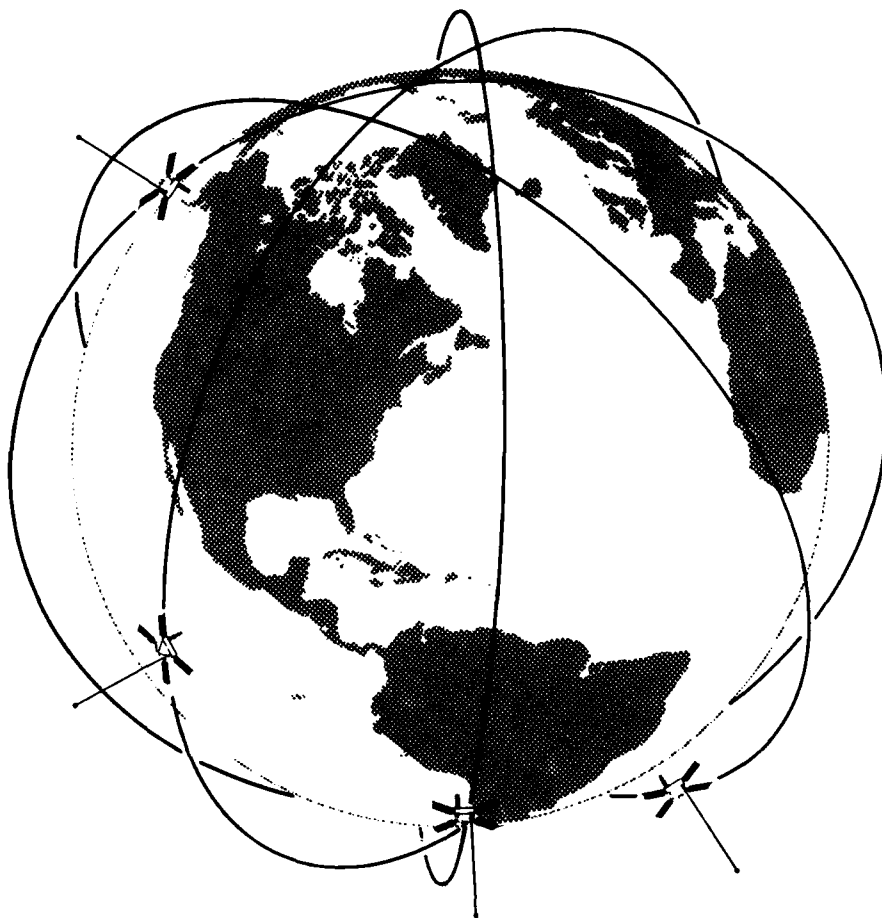


Figure 1 — The SARSAT constellation.

transmission to the next "visible" terminal. The additional time to generate an alert will depend on the number and distribution of terminals in the SARSAT system. A fifth satellite in the constellation would improve the coverage in both modes. The low power output of the existing beacons dictates the maximum useful beacon-to-SARSAT distance and constrains the maximum SARSAT altitude to about 1000 km.

The SARSAT program plan calls for four shuttle launches. A Payload Assist Module augmented with an on-board, hydrazine-fueled orbit adjust and transfer subsystem will lift the SARSAT from its shuttle transfer orbit to its final orbit in the constellation.

The analysis in Ref. 3 suggests that several different constellations of four or five satellites are acceptable. All are comparable in satisfying search and rescue requirements. The choice among these alternatives should come from other considerations, for

example, launch inclinations and the availability of shuttle launches at particular times.

### The Satellite

SARSAT (Fig. 2) will weigh nearly 700 lb and will occupy about five linear feet of the shuttle's cargo bay area. The spacecraft power system (125 W average) will consist of nickel-cadmium batteries charged by solar cells covering the surfaces of four solar panels. The thermal subsystem, consisting of heaters for the batteries and boom motors, louvers, and passive radiators, will dissipate 60 to 150 W of heat and maintain the spacecraft temperature in the range of 5 to 30°C. The satellite will be controlled with a VHF (148 to 149 MHz) command subsystem, operating in real-time and in delayed-execution modes, and an L-band (1544 to 1545 MHz) downlink telemetry subsystem. The command/telemetry subsystems will have their own antennas mounted on the solar panels. Redundant, motor-

ized booms and passive hysteresis energy dissipation will provide  $\pm 10^\circ$  pitch and roll (gravity-gradient) attitude control. To accomplish the necessary orbit adjustment maneuvers and the interim spin-stabilized mode, the spacecraft incorporates a hydrazine-fueled orbit adjust and transfer subsystem. A three-axis vector magnetom-

eter and spinning digital sun sensors provide the attitude determinations ( $\pm 2^\circ$ ) required for orbit adjustment maneuvers. All these subsystems support the SAR repeaters (the 121.5/243 and 406 MHz uplink antennas, the receivers, and the 1544.5 MHz downlink transmitter and antenna) and the (406 MHz) SAR Processor/Memory Unit.

## The Ground System

The SARSAT ground system is constructed around a network of sponsor-supplied local user terminals. A master control station at one terminal will contain the necessary equipment to perform routine SARSAT command and telemetry operations. It will also be the communication center for the ground-based network of terminals; it will collect Doppler data, update SARSAT orbits, and transmit orbit information to the remote terminals. Each terminal in the network (including the master control station) will collect and process real-time beacon signals whenever both an activated beacon and a terminal are in view of a SARSAT. In addition, each terminal will process the global mode (406 MHz) stored data. The transfer of data from the SAR Processor/Memory Unit will take place at the master control station and at the remote terminals. In the latter case, the master control station will load the satellite memory with delayed-execution data transfer commands.

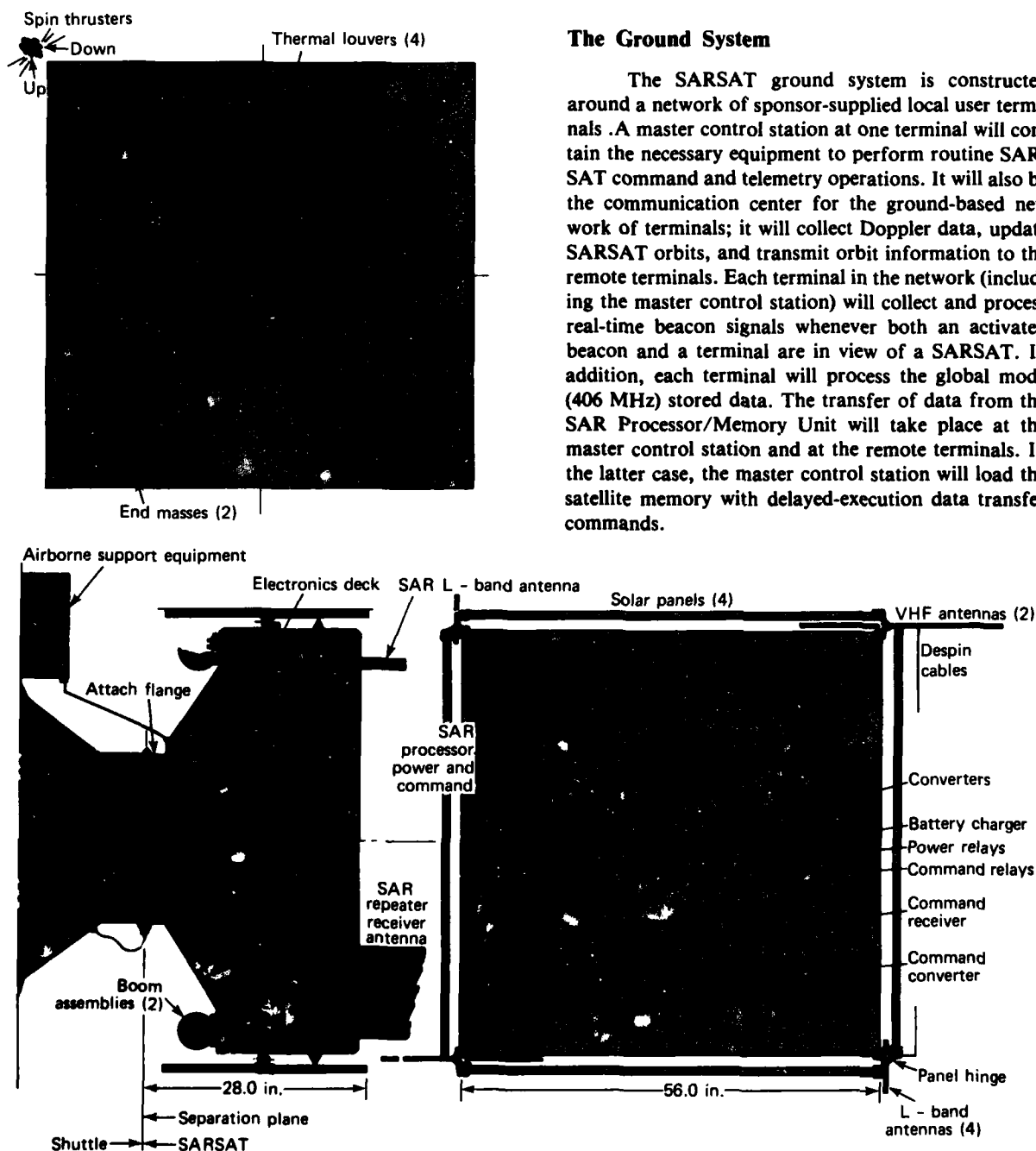


Figure 2 — The SARSAT configuration.

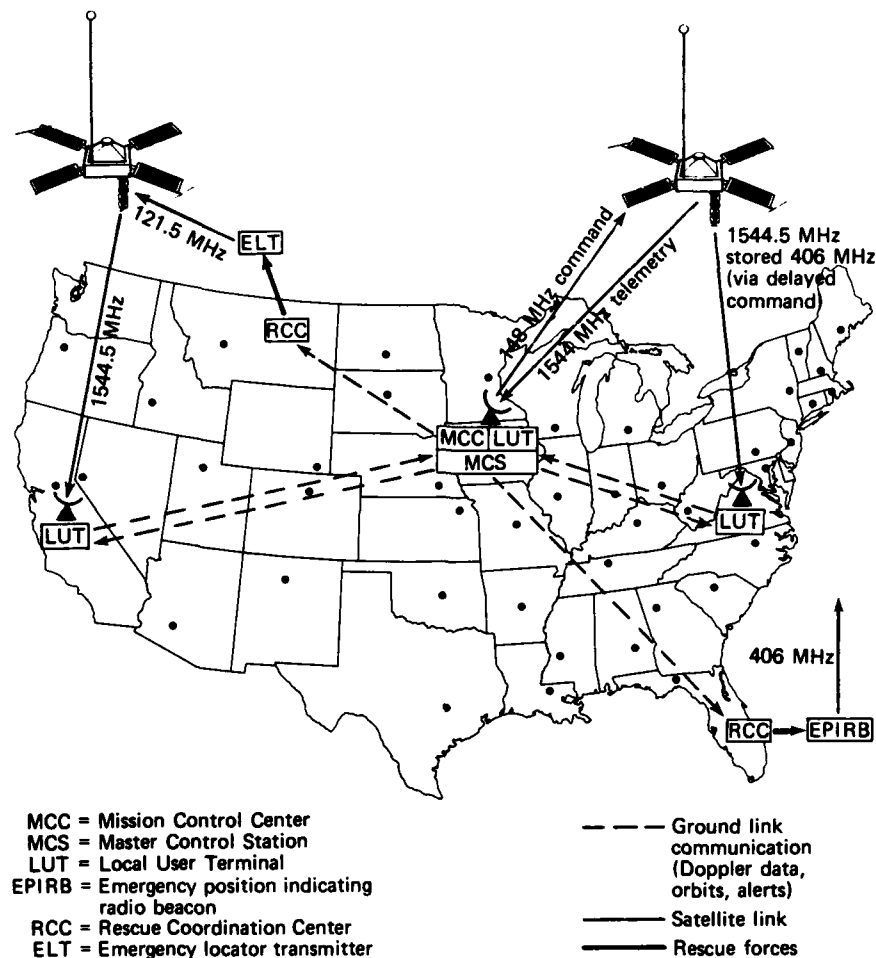


Figure 3 — The conceptual ground system for SARSAT.

Figure 3 illustrates a ground tracking system in the continental United States composed of three terminals. The master control station is in the same complex as the mission control center. The scenario illustrated includes two SARSAT's, one downed rescue beacon in Canada, and a downed (experimental 406 MHz) rescue beacon in the Atlantic Ocean. SARSAT-A is in view of the east coast terminal and is transmitting the stored data (via delayed commands from the master control station) collected during an earlier transit over the downed beacon. The station is performing routine command/control on SARSAT-A. SARSAT-B is relaying (in real time) the 121.5 MHz signal from the downed rescue beacon to the west coast terminal. The terminals send the alerts and the Doppler data (dashed lines) to the master control station/mission control center. The mission control center alerts the appropriate rescue coordination center to start operations. Having collected sufficient Doppler data for SARSAT-A, the master

control station computes new orbit parameters and transmits the updated orbit to the terminals (dashed lines).

#### ACKNOWLEDGMENT

APL participants in the SARSAT program are: W. E. Allen (power subsystem), H. D. Black (mission analysis), A. Eisner (technical coordination/mission analysis/system summary), H. G. Fox (mechanical structure), A. L. Lew (command/telemetry), F. F. Mobley (orbit adjust and transfer subsystem/attitude subsystem), J. B. Moffett (editor), J. Nagrant (power/thermal/payload), P. E. Partridge (reliability and quality assurance), V. L. Pisacane (system consultant), K. A. Potocki (system consultant), E. F. Prozeller (ground station), J. C. Ray (attitude subsystem), A. C. Reymann (mechanical structure), R. M. Rhue (command/telemetry), T. L. Roche (payload inte-

gration), J. F. Smola (orbit adjust and transfer subsystem), R. K. Stilwell (antennas), J. G. Wall (management plan/cost estimates), and C. A. Wingate (thermal subsystem).

## REFERENCES

<sup>1</sup>Space Department, *Search and Rescue Satellite*, JHU/APL SDO 6460.1-3 (Jun 1982).

<sup>2</sup>D. J. McKinnon, *SARSAT Summary*, Department of National Defence, Ottawa, Ontario (Jun 1981).

<sup>3</sup>H. D. Black, A. Eisner, and J. A. Platt, "Choosing a Satellite Constellation for the Search and Rescue Satellite System," to be presented at RTCM Assembly Meeting, Savannah, Ga. (18-20 Apr 1983).

This work was supported by NASA, the U.S. Coast Guard, and the U.S. Air Force.

## THE SATELLITE MISSILE TRACKING PROGRAM

T. Thompson and C. W. Meyrick

*The Satellite Missile Tracking Program is an instrumentation system to determine missile trajectories and identify sources of error. It was developed to support Trident missile flight tests. Trajectory determinations are made from radio frequency measurements between the test missile and satellites with precisely determined orbits. The system has been fully evaluated and, having met its objectives, is now used routinely to support accuracy evaluations.*

## BACKGROUND

The improved-accuracy Trident program, which followed Poseidon, required refinement in all areas of test and evaluation to ensure missile system capability. The Satellite Missile Tracking (SATRACK) system provides both instrumentation and analytical improvements for the evaluation of test flight accuracy.

The SATRACK measurement concept is illustrated in Fig. 1. Radio frequency transmissions from the Department of Defense Global Positioning System (GPS) satellites are relayed by the missile to data collection equipment on the launch-area support ship and the down-range support ship. The ships also receive and record missile telemetry data and act as centers to support range safety.

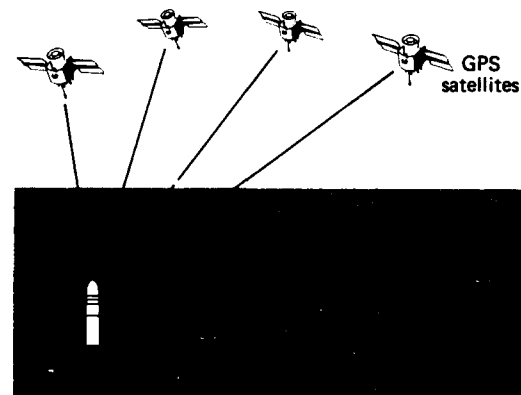


Figure 1 — The SATRACK measurement concept.

GPS transmissions provide a basis for distance and velocity measurements along the paths between the test missile and each in-view satellite. Four in-view satellites form the base of an inverted pyramid (the satellites are at an altitude of approximately 11,000 mi) and the missile is instantaneously at the apex. Because the positions of the satellites (at the four corners of the base of the pyramid) are known, the position of the missile at any instant can be determined from the measured distance along each of the four satellite-to-missile paths. Similarly, a measurement of the velocity along each

path provides a basis for determining the missile velocity at any point in the flight trajectory.

Distance and velocity are not directly measurable with radio transmissions. Radio distance is usually measured by transmitting a pulse of radio energy and then listening for the return. The time between transmission and receipt is then converted into distance through knowledge of the propagation velocity of the pulse signal. This, of course, is the standard radar technique. One important difference between radar methods and GPS positioning is that the GPS measurements are not based on two-way transmissions. Each satellite transmits the equivalent of a pulse signal, and the time of receipt of each pulse can be identified on the missile "clock." Although the GPS is responsible for maintaining a common clock (i.e., synchronization of all satellite transmissions), there is no way for the missile clock to be synchronized precisely with the satellite clocks. Therefore, receipt time is not directly convertible to distance because the assumed transmission time indicated by the missile clock is usually in error. For this reason, signals from four satellites are needed in order to determine the three components of position. The four distance measurements to the four in-view satellites provide the data necessary to determine the three components of position and the clock error. An equivalent result is achieved by determining the differences in the time-of-arrival measurements for each of three independent satellite measurement pairs. This method removes the missile clock error from the missile position computation and is the one actually used in SATRACK.

To simplify the missile hardware, the SATRACK system is based on relaying satellite signals to the two support ships (see Fig. 1). The signals from GPS received at the missile are converted to a different output frequency and are retransmitted to the support ships. Therefore, the signals received at the ships have added propagation delays arising from the characteristics of the missile hardware and the missile-to-ship transmission path. However, when time-of-arrival differences among the satellite signal arrival times are determined relative to the ship clock, all delays beyond the missile GPS antennas (being common to all transmissions) are removed by the computation, greatly simplifying the processing system.

The process of recovering the measurement data for missile trajectory determination is not actually accomplished on the support ships. Again in the interest of simplicity, the ships are equipped with a single receiver and wideband recorder that recover all the GPS satellite signals simultaneously without separating or making detailed measurements of them. The process of recovering signal data, referred to as signal tracking, is

accomplished at an APL processing center by replaying the tapes recorded on the support ships.

After the tracking data are recovered, corrections are applied, including those for the estimated effects of transmission through the ionosphere and troposphere, for antenna interferometry and offset (i.e., displacement of antennas from the guidance reference position), and for relativity. The corrected tracking data are passed to the final postflight data processor (Fig. 2) where the satellite-to-satellite differences are formed and used to estimate the missile trajectory.

The measurement of a missile trajectory is not the end objective of SATRACK. Using information from the submarine navigation and fire control systems and its own guidance system, the missile is operating relative to its internal trajectory estimates. Therefore, the external trajectory measurements provide insights into weapon performance.

The SATRACK processing concept uses a traditional filtering technique, as shown in Fig. 2. The missile guidance model begins with an initial estimate of its guidance parameters, the uncertainty in those parameters, and an estimate of the missile initial conditions. Using those data and the missile accelerometer measurements (recovered by telemetry), the model for missile motion predicts the new velocity and position of the

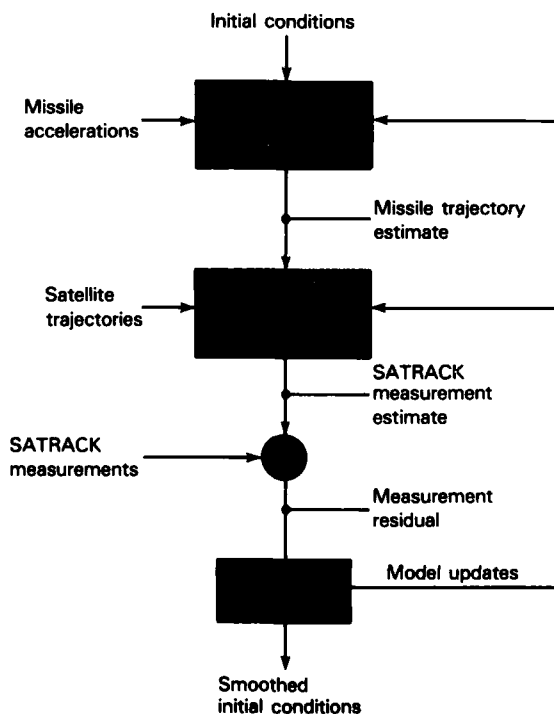


Figure 2 — The SATRACK processing concept.

missile (i.e., its trajectory). The predicted missile trajectory and the satellite trajectories are used to compute the expected SATRACK measurement data for the corresponding interval. The estimated and measured data are then compared and the difference (the residual) is available to the filter. The filter acts on the residuals to make adjustments to the model parameters and to refine the initial conditions in order to reduce subsequent residuals. This may be recognized as a normal Kalman filter process, but the actual process used for SATRACK was modified so that updates of all model parameters were not attempted (e.g., satellite ephemeris errors are normally not updated). At the completion of data processing, there is a refined estimate of all model parameters and a refined estimate of missile initial conditions.

The primary product of the processing is an estimate of the contribution of individual error sources to the total weapon system impact error for each flight.

Figure 3 illustrates the method commonly used to summarize SATRACK error estimates. The origin of the cross-range and down-range miss axis represents the missile aim point. The various error contributors are represented by vectors. For example, the miss contribution allocated by the SATRACK system to the initial condition error of the launch platform (the submarine) is shown as the vector from the origin to the upper left quadrant. The components of this vector are estimates of the position, velocity, and orientation errors of the submarine. The uncertainty in that estimate is indicated by the uncertainty ellipse at the head of the vector.

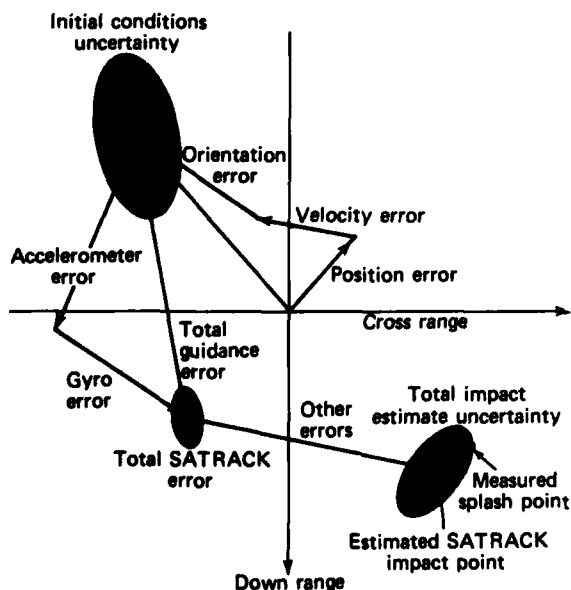


Figure 3 — Hypothetical SATRACK test results.

Similarly, the total guidance error estimate is the vector sum of accelerometer and gyro error components. The other vector as shown includes measurements of reentry and deployment made by a system separate from SATRACK. When all the error vectors are added, the result is the total miss and a projection of SATRACK estimates to the impact point. The impact point is also measured independently by a splash detection system; a comparison with that measurement tests the consistency of the SATRACK process.

## EXPERIENCE WITH SYSTEM USE

As experience was gained with SATRACK, data processing efficiency improved and a greater understanding of system errors was achieved. Two items of particular concern at the onset were the accuracy of the GPS satellite ephemeris and clock information, and the accuracy of the estimates to correct for the effects of transmission through the ionosphere.

A "static missile" test is conducted as part of every Trident missile test. It consists of recording the GPS satellite signals received by a stationary antenna located at APL and processed through hardware that simulates the translator in the missile and the recording equipment on the support ships. The signals are processed similarly to the actual flight test data. However, the location of the antenna (the static missile) is known in this case, and thus any motion of the missile or variance in position indicated by the data is the result of system errors. The principal errors are in the ephemeris and clock data for the GPS satellites and in the estimate of corrections to compensate for the effects of transmission through the ionosphere. The results from 20 tests, shown in Table 1, are consistent and indicate that the ephemeris and clock data are accurate enough to meet the operational SATRACK system requirements specified for Trident I tests.

The main source of error in the operational SATRACK system is the result of having to estimate corrections to compensate for the effects of transmission through the ionosphere because of being limited to the single frequency used by the GPS satellites. Two-frequency data available for the transmissions from the pseudosatellite transmitters located on the ground can be used to measure the ionospheric effects in the path from the pseudosatellite to the missile; however, that path traverses a different portion of the ionosphere than do the transmissions from the GPS satellites; therefore, it is necessary to use a model of the ionosphere to calculate the corrections for the latter signals.

The model is normally fit with the two-frequency data from the pseudosatellite transmissions. Early in

**Table 1 — Results of SATRACK static missile tests.**

Range Residual (ft)	Range Rate Residual (ft/s $\times 10^{-4}$ )
3.1	59
21.5	16
16.1	21
12.9	48
15.8	11
17.3	15
18.2	7
13.0	28
17.0	58
17.9	26
18.9	36
33.3	29
27.6	14
11.1	11
8.1	11
29.4	49
18.7	73
22.1	28
22.6	28
26.1	48
Mean	31
Std. deviation	56

the development of the SATRACK system, it was decided that a sophisticated model of the ionosphere should be used in order to minimize error. Simplified models were tried, and the results showed that a properly employed, simple, spherically symmetrical model gave comparable results for SATRACK purposes. Figure 4 shows examples of the ionospheric corrections calculated at the L1 frequency for the same signals using the sophisticated and the simple, spherically symmetrical ionospheric models. From an overall system standpoint, the estimated corrections for the effects of transmission through the ionosphere remain the largest source of error and will likely remain so until two frequencies are used. The use of two frequencies will allow ionospheric effects to be calculated on the basis of data from the actual transmission paths.

## SYSTEM PERFORMANCE

Table 2 summarizes the trajectory measurement uncertainties that have been estimated for all flights processed or reprocessed by SATRACK through April 1981. The uncertainties are given as three-dimensional values (i.e., the root sum square (rss) of the position and velocity uncertainties along three orthogonal axes) estimated at reentry body deployment (i.e., separation from the missile control section). The original goal for a SATRACK trajectory estimation was 40 ft and 0.05 ft/s along each axis, resulting in an rss of 69 ft and 0.087 ft/s. The mean values for the 20 flights are 35 ft and 0.089 ft/s.

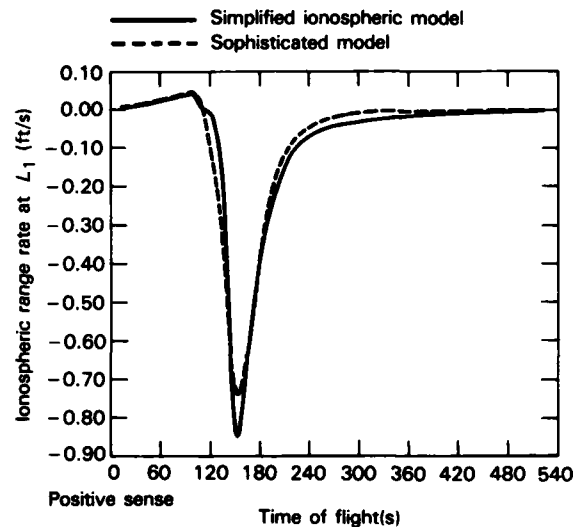


**Figure 4 — Comparison of atmospheric corrections calculated with the sophisticated and the simple ionospheric models.**

**Table 2 — SATRACK trajectory measurement characteristics at deployment.**

Test Date	3D Velocity (ft/s)	3D Position (ft)
Aug 1979	0.099	38
Dec 1979	0.092	40
Feb 1980-1	0.110	40
Feb 1980-2	0.087	32
Feb 1980-3	0.090	28
Feb 1980-4	0.086	29
Mar 1980	0.090	32
Apr 1980-1	0.089	36
Apr 1980-2	0.085	36
May 1980-1	0.090	41
May 1980-2	0.088	38
May 1980-3	0.086	37
Jun 1980-1	0.086	31
Jun 1980-2	0.084	35
Jun 1980-3	0.084	33
Jun 1980-4	0.089	32
Jul 1980	0.071	36
Aug 1980	0.089	34
Oct 1980	0.087	29
Apr 1981	0.091	41

The values for trajectory uncertainties shown in Table 2 are internal processor estimates; they reflect the state of understanding of the measurement system represented by the mathematical model. An independent assessment of the uncertainties can be inferred from the impact difference measurements used for consistency testing (Fig. 3). Table 3 summarizes the down-range and cross-range differences between the independent measurement of splash point and the SATRACK projected values for all the flights given in Table 2. The

**Table 3 — Normalized splash consistency differences.**

Test Date	Down Range	Cross Range
Aug 1979	-1.46	-0.09
Dec 1979	-0.47	0.97
Feb 1980-1	-0.15	-1.05
Feb 1980-2	-1.78	0.00
Feb 1980-3	0.42	-0.78
Feb 1980-4	0.26	-1.31
Mar 1980	0.47	0.30
Apr 1980-1	0.86	-0.08
Apr 1980-2	1.63	0.61
May 1980-1	1.08	-0.68
May 1980-2	-0.94	-1.27
May 1980-3	1.21	-0.18
Jun 1980-1	-0.05	-0.80
Jun 1980-2	0.78	0.25
Jun 1980-3	0.31	0.15
Jun 1980-4	0.47	1.50
Jul 1980	0.98	-0.08
Aug 1980	-0.84	-1.03
Oct 1980	1.68	1.17
Apr 1981	-0.99	-0.42
Mean	0.17	-0.14
Std. deviation	0.99	0.80

numbers are normalized with respect to the uncertainty in the difference measurement; that is, unity identifies a distance between the two measurements that is exactly equal to the estimated uncertainty in determining that difference. To project SATRACK measurements to impact, errors in deployment and reentry with their corresponding uncertainties are provided from a separate measurement and analysis. Uncertainty in the impact difference includes the total SATRACK uncertainty, the deployment and reentry uncertainty, and the uncertainty in making the independent splash measurement. Although the differences between the impact measurements show a small bias, the level is not statistically significant for the sample size. On the basis of the near-

zero mean and the near-unity standard deviation of the consistency data, the estimates of trajectory uncertainty (Table 2) are consistent with the independent impact measurements.

## CONCLUSIONS

Before SATRACK was developed, the determination of a missile trajectory from satellite-based measurements had never been demonstrated. The SATRACK effort was constrained to use a poor missile antenna and low GPS satellite signal levels. Those factors required the use of the unique postflight receiver technique. The signal tracking processes were analytically sound, but there was little margin for error. However, SATRACK fully demonstrated the unique signal tracking technique and provided the first precision missile tracking demonstration from satellite measurements.

SATRACK provides a useful test capability for the Trident I missile. It has fully met its performance goals and has provided the groundwork for the next-generation accuracy evaluation system.

## ACKNOWLEDGMENT

The authors wish to acknowledge D. Duven, J. Vetter, M. Feen, and S. Deines who assembled the material for this article.

---

This work was supported by the Strategic Systems Projects Office, SP-25.



## **OCEAN SCIENCE AND TECHNOLOGY**

## INTRODUCTION

The studies of the oceans and the technologies related thereto are legion. Here at the Laboratory, the particular ocean studies are principally those that relate to or derive from the temporal and spatial characteristics of the physical properties and processes of the waters in their natural state and, often, as altered by mechanisms of man. As would be expected, almost all such explorations are linked, more or less closely, with Laboratory efforts to bring the understanding gained to bear on a practical problem under consideration or investigation.

In the field of ocean-related technology, the Laboratory identifies or, more often, develops and then applies advanced techniques that offer promise of accomplishing a particular task, defining a technical issue, or resolving a technical uncertainty. The range of these technological efforts at APL is wide indeed: from the development of a tiny sensor that establishes a new capability for measuring a certain parameter of the ocean or extends an existing capability to new heights, to the specification of a massive system for converting to electrical energy the temperature difference between the depths and the surface of the ocean.

The prospect is that the Laboratory's work in these and other matters related to the earth's environment will grow as the thirst for knowledge in this field continues unslaked.

AD-A139 624

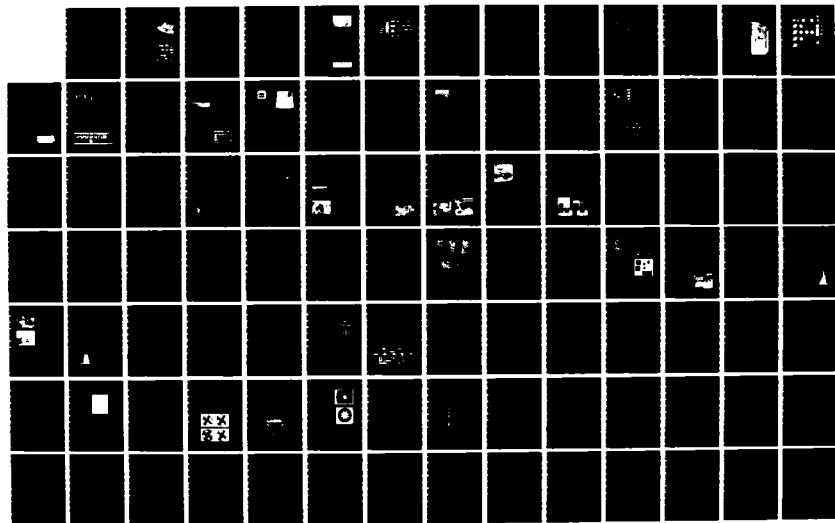
DEVELOPMENTS IN SCIENCE AND TECHNOLOGY(U) JOHNS HOPKINS  
UNIV LAUREL MD APPLIED PHYSICS LAB 1982 JHU/APL/DST-10  
N00024-83-C-5301

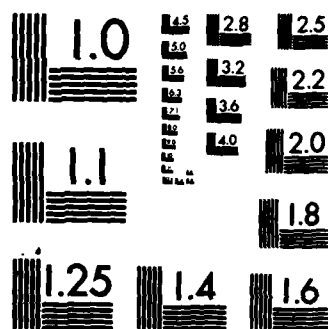
2/3

UNCLASSIFIED

F/G 14/2

NL





MICROCOPY RESOLUTION TEST CHART  
NATIONAL BUREAU OF STANDARDS-1963-A

## MINIATURE OCEANOGRAPHIC FLUOROMETER

A. B. Fraser and R. P. H. Lee

*Miniature fluorometers for sensing very dilute fluorescein tracer in the ocean were developed and tested. Sensitivities (expressed as the rms noise equivalent weight fraction of dye in the water) of  $3 \times 10^{-11}$  in a 0- to 2-Hz passband and baseline drift on the order of  $1 \times 10^{-11}$  per hour were achieved.*

### BACKGROUND

Fluorescent tracers are well known marking substances used in the study of motions and mixing of water masses.<sup>1</sup> Sodium fluorescein dye is inexpensive, is water-soluble, and provides a brilliant green-yellow fluorescence. Most fluorescent tracer studies are performed by a laboratory analysis of water samples. Specialized submersible and towable fluorometers have been developed for cases where large amounts of real-time data are required to describe oceanic masses.<sup>2</sup> The fluorometers reported in this article suit a particular need for a very small fluorometer for the highly sensitive, *in situ* oceanographic determination of fluorescence. The "in-fairing" fluorometers are but slightly larger than one unit of the oceanographic chain fairings that APL usually uses on its oceanographic research chains. The fluorometers are 0.77 in. thick, 4 in. high, and 4 in. long (about 2 by 10 by 10 cm), with 1 in. projections above and below the trailing edges. Figure 1 shows a fluorometer with the cover removed. The form of the fluorometer housings resembles that of the normal oceanographic chain fairing units closely enough for them to roll through the automatic chain-handling hardware the same way that the fairings do. A fluorometer weighs 2 lb (0.9 kg).

### DISCUSSION

The major design features were modulated illumination of the water sample, synchronous detection of sensed light, normalization of measured fluorescence according to the brightness of the excitation, and miniaturization of all electronics and optics. Figure 2 is a block diagram of the fluorometer.

#### Electronics

All optical fluorometers must have a light source that illuminates a sample with short-wavelength light, a chamber to hold the sample, and a receiver that senses the light of longer wavelengths that the sample emits by

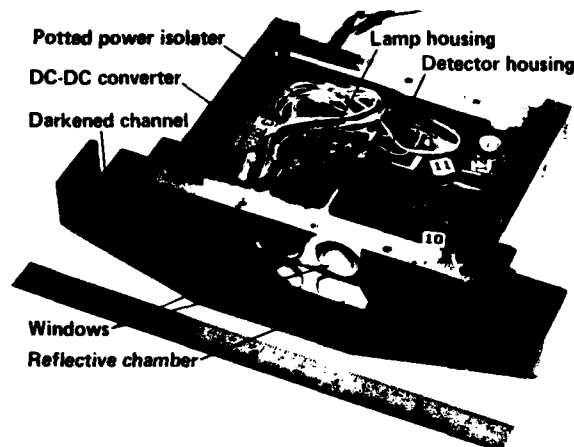


Figure 1 — The fluorometer with its cover removed.

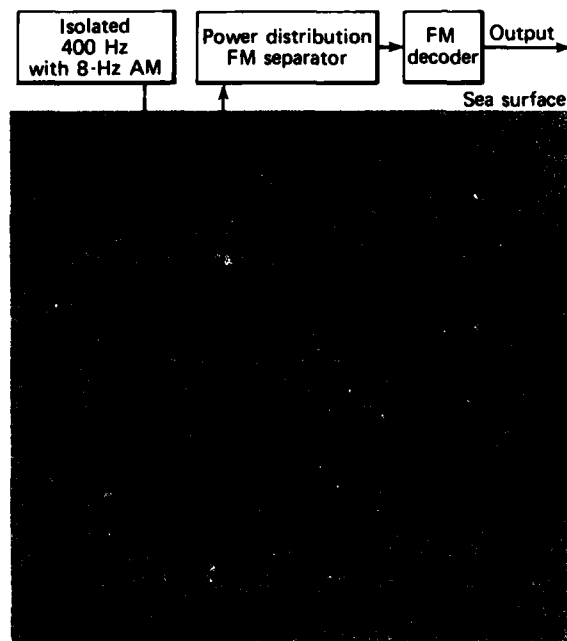


Figure 2 — Block diagram of the in-fairing fluorometer system.

fluorescent processes. Those assemblies appear just above the lower left corner of Fig. 2.

One of the most significant system design features is the modulated current source drive for the halo-

gen lamp that provides the illumination. A 400-Hz carrier is multiplied by an 8-Hz sinewave. The brightness of the lamp flickers at 16 Hz in response to the 8-Hz modulation. Green fluorescence stimulated by the blue illumination flickers synchronously with the 16-Hz fluctuation in the excitation. A 16-Hz, fourth-order band-pass amplifier is used to amplify the photoelectric signals generated by the green fluorescent light in the photodetector. The 16-Hz amplified AC signal representing fluorescence is entered at the numerator port in a divider circuit. The divider circuit normalizes the numerator signal, dividing it by a DC level that is proportional to the average fluctuating blue brightness from the lamp. The rectifier that provides the normalizing signal also produces a square-wave synchronizing signal that is in phase with the 16-Hz lamp brightness. Those circuits appear across the bottom of Fig. 2. Normalization with the slowly changing lamp brightness provides a time-invariant instrument calibration factor and minimizes baseline drift.

Because the frequency and phase of all signals of fluorescent origin are known, the noise at the system output can be reduced greatly by maximizing the contribution to the final output of in-phase, 16-Hz signals and by minimizing the contributions to the output by all other signals. A synchronous rectifier (or a synchronous detector), at the right near the bottom of Fig. 2, provides the desired high sensitivity to the 16-Hz signals and minimizes interfering noise. The greatest advantage of the synchronous rectification technique is its suppression of large system noises and "drift" near zero frequency. The output of the synchronous rectifier is low-pass filtered to match the system's electrical bandwidth (which is set by the fluid flow in the sample chamber) and to remove the 32-Hz ripple from the synchronous rectifier.

A linear signal proportional to fluorescence is provided at the output of the low-pass filter following the synchronous rectifier. It is converted to a 50%-duty-factor, square-wave FM signal by a voltage-to-frequency converter. The square-wave FM signal modulates, by means of an optical isolator, the DC current drawn by the fluorometer. Those blocks appear near the middle of Fig. 2. The FM signal is stripped from the supply current by on-ship instrumentation, and a linear frequency-to-voltage converter provides analog signals to the users.

### Optical Design

The most important parts of the optical design are the lamp, its blue exciter filter, the chamber for the water with fluorescent dye, the green barrier filter, and the photodetector. The small tungsten halogen lamp has

high blue brightness. A filter consisting of dye and interference components allows only the blue wavelengths of the lamp's light to pass to the water sample.

The sample chamber has an unusual design. It is lined with a chromium-plated reflector that causes the blue exciting light to pass through the sample several times before being lost through absorption or by passing into the inlet or outlet passageways. The reflecting chamber also reflects green fluorescent emissions several times before they are lost. These reflections increase the fraction of emitted fluorescent green light that eventually strikes the photodetector aperture.

Green light of fluorescent origin in the sample chamber strikes the barrier filter that is in front of the detector. The barrier filter consists of yellow and green dyed plastic sheets. The dye filters cause especially high rejection of blue light at the low angles of incidence of most of the blue excitation. The orange-red rejection of the dye filters also prevents the fluorometer from having an appreciable undesired sensitivity to rhodamine, which is often used in conjunction with fluorescein in sea tests.

The photodetectors are gallium arsenide phosphide (GaAsP) semiconductor photodiodes. They are highly sensitive to light from the ultraviolet region up to the far visible red, but they do not respond to infrared wavelengths. The insensitivity to infrared light simplified the filter design, and the GaAsP sensors have proved to be very stable and sensitive.

### Field Results

Several in-fairing fluorometers were tested at sea. Two were different from the above description but only in minor details. In the sea tests, fluorescein dye was ejected along a vertical line that was towed horizontally through the Gulf Stream. The result was a "sheet" of dye that diffused and sheared in the ocean. Figure 3 shows a typical traversal of such a dye sheet by two in-fairing fluorometers. The calibration factors for time, space, and dye concentration are shown in Fig. 3. Shearing of about 15-m occurred over the 14-m vertical distance between the two fluorometers.

The rms noise on each fluorometer was estimated to be a  $3 \times 10^{-11}$  dye fraction. Drift is very difficult to measure; it was estimated at no more than  $1 \times 10^{-11}$  per hour. Noise levels were the same in the laboratory and at sea. Five units were calibrated precisely in the laboratory; the calibration range was  $3 \times 10^{-11}$  to  $1 \times 10^{-7}$ , and the calibration curve was highly linear. While this article was being prepared, the in-fairing fluorometers completed their third and fourth successful at-sea tests.

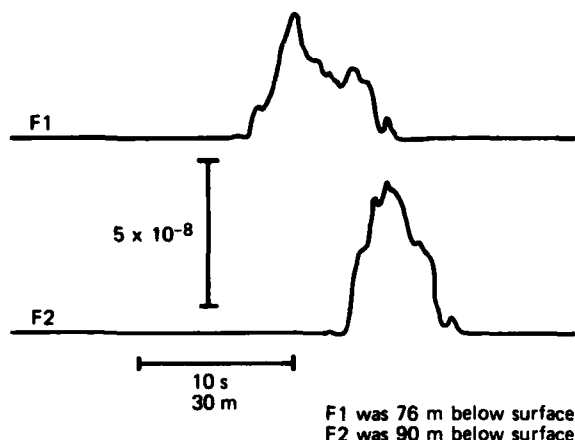


Figure 3 — Sheared dye as indicated by a pair of in-fairing fluorometers.

## ACKNOWLEDGMENTS

C. D. Mitchell of APL is especially cited for his excellent machine tool work that extended over hundreds of hours and all phases of fabrication. Many other co-workers contributed vital ideas and efforts; their contributions are much appreciated.

## REFERENCES

- <sup>1</sup> J. F. Wilson, Jr., *Techniques of Water-Resources Investigations of the United States Geological Survey, Book 3, Applications of Hydraulics*, U.S. Government Printing Office, Washington (1968).
- <sup>2</sup> G. S. Keys and B. F. Hochheimer, "The Design of a Simple Fluorometer for Underwater Detection of Rhodamine Dye," *Sea Tech.* 18 (Sep 1977).

This work was supported by the Strategic Systems Projects Office.

## A HELICOPTER-DEPLOYABLE INSTRUMENTED SPAR BUOY FOR OCEAN HEAT FLUX MEASUREMENTS

C. V. Nelson and R. G. Chappell

*A large, instrumented spar buoy has been developed by APL to obtain meteorological data at sea. A data acquisition system on the buoy records and transmits the environmental data to a remote receiving station for processing and recording. The buoy was deployed by helicopter and moored in the Tongue of the Ocean in the Bahamas for six days in January 1982 to monitor the ocean/air heat flux continuously during an oceanographic experiment.*

## BACKGROUND

Energy and momentum exchanges between the ocean and the atmosphere strongly influence the weather, the sea state, and the character of the mixed layer of the ocean. It is known, for example, that sea-surface temperature changes, which communicate with the atmosphere via ocean-air heat fluxes, can give rise to weather pattern anomalies, hurricanes, and long-term

climatic changes. Seasonal variations in the depths of the upper-ocean mixed layer occur largely in response to changes in the surface heat and momentum fluxes.

Accurate measurement of the surface heat flux is needed to support efforts in these and other areas of oceanographic research. The fluxes of interest are the sensible, evaporative, and radiative ones. The simplest and most convenient way to estimate sensible and evaporative heat fluxes at sea is to make use of the bulk aerodynamic method, by which the fluxes are calculated from meteorological measurements using parameterized formulas. The radiative flux can be measured directly by net radiometers.

To measure the needed meteorological and oceanographic parameters accurately at sea is a challenging task. Measurements from ships are infrequent and are limited in duration by ship operating costs. In addition, the measurements can become severely contaminated by the presence of the ship. To overcome

these problems, APL designed, built, and tested an easily deployed, instrumented spar buoy for meteorological measurements at sea.

## DISCUSSION

The spar buoy is designed to be a stable platform for open-ocean meteorological measurements. It is instrumented to measure

- Air temperature
- True wind speed and direction
- Net radiation (0.2 to 3.0  $\mu\text{m}$  and 0.2 to 60  $\mu\text{m}$ )
- Relative humidity
- Surface water temperature

Sensor data are recorded by an on-board magnetic tape recorder and are transmitted to a remote receiving station by a VHF telemetry system.

Figure 1 shows the buoy being deployed by the helicopter. The buoy is approximately 20 m long and weighs about 1900 kg with the virtual mass chamber attached. The main structure consists of a triangular arrangement of aluminum tubes, 10 cm in diameter, mounted on 61 cm centers. Buoyancy is provided by six air-filled aluminum chambers. The meteorological sensors are located approximately 6 m above the mean water line. Ballast weights and a battery pack are located at one end of the buoy to provide the proper righting moment for stable operation in seas up to state 3+. Additional stability is provided by a virtual mass chamber suspended below the buoy.

Two booms at the top of the buoy hold the wind instruments 1 m away from the main buoy structure. This arrangement ensures that one of the wind sensors is always upwind of the main structure. A third identical boom holds the two net radiometers away from the main structure to minimize the amount of buoy structure in their field of view. The sensors for air temperature and relative humidity are located within a naturally aspirated radiation shelter mounted below the top plate of the buoy. A water temperature thermistor is mounted on the buoy approximately 3 m below the water line.

The sensor electronics and data acquisition system are in a water-resistant housing approximately 4.6 m above the water line. A radar reflector and xenon flash lamp are located above the electronics housing.

Figure 2 is a schematic diagram of the sensor electronics and data acquisition system. The sensor electronics consists of bridge circuits for the thermistor and relative humidity sensors, instrumentation amplifiers for the net radiometers, and frequency-to-

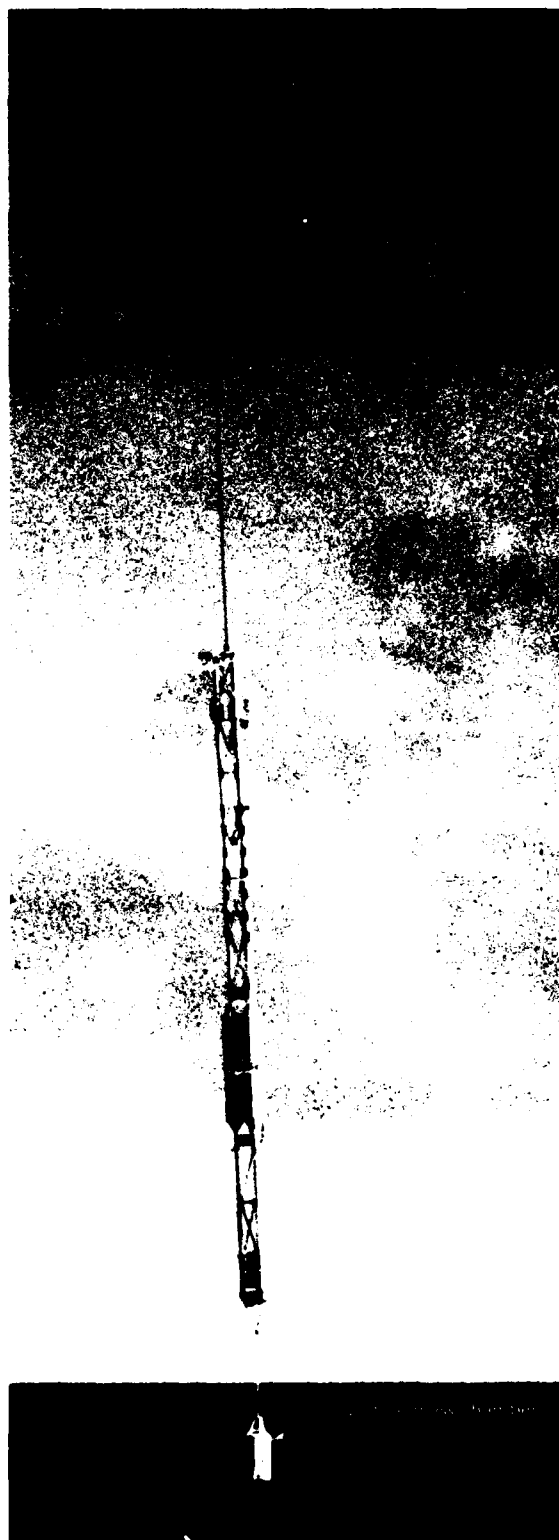


Figure 1 — Helicopter deployment of the spar buoy.

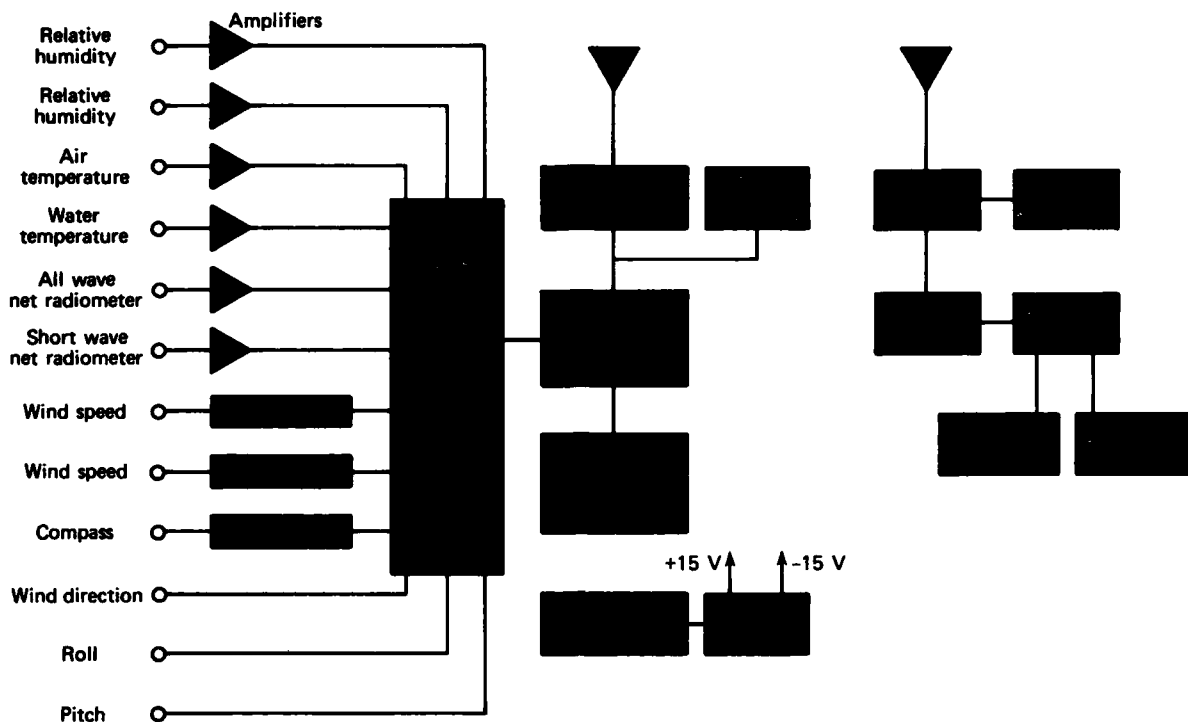


Figure 2 — Electronics for the sensors and data acquisition system.

voltage (F/V) converters for the wind-speed sensors. A low-power, microprocessor-based data acquisition system is used to sample the sensors once per second and to average the readings for 1 min before the data are transmitted to the remote receiving station. The internal tape recorder records hourly average readings.

The major components of the data acquisition system include a CMOS microcomputer, a CMOS 12-bit analog-to-digital converter, a 16-channel analog multiplexer, a time-code generator, a frequency-shift keying circuit, a 5-W, 168.5-MHz transmitter, and a miniature cassette tape recorder.

Primary power for the electronics is provided by three commercial, 12-V, lead-acid batteries connected in parallel. The battery capacity allows the system to operate for a minimum of 10 days without recharging.

The remote receiving station includes a 168.5-MHz receiver, an analog tape recorder, a serial interface, a desk-top computer, a line printer, and an X-Y plotter. The analog recorder records the raw data from the FM telemetry receiver and serves as a backup to the computer system. The serial interface demodulates the FM data and provides a serial data stream to the computer. The data are stored by the computer on magnetic tape and displayed on the line printer and

plotter in real time. Twelve hours of 1-min-averaged data are stored on each tape.

The deployment and recovery of a large buoy are difficult tasks that commonly require a large surface vessel outfitted with appropriate handling equipment. A ship of this type was not available to support the experiment for which this buoy was designed. Moreover, schedule constraints prevented us from waiting for calm seas in order to not damage the delicate instruments during deployment from a small vessel. To overcome these problems, we designed the buoy to be deployed and recovered by helicopter. Figure 1 shows the helicopter in process of executing this unique and extremely simple deployment. Both deployment and recovery were effected without incident.

The field test of the buoy was conducted in January 1982 in the Tongue of the Ocean; six days of continuous data were recorded. Figure 3 shows the ocean/air heat flux for a three-day interval when a cold front moved through the area. A large change in heat flux results in substantial cooling of the upper ocean. The ability to deploy instrumentation of this type readily is extremely valuable for studying this and other air/sea interaction processes when time series information is needed.

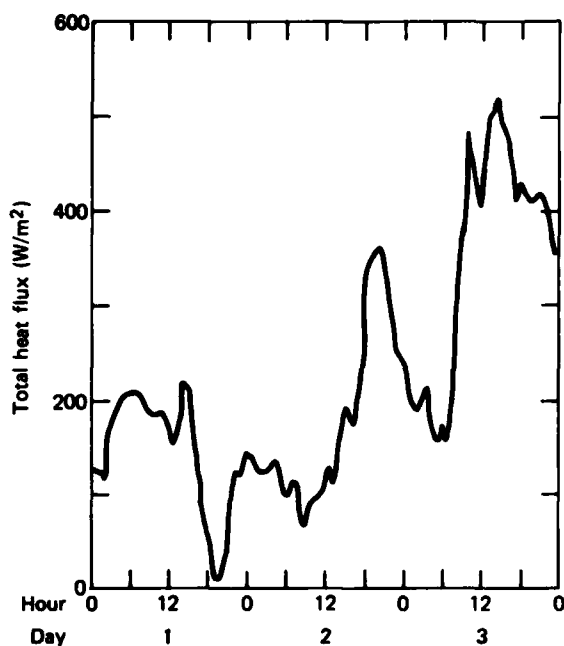


**Figure 3** — Ocean/air heat flux estimated from the spar buoy measurements.

#### ACKNOWLEDGMENT

The following people contributed to the development of this buoy: W. A. Venezia (General Offshore Corp.) and J. F. George, C. W. Anderson, J. R. Kime, V. Del Guercio, J. B. Allison, and J. Clinedinst (APL).

#### REFERENCE

<sup>1</sup> C. V. Nelson, *Standard Krypton Meteorological Measurements*, JHU/APL STD-R-688 (Sep 1982).

This work was supported by the Strategic Systems Projects Office.

# A SHIPBOARD REAL-TIME DATA ACQUISITION AND DISPLAY SYSTEM FOR OCEANOGRAPHIC MEASUREMENTS

R. E. Ball, J. E. Coolahan, V. Vigliotti, and R. F. Cohn

*A data acquisition and display system that features a signal correlator to aid in the real-time identification of oceanographic phenomena has been developed by the Ocean Data Acquisition Program Office of the APL Strategic Systems Department. The Minimal Installation Data Acquisition System-II also provides for the collection of a variety of ship system and oceanographic sensor data for posttest analysis.*

## BACKGROUND

The collection of oceanographic data is an ongoing APL task that has been at the heart of a number of controlled experiments over the last several years. In 1982, the Ocean Data Acquisition Program (ODAP) Office completed the development and shipboard installation of two Minimal Installation Data Acquisition Systems (MIDAS-II). A unique feature of the systems is a software module that correlates the outputs of multiple vertically spaced sensors in real time to aid system operators in the highly confident identification of oceanographic features. The systems were designed to acquire and record ship motion data and oceanographic sensor data for use in post-test laboratory analysis and to provide for the real-time processing and display of such data.

## DISCUSSION

### Data Acquisition System Functions

MIDAS-II is a modular, computer-controlled system comprising commercially available computer equipment and peripheral units, special-purpose hardware, a standard operating system, and special-purpose application software. It is designed to:

1. Acquire oceanographic sensor data in both analog and multiplexed digital formats;
2. Acquire ship position and motion data in synchro and event formats;
3. Record data on digital and analog magnetic tape;
4. Display acquired data in real time on a cathode ray tube (CRT) and a strip-chart recorder;

5. Permit the operator to interact with the data acquisition and display programs to select data channels for display; and
6. Compute in real time and display on the CRT the correlated response to a given change in ocean parameters of selected oceanographic sensors.

Figure 1 is a functional block diagram of the major MIDAS-II data acquisition units and the equipment with which they interact.

### Data Acquisition Hardware

The MIDAS-II special-purpose hardware units were developed to satisfy the requirements for data interfaces to shipboard and special oceanographic sensor systems, including those for ship position and motion, the analog sensors, the serial digital sensor, and timing inputs.

The platform interface unit is an improved version of a unit previously developed by the Interstate Electronics Corp. under direction of the ODAP Office. It provides the interface between MIDAS-II and the ship's position and motion sensing equipment. It can interface 36 synchro signals and 15 voltage-change events. Each synchro signal is converted twice a second to a highly accurate binary representation. The binary synchro and event data words are assembled into a single data block and transmitted via a standard serial interface to the PDP-11/34A minicomputer.

Low-level analog sensor signals are routed to the analog processing unit where selectable gain, filtering, and root-mean-square averaging operations may be applied. It provides processed narrowband and wideband outputs. Each processing channel is configured with plug-in components and jumpers to optimize the signal processing parameters for individual sensors. The wideband outputs are available for recording at a wideband analog recorder. The narrowband outputs are routed to an analog-to-digital (A/D) converter for input to the PDP-11/34A minicomputer. Sixteen channels of additional oceanographic sensor data are acquired by a separate sensor control panel and are transmitted via a serial interface to the minicomputer.

MIDAS-II timing-rate and time-of-day inputs are provided by a time code generator/translator that is

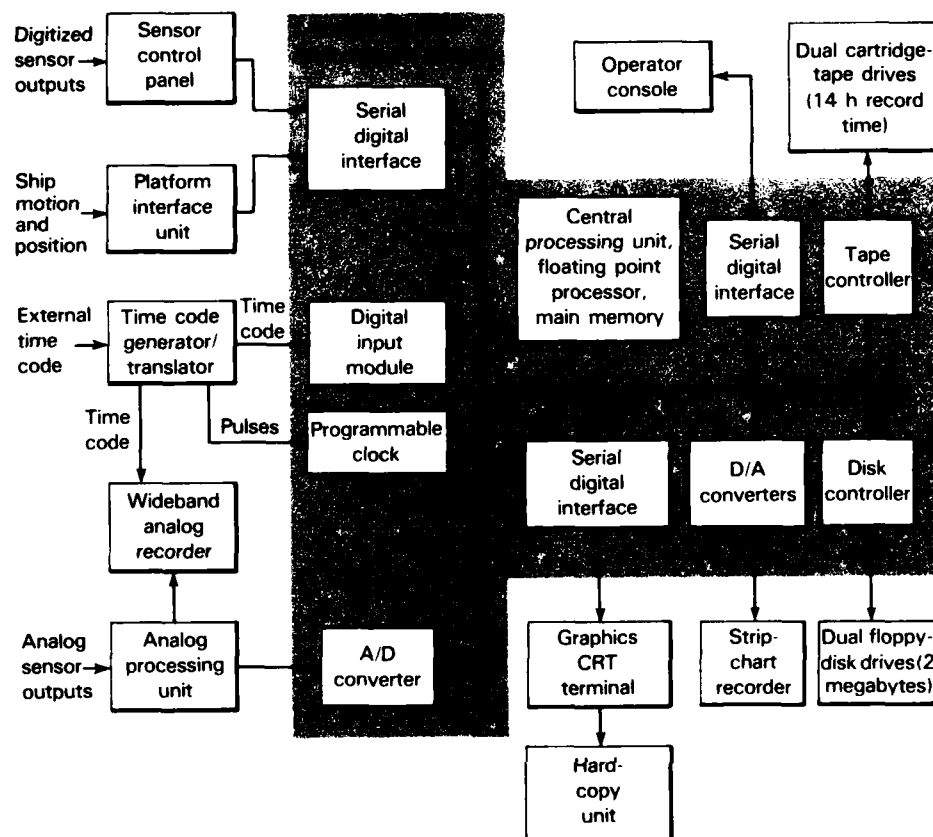


Figure 1 — Functional diagram of MIDAS-II.

synchronized to an externally generated time code. The digital input module receives the time-of-day information, updated once per second, that is used as the system time reference. Timing pulses from the time code generator/translator are input to a programmable clock for synchronization of software-controlled A/D sampling and data display outputs.

The MIDAS-II supporting peripherals are standard devices that perform data storage, off-line program storage, data display, and system operator input/output. Each of these off-the-shelf commercial units was selected for its compatibility with the PDP-11/34A hardware and operating system software and for its functional capacity. The units were packaged in rugged module shells designed for protection and for ease of stacking aboard ship.

#### Data Acquisition Software

The APL-developed MIDAS-II software may be divided into two broad categories: real-time data acquisition and data display.

The acquisition software is composed of a data acquisition control program and a disk-to-tape buffering program. The display software includes a real-time display program and a correlated signal program. The relationships among the various data acquisition programs are indicated in Fig. 2.

#### Correlated Signal Program

The correlated signal program was designed to be used for the real-time two-dimensional identification of oceanographic phenomena in the vertical plane. Those phenomena are detected by an algorithm that emphasizes the vertical correlation of several oceanographic sensor outputs. The signals available for display on the graphics CRT terminal are prewhitened sensor outputs and two software-generated signals, called COM (combined) and CSD (combined standard deviations). The sensors designated for prewhitening first have their scale changes and their wild points removed. Then they are prewhitened by a single-pole, single-zero digital filter and are finally high-passed by a two-pole

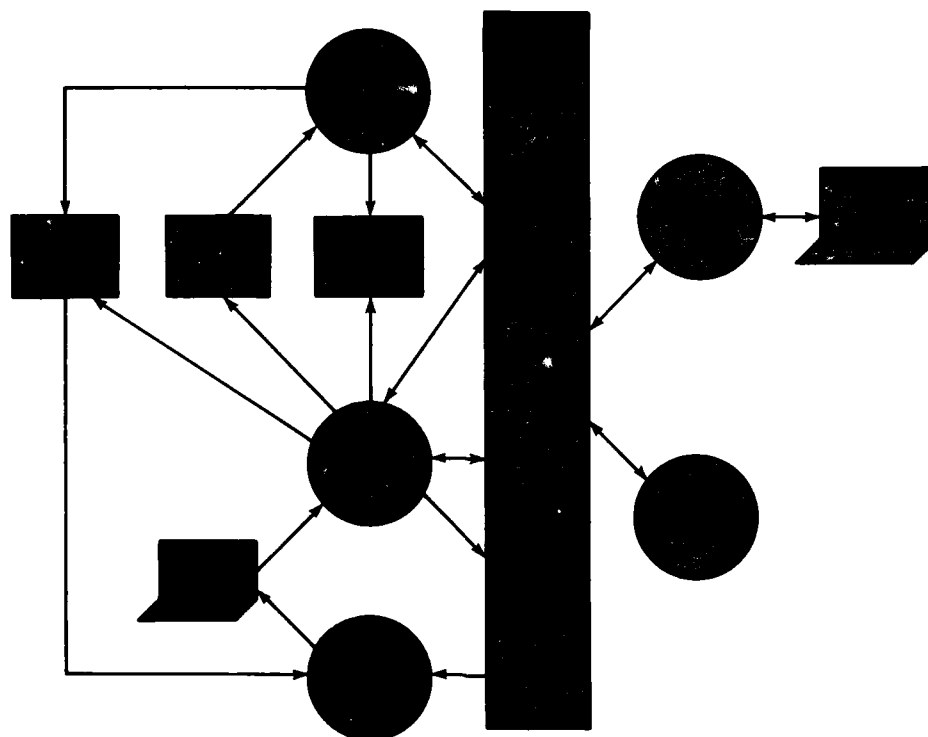


Figure 2 — Relationships among MIDAS-II data recording and display programs.

Butterworth digital filter. The COM signal is formed by first computing for each sensor an energy that is the sum of the square of all data points over a sliding time window. The COM signal is the normalized product of the individual sensor energies. Normalization is based on running estimates of the COM signal's mean and standard deviation. In equation form,

$$COM = \left( \frac{1}{\mu + B * \alpha} \right) \cdot \sqrt{\prod_{i=1}^N \left[ \left( \frac{1}{LENWD} \right) \sum_{j=1}^{LENWD} (S_{ij})^2 \right]}$$

where

- $N$  = number of sensors,
- $LENWD$  = window length (typically 75 samples, for a 5 Hz sampling rate),
- $B$  = scaling coefficient (typically 30),
- $\mu$  = estimated COM signal mean,
- $\alpha$  = estimated COM signal standard deviation, and
- $S$  = raw sensor signal.

The CSD signal is the number of estimated standard deviations by which the present COM signal value exceeds the estimated mean value. It has discrete output levels from zero to a variable maximum. Its advantage is that insignificant background level fluctuations are not displayed; therefore, the strength and the time scale of the vertical coherence may be evaluated by observing in real time the discrete number of standard deviations. CSD responds both to the energy present in the sensor signals and to the number of sensors showing coherent activity. Strong responses during a quiet background may well exceed 30 standard deviations, the typical setting for maximum signal display. Figure 3 is an example of a real-time display of the CSD signal plus operator-selected single-sensor outputs. The visual examination of hard copies of real-time CRT plots containing identifiable phenomena confirms that the CSD signal responds to those events while maintaining an excellent signal-to-noise ratio in comparison to any individual sensor response.

This work was supported by the Office of the Chief of Naval Operations, OP-009E1.

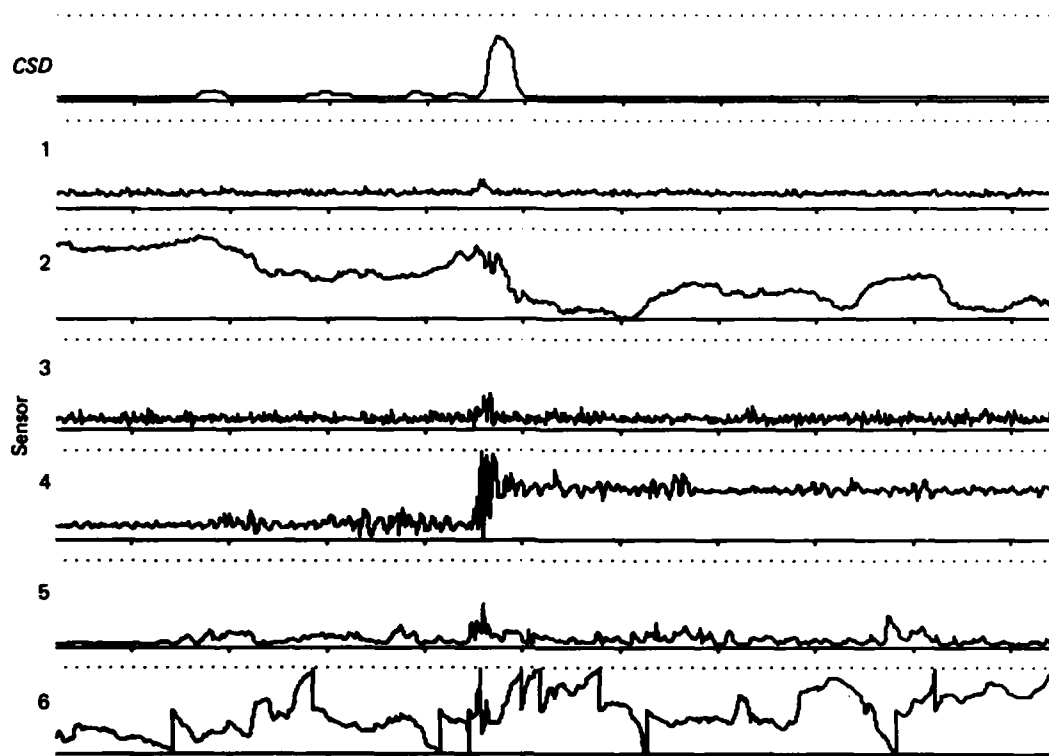


Figure 3 — Real-time display of the CSD signal and of single-sensor outputs.

## A PDP-11 BASED OCEANOGRAPHIC DATA ACQUISITION SYSTEM

R. B. Harris III (Sachs/ Freeman Assoc., Inc.) and  
S. J. Bockstahler-Brandt (APL)

*The APL Submarine Technology Division conducts a variety of oceanographic experiments requiring time-series data acquisition and recording. Recent experiments have called for data acquisition from custom, digital, microprocessor-based instruments as well as from conventional analog systems. In addition, it has become increasingly desirable to have real-time data validation and display capabilities included in data acquisition systems. A general-purpose, minicomputer-based data acquisition system has been developed to meet those needs for low- to medium-rate data recording.*

### DISCUSSION

The data acquisition (DAQ) program operates on a PDP-11 minicomputer (Fig. 1). The minicomputer and its peripherals have been strengthened for use in the field. The modular construction of the computer components allows them to be assembled quickly and flexibly into a configuration that meets the specific requirements of a given experiment.

Figure 2 shows the flow of data through the components of DAQ. Analog sensor systems are connected to the computer by an analog-to-digital converter. Digital sensor systems such as the AIP thermal gradiometer, the APL multiplexed temperature system, and the Parascientific digital depth computer are connected directly to the computer using standard PDP-11 components. The output of the system is recorded on nine-track magnetic tapes containing data received from the sensors. A cathode ray tube (CRT) and a printer are used for real-time data display and hard copy. The CRT is also used to display messages generated by a data validation program that monitors the data for indications of sensor malfunctions.

Like the computer hardware, the DAQ software is divided into modules. Device-dependent modules receive data from the sensor systems and place them in data buffers in the computer memory; when a buffer is filled, its contents are written on tape by the magnetic tape output module. The operation of a pool of buffers is maintained by the buffer control module, allowing input and output to occur simultaneously.

An important feature of DAQ is the degree of flexibility that permits the system to be reconfigured quickly and easily, even in the field. The programmer need not be experienced in PDP-11 assembly language. The key to this flexibility is that details specific to a particular sensor system are isolated in a single device-de-

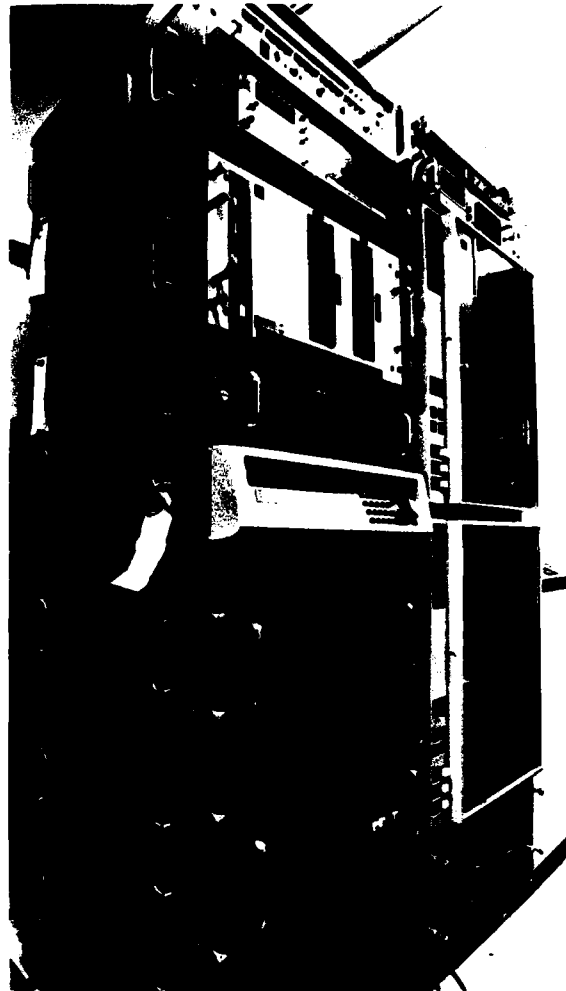


Figure 1 — The PDP-11 minicomputer in a typical at-sea configuration.

pendent module. One or more device-dependent modules are bound together with the generic modules to form a data acquisition system custom-tailored for the needs of an experiment.

Most modules contain no information specific to the data-acquisition requirements of a given experiment. Instead, such information is stored in lists in a single, configuration-specific module. The lists determine the order of execution of routines in the generic and device-dependent modules and thus control the op-

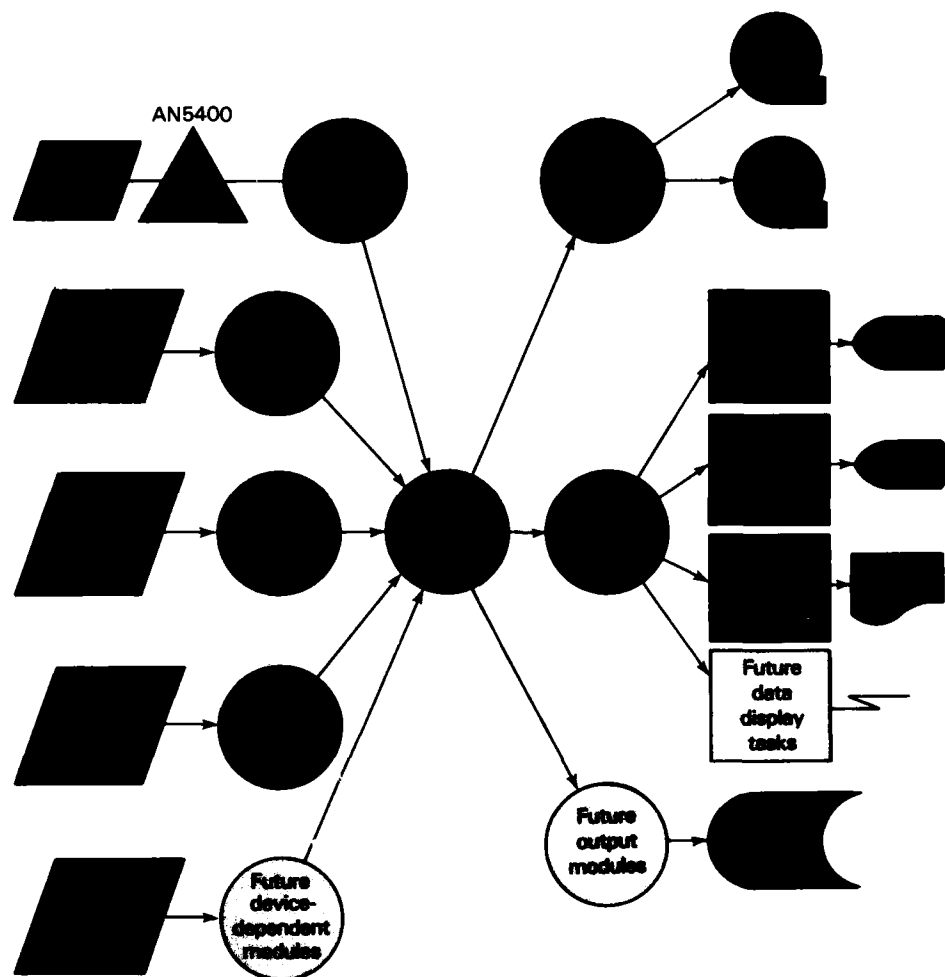


Figure 2 — Data flow through DAQ.

eration of DAQ. For instance, the list of sensors to be sampled is contained in the configuration-dependent module.

The concept of list-driven operation is extended to allow device-dependent modules to affect directly the operation of generic modules. Advanced programming techniques allow a device-dependent module to put its own name on a list that is accessed by a generic module: e.g., the list of modules that require activation during the initialization of data acquisition. This feature further reduces the interdependence of the DAQ modules.

Real-time data validation and display are made possible by the data-display task interface module, which makes the data buffer contents available to other programs. Those programs can carry on activities such as printing or graphing the data in real time and checking for sensor malfunctions. All data-display tasks are

carried out at a lower priority than are other DAQ functions and thus do not interfere with the primary mission of recording the data on tape.

## RESULTS

DAQ has been used successfully in two at-sea experiments conducted by the Submarine Technology Division. About 800 data tapes from analog and digital sensors have been acquired. At least 10 custom data validation and display programs have been developed for DAQ. It has been reconfigured both at the Laboratory and at sea with relative ease. Such flexibility and ease of use, which are of great economic and operational value, are a direct result of the modular design wherein specific functions and related information are isolated in independent modules.

## ACKNOWLEDGMENTS

The following people also contributed to the implementation of DAQ: D. J. Sides, L. E. Karner, S. M. Miller, and A. P. Rosenberg.

This work was supported by the Strategic Systems Projects Office.

## A DISTRIBUTED, INTELLIGENT OCEANOGRAPHIC DATA ACQUISITION SYSTEM FOR TOWED SENSOR ARRAYS

D. A. Kitchin, A. B. Fraser, L. E. Karner, R. P. H. Lee, and C. S. Best

*An expandable, flexible, intelligent, towed oceanographic data acquisition system has been developed to meet the APL Submarine Technology Division's needs for the 1980's. The system offers significant improvement over past approaches, most notably by incorporating microprocessors and network topology. Thus, it monitors both measured data and system performance and can preprocess data prior to recording and display.*

## BACKGROUND

As theoretical and experimental understanding of the ocean has improved in recent years, higher spatial resolution and more accuracy have been required from an ever-expanding variety of oceanographic sensors. With the increasing volume of data, it has become desirable to preprocess and compact the data and monitor its quality prior to recording or display, thereby reducing the overhead on acquisition and analysis computers. Furthermore, because only a few signal conductors are available in a towed array, a distributed acquisition system that digitizes adjacent sensors *in situ* and shares a high-speed serial digital bus has been sorely needed. This article describes the development of the Densely Instrumented Towed System (DITS) that was designed specifically to address these and other problems common to past oceanographic data acquisition systems.

## DISCUSSION

Architecturally, DITS is a distributed, intelligent (i.e., adaptive) data acquisition network incorporating selected features from the EIA RS422 and MIL STD 1553 bus protocols. Bus contention between stations is resolved and throughput is maximized by a scheme that determines positional priorities by the use of a few extra signal paths to eliminate the overhead found in other popular networks. Data are transferred in small scan packets from up to 62 underwater acquisition modules (UAM's) (Fig. 1) at a rate of 1 megabit per second to a shipboard DITS control unit (Fig. 2). Each data packet (and implicitly each sensor channel) is identified uniquely to aid in routing the data to different destinations: recording buffers, displays, etc.



Figure 1 — The underwater acquisition module for up to 30 sensors.

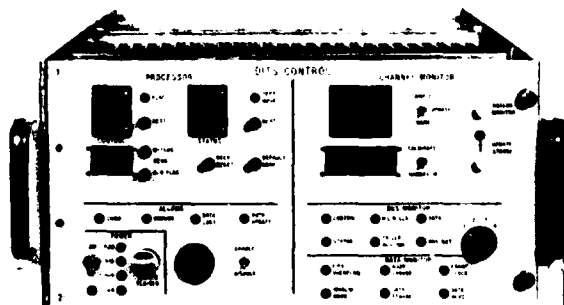


Figure 2 — The DITS control unit.

Each UAM is housed in a tiny pressure vessel measuring only 9 by 4.375 by 0.925 in. It contains watertight, wire feed-throughs and a special lid seal (not an O-ring). Each UAM is attached to a faired tow cable and to the sensors by means of wire harnesses (Fig. 3).

Within each UAM, a general-purpose modifiable preamplifier for each channel conditions the analog signals before they are presented to a multiplexer. Each preamplifier can include any combination of zero suppression, gain, preemphasis, and anti-alias filtering. A 32-to-1 multiplexer, a programmable gain amplifier, a sample-and-hold amplifier, and a 16-bit analog-to-digital converter are used to acquire data in digital format. To prevent ground loops and monitor leaks to seawater, each UAM isolates power magnetically and signals optically and contains a built-in megohmmeter and a leak detector/power shutoff. If a leak or some other failure does occur in one or more modules, the bus protocol allows the bus to continue functioning to support the remaining operational modules.

The Intel 8751 microcomputer/controller within each UAM contains firmware to (a) parse and execute numerous commands; (b) save, modify, or recall configuration-dependent parameters from a nonvolatile memory; (c) support sampling, subsampling, and tape-

frame-rate scans of sensors and housekeeping functions; (d) send test patterns; (e) convert data via each sensor's transfer function to engineering units; (f) format the data to the bus protocol; and (g) monitor and maintain the quality of the data by means of special algorithms.

The special algorithms are an integral part of the DITS acquisition philosophy that takes advantage of the small vertical gradients and horizontal near-invariability of the ocean. Basically, the point at issue is that even though the possible range of measured values in the ocean is quite large, the range measured in a particular area and depth is very small. This property permits similar sensors in each UAM to be zero-suppressed identically and adjusted in gain to optimize the range-versus-resolution trade-off for a particular ocean gradient. This feature has the fringe benefit of compressing the data significantly, thereby allowing more recording time per data tape, because the zero suppression is shared by many channels and the optimum gain ensures that nearly all of the digitized bits are active rather than static. Although most of the time these programmable settings remain fixed, an adaptive firmware algorithm that monitors the measurements may change the settings in response to significant changes in mean sensed properties. Adjustments can occur either instantaneously in stepwise fashion for initialization or as a slow ramp that is transparent to the quality of the data.

The control unit, which can accept up to four serial busses, distributes the data packets to the host computer interface, real-time display, and monitoring functions. The control unit can also be configured for data playback from the host computer for quick-look time-series analysis. The display/monitor functions include 32 channels of analog output for strip charts or spectrum analyzers, a hexadecimal display, and a data quality/dropout monitor that scans periodically through each sensor. Firmware in the control unit mi-

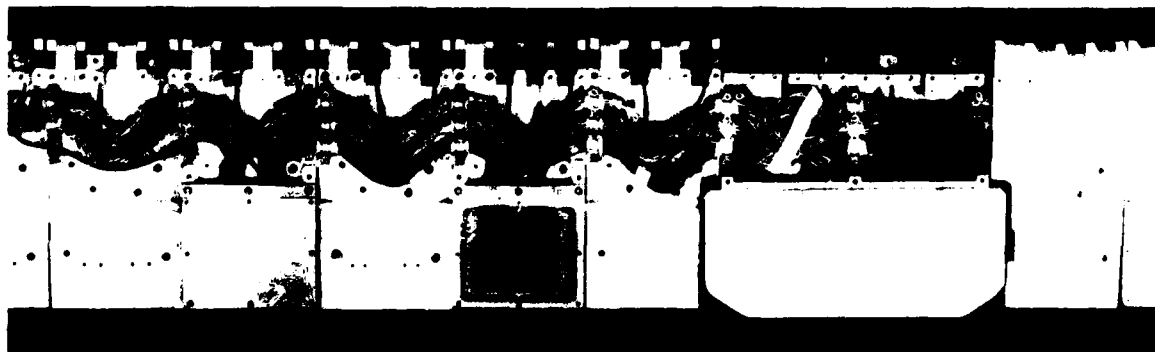


Figure 3 — Exposed section of the towed oceanographic array with UAM and sensors.

crocomputer gives an alarm when certain error or update conditions are reported; parses and executes system commands either from the host computer or from the front panel; and saves, recalls, or modifies a non-volatile, content-addressable memory that enables any sensor to appear on any display channel.

The host computer, usually a DEC PDP-11/34, contains special support software to drive the control unit interface and monitor its performance, to examine the mean and standard deviation of any sensor in real time, and to control overall system functions. The DITS control task, in particular, makes the encoding and decoding of commands, status, sensor transfer function coefficients, and configuration parameters very "user friendly" by using the versatile constructs of the DEC-supplied, table-driven parser in conjunction with routines from the system object library to perform command-line processing.

The DITS prototype (minus a few of the more complex firmware features mentioned) was tested successfully during a recent at-sea test. Data are currently being processed for a performance evaluation and design review.

## ACKNOWLEDGMENTS

For help in layout, assembly, programming, testing, calibration, and management, we wish to thank H. K. Charles, Jr., G. J. Farruggia, L. A. Fuhrmann, Jr., J. R. Hillier, A. F. Hogrefe, I. R. Hunter, L. A. Meyer, M. W. Roth, J. T. Velky, and E. N. Wallace.

---

This work was supported by the Strategic Systems Projects Office.

## AN OCEANOGRAPHIC DATA ANALYSIS SYSTEM

B. E. Raff

*An Oceanographic Data Analysis System was developed as a microprocessor-controlled oceanographic survey tool that automates routine and tedious analyses associated with airborne bathythermic surveys.*

### BACKGROUND

Various oceanographic experiments frequently entail making measurements of the background mesoscale thermal field. This field has characteristic spatial scales of 50 to 500 km and temporal scales of several days to several weeks. Experiments concerned with mesoscale descriptions include measurements of acoustic propagation through a variable environment and practically any physical or biological survey in proximity to regions of high variability such as oceanic fronts, rings, and eddies. It is of particular benefit to characterize the mesoscale field in a period short enough to capture a synoptic description and to produce timely data in order to use the derived environmental descriptions to make

in-process modifications of the survey design. This objective has been reached recently by an Oceanographic Data Analysis System (ODAS) that was designed for use with airborne expendable bathythermographs (AXBT's).

### DISCUSSION

The AXBT's are designed to measure vertical temperature profiles. They are deployed from aircraft, descend to the ocean surface, release a sounding thermistor probe, and telemeter subsurface data to the airplane (Fig. 1). Although their use is generally straightforward, there are practical problems because they have peculiar faults that can affect data adversely if not detected and corrected.

The AXBT is essentially a buoy with a radio frequency transmitting antenna only 6 to 12 in. above the ocean surface. In other than calm seas, ocean waves and spindrift "ground" this short antenna and tempor-

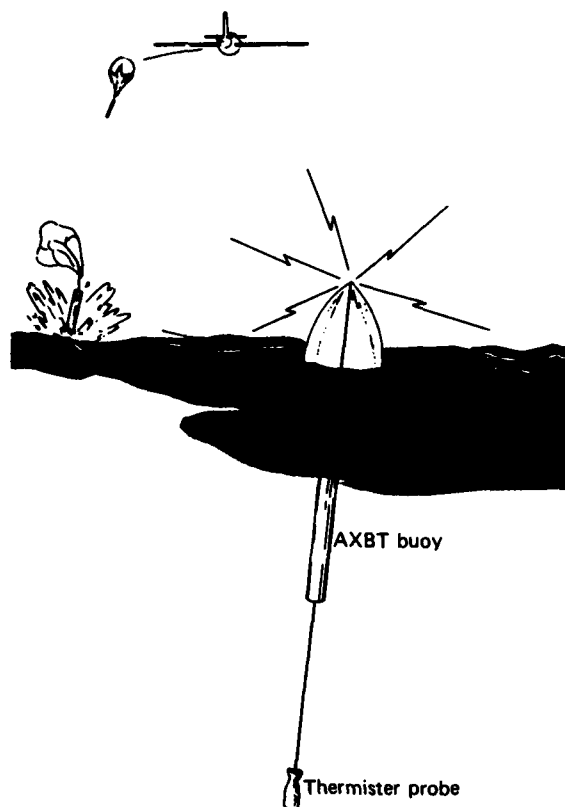


Figure 1 — Deployment of an AXBT.

arily interrupt data transmissions. Another problem is a false start (i.e., the indicated origin of the depth scale is offset from zero). The AXBT data signal is supposed to appear the instant the thermistor probe is released from the buoy. Owing to various mechanical and electrical malfunctions, a false start can misstate the true temperature/depth relationship.

Their imperfections notwithstanding, AXBT's (which have been available for two decades) have played an important role in Navy antisubmarine warfare operations. At the same time, however, their use in scientific survey efforts has been relatively infrequent until recently when increased awareness of the importance of mesoscale variability to undersea warfare has sparked an increased interest in AXBT surveys to the point where the Naval Oceanographic Office now regularly sponsors large AXBT surveys for environmental mesoscale characterizations. This "popularity" gave rise to another problem; the capacity to process AXBT data could not keep pace with the increased demand. A new approach to processing that would routinely and efficiently handle large quantities of data was clearly needed. ODAS, an airborne recording and analysis system that automates routine and tedious work and

thereby expedites data analysis, was developed to fill this need.

ODAS is shown in Fig. 2; Fig. 3 is a block diagram of the system. The design responded both to very specific aspects of AXBT data processing and to more general aspects of oceanographic analyses. ODAS specifications and capabilities are outlined in Table 1. The concept inherent in the use of ODAS for oceanographic research is discussed below.

Bathythermographs produce vertical samplings of the ocean thermal field (Fig. 4). An AXBT mesoscale

Table 1 — ODAS specifications.

#### AXBT processing

- 5 channel capacity
- $\pm 5$  millidegree C accuracy
- 5 Hz sampling rate
- Automatic start feature
- False start protection
- Data editing
- Profile analysis
- Bathybooking messages

#### Navigation processing

- LTN-51, LTN-72, or VLF Global 500
- Records latitude, longitude, heading, and airspeed

#### General data acquisition

- 8 channel capacity
- 200 Hz data throughput
- 12 bit analog/digital
- $\pm 5$  V dynamic range

#### Recording

- Raymond 6412 cartridge drive
- Standard 4 track data cartridge

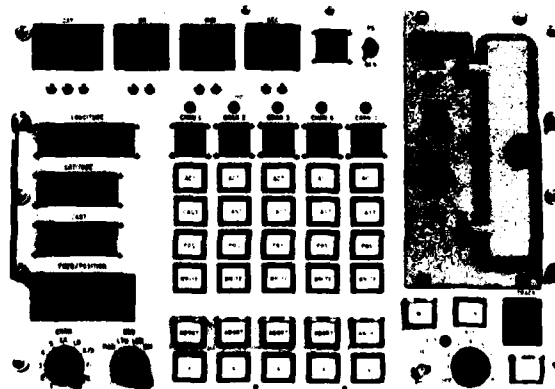


Figure 2 — The Ocean Data Analysis System.

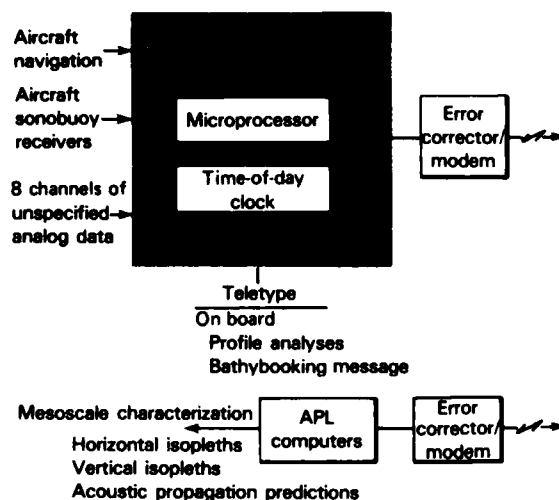


Figure 3 — Block diagram of ODAS.

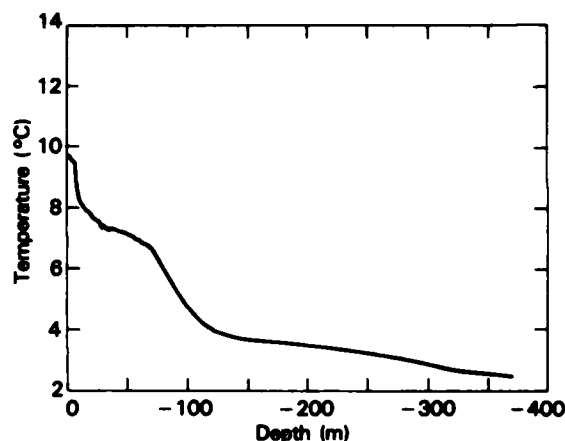


Figure 4 — Example of a temperature profile.

survey consists of discrete samplings spaced 10 to 30 km apart (Fig. 5). Several standard oceanographic products are generated from such a survey: temperature contours at constant depths, depth contours at constant temperatures, and vertical contours of temperature. Some examples are shown in Fig. 6. Prior to the development of ODAS, the production of such isopleths had been an intensive hand-plotting operation subject to individual interpretation.

In addition to recording aircraft sensor and navigational data, ODAS has error-checking hardware and software to detect AXBT fault conditions and to flag faulty data (Fig. 3). This real-time, error-detection feature significantly expedites data generation. Moreover, ODAS yields several types of data for immediate on-board examination so that operators may identify envi-

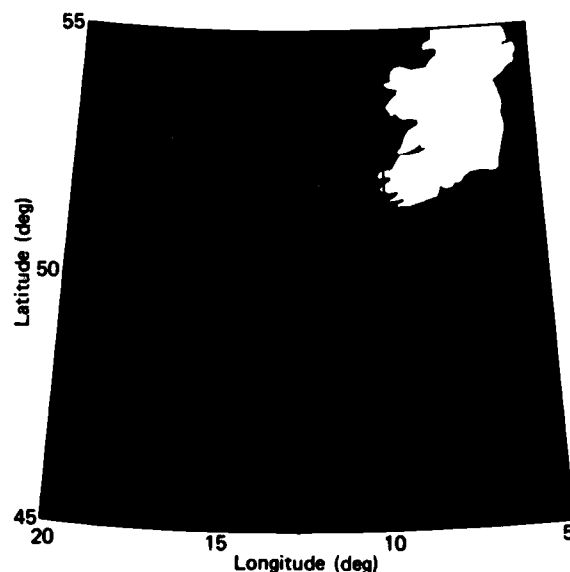


Figure 5 — Example of a mesoscale survey (points indicate AXBT deployment locations).

ronmental features easily and, if needed, modify survey operations to achieve the desired environmental descriptions. The near-real-time outputs for each profile are classified into temperature/depth pairs at given temperatures, temperature/depth pairs at given depths, profile inflection points, and so-called "bathybooking" messages.

The latter two outputs need further explanation. Each profile, such as the one shown in Fig. 4, can be approximated by a sequence of line segments connected at major profile inflection points (8 to 15 such points are customary). The points can be encoded into a special format (a bathybooking message) and sent to the Fleet Numerical Oceanographic Center (FNOC), which maintains a large historical data base of bathythermographs.

When the survey aircraft has landed, the bathybooking messages are dispatched quickly to FNOC, and the entire AXBT data set is transmitted to APL for further analysis. At APL, the data are processed on general-purpose computers using objective mapping techniques to produce the horizontal and vertical isopleths shown in Fig. 6.

## RESULTS

ODAS has proven to be a useful tool of significant capability in oceanographic research. It has been flown on numerous survey missions over the Atlantic and Pacific Oceans for the United States and the United

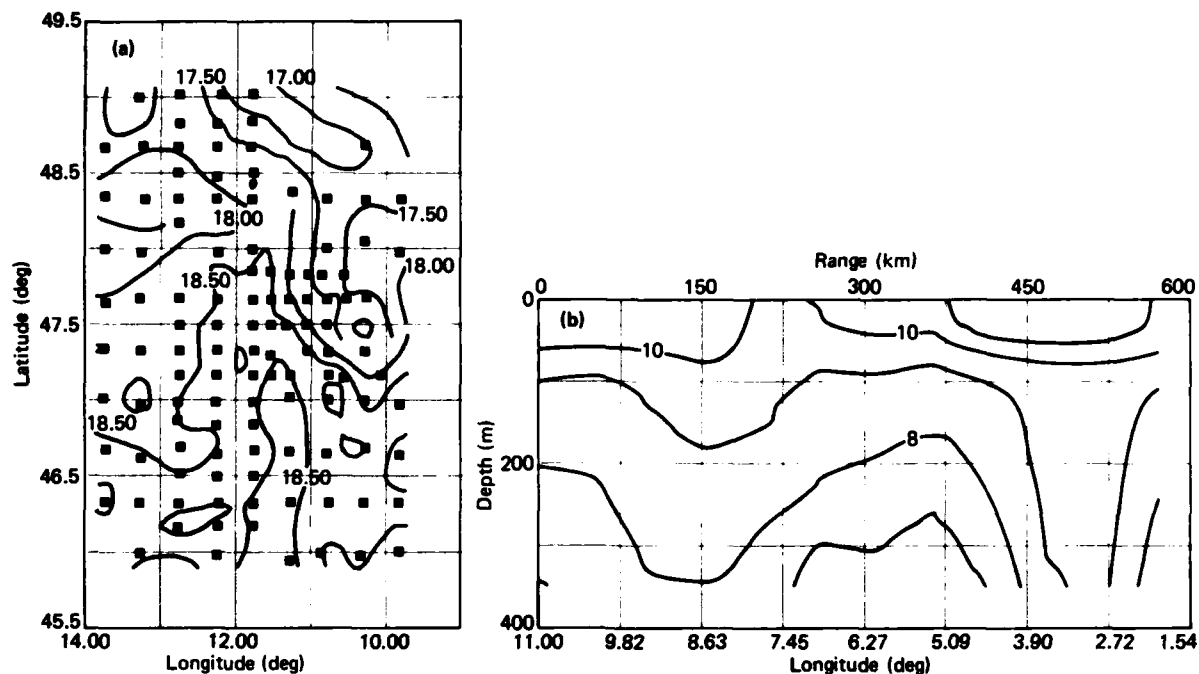


Figure 6 — Examples of temperature contour maps, (a) horizontal and (b) vertical.

Kingdom. Its use has proven that complete mesoscale thermal descriptions can be available within hours of aircraft landing. This point is particularly significant. AXBT surveys are frequently used for reconnaissance in conjunction with ship operations. Timely mesoscale descriptions provide a most effective basis for directing

ship operations and for using survey time, a capability that has been demonstrated during many of the surveys mentioned above.

This work was supported by the Strategic Systems Projects Office.

# THE CHARACTERIZATION OF MESOSCALE OCEANOGRAPHIC FEATURES

J. J. Ousborne

*The ability of a satellite altimeter to provide useful oceanographic information depends, in part, on the data processing system. Several signal-processing algorithms were assessed to determine the level of performance that can be achieved in detecting and estimating oceanographic features and to identify an algorithm for processing altimetry data from the GEOSAT satellite scheduled for launching in 1984.*

## BACKGROUND

The quantified knowledge of oceanographic parameters is a key factor in evaluating Naval system performance, tactics, and vulnerability. In the past, *in situ* measurements have been the primary means of environmental surveillance. As the extent of geographic regions of interest expands and the need for synoptic coverage grows, remote sensors will become the only realistic way to characterize the environment. Although spaceborne infrared sensors now provide some measure of characterization of the mesoscale oceanographic field, they have limited utility in areas where cloud cover greatly reduces their ability to image the sea surface. In contrast, a satellite altimeter provides all-weather surveillance and potentially can fulfill the Navy requirement for oceanographic characterization. The exploitation of the altimeter's capability is an especially timely consideration, owing to the near-term availability of the GEOSAT altimetry data.

GEOSAT, a geodesy satellite that will carry a high-resolution altimeter system, is scheduled to be launched in the fall of 1984. It will be used as a stable platform from which measurements of the vertical distance to the ocean surface will be made (Fig. 1). When the altimetry data are merged with accurate orbital information, undulations in the mean sea level, predominantly induced by the earth's geoid, will be revealed.

Although the earth's geoid produces the dominant sea-surface signature, other environmental features produce potentially exploitable signals in the altimetry data as well. For example, the sea-surface topography measured by the altimeter contains fluctuations induced by tides, barometric pressure loading, surface-wave effects, and geostrophically balanced surface current systems related to mesoscale features. Mesoscale features are of significant interest to the Navy and possibly can be identified and characterized by appro-

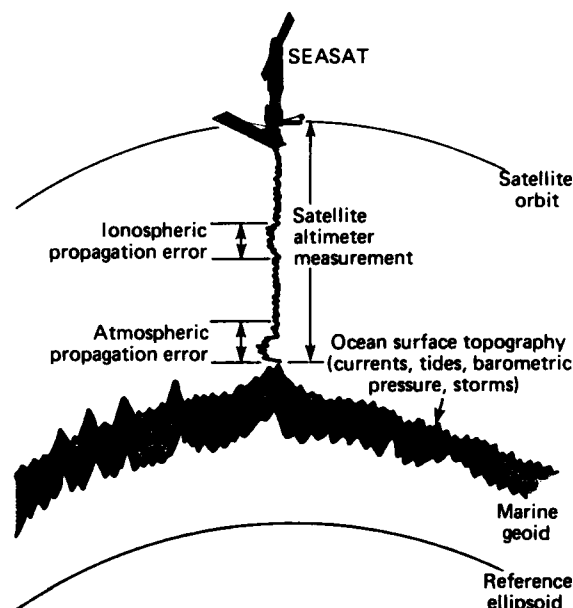


Figure 1 — Altimeter measurement of distance to ocean surface.

prate use of altimetry data. The mesoscale feature of greatest interest is the eddy, an identifiable characteristic of which is an elevation or a depression (i.e., a negative elevation) of the sea surface in its immediate vicinity. Typical eddies have diameters of 50 to 200 km, surface elevations with  $\pm 30$  to 100 cm maximum amplitudes, and translational velocities of 1 to 8 km per day. It is expected that an altimetric system such as GEOSAT will be able to detect and track such eddies.

## DISCUSSION

Altimetry data are inherently one dimensional (1D); the satellite altimeter measures the surface topography along the satellite ground track and produces a topographic time history. However, an aggregate of satellite orbits can be combined for two-dimensional (2D) processing. The proposed GEOSAT orbit will produce a ground-track pattern (Fig. 2) that maps one track every third day in each fundamental sector. Each track will be a fixed distance from the previous one; after a certain number of days, the pattern will complete its coverage of the fundamental sector and will then repeat the process. At the stage shown in Fig. 2,

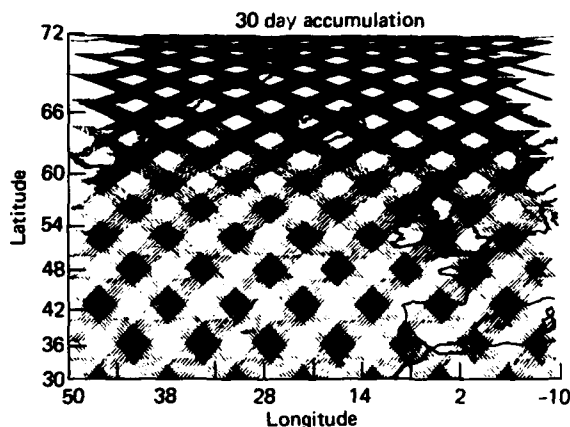


Figure 2 — Satellite ground track pattern.

coverage is half completed. In addition, data from ascending (south to north) and descending satellite paths can be combined.

When processing altimetry data, it is necessary to incorporate a way to make a decision as to whether a mesoscale signature or, alternately, noise only is present at a specific geographic location. If a feature is detected, estimates of its parameters (elevation and diameter) are needed. The capability of the system is now limited by both geophysical noise and system noise. The eddy signature and the noise are such that not all the optimality criteria of conventional detection and estimation theory can be met; hence, it was necessary to select a "best" algorithm by comparing a set of detectors. The assessment was completed in two steps. First, stationary eddy detection performance was assessed to provide a basic understanding of the detection and estimation process without the complications introduced by eddy translation. Then, the effects of eddy translation were assessed.

Matched filters (1D and 2D), a 2D maximum *a posteriori* (MAP) estimator-correlator, and a 2D Kalman filter estimator-correlator were considered. The performance of the matched filter was evaluated by the numerical implementation of analytical equations. An analytic evaluation of the MAP and Kalman filter estimator-correlators was not feasible; accordingly, a Monte Carlo simulation was used.

A comparison of the performances of the 1D and 2D matched filters demonstrates the advantage of 2D processing for the larger-diameter eddies that are crossed by several satellite ground tracks. It is apparent from Fig. 3 that median-amplitude, large-diameter eddies are significantly more detectable with 2D processing. In the example, five or six ground tracks intersect the feature; three or four of them contribute most to its

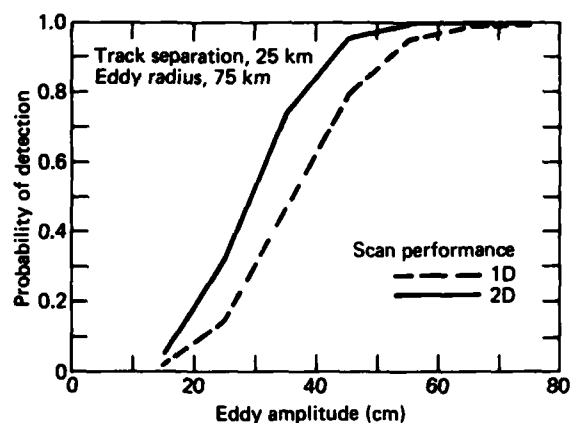


Figure 3 — Comparison of performance of 1D and 2D filters.

detectability. Ground tracks near the edge of the feature show very small surface signatures and do not add significantly to detectability. As might be expected, the 2D processing advantage is less for smaller diameter eddies that are intercepted by fewer ground tracks.

The filter performances were evaluated by comparing the detection probabilities at various satellite cross-track separations. For each separation, the probability of detection was determined by averaging over a typical range of eddy amplitudes and diameters. The performance for the scan detectors is shown in Fig. 4. Predictably, system performance improves as the cross-track separation decreases and as more tracks per eddy are available. Note that the performances of the 1D and 2D detectors converge at large cross-track separations, showing the diminution of the 2D advantage as the number of crossings is reduced.

The performances of the MAP and Kalman filters were evaluated at only a few cross-track separations. At those particular separations, the performance

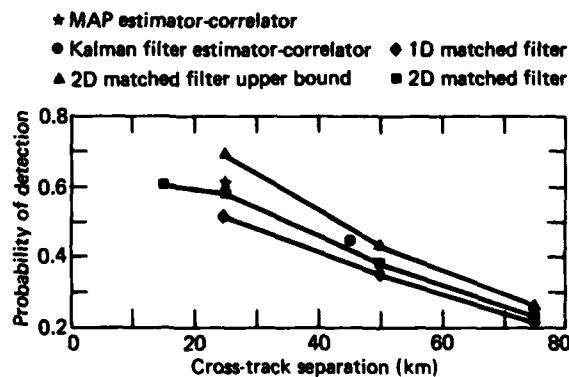


Figure 4 — Comparison of performance of 1D and 2D scan detectors.

of each estimator-correlator lay between that of the 2D single matched filter and a theoretical upper bound. Although the MAP performance is relatively good, that detector would not be suitable for an operational system because it is nonlinear and convergence is not ensured. Hence, the appropriate choice of a system filter is between a 2D multiple matched filter and a Kalman filter.

Up to this point in the analysis, the eddies were treated as stationary. In fact, most eddies observed do translate, and the movement can affect detector performance. Eddy translation does not affect the performance of 1D detectors, which sample the feature nearly instantaneously, but it does smear the feature signature derived from 2D systems, which depend on successive crossings.

In the proposed GEOSAT orbit, successive ground track intersections with an eddy will be separated by three days. During that period, the eddy will translate, and each ground track will intersect it at a position offset from that at which it would have done had the eddy been stationary. Depending on the translational velocity of the eddy, the signature as resolved by an altimeter will be elongated (the eddy velocity is in the direction of ground track evolution), skewed (the eddy velocity is perpendicular to ground track evolution), or foreshortened (the eddy velocity is diametrically opposite to ground track evolution). The net effect of feature smearing is a reduction of detectability. An example of the degradation in performance of the sweep detector (using only ascending or descending satellite tracks, but not both) is shown in Fig. 5 for a typical range of eddy velocities. As would be expected, high velocity produces greater degradation; even so, the degree of degradation is not severe.

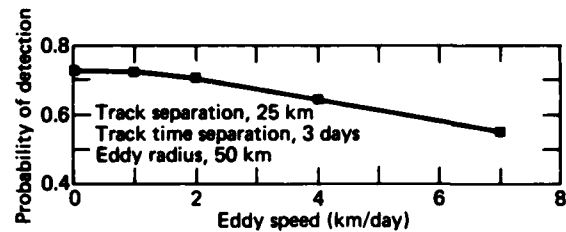


Figure 5 — Effect of eddy velocity on sweep detector performance.

The salient findings of this parametric study and examples of algorithm performance for several eddy sizes and translational speeds have been given here. From the results reported in detail to the Navy, it was concluded that it should be possible to process altimeter data to achieve a reasonable probability of detection (about 0.5) of eddies having characteristics in the typical range of amplitudes, diameters, and translational speeds.

#### ACKNOWLEDGMENTS

The 2D Kalman filter detection and estimation analysis was performed by J. Woods at Rensselaer Polytechnic Institute.

This work was supported by the Strategic Systems Projects Office.

## AID CONTROL AND MONITOR SYSTEM

T. H. Man, E. E. Mengel, and C. A. Twigg

*A microprocessor-based system for the remote control and monitoring of distant, unmanned navigational aids has been designed for the U.S. Coast Guard. APL will supply the engineering drawings and documentation necessary for the Coast Guard to procure operational systems from commercial vendors and to install and operate the systems when delivered.*

### BACKGROUND

The U.S. Coast Guard traditionally has provided to the maritime community a variety of navigational aids including manned lighthouses that contain a major light and a fog horn, a radio beacon, or both. In 1968, a project was begun to convert the lighthouses to unmanned operation by using sophisticated automatic equipment, some of which was installed in the lighthouses and some at master sites, to control and monitor the aids. Since that time, it has been recognized that it would be desirable to monitor or control from the master sites a number of secondary aids such as large buoys or beacons. Until now, however, the lack of an inexpensive and standardized remote control and monitor system has precluded implementation of the concept. The aim of this project is to develop a modular Aid Control and Monitor System (ACMS) that will both replace the current system of controlling unmanned lighthouses and, in a minimal configuration, monitor and control less complex aids as well.

The first phase of this effort was the development of a modular, microprocessor-based system that monitors the status of devices at a distant station, communicates status information to the master station upon request, and executes commands generated by the master station. The second phase of the project was the development of a system whereby the master station will be able to interrogate up to 48 distant stations and display the status of monitored aids to operating personnel at the master site.

### DISCUSSION

The system designed by APL consists of:

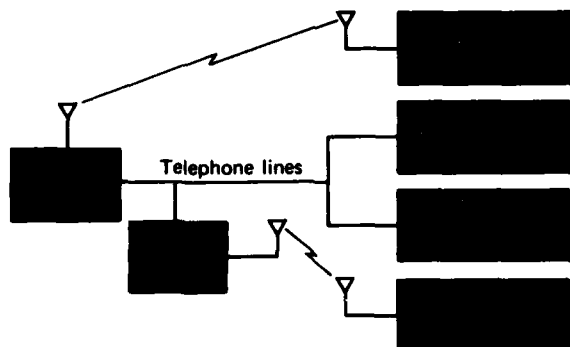
1. Remote terminal units (RTU's), installed in the navigational aids, that monitor the status of elements of the aids and control the receipt of commands from and the transmission of status messages to the master terminal unit.
2. A master terminal unit (MTU) that transmits commands to the RTU's, receives status information from them, displays the status on a touch-sensitive cathode ray tube (CRT), stores on tape information relative to lighthouse status changes, and informs the operator what action should be taken in the event of a detected failure.
3. A transfer terminal unit that is used to enable communication between the RTU and the MTU when that communication would otherwise be impossible or unreliable as, for example, when stations are separated by more than the line-of-sight RF range.

Figure 1 shows the various elements of the system and illustrates the use of RTU's in three kinds of installations: an unmanned lighthouse, a large navigational buoy, and an independent radio beacon. The communication links between the MTU and the RTU's include UHF radio, local telephone, and commercial telephone networks.

All three systems use the same enclosure, electronic modules, and (where applicable) software. The selected electronic hardware uses a modular bus system that is available commercially from several vendors and maintained by them. A modular approach allows the Coast Guard to change the equipment configuration easily for the different RTU applications and, further, provides flexibility to accommodate future functional changes in the system.

The RTU (Fig. 2) monitors 32 status lines and controls 8 command lines. It can communicate with the MTU by means of dual UHF transceivers, over a telephone line, or by UHF to a transfer terminal unit and thence by telephone line (Fig. 1). The Coast Guard has identified uses for 22 status lines and 5 command lines; the remaining 10 input and 3 output lines are available for future use or for additional signals that may be required for nonstandard installations. The spare data communication channel (shown as a dashed line in Fig. 2) is used by installation personnel for setting up the microprocessor and by maintenance personnel for troubleshooting and diagnostics.

The status signals are generated by sensors and electronic circuitry already in the lighthouse. Those signals now sent from the RTU convey to the master station information on conditions or failures in primary, secondary, and emergency navigational aids and their



**Figure 1 — Elements of the Aid Control and Monitor System.**

power sources. As appropriate to conditions indicated by the status reports, the master station generates and transmits, by means of the MTU, command signals that activate command relays or other electronic equipment in the lighthouse. The various signals to and from the RTU microprocessor are coupled to the rest of the lighthouse electronics equipment by amplifiers, that are electronically isolated by optical links to reduce the possibility of mutual interference by the microprocessor and the lighthouse.

The RTU system software monitors the communication ports for commands from the MTU and also monitors the status inputs to sense and communicate changes. Status inputs are those that indicate the conditions of the main light primary or secondary, the fog horn primary or secondary, primary and secondary AC power, emergency power, etc. If a status report indi-

cates that the normal lamp or fog horn characteristics have been altered, the RTU sends a status-change message to the MTU, thereby alerting personnel at the MTU to take appropriate action. Such actions can range from sending a repair order to maintenance personnel to issuing an official Notice to Mariners that a major navigational aid is inoperative.

Figure 3 shows the components of the MTU, including the microprocessor system, the touch-sensitive CRT with a removable keyboard, a tape recorder, a modem, and the transceivers. The status information at each RTU is stored in the MTU microprocessor memory and displayed to the operator on the CRT. If a problem is reported by an RTU, the information is displayed and the options for actions are presented; the operator can then command the system by simply touching the appropriate portions of the CRT screen. This feature allows minimally trained personnel to be able to react properly with the "user friendly" system.

A detachable keyboard enables experienced personnel to enter the initial setup information for the individual RTU's and then remove the keyboard to preclude the inadvertent entry of further changes. All RTU messages are stored on magnetic tape so that system failures can later be analyzed in detail. The setup information also is stored on tape to enable proper reinitialization after a power failure.

The MTU communicates using UHF transceivers or (via a modem) the telephone line. In order to minimize transmission errors that have plagued the current system, an error-correcting code is incorporated. It prevents certain types of errors from disrupting the mes-

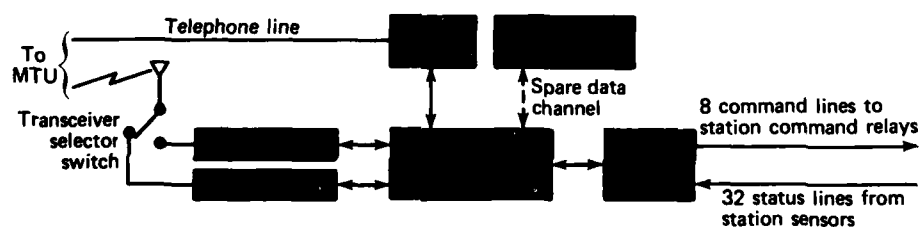


**Figure 2 — The remote terminal unit.**

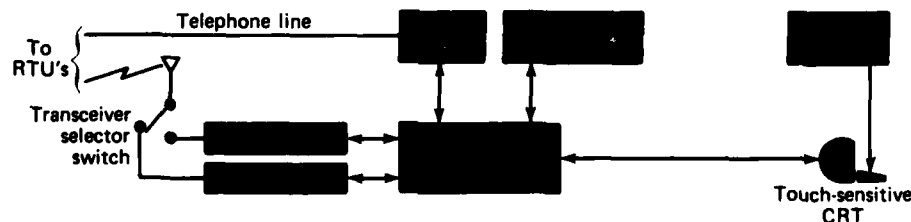


**Figure 3 — The master terminal unit.**

sage. The formatting for this feature appears in the microprocessor software for both the RTU and the MTU.

## **SUMMARY**

The design of the RTU and MTU electronic hardware and of the RTU software was completed during this period. A breadboard RTU was constructed, subjected to environmental testing at APL, and installed for field testing at a Coast Guard engineering test facility. The next phase of the project will produce prototype hardware and software for the RTU and the MTU and the drawings required for the acquisition of both items.

## **ACKNOWLEDGMENTS**

The authors would like to acknowledge and thank W. R. Powell for his leadership as program manager for the Aid Control and Monitor System.

The authors also wish to acknowledge the efforts of J. Baldassano, R. L. Cannon, D. C. Culver, H. L. Smigocki, D. L. Snope, and P. Whitman, who contributed to the design and development of the system.

---

This work was supported by the U.S. Coast Guard.

**BIOMEDICAL SCIENCE AND ENGINEERING**

## INTRODUCTION

The collaborative biomedical program between the Applied Physics Laboratory and The Johns Hopkins University's School of Medicine began in 1965. The program brings together the expertise in medical and biological sciences found at the Medical School with those in the physical sciences, engineering, and mathematics found at APL, in order to solve significant problems in biomedical science and health-care delivery. From the beginning, the collaboration has received strong support from the University's leadership and encouragement from the Navv, APL's principal sponsor. The strength of the collaboration is evidenced by the joint appointments made within the two University divisions: 17 members of the APL staff have appointments at the Medical School, and 16 members of the medical faculty have Principal Professional Staff appointments at APL.

Currently, there are active projects in ophthalmology, neurosensory research and instrumentation development, cardiovascular systems, patient monitoring, therapy and rehabilitation, clinical information systems, and clinical engineering. Forty-four APL physical scientists and engineers are working in collaboration with Medical School biomedical scientists and clinicians on those projects. Their research and development results are published in the peer-reviewed scientific and medical literature. Since the program's inception, over 350 papers have been published, and there are even more published abstracts and presentations at major scientific and medical meetings.

The articles appearing in this year's *APL Selected Accomplishments* indicate the breadth of the collaborative biomedical effort. In cardiovascular research, there is an article suggesting that geometric features of arteries could be risk factors for vascular disease. In ophthalmology, a microwave-induced cellular change in the corneal endothelium has been observed at exposure levels previously thought to be biologically safe. The third article describes a computer-controlled robot arm designed for individuals with high-spinal-cord damage (quadriplegics). Next, a description is presented of the successful testing in diabetic dogs of the Programmable Implantable Medication System developed at APL. The last article reviews APL's productive effort in assisting the Johns Hopkins Medical Institutions to develop several computer recordkeeping and information systems.

## POSSIBLE GEOMETRIC RISK FACTORS FOR ARTERIOSCLEROSIS

M. H. Friedman, O. J. Deters, F. F. Mark, and  
C. B. Barger (APL) and G. M. Hutchins (JHMI)

*Hemodynamic data obtained in pulsatile flow through casts of human aortic bifurcations reveal four geometric features whose variation from one individual to another is sufficient to cause significant variability in the shear stress on the vessel wall. Correlations between measured shear stress and vessel wall thickness suggest that hemodynamics may mediate the formation of arteriosclerotic lesions. Consequently, the geometric features that have been identified may account for some of the variability in the location and rate of development of the disease, indicating that particular geometric features of arteries could be risk factors for vascular disease.*

### BACKGROUND

Much of the credit for the recent decline in mortality resulting from cardiovascular disease has been attributed to the identification of certain aspects of an individual's lifestyle, genetic makeup, and disease state that appear to predispose to arteriosclerosis. A recent tabulation by Anyanwu et al.<sup>1</sup> lists 21 such "risk factors." In spite of the large number of identified or proposed risk factors, they are incapable of explaining half of the variance in arterial disease among individuals and populations. One conclusion is that there are other risk factors that have not yet been identified.<sup>2</sup> This situation, together with the facts that (a) many hypotheses dealing with the onset and development of arteriosclerosis invoke hemodynamic factors and (b) all fluid dynamic variables are affected by the geometry of the channel through which the fluid flows, led to the proposal of geometric risk factors that increase one's susceptibility to disease.<sup>3</sup> Thus, experimental procedures were developed to identify these factors.

### DISCUSSION

The dependence of hemodynamic variables on local arterial geometry is examined by selecting at autopsy relatively uninvolved human arterial segments, passing a life-like pulsatile flow through casts of each vessel's lumen, and using laser Doppler anemometry to measure time-dependent velocities at multiple sites near the wall of each cast.<sup>4</sup> The specimens selected for casting and hemodynamic study are chosen to reflect the range of normal variations in arterial geometry, and their particular contours are preserved in radiographs,

photographs, the luminal mold from which the cast is prepared, and the cast itself.

The anemometry results<sup>5</sup> show that the flow in the normal human aortic bifurcation, although complex, is not turbulent. Neither is separation a prominent feature; transient eddies have been observed on occasion, but they occur only in diastole and are very weak.<sup>6</sup> Accordingly, major emphasis has been placed on the influence of arterial geometry on wall shear rate, a quantity that can be computed readily from the velocity data.<sup>4</sup> Furthermore, consideration will be limited here to only the outer wall of the aortic bifurcation because this is where most of our velocity data have been taken. A paradigm has been developed to identify readily the most important geometric features influencing internal shear at other locations.

The geometric features of interest are identified by comparing the experimental shear at each site along the outer wall with the value that would have been observed at that cross section were the flow at the site fully developed and parallel. Except for a very short region immediately upstream of the flow divider tip, the cross sections of the aorta and iliacs can be approximated as elliptical; for fully developed pulsatile flow through an elliptical pipe whose axes are  $a$  and  $b$ , the mean shear rate at the end of axis  $a$  is

$$\langle \dot{S} \rangle = \frac{32 \langle q \rangle}{\pi a^2 b}, \quad (1)$$

where  $\langle q \rangle$  is the mean flow rate through the pipe.

The actual shear rate at the site will naturally differ from that given by Eq. 1. To isolate the contribution to that difference of individual variations in geometry (in addition to local cross section, whose effect is already included in the equation), it is convenient to introduce the concept of the "average bifurcation." The longitudinal variation of mean shear rate along the outer wall of the average aortic bifurcation is postulated to be

$$\langle \dot{S} \rangle = \frac{32 \langle q \rangle}{\pi a^2 b} P(z/d). \quad (2)$$

The function  $P(z/d)$  measures the influence of the branching geometry of the average bifurcation on the mean shear rate that would be observed at a site on the outer wall were the flow fully developed and parallel at that site. The argument of the function is longitudinal distance,  $z$ , normalized by a characteristic diameter,  $d$ , of the parent aorta. The effects of the particular geometry of each vessel are seen as deviations between the actual shear rate at a site and that predicted by Eq. 2. The largest deviations are used to identify those geometric features of real arteries that have the greatest effect on the mean shear rate along the outer wall.

The paradigm outlined above was applied to data obtained at 52 sites in six casts of minimally diseased aortic bifurcations. Since there is no a priori analytical form for  $P(z/d)$ , it was estimated by polynomial fitting of  $\pi a^2 b \langle \dot{\gamma} \rangle / (32 \langle q \rangle)$ , termed the "reduced shear rate," versus  $z/d$  (Fig. 1). Because the vessel cross section and  $\langle q \rangle$  change discontinuously on passing from the aorta to the iliacs, reduced shear data in the parent and daughters were correlated separately. The data obtained in the aorta does not support a polynomial of degree greater than unity; a quadratic minimizes the standard error of estimate of the data obtained in the iliac arteries. The fits indicate that the bifurcating geometry causes a broad minimum in reduced shear, the minimum occurring a short distance into the daughter.

Deviations from the correlations in Fig. 1 are presumed to be due to particular geometric features of the individual bifurcations. The most important features were sought by searching for geometric explanations of the deviations at the 11 sites where the reduced shear deviated from the best fit by more than one standard error of estimate. The wall contours of each branch were obtained from radiographs of the original vessel, photographs of the mold, and coordinate and angle data obtained during the hemodynamic measurements in the cast.

It was found that four specific geometric features were sufficient to explain the deviations at the 11 sites. Those features, illustrated in Fig. 2, are described below:

1. A flow divider that is offset from the aortic axis induces considerable asymmetry in the flow field and promotes increased secondary flows. The secondary flows are accompanied by an inordinately high shear stress in the aorta on the lateral wall that is farther from the tip and a low shear stress on the opposing lateral wall.
2. In most cases, the aortic contour continuously curves away from the vessel axis as

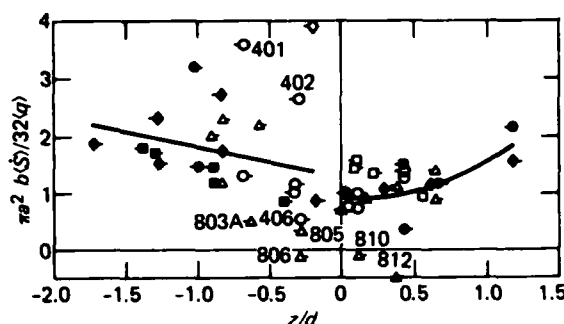


Figure 1 — Reduced wall shear rate measured in casts versus normalized longitudinal distance. The  $z$ -axis is coincident with the approximate centerline of the terminal aorta;  $z = 0$  at the flow divider tip and increases distally. The normalizing diameter is that of a circle whose area is the same as that of the aorta at  $z = -1$  cm:  $d = (ab)^{1/2}$ . The symbols, which are tagged to designate the left and right sides of the original vessel, identify data obtained in each of the six casts. The serial numbers of sites identified in Fig. 2 are shown adjacent to the corresponding data point. The data point at  $(-0.16, 3.89)$  lies well above the regression line for two reasons: the site is on an outer wall that is farther from an offset flow divider (see below), and it lies so close to the iliac origins that the cross section is no longer even approximately elliptical. The effect of the latter can be as much as a doubling of the reduced shear rate. The contralateral site at  $(-0.18, 0.83)$  lies close to the regression line because, in this case, the effect of flow divider offset opposes that of the nonelliptical cross section.

the flow divider is approached. Occasionally, an inward curvature is observed in the aorta, causing a very gentle intrusion in the flow. Shears in the neighborhood of such intrusions are surprisingly high.

3. When a daughter branch curves away from the parent at an unusually large angle, the outer wall of that branch is exposed to inordinately low shears.
4. In an asymmetric branch, where one iliac makes a large angle with the aorta and the other iliac closely follows the aortic axis, the branch geometry approaches that of a parent and a side arm. In such cases, sites on the continuing parent opposite the side arm can be exposed to relatively low shears. This effect is expected to be sensitive to flow partition and the relative areas of the daughter vessels and the parent.

The fluid mechanical effects of some of these geometric features have been demonstrated earlier, in numerical studies or in experiments with simpler models. Of importance is the finding that the variability of these particular features in real arteries is enough to cause



**Figure 2** — Tracings of the luminal molds of two vessels used in this study. Arrows point to sites where the reduced shear rates deviated from the best fits in Fig. 1 by more than one standard error of estimate. Sites 401 and 402 are in the neighborhood of an incurving aorta; they, and site 406, precede an offset flow divider tip; sites 806, 810, and 812 are on the outer wall of a markedly angulating branch; and sites 803A and 805 are on the opposite outer wall.

major variations in the hemodynamic environment at the intimal surface. Of course, the cross section at a site will also influence the wall shear, through the coefficient of  $P(z/d)$  in Eq. 2.

On the basis of the data presented here and in other work, it is possible to suggest a number of candidate geometric risk factors. A protocol pursued in parallel with that reported here has demonstrated<sup>4</sup> a negative correlation between interfacial shear rate and intimal thickness; that is, the intima is thinner where the shear is higher. If this correlation continues to gain experimental support, then large and asymmetric branch angles may be geometric risk factors. An offset flow divider tip appears to be a likely candidate as well, since it is responsible for both inordinately high and inordinately low mural shears.

## REFERENCES

- <sup>1</sup>E. Anyanwu, H. Dittrich, V. Jelesijevic, B. Druen, E. R. Krefting, and H. Hohling, "Coarctation of the Aorta. A Risk Factor in Children for the Development of Arteriosclerosis," *Atherosclerosis* **39**, 367-381 (1981).
- <sup>2</sup>*Arteriosclerosis 1981, Report of the Working Group on Arteriosclerosis of the National Heart, Lung and Blood Institute*, NIH Publication 81-2034, 1, p. 30 (Jun 1981).
- <sup>3</sup>M. H. Friedman, V. O'Brien, and L. W. Ehrlich, "Calculations of Pulsatile Flow through a Branch. Implications for the Hemodynamics of Atherogenesis," *Circ. Res.* **36**, 277-285 (1975).
- <sup>4</sup>M. H. Friedman, G. M. Hutchins, C. B. Barger, O. J. Deters, and F. F. Mark, "Correlation between Intimal Thickness and Fluid Shear in Human Arteries," *Atherosclerosis* **39**, 425-436 (1981).
- <sup>5</sup>M. H. Friedman, C. B. Barger, G. M. Hutchins, F. F. Mark, and O. J. Deters, "Hemodynamic Measurements in Human Arterial Casts, and their Correlation with Histology and Luminal Area," *J. Biomech. Eng.* **102**, 247-251 (1980).
- <sup>6</sup>F. F. Mark, C. B. Barger, O. J. Deters, G. M. Hutchins, and M. H. Friedman, "Velocity Measurements of Pulsatile Flow through a Cast of an Asymmetric Human Aortic Bifurcation," in *Proc. ASME Biomech. Symp.* AMD-43, pp. 47-50 (1981).

This work was supported by NIH grant HL21270.

## A MICROWAVE-RELATED CORNEAL EFFECT

H. A. Kues (APL) and L. W. Hirst, S. A. D'Anna, and G. Dunkelberger (JHMI)

*A microwave-induced cellular change was found to occur in the corneal endothelium of rabbits and sub-human primates for microwave exposure levels previously thought to be biologically safe.*

### BACKGROUND

The sight path of the eye includes four major elements of tissue: the cornea, iris, lens, and retina. Each element contributes to the maintenance of clear vision by means of specific functions, and each may be divided into a number of components.

The cornea (Fig. 1) is made up of the epithelium, Bowman's membrane, stroma, Descemet's membrane, and endothelium. The transparency of the cornea is due to its ordered structure, avascularity, and deturgescence. Deturgescence, the state of relative dehydration of the corneal tissue, is maintained by the anatomic integrity and active cell "pumps" of the endothelium and epithelium. In turn, the state of dehydration plays a definite role in preserving corneal transparency.

The endothelium is composed of a single layer of approximately one-half million thin and mostly hexagonal cells. It is more important in the mechanism of dehydration than the epithelium. Chemical or physical damage to the endothelium of the cornea is far more

serious than epithelial damage. Destruction of the endothelial cells may cause marked swelling of the cornea and resultant loss of transparency. It is in endothelial cells that cellular damage was found to occur in subhuman primates and rabbits after low-level microwave exposure.

The rabbit corneal endothelium is known to repair itself rapidly through mitosis. The adult primate and human endothelium, unlike that of the rabbit, does not repair itself through cell division. Once endothelial cells of these species are damaged, they die and drop out. The resulting lesions are filled in by surrounding cells that increase in size and migrate. Consequently, an overall reduction in cell population occurs.

The concern over the possibility of harmful ocular effects as a result of microwave exposure is not new. Ocular research in the past has established a firm relationship between microwave exposure and the formation of lens opacities or cataracts in test animals. However, the level of microwave exposure found necessary for cataractogenesis is in excess of 100 mW/cm<sup>2</sup> or at least ten times the amount of exposure allowed under the most conservative safety standards. This level is thought to be well into the "thermal damage zone." In contrast, the effect on the endothelium that we describe occurs at microwave levels close to those presently allowed by the microwave exposure safety standard.

### DISCUSSION

Subhuman primates (cynomolgus monkeys) and rabbits (Dutch-belted pigmented) were subjected to specular microscopic examinations both prior and subsequent to predetermined low-level microwave exposures. The apparatus used for the animal irradiations is shown in Fig. 2. The 2.45 GHz continuous (CW) microwaves were generated by a microwave signal source driving a traveling wave tube (TWT) amplifier. The microwave energy was transmitted through a coaxial cable to a bidirectional coupler that was configured as a reflectometer to measure both forward and reflected input power on associated power meters. The microwaves then passed through the directional coupler into a coaxial-to-waveguide transition source located within the absorption chamber. The source was positioned over the ocular area to be irradiated at a height sufficient to allow a 10 cm gap between it and the ocular surface. In-

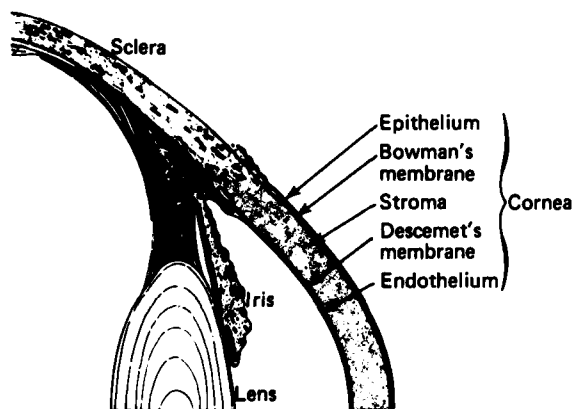


Figure 1 — Anatomy of the anterior eye.

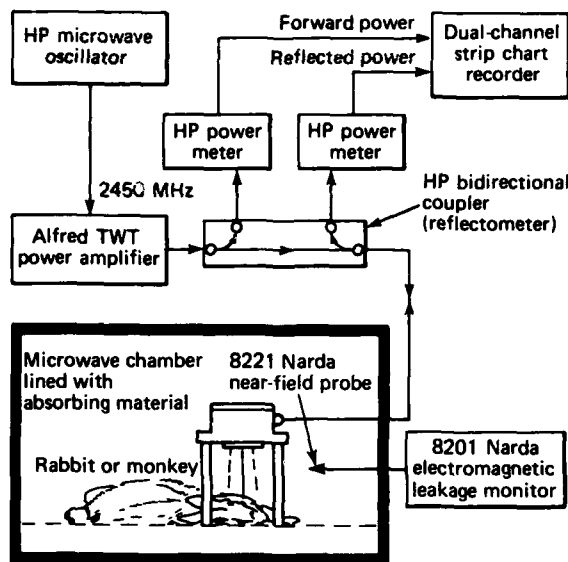


Figure 2 — The experimental microwave apparatus.

put and relected power levels were recorded on a dual-strip-chart recorder during each four-hour exposure. The 2.45 GHz pulse irradiations were performed as indicated above with one exception: a pulsed signal source was used in place of the CW source and the TWT power amplifier.

The microwave power density at the cornea was determined prior to each exposure before the animal was placed in position, by means of a calibrated microwave field probe. The anesthetized animal was placed in the absorption chamber either in a supine position, with both eyes directed toward the microwave source, or in a lateral position, which allowed the nearer eye to be exposed.

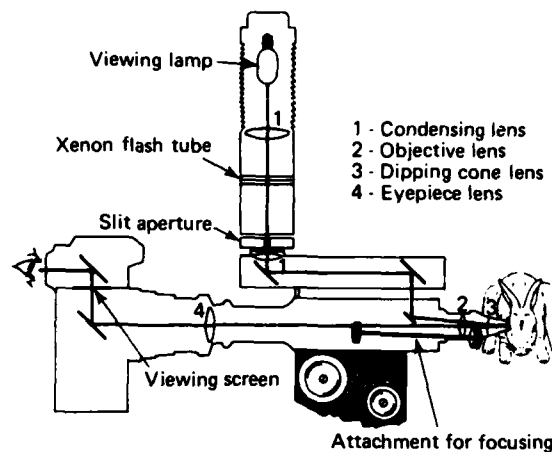


Figure 3 — The biospecular microscope.

A contact specular microscope (Fig. 3) was used to observe and photograph the *in vivo* corneal endothelium of both eyes. The examinations were performed immediately before exposure and four hours after. Additional follow-up photographs were taken 16 to 72 hours postexposure. Nonirradiated animals were also examined; they had been treated exactly the same as the exposed animals except that they had received no microwave exposure.

Table 1 summarizes the results to date of our assessment of the 2.45 GHz microwave exposures and how they affect the rabbit corneal endothelium. Since rabbit corneal endothelium is known to repair itself rapidly, it was not considered unusual that the one-

Table 1 — Microwave-related endothelial effects (data for rabbit, 2.45 GHz)

Microwave Frequency Mode*	Single Four-Hour Exposure Level (mW/cm <sup>2</sup> )	Preexposure Endothelial Condition Normal/Abnormal	Four-Hour Postexposure Endothelial Condition Normal/Abnormal**	16- to 24-Hour Postexposure Endothelial Condition Normal/Abnormal
2.45 GHz CW	5	2/0	2/0	2/0
2.45 GHz CW	10	11/0	10/1	7/3
2.45 GHz CW	20	8/0	8/0	7/1
2.45 GHz pulse	10 av.	4/0	3/1	1/2
2.45 GHz pulse	20 av.	1/0	1/0	0/1
Sham exposure	0	6/0	6/0	6/0
Nonexposed control eyes		26/0	26/0	26/0

\*In the pulse mode, pulses were 10  $\mu$ s wide and had a 300 pps repetition rate.

\*\*Cellular changes observed four hours postexposure were considered minor in degree.

week postexposure examinations showed complete repair of the damaged areas.

Cellular abnormalities similar to those shown in the rabbits were exhibited by 10 subhuman primates. While preliminary results with primates indicate that a four-hour exposure to 20 to 30 mW/cm<sup>2</sup> of CW irradiation at 2.45 GHz will produce cellular effects, a four-hour exposure of pulsed microwaves at 2.45 GHz produces similar effects for as low as, and possibly even below, 10 mW/cm<sup>2</sup> average power.

Figure 4a is a wide-field, specular-microscope photograph of a normal primate endothelium before microwave exposure; Fig. 4b is a photograph representative of a series taken 48 hours after exposure. The dark areas clearly portray cellular changes subsequent to exposure.

In order to determine that a thermally damaging level was not produced by our microwave exposures, *in*

*vivo* temperature measurements were made using a non-perturbing fluoroptic thermal probe system. Exposure levels for all cases were set at 20 mW/cm<sup>2</sup> of CW microwave irradiation at 2.45 GHz. Measurements were taken first with only the probe in the chamber. The microwave chamber temperature increased 3°C during the four-hour test irradiation; the room temperature increased 2.7°C during the same period. Measurements were taken with a fluoroptic probe implanted in the anterior chamber and butted against the endothelial layer of the upper eye of an anesthetized rabbit lying on its side within the chamber. After four hours of exposure, the temperature increased 0.9°C. Measurements were taken with a fluoroptic probe placed on the outer central cornea and under the closed eyelid of one eye of an anesthetized primate lying supine within the chamber; measurements were also taken in the unexposed eye. After four hours of exposure, an increase of 0.2°C was measured in the exposed eye and of 0.1°C in the unexposed eye. It was determined from these experiments that the cellular effect we are observing is not caused by direct thermal damage.

The long-standing United States safety standard for microwave exposure was recently replaced. The old standard recommended 10 mW/cm<sup>2</sup> as the maximum chronic exposure level for all microwave frequencies. The new standard recommends 1 mW/cm<sup>2</sup> up to 1.50 GHz and 5 mW/cm<sup>2</sup> beyond 1.50 GHz. Our preliminary data suggest an observable effect at approximately 10 mW/cm<sup>2</sup> for exposure to 2.45 GHz; this is quite close to the allowed 5 mW/cm<sup>2</sup> level of the new standard. On the basis of histological findings in affected eyes, cellular changes might occur in the endothelium at exposure levels below the 10 mW/cm<sup>2</sup> level. Furthermore, the effect of long-term, low-level microwave exposure on the cornea has not been fully investigated. Should such cellular changes be compounded over extended periods of time, it is conceivable that marked endothelial thinning and perhaps even corneal clouding could result.

In addition to the possibility of human health decrement, interest exists in learning something about the mechanisms involved in the interaction of cells and microwaves. Although cellular changes have been noted upon microwave exposure, the actual mechanisms through which damage occurs remain unknown. Investigation of such mechanisms is crucial to the understanding of the interaction between microwaves and living organisms.

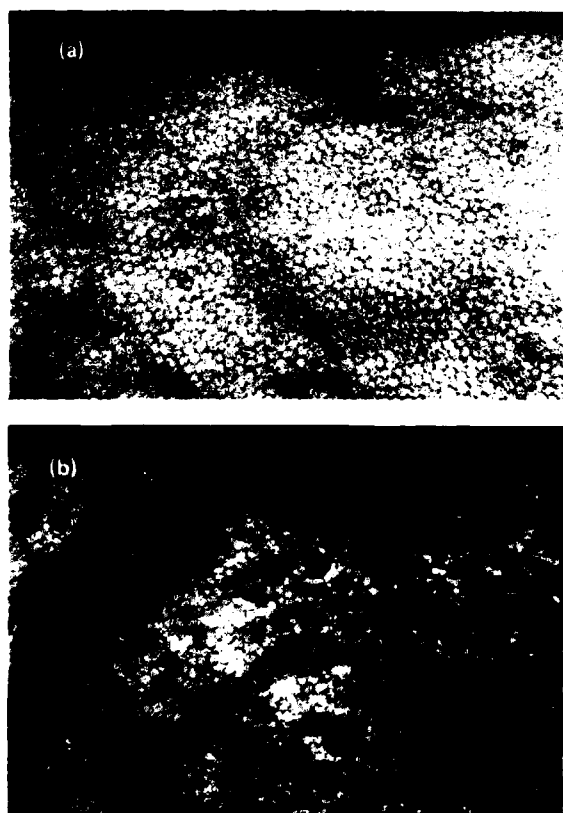


Figure 4 — (a) Specular microscope photograph of a normal primate endothelium before microwave exposure. (b) Specular microscope photograph of a primate endothelium 48 hours after exposure. The dark areas are cellular changes induced by the microwave exposure.

## ROBOTIC ARM TO PROVIDE MANIPULATIVE CAPABILITY TO THE DISABLED PERSON

W. Schneider, J. H. Loveless, and W. Seamone

*A computer-controlled robotic arm designed for high-spinal-cord injured persons has been under development at APL for the past several years. New features added to the system now make it ready for clinical evaluation.*

### BACKGROUND

High-spinal-cord injury can cause total loss of control in lower- and upper-limb functions and thus begot a devastating handicap. Opening the door to self-reliance for a person so handicapped has long been a goal of the Veterans Administration (VA). For the past 10 years, the VA has sponsored several research programs in the United States to develop assistive devices for the quadriplegic. The application of robotics is one potential solution to this critical problem. Stanford University and APL are among the institutions investigating the use of robotics for high-spinal-cord injured persons.

An advanced model of the robotic arm/work table being developed at APL under VA sponsorship is now undergoing clinical testing at the Spinal Cord Injury Unit at the VA Medical Center in Richmond, Va. Continued engineering development of the robotic arm/work table system at APL during 1982 has added features that enhance its potential value to the quadriplegic. Among the improvements are programming techniques to simplify the use of prestored motion trajectories that allow practical management of the typewriter, telephone, books, etc., as well as a computer for vocational or personal use. With these improvements, the occupational therapist or user can easily program the motions of the robotic arm. The addition of a chin-operated system for Morse code allows the user to operate a personal computer with minimum assistance; it requires only that disks be changed. Another important improvement — the self-feeding mode — expands the system's capability and allows the quadriplegic to eat food such as sandwiches, hot dogs, and french fries. This change augments the earlier capability for eating bite-size food.

### DISCUSSION

The APL robotic system uses a structured work table concept<sup>1</sup>; that is, the components are located on the work table in a way that allows the robot to use prestored motion trajectories to carry out a desired

function. The concept makes manageable, for example, the difficult task of putting a single sheet of paper into the typewriter. The system is designed for the highly disabled person who is unable to use his arms or hands but who has nearly full motion of the head and neck. Such motions are enough to control the robotic system by means of a chin-operated controller mounted on the wheelchair. The controller also runs the quadriplegic's electric wheelchair.<sup>2</sup> This duality of control gives the quadriplegic a much needed mobility as well as a way to manipulate tasks made possible by the robotic arm.

The robotic arm is a six-degree-of-freedom, computer-controlled, anthropomorphic limb whose individual degrees of freedom may be controlled directly by selecting the joint to be moved. The user may also select prestored trajectories to accomplish a specific task. To stop a preprogrammed trajectory at any time, the user merely pushes the chin-controller pulse switch.

The redesigned keyboard, editor, and file handler for the application program are important new features. The motions of the robotic arm are specified by functional keys on the programming keyboard, which is shown in Fig. 1 temporarily located near the front of the table. The keyboard is plugged into the robotic arm to make program changes but is removed during normal operations. Editing keys allow the sequentially numbered commands to be inserted and deleted easily. Motion sequence files (prestored robotic arm trajectory motion sequences) are identified by page name (collection of files) and program name (specific file). These names are specified with alphanumeric keys. All files



Figure 1 — Robotic arm/work table with programming keyboard plugged into arm.

reside in battery-backup CMOS (complementary metal-oxide semiconductor) read-write memory, and all file handling is transparent to the user.

The functional keys define language elements (similar to those of Basic) for the easy specification of motion sequences. There are commands for motion to a point, conditional and unconditional branching, stimulation and sensing of external devices, jumps to other motion sequences, pauses, and so on.

The following tasks (only a partial list) use pre-stored application programs in the current model of the robotic system:

- Move mouthstick into position
- Pick up telephone and place it in position for use
- Hang up telephone
- Pick up Kleenex tissue
- Move typewriter forward
- Put sheet of paper into typewriter
- Remove sheet of paper from typewriter
- Pick up any of five books in reading stand
- Return book to storage location
- Eat sandwich from plate
- Eat with spoon from plate
- Eat from bowl

Another important new feature on this work table is a chin-operated Morse code system to command a personal computer instead of the keyboard. A standard Morse code keyer operated by minute motions of the chin gives the user full control of all keyboard characters, including the control and shift keys. This keyer is shown on the work table in Fig. 2. Because the keyboard is not used directly, it can be moved to the rear of

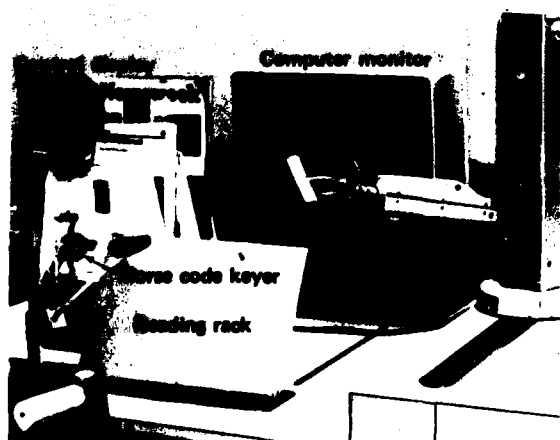


Figure 2 — Morse code interface for robotic arm/work table.

the work table. A series of audible dots or dashes generated by chin motions sends, via a single chip microprocessor, the appropriate ASCII characters to the computer. This approach was verified by tests with quadriplegic volunteers using an Apple computer. Speeds of 60 characters per minute are easily achievable, and simultaneous key entries such as those required with the control, shift, or repeat keys are accommodated. In demonstrations at APL, word-processor programs such as Applewriter or Magic Window and electronic spreadsheet programs such as Visicalc were shown to be practical. The demand for this Morse code interface with the Apple computer was great enough to convince a manufacturer to sign a license arrangement with APL to manufacture and sell the device.

Self-feeding by the quadriplegic is one of the important tasks to be evaluated with this system. During the past year, the devices and the prestored programs used for self-feeding were improved. A new spoon arrangement with a functional wire clamp (Fig. 3) allows the user to eat such things as sandwiches, hot dogs, french fries, and lettuce. Self-feeding takes place on the right side of the table, and two bowls and a plate may be used. As the user approaches the desired portion of food or the sandwich with the spoon, the wire clamp is retracted. Clamp motion is activated to hold the food during the appropriate part of the cycle (Fig. 4). After the sandwich or other food has been brought to the mouth and most of it has been eaten, the user may command the clamp to open so that he may take the last bite off the spoon. In the prestored eating program using the bowl, the spoon is preprogrammed to go into the bowl, pick up a bite-size portion, scrape the bottom of the

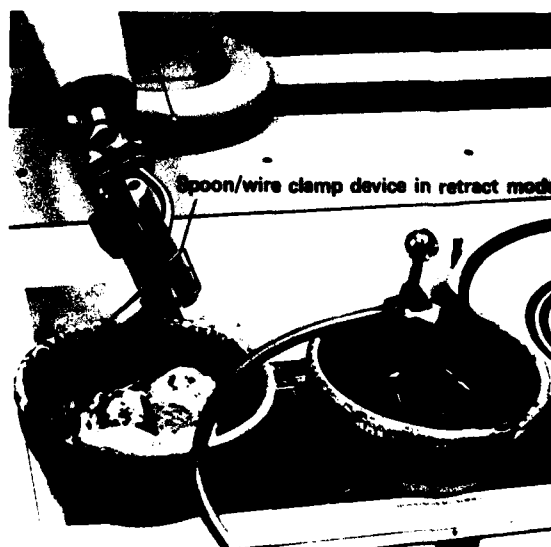
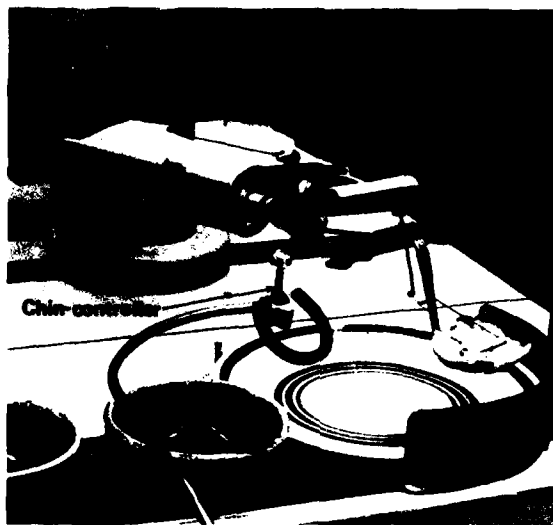


Figure 3 — Self-feeding arrangement with robotic arm.



**Figure 4** — Self-feeding arrangement to permit handling of bread and sandwiches.

spoon to remove drippings, and proceed to the user's mouth. While eating, the user may command a change to any of several eating modes, e.g., from bowl to plate or from plate to bowl. The self-feeding mode was tested at APL and shows great promise as a practical eating arrangement. An evaluation is planned at the VA Centers in Richmond and Cleveland.

## SUMMARY

Design features added during 1982 have improved the capability of APL's robotic arm/work table system for self-feeding, programming of prestored motions, and communicating with a personal computer. After eight years of development, it is now ready for serious clinical testing at two VA Spinal Cord Injury Centers. This evaluation testing is expected to yield quantitative data on the value of robotics for the daily needs of the high-spinal-cord injured person.

## REFERENCES

- <sup>1</sup>W. Schneider, G. Schmeisser, and W. Seamone, "A Computer-Aided Robotic Arm/Worktable System for the High-Level Quadriplegic," *Computer* (Jan 1981).
- <sup>2</sup>W. Seamone and G. Schmeisser, "New Control Techniques for Wheelchair Mobility," *Johns Hopkins APL Tech. Dig.* 2, 179-184 (1981).

---

This work was supported by the Veterans Administration.

## USE OF A PROGRAMMABLE IMPLANTABLE MEDICATION SYSTEM TO CONTROL PLASMA GLUCOSE LEVELS IN DIABETIC DOGS

R. E. Fischell and W. E. Radford (APL), C. D. Saudek (JHH), and J. R. Champion (APL)

*The Programmable Implantable Medication System developed at APL has been implanted and used to control plasma glucose levels in diabetic dogs. This work is part of the ongoing bench and animal studies of the system's efficacy in the treatment of diabetes.*

### BACKGROUND

In 1980, some 1.3 million Americans required insulin injections at least once each day. Insulin delivered in such a manner prolongs the life of the diabetic but it does not provide the same measure of blood glucose control as a normal pancreas. Long-term hyperglycemia (increased plasma glucose concentration) is believed by many medical researchers to be the cause of the long-term complications of diabetes, i.e., blindness, kidney failure, heart disease, nerve degeneration, and gangrene.<sup>1</sup>

The potential of insulin infusion pumps to provide improved control of blood glucose in the insulin-dependent diabetic has been discussed in the literature.<sup>2,3</sup> Externally worn insulin pumps are widely marketed at present. The Programmable Implantable

Medication System (PIMS) developed at APL is undergoing bench and animal studies to determine the system's efficacy in the treatment of diabetes and has been used to control plasma glucose levels in diabetic dogs.

PIMS consists of an Implantable Programmable Infusion Pump (IPIP), an implanted device that controls the release of medication, and the necessary support equipment. Figure 1 diagrams the patient's and the physician's equipment. IPIP can be programmed by the physician; additional programming for self-medication can be performed (at the physician's option) by the patient himself. The patient's programming unit is a hand-held device used by the patient to communicate with the IPIP for self-medication. The physician will have a medication programming system, consisting of a "smart" terminal called a medication programming unit (to be used by the physician for programming the IPIP) and a paper printer (which provides a permanent record of the IPIP programming). A communication head serves as both transmitting and receiving antennas. Communication can also take place via telephone transceivers, as shown.

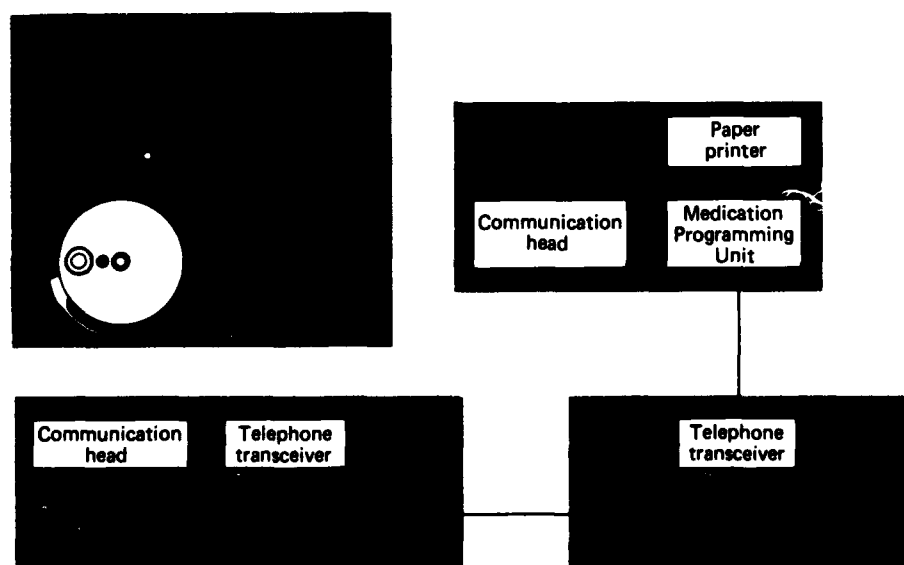


Figure 1 — The Programmable Implantable Medication System.

The IPIP has a CMOS 1802 microprocessor-based microcomputer system. Programming of the IPIP is performed after implantation by means of the unit's command and telemetry systems. The command system sends instructions and programming information by radio into the implanted IPIP. The radio telemetry system confirms receipt of the stored program and also sends out data relating to functions of the IPIP. The medication programming system is used by the physician to program a basal medication delivery profile. The physician has the option to program a 2  $\mu$ l infusion pulse for each quarter-hour interval in a repeating 24-hour cycle. In addition, as many as six different supplementary delivery schedules can be programmed by the physician to meet the individual patient's needs. Medication will be delivered according to these schedules when the patient uses his programming unit to initiate the appropriate command.

The patient's programming unit is used by the patient (at the physician's option) to request the preprogrammed, supplementary medication profiles. It can direct the IPIP to deliver full-basal and half-basal infusion rates in addition to any one of the six separately programmable supplementary delivery schedules. It can shut off all medication flow for from one hour (minimum) to eight hours (maximum). The patient can also countermand a previously commanded medication instruction. The basal programming is resumed automatically at the end of the one to eight hour shutoff period.

The IPIP can simulate the basal and postprandial insulin profiles delivered by the normal pancreas. Using his system, the physician can construct infusion patterns to meet the individual patient's need. Once programmed, the 24-hour basal cycle will continue automatically unless the patient uses his unit to decrease the basal infusion by half or shut delivery off for up to eight hours. The patient's unit also allows him to command a postprandial insulin profile appropriate to the meal consumed.

The IPIP reservoir capacity is 10 ml. Filled with the proper concentration of insulin, this could provide about three months of blood glucose control for most patients. It is refilled by inserting a hypodermic needle into a septum-covered antechamber in the IPIP.

## DISCUSSION

Currently, PIMS is undergoing bench and animal trials for the diabetes application. The initial two implantations in diabetic dogs (October 1981 and February 1982) were terminated for technical reasons, including the aggregation of insulin in a catheter and unacceptable valve backleaking. The communication,

programming, interrogation, and refill systems were shown to function properly in the initial trials.

On 5 May 1982, a third IPIP was implanted in a diabetic dog at the Johns Hopkins Hospital. Figure 2 shows plasma glucose levels in the dog for the month prior to implantation. He was given two injections of insulin a day in an attempt to control plasma glucose. With this optimum regimen of subcutaneous insulin, his plasma glucose levels varied from the low 30's to a high of 452 mg/dl. On the day following implant, the plasma glucose varied from 60 to 310 mg/dl and decreased progressively the first six days after implantation.

The results for days 18 to 23 are shown in Fig. 3. By the eighteenth postoperative day, the blood glucose levels were within the normal range of 75 to 90 mg/dl. These results were accomplished by feeding the dog at 9:00 a.m. and selecting a basal rate of 0.72 unit per hour from 9:00 a.m. to 5:00 p.m. and a lower basal rate of 0.42 unit per hour from 5:00 p.m. to 9:00 a.m. Fifteen minutes before the dog was fed, a supplemental infusion of insulin of 21.2 units was begun and was given over a period of eight hours. The supplemental infusion was rapid at first and then fell exponentially. A major difference between the metabolism of dogs and humans is that humans absorb their food in a much shorter time so that a three-hour period of supplemental infusion is typical of the human and an eight-hour supplemental delivery of 21.2 units (Fig. 4) is more typical of the diabetic dog's requirement.

On days 21 to 23, the dog ate in a shorter time. Consequently, his plasma glucose level rose to somewhat higher levels than those reached during days 18 to 20. By day 30 of the experiment, the dog developed an infection around the implanted IPIP and it was necessary to remove the infusion pump and its catheter.

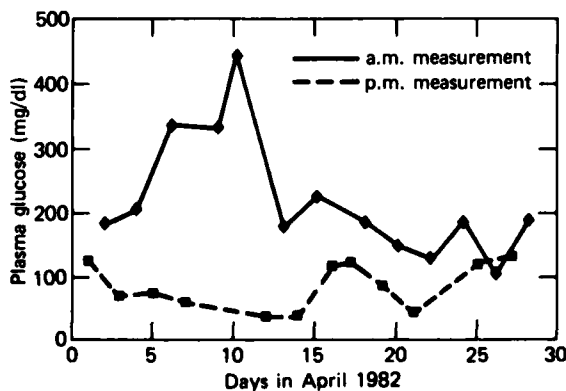


Figure 2 — Plasma glucose levels in the diabetic dog receiving two injections of insulin a day, before IPIP implantation.

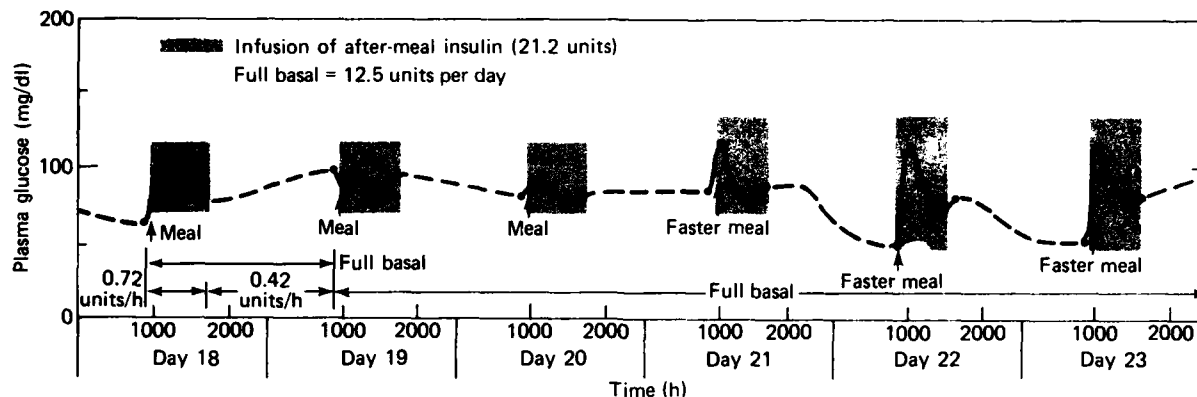


Figure 3 — Plasma glucose levels in the same dog days 18 to 23 after IPIP implantation.

Figure 4 shows the telemetered record of insulin infusion for the dog on 23 May 1982. These data were obtained from the random access memory within the implanted IPIP. In fact, the data were requested by a command signal emanating from APL and sent by telephone to the telephone transceiver at Johns Hopkins Hospital, 25 miles away. Once interrogated, the implanted IPIP read out by telemetry the data shown in Fig. 4. From these data we see that, in fact, the basal rate was 0.42 unit per hour between the hours of 5:00 p.m. and 9:00 a.m. and 0.72 unit per hour from 9:00

a.m. to 5:00 p.m. The supplemental dose of 21.2 units is shown in Fig. 4 in its exact time format. The supplemental infusion was controlled by a command from the patient's programming unit as per system design.

A comparison of the preimplant hyperglycemia (Fig. 2) with the postimplant glucose levels (Fig. 3) clearly demonstrates that PIMS, in providing computer-controlled release of insulin, achieves far better control of plasma glucose than is obtainable by two daily injections. Specifically, both the peak values of

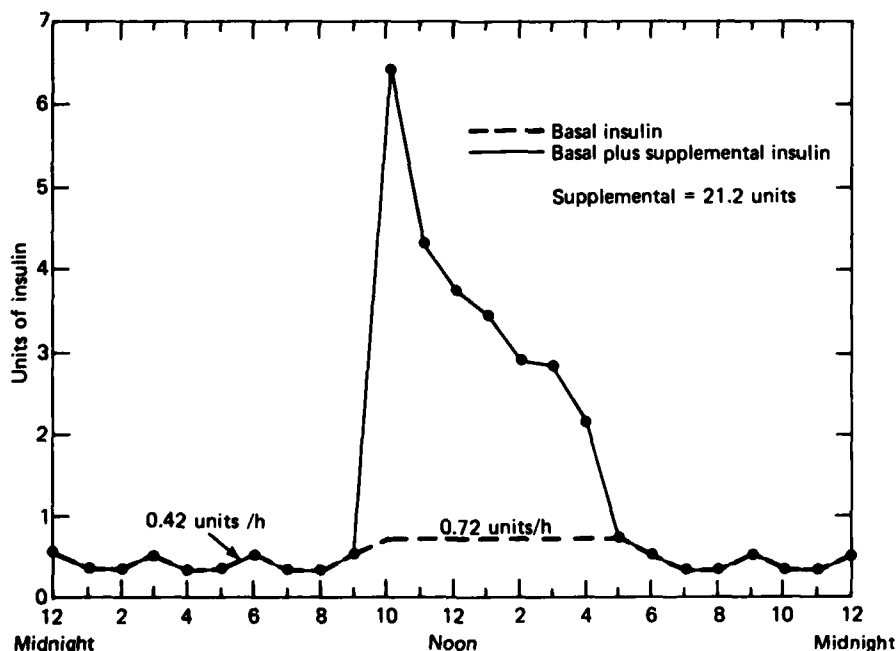


Figure 4 — A record of the insulin infused by the IPIP into the diabetic dog, day 23 after implantation.

plasma glucose and its excursions during the day are dramatically reduced by the use of IPIP. It has also been demonstrated that the patient's programming unit, the medication programming system, and the telephone transceiver performed in a completely satisfactory manner.

After more testing, it is expected that PIMS will be made available for trials with human diabetic patients who could profit from the improved therapy that PIMS should be able to provide.

### ACKNOWLEDGMENTS

The development of the PIMS resulted from the efforts of many APL staff members as well as employees of the Parker-Hannifin Corp.

### REFERENCES

- <sup>1</sup> M. Brownlee and G. F. Cahill, "Diabetic Control and Vascular Complications," in *Atherosclerosis Reviews* 4, Raven Press (1979).
- <sup>2</sup> J. V. Santiago, A. H. Clemens, W. L. Clarke, and D. K. Kipnis, "Closed-Loop and Open-Loop Devices for Blood Glucose Control in Normal and Diabetic Subjects," *Diabetes* 28, 71-84 (1979).
- <sup>3</sup> *New Approaches to Insulin Therapy*, K. Irsigler, K. N. Kunz, D. R. Owens, and H. Regal, eds., MTP Press Ltd., Lancaster, England (1981).

This work was supported by the APL Development Fund, the NASA Goddard Space Flight Center Technology Utilization Office, and the National Institutes of Health.

## TECHNICAL SUPPORT IN INFORMATION SYSTEMS

B. I. Blum

*From 1975 to the present, through an interdivisional assignment, APL has technically supported the Johns Hopkins Medical Institutions in the development and evaluation of clinical information systems. Several significant systems have been implemented, and a staff of University and Hospital employees was hired and trained to manage all subsequent development activities. This article reviews the major accomplishments of that period.*

### DISCUSSION

#### The Minirecord System

In 1974, APL, the Department of Biomedical Engineering, and the management of the Hamman-Baker Medical Clinic began a collaborative effort to develop an inexpensive, computer-stored medical record that would improve follow-up and continuity of care to the 7000 chronically ill patients treated by the clinic. Designed to give on-line access to a minimal essential medical record, it was called the Minirecord System.

After developing a prototype system on the APL computer, the collaborators created a data base and modified programs to operate from the Hospital's computer. The system was then linked to an appointment system to produce a two-page "encounter form" that would be available before each patient's visit. Encounter forms could also be printed on demand for unscheduled patients. The first page contained registration information such as the patient's address and insurance coverage. The second page (Fig. 1) contained the list of current problems, a summary of medication, and a history of visits to other clinics. In actual practice, the physician wrote the progress note on this page and updated the problem list as part of the note. The original of this note became part of the medical record, and a copy was used to update the problem list. The first page of the encounter form was also used to order tests and prepare charges.

The Minirecord was available on-line in the Emergency Room, the Walk-In Clinic, the Medical Clinic, and selected inpatient units. The system was well received and remained in operation until 1982 when the

# THE JOHNS HOPKINS HOSPITAL OUTPATIENT DEPARTMENT NOTE

CLINIC MED (141) DATE 03/06/79 HISTORY NO: NAME:

TEMP WT B.P.

4 VISIT(S) SINCE LAST MED ENCOUNTER (12/19/78)

ER 01/04/79.  
DIAB MAN 01/10/79.  
SUR FOLL 02/07/79.  
PCC 01/04/79.

LAB RESULTS: DONE IN CLINIC GUAIAC + NON + HCT

UR STAIN UA

<input checked="" type="checkbox"/> CHECK ALL PROBLEMS TREATED THIS VISIT. WRITE IN TO ADD; LINE OUT TO DELETE		
PROBLEMS ADDRESSED LAST VISIT		OTHER PROBLEMS AND PRIOR CONDITIONS
1( ) DISCH FROM HAL-8 ON 012879		5( ) FLANK PAIN
2( ) HBP		6( ) FOLLICULITIS
3( ) HEADACHES		7( ) OMD
4( ) DIABETES-INSULLIN REQUIRED		8( ) SCHIZOPHRENIA
ADDITIONAL PROBLEMS THIS VISIT:		9( ) DIABETIC RETINOPATHY
		10( ) DIABETIC NEUROPATHY
		11( ) DJD LUMBAR SPINE
		12( ) NEUROGENIC BLADDER
		13( ) ASCVD WITH H/D PAT
		14( ) PENICILLIN ALLERGY
		15( ) RECURRENT UTI'S
**WRNG. ONLY 1 CHAR OF TEXT REMAINING		
CURRENT MEDICATIONS (WRITE IN TO ADD; LINE OUT TO DELETE. INDICATE NO REFILL/REFILL IF DESIRED)		
16 NPH INSULIN		
SPECIAL PT. <input type="checkbox"/> PROVIDER NUMBER _____ SIGNATURE _____		

Figure 1 — Encounter form, page 2.

Medical Clinic was replaced by the Johns Hopkins Internal Medicine Associates. A multiclinic expansion of the Minirecord System, called the Core Record System, was implemented in 1980 and is currently in use in the Emergency Department, the Orthopedic Clinics, and the Oncology Center.

### **The Oncology Clinical Information System**

When the Minirecord System development was coming to a close, preparations were under way to open a comprehensive Oncology Center that would provide facilities for 56 inpatients, 500 outpatients per week, radiation therapy, and research laboratories. Because of the success of the Minirecord System, APL was asked to direct work on a system for the Oncology Center.

The needs of the Oncology Center were quite different from those of the Medical Clinic, which had required a short problem list at very low cost. The Oncology Center used complex protocols, collected as many as 100 data elements per patient-day, and followed its patients for years. It needed tools to manage and present clinical data in formats that would support decision-making. There also was need for computer reminders of protocol-directed care as well as tools for retrospective analysis of patient data.

The system was implemented in four phases. The first was a prototype that operated on the APL computer and provided insights into the most useful data formats for patient care. The second and third phases addressed the management of patient data and automated support for protocol-directed care. The fourth phase, development of facilities for data analysis, will be completed in mid-1983.

The Oncology Clinical Information System contains information on some 37,000 patients, including 90% who were treated at the Oncology Center. The available data include text abstracts, test results, therapy summaries, and administrative information. Data presentations and care plans are produced each day and delivered in time for morning rounds or outpatient visits. Among the most useful output formats is the printer plot (Fig. 2). The plot shows the first 36 days of therapy of a leukemia patient treated with a combination of two antitumor drugs. The platelet and white blood cell counts are plotted on a logarithmic scale. Below this scale are shown the administration of chemotherapy and antibiotics, the transfusion of blood products, and the temperature in degrees above normal.

To illustrate how such plots can be used for patient care, note how it combines information to review the patient's progress. Therapy for leukemia with Cytosine Arabinoside and Daunomycin was begun on Febru-

ary 16. Under the convention used by this protocol, that date is renumbered treatment day 1 (TX DAY). In accordance with a laboratory research model of cell kinetics, a second cycle of Cytosine Arabinoside chemotherapy is given beginning on day 8. The effect of the treatment is readily seen. A large number of malignant leukemic cells, plotted as white blood cells (W), are eliminated, the value falling from a pretreatment level of 80,000 to 100 by day 5.

At the bottom of the plot, the patient's maximum daily temperature is indicated in degrees (centigrade) above normal. The temperature was elevated at the outset of treatment; when the problem of bone marrow aplasia is added, two antibiotics are given. The temperature then falls to normal. Protocols for the management of fever in the absence of normal white blood cells are a routine part of the organized approach to clinical management and must be considered in the design of the computer display.

To continue with this illustration, the effect of a standard protocol for administering blood platelets is also seen. Platelets (plotted as P on the graph) are monitored daily. When the platelet level in the blood falls below 20,000/mm<sup>3</sup>, there is a danger of hemorrhaging, and platelet transfusions are given. The plot uses a horizontal line drawn at 20,000 to provide a visual guide for the medical management team. In this case, transfusions of platelets correlate well with higher platelet levels on the following day.

By day 19, normal white blood cells are seen to be returning; by day 32, the patient's leukemia is shown to be in remission and he is ready for discharge. This particular plot presents a summary of treatment and responses; its daily availability becomes a mechanism for the early detection of trends that require new or different interventions.

### **Other Activities**

While most of the interdivisional activity was related to the above two projects, other responsibilities included teaching and course development, implementation of smaller systems for other clinical departments, and software engineering. In the seven years of the assignment, 50 papers were published or presented at scientific meetings. A representative bibliography is provided.

The APL staff was assigned temporarily to individual projects on an *ad hoc* basis. It was decided, however, that the Medical Institutions should have their own staff. By late 1982, the Department of Biomedical Engineering had a faculty member and staff fully able to assume the responsibilities of the Clinical Informa-

Chemotherapy is given in two 3-day cycles 1. The malignant leukemic cells 2 are eliminated 3. Antibiotics 4 are prescribed for infection, and the temperature becomes normal 5. The platelet count falls 6 and platelets are transfused 7. The plot has waving lines for low platelet count 8, which increases the risk of hemorrhage, and for low white blood cell count 9, which increases the risk of infection. By day 32 10, the patient is in remission.

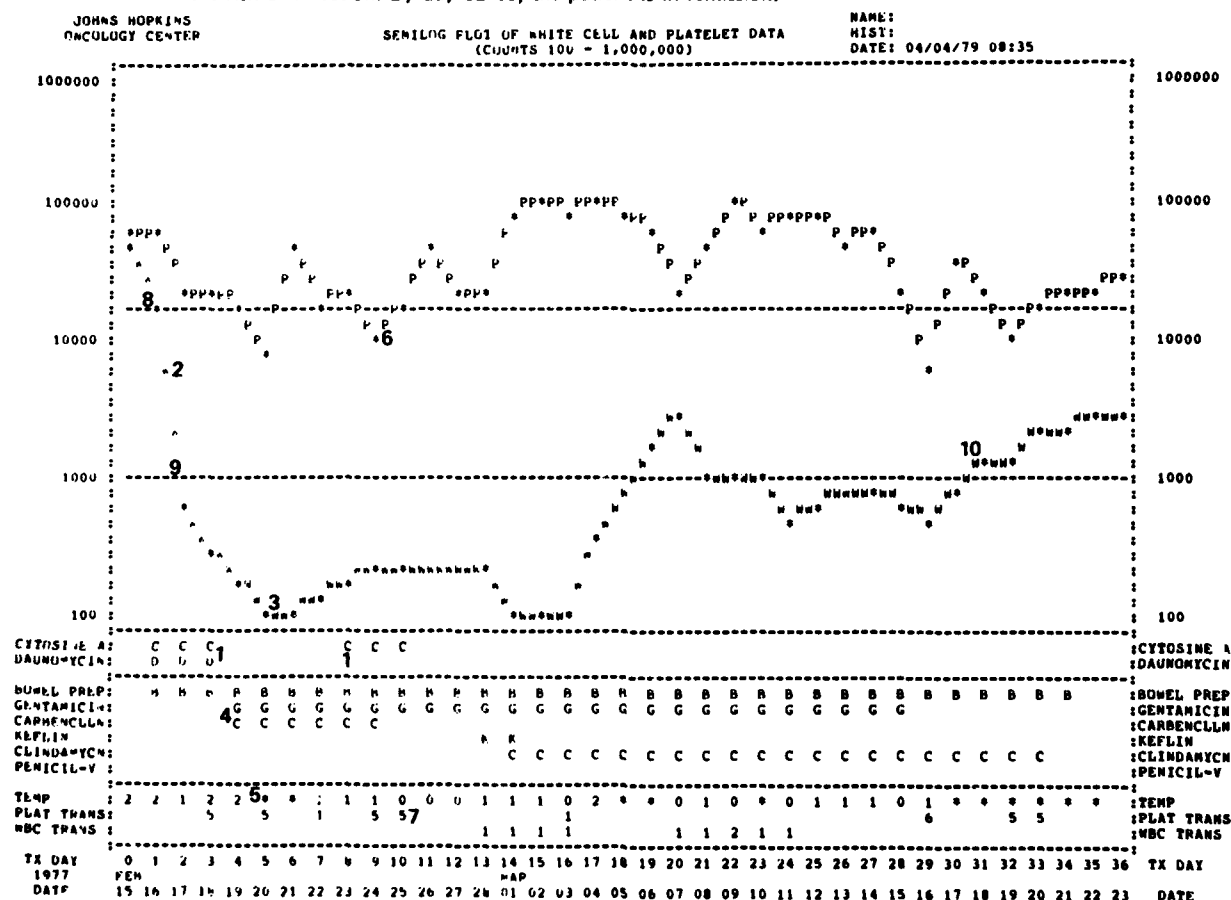


Figure 2 — Printout record of 36 day therapy.

tion Systems Division, and the Oncology Center had a staff trained in the operation and maintenance of the Oncology Clinical Information System. APL's expertise was thus transferred to the Medical Institutions, and the author's seven-year assignment came to an end. However, the developed information systems will continue to be an integral part of patient care at the Johns Hopkins Hospital.

## BIBLIOGRAPHY

### The Minirecord System

C. Johns, D. Simborg, B. Blum, and B. Starfield, "A Minirecord: An Aid to Continuity of Care," *Johns Hopkins Med. J.* 140, 277-284 (1977).

B. Blum, C. Johns, E. McColligan, C. Smith, and D. Steinwachs, "A Low Cost Ambulatory Medical Information System," *J. Clin. Eng.* 4, 372-378 (1979).

B. Blum, R. Johns, and E. McColligan, "An Approach to Ambulatory Care Medical Records," International Conf. on Systems Science in Health Care, Montreal (14-17 Jul 1980).

### The Core Record System

E. McColligan, B. Blum, and C. Brunn, "An Automated Core Medical Record System for Ambulatory Care," *J. Med. Syst.* (in press).

E. McColligan and B. Blum, "Evaluating an Automated Core Medical Record System for Ambulatory Care," American Medical Informatics Association Meeting, San Francisco (2-5 May 1982).

### The Oncology Clinical Information System

B. Blum, R. Lenhard, H. Braine, and A. Kammer, "A Clinical Information Display System," in *Symposium in Computer Applications in Medical Care*, Washington, pp. 131-138 (3-5 Oct 1977). Reprinted in *Computers and Medicine*, V. Sondak, and H. Schwartz, eds. Artech House, Inc., Dedham, Mass. (1979).

B. Blum and R. Lenhard, "Privacy and Security in an Oncology Information System," in *Symposium in Computer Applications in Medical Care*, Washington, pp. 500-508 (5-9 Nov 1978). Reprinted in *Computers in Medical Administration*, V. Sondak, ed., Artech House, Inc., Dedham, Mass. (1979).

B. Blum and R. Lenhard, "An Oncology Clinical Information System," *Comput. Mag.* 12, 42-50 (Nov 1979).

E. McColligan, B. Blum, R. Lenhard, and M. Johnson, "The Human Element in Computer Generated Patient Management Plans," Conf. of the Society for Computer Medicine, San Diego (24-27 Sep 1980). Reprinted in *J. Med. Syst.* 3 (1982).

B. Blum and R. Lenhard, "Experience in Implementing a Clinical Information System," MEDINFO 80 Conference, Tokyo (29 Sep-4 Oct 1980).

B. Blum and R. Lenhard, "Displaying Clinical Data for Decision Making," *J. Clin. Eng.* (Jun 1982).

R. Lenhard, B. Blum, J. Sunderland, H. Braine, and R. Saral, "The Johns Hopkins Oncology Clinical Information System," in *Proc. Symp. on Computer Applications in Medical Care*, 28-43 (1982).

### Education and Other Activities

R. Johns and B. Blum, "The Use of Clinical Information Systems to Control Cost as Well as to Improve Care," *Trans. Am. Clin. Climatol. Assoc.* 90, 140-152 (1978).

B. Blum and R. Johns, "Computer Technology and Medical Costs," in *Information Processing 80*, S. H. Lavington, ed., North-Holland Pub. Co., pp. 903-906 (1980).

B. Blum, "Review of the Established Benefits of Automated Information Systems in Patient Care," in *Application of Computers in Medicine*, IEEE TH 0095-0 (Mar 1982).

B. Blum, ed., *Sixth Annual Symp. on Computer Applications in Medical Care*, Washington (1982).

B. Blum, "A Methodology for Information System Production," in *Twenty-Sixth Meeting of the Society for General Systems Research on System Methodology I*, pp. 278-282 (1982).

B. Blum, "A Tool for Developing Information Systems," in *Automated Tools for Information Systems Design*, H. J. Schneider and A. I. Wasserman, eds. North-Holland Pub. Co. (1982).

B. Blum and R. Haughton, "Rapid Prototyping of Information Management Systems," *Software Engineering Symp.: Rapid Prototyping ACM SIGSOFT*, Columbia, Md. (19-21 Apr 1982).

---

This work was supported by the Johns Hopkins Medical Institutions.

**ENERGY, ENGINEERING, AND CIVILIAN TECHNOLOGY**

## INTRODUCTION

Efficient energy generation and use are implicit in much of APL's missile propulsion and satellite systems work. An APL evaluation of alternative, long-range, nondepleting sources of energy identified solar and geothermal energy sources as being especially attractive to meet future national requirements. Tests exploiting one aspect of solar energy, the thermal gradient between the surface and the deep ocean, indicate that Ocean Thermal Energy Conversion (OTEC) may provide a practical and economical way to produce electricity, chemicals such as ammonia for fertilizers, and synthetic fuels such as methanol. Methanol has promise both for fuel cell use to regenerate electricity and as an automotive vehicle fuel. The APL Ocean Energy Program assists the Department of Energy in the technical assessment of those concepts.

APL also assists the Department of Energy in the assessment of geothermal resources and applications in the Eastern United States. Knowledge gained from the two programs, along with the analysis of worldwide geothermal resources, has suggested the potential of hybrid geothermal/ocean thermal energy conversion (GEOTEC) plants. The GEOTEC system combines geothermal resources with OTEC power-cycle technology and seawater cooling. It may permit the useful production of electric power at sites where neither technology alone would be suitable.

APL has been studying the environmental effects of energy facilities since 1971. A major activity has been the evaluation for the State of Maryland of the potential environmental, economic, and social impacts of all power-generating facilities proposed for development and construction in the state. In addition, generic studies are conducted for the State of Maryland and other public agencies in technical areas related to the location of energy facilities, their impact, and the mitigation of any adverse impacts.

Other energy projects have included the development and testing of high-speed flywheels for energy storage, and fundamental photovoltaic research to develop thin-film techniques leading to inexpensive solar cells.

Electronic devices pervade the entire APL research development and testing effort. Much of the electronics is designed with tight packaging constraints and must operate under severe environmental conditions. For a number of years, APL has been involved in the design and fabrication of special-purpose micro-electronic devices that can provide the required high reliability in undersea, space, and biomedical applications.

Through a variety of special projects, APL has participated in and contributed to programs for developing and applying modern technology to civil programs. Among them, the APL Transportation Program has been active since 1969. Its efforts have included research directed at the development of automated guideway transit command and control systems and at the provision of technical assistance to public agencies in the conduct of their automated transit and other transportation programs.

The articles in this section are examples of recent APL accomplishments in energy, microelectronics engineering, and urban transit technology.

# THE DEVELOPMENT OF GEOTHERMAL ENERGY IN THE EASTERN UNITED STATES

F. C. Paddison and A. M. Stone

*Over the past five years, the Laboratory and the JHU Center for Metropolitan Planning and Research have investigated the practicality and economics of the direct use of geothermal energy in the Eastern United States. These efforts had resulted in the expansion of the use of geofluids in Hot Springs, Ark., and of geothermal systems in South Dakota and New York. Legislative and planning activities in Maryland, Virginia, and Delaware also increased as a result.*

## BACKGROUND

APL served as the Technical Assistance Center for most of the Eastern United States as part of an ER-DA (later DOE) commercialization program to assist and expedite the introduction of geothermal energy. Figure 1 shows the regions of concern, together with the areas of potential geothermal interest. APL also made recommendations for government-sponsored research and development and for tax and incentive programs and initiated efforts to obtain comprehensive geothermal legislation in the Delmarva Peninsula.

Because the importance of cost prediction and its sensitivity to changes in system parameters or economic factors were recognized, a comprehensive computer code for the economic evaluation of a geothermal prospect was developed. The model, called GRITS (Geothermal Resource Interactive Simulation), is currently in use by the geothermal industry infrastructure.

## DISCUSSION

Fifteen technical studies of the application of geothermal energy to specific end uses were carried out. Each study was limited to approximately 100 hours of engineering effort, some of which was subcontracted to enhance the development of an infrastructure for this new industry. This limited engineering and economic feasibility study was intended as a prelude to detailed design by industry.

Table 1 lists the principal projects that APL supported. A brief review of the work done at the Naval Air Rework Facility (NARF) in Norfolk, Va., will serve to give the flavor of the technical assistance process in space heating, while a similar review of the liquified natural gas (LNG) gasification study for Cove Point, Md., will illustrate the industrial process heat effort.

Table 1 — Technical assistance.

### Space heating

Hot Springs, Ark. — bath house  
Pittsville, Md. — middle/elementary school  
Naval Air Rework Facility, Norfolk, Va.  
Crisfield, Md. — high school  
Community Center, Ocean City, Md.  
St. Mary's Hospital, Pierre, S. Dak.

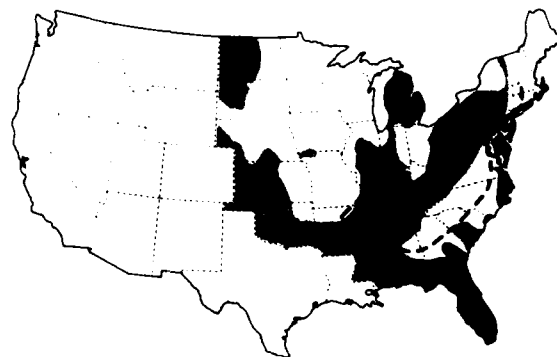
### District heating

Cape Charles, Va.  
Dover AFB, Del.  
Philip, S. Dak.  
Naval Submarine Support, Kings Bay, Ga.  
Wallops Flight Test Center, Va.  
McGuire AFB, N.J.

### Industrial process heat

Clinton Corn Products, N.Y. — wet mill processing  
Cove Point, Md. — LNG gasification  
Eastern Shore, Md. — poultry processing  
Talbot Co., Md. — mariculture  
Lewes, Del. — recovery of MgCl

**NARF.** The cost of heating one aircraft hangar by means of geothermal energy was compared with the cost of the existing oil-fired hot-water system. A 2500 ft



- Sedimentary rocks of depth greater than 1219 m (4000 ft) below surface. (Contours adapted from map of North America - 1967)
- Approximate areas of thermal anomalies under investigation by Costain et al. of VPI&SU. (From Gruy Federal report DOE/NVO/1558-7, Dec 1979)
- Limit of coastal plain sediments

Figure 1 — Coastal plain and interior sedimentary basins with potential for hydrothermal resources, Eastern United States.

well delivering 225 gpm of water at 107°F with a 1500 ft maximum drawdown appears feasible. The heating load is intermittent (both annually and diurnally) but a thermal storage reservoir could furnish heat at a rate three to four times that of the well itself. A redesign for radiant floor heat would increase the percentage of geothermal use. The existing oil-fired system would be used as a supplement for the coldest ambient conditions. Several designs for this dual system evolved, the most elaborate of which uses thermal storage at 140°F and two heat pumps to reduce the reinjection temperature to 65°F. The submersible well pump is rated at 85 hp; suitable circulating pumps and heat exchangers would complete the installation. The existing system uses 73,100 gallons of oil per year on the average. Savings in oil with the geothermal system can be used to amortize the refit cost. The time to amortize the capital cost could be as short as 11.5 years.

**LNG Vaporization.** At the request of the Columbia LNG Corp., APL performed a preliminary feasibility analysis for obtaining 8000 gpm of geothermal water to gasify LNG prior to its insertion in the interstate pipeline. At Cove Point, 5% of the LNG is normally consumed in gasification, thus substantially reducing revenues.

The hydrologic/geologic resource was approximated as a confined, horizontal, isotropic, homogeneous, infinite aquifer with a transmissibility of 0.50 cm<sup>2</sup>/s, a storage coefficient of about 10<sup>-3</sup>, and a temperature in the range of 100 to 125°F. Reinjection of the geothermal fluid is mandatory, but the reinjection (and supply) wells must be sited to minimize drawdown. Although the drawdown is less for close spacing of the production well and the reinjection well, the time for thermal breakthrough and cooling of the production zone is greater. Thus a compromise must be sought. Calculations of drawdown and thermal breakthrough as a function of well separation indicate that between 1 and 2 km would be adequate. These figures permit the necessary well field size to be determined. For example:

<b>Drawdown</b>	540 to 590 ft at 100 gpm 1600 to 1800 ft at 300 gpm
<b>Thermal breakthrough time</b>	160 to 640 yr at 100 gpm 53 to 215 yr at 300 gpm

On the basis of these results, a rectangular grid of 32 pairs of wells with a lattice spacing of 4921 ft was recommended.

#### **Economic Assessment**

The application of geothermal energy to a particular industry's energy needs depends in large measure on economics. The GRITS computer program for the

economic evaluation of geothermal energy was written to estimate the cost of geothermal energy delivery systems and the revenue stream. The program is interactive, allowing the user to vary a wide range of resources, demands, and financial parameters in order to observe their effect on the delivered costs of geothermal energy in direct-use applications. GRITS differs from many other programs in that it is a temporal simulation that produces a series of annual cost and revenue estimates for the life of a project.

Figure 2 is a block diagram of the GRITS model. Tables 2 and 3 illustrate its utility in comparing the costs of geothermal space heating in three different resource and environmental areas. The discounted average cost as a function of design ambient temperature (i.e., the temperature at which an auxiliary peaking plant begins to contribute heat to supplement the geothermal system) is shown in Fig. 3 for the three areas. Figure 4 shows the costs for these same areas as a function of the flow rate for each geothermal well.

The cost of geothermal energy for industrial process heat can be substantially lower than for space heating because of the lower cost of the distribution system and the greater utilization of the resource. Figure 5 shows the variation of average discounted cost as a function of utilization factor.

## **RESULTS**

Members of the Geothermal Commercialization Program have made personal visits to almost every eastern state and have published papers and held annual coordination meetings. State agencies and interested groups and individuals now are knowledgeable about geothermal possibilities in their area and in the East in general. For example, a well drilled in Auburn, N. Y. shows good possibilities for application, there are four demonstrations in South Dakota, and bath houses are being heated at Hot Springs, Ark.

A comprehensive economic evaluation model for geothermal energy has been developed and disseminated to industry and other interested groups to aid in their application studies.

A number of areas for future research have been identified. The use of extremely low frequency signals from the Clam Lake installation in Wisconsin to probe for conducting bodies lying 1 to 10 km below the surface could be helpful when prospecting for geothermal resources. Also a systematic processing of logs of existing deep wells would establish water availability below the surface, the major uncertain geothermal parameter.

In the applications area, the development of an ammonia-cycle refrigerator using geothermal fluids in



Parameter	East	West	
	Salisbury, Md.	Thermopolis, Wyo.	Boise, Idaho
Production well depth, ft (m)	5000 (1524)	3000 (914)	1200 (365)
Reinjection well depth, ft (m)	5000 (1524)	3000 (914)	1200 (365)
Wellhead temperature, °F (°C)	140 (60)	170 (77)	170 (77)
Reinjection temperature, °F (°C)	90 (32)	110 (43)	110 (43)
Flow, gpm (m <sup>3</sup> /h)	225 (51)	500 (114)	1000 (227)
Drawdown (% of well depth)	15	10	10
Transportation distance to users, mi. (km)	0.25 (0.4)	3 (4.8)	1 (1.6)
System design temperature, °F (°C)	45 (7.2)	24 (- 4.4)	17 (- 8.3)
Minimum ambient temperature, °F (°C)	- 5 (- 21)	- 28 (- 33)	- 13 (- 25)
Weather statistics for	Richmond, Va.	Casper, Wyo.	Boise, Idaho

**Table 3 — Sensivity analysis: comparison of eastern and western resources, selected values, space heating.**

Seven commercial buildings at 9 Btu/ft<sup>2</sup>/degree day — five with 4000 ft<sup>2</sup>, two with 10,000 ft<sup>2</sup>:

Year	% Using Geothermal
1	50
2	75
3	100

Residential buildings (including domestic hot water) at  $20 \times 10^6$  Btu/yr/residence; the maximum number of residences supplied is 267 for Salisbury, Md., 410 for Thermopolis, Wyo., and 730 for Boise, Idaho:

Year	% Using Geothermal
1	15
2	23
3	31*

\*Continues to increase at 8% per year until maximum is reached.

Types	% of Total	Area (ft <sup>2</sup> )	Demand (Btu/h/°F)
Single family	20	1600	1200
Townhouses	40	1000	780
Garden apartments	40	1000	420

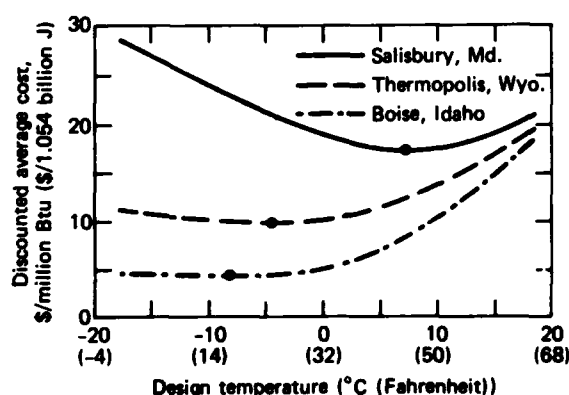


**Figure 3 — The discounted average cost for geothermal space heating versus system design temperature.**

the 150°F range would provide air conditioning and extend the well usage, a critical economic parameter.

Finally, inversion of the Einstein-Szilard patented refrigerator could provide a geothermal compressor for a refrigerant in a heat pump without the need for a mechanical compressor. Its successful development would improve efficiencies by a factor of about 3.

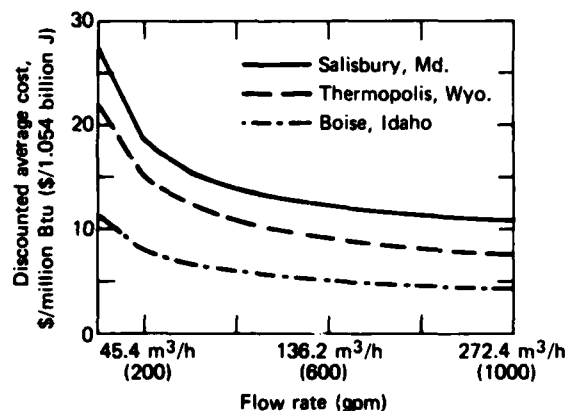


**Figure 4 — The discounted average cost for geothermal space heating versus flow rate.**

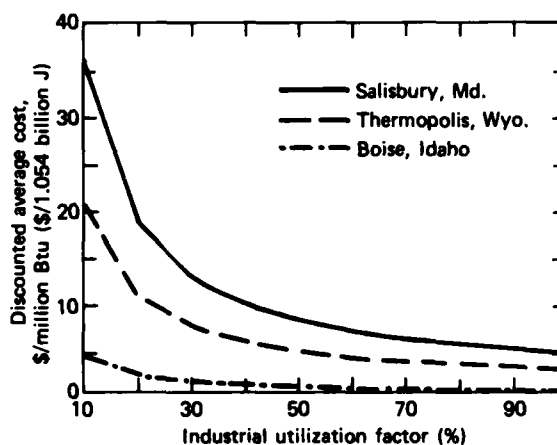


**Figure 5 — Discounted average cost for geothermal space heating versus industrial utilization factor.**

## ACKNOWLEDGMENTS

Many individuals at APL and The Johns Hopkins University Center for Metropolitan Planning and Research contributed to this effort. The following should be mentioned in particular: C. S. Leffel, Jr., J. E. Tillman, W. J. Toth, K. Yu, F. K. Hill, R. Von Briesen, and F. Mitchell (all from APL) and W. F. Barron, P. Kroll, R. Weissbrod, and S. M. Kane (from the Micro Center).

## SELECTED REFERENCES

- <sup>1</sup> *Geothermal Energy Development in the Eastern U.S. - Final Report*, JHU/APL QM-81-130 (Oct 1981).
- <sup>2</sup> S. M. Kane, W. F. Barron, F. C. Paddison, and P. Kroll, "GRITS - A Computer Program for Economic Evaluation of Geothermal Energy," *ASHRAE Trans.* 88 (Jan 1982).
- <sup>3</sup> J. E. Tillman, "Eastern Geothermal Resources: Should We Pursue Them?" *Science* 210 (7 Nov 1980).
- <sup>4</sup> W. J. Toth, "Geothermal Markets on the Atlantic Coastal Plain"; F. C. Paddison, "A Prospectus for Geothermal Energy - The Atlantic Coastal Plain"; and W. F. Barron and R. Weissbrod, "Cost Analysis of Hydrothermal Resource Applications in the Atlantic Coastal Plain"; in *Geothermal Resources Council Transactions*, Special Report No. 5 (Apr 1979).
- <sup>5</sup> K. Yu and F. C. Paddison, "Technical Assistance - Hydrothermal Resource Application, the Eastern U.S."; A. Goodman, "Geothermal Market Penetration in the Residential Sector: Capitol Stock Impediments and Compensatory Incentives"; W. F. Barron, R. Dubin, and S. M. Kane, "An Analysis of Benefits and Costs of Accelerating Market Penetration by a Geothermal Community Heating System"; and W. J. Toth and W. F. Barron, "GRITS: A Computer Model for Economic Evaluations of Direct Use of Geothermal Energy"; in *Geothermal Resources Council Annual Meeting Transactions* 4 (Oct 1980).
- <sup>6</sup> S. M. Kane, "Industrial Applications of Geothermal Energy in Lewes, Delaware: An Economic Analysis"; and C. Uhrmacher, "Technical Feasibility of Use of Eastern Geothermal Energy in Vacuum Distillation of Ethanol Fuel"; in *Geothermal Resources Council Annual Meeting Transactions* 5 (Oct 1981).
- <sup>7</sup> C. S. Leffel and R. A. Eisenberg, *Geothermal Handbook*, JHU/APL SR-77-1 (Jun 1977).
- <sup>8</sup> W. J. Toth and F. C. Paddison, "Geothermal Energy Markets on the Atlantic Coastal Plain," *Energy Tech.* VI (Feb 1979).
- <sup>9</sup> F. C. Paddison, C. S. Leffel, Jr., W. J. Toth, and R. Weissbrod, "Direct Applications of Geothermal Energy in the Eastern United States and Estimates of Life Cycle Costs," presented at American Institute of Industrial Engineers Seminar - Life Cycle Costing (Oct 1978).
- <sup>10</sup> A. M. Stone, "Geothermal Energy - An Overview"; and F. C. Paddison and K. Yu, "Use of Geothermal Energy in the Eastern United States"; *Johns Hopkins APL Tech. Dig.* 1 (Apr-Jun 1980).

This work was supported by the Department of Energy, Division of Geothermal Energy.

## APPLICATION DESIGN, IMPLEMENTATION, AND RELIABILITY TESTING OF THE CERAMIC CHIP CARRIER

H. K. Charles, Jr., G. D. Wagner, B. M. Romenesko, and R. E. Hicks

*The ceramic chip carrier, which is compact and easy to use and test, is a highly reliable integrated-circuit packaging technique. Because of its hermeticity, high density of input/output interconnects, straightforward attachment by solder reflow, and relatively small size, it is ideally suited for packaging large-scale and very-large-scale integrated circuits for use in stringent environments such as space satellites, biomedical implants, and underwater instrumentation.*

### BACKGROUND

As a developer of prototype electronic systems, APL has an ever-increasing need to use miniaturized assembly and packaging techniques that not only satisfy

the requirements of stringent application environments but also meet the standards of the electronics industry for economy, ease of assembly, and reliability. The ceramic chip carrier is a modern, miniaturized packaging technique that is rapidly becoming a standard of the industry. Before such a method could be introduced into APL systems, an extensive program in the attachment, reliability testing, and application design of ceramic chip carriers had to be undertaken.<sup>1,2</sup>

Chip carriers with up to 48 inputs and outputs have already been used successfully in both the Implantable Programmable Infusion Pump and the Patient Programming Unit of the Programmable Implantable Medication System (PIMS). Figure 1 illustrates a completed microprocessor-based controller board used

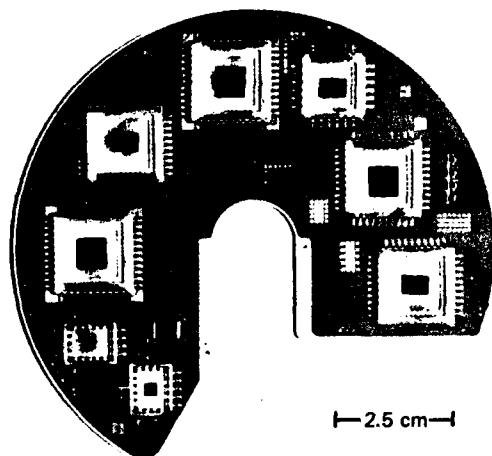


**Figure 1** — Controller board of the Implantable Programmable Infusion Pump, showing the use of ceramic chip carriers with a multiconductor-level, thick-film ceramic substrate.

in the PIMS implant unit. An automatic implantable defibrillator application that is currently in the final design phase will use ceramic chip carriers with up to 132 input and output terminations as well as some small-footprint custom carriers of 84 "leads." In the development of that and other APL systems, many large-scale and very-large-scale integrated circuit chips have been packaged in ceramic chip carriers and subsequently attached by the reflow method to a variety of thick-film, multiconductor-level ceramic circuit boards, thin-film metallized ceramic substrates, and printed wire boards. Other designs use complex multiconductor-level cofired ceramic substrates and high-density printed wire boards with large numbers of ceramic chip carriers with 100 or more leads and the associated pin grid arrays.<sup>3</sup>

## DISCUSSION

### The Ceramic Chip Carrier

The ceramic chip carrier (Fig. 2) is basically a square or rectangular, multilayer, ceramic package with a pattern of gold metallization pads on the bottom and an internal cavity into which semiconductors and perhaps small hybrids can be placed, depending on carrier height and input/output requirements. (Side metallization castellations and metal leads for strain relief are used on some versions.) The top edge of the cavity has a metal sealing surface that accepts a conventional plated metal (Kovar) lid. In some cases, conformal coating with epoxies or polyimide resins can be done instead of

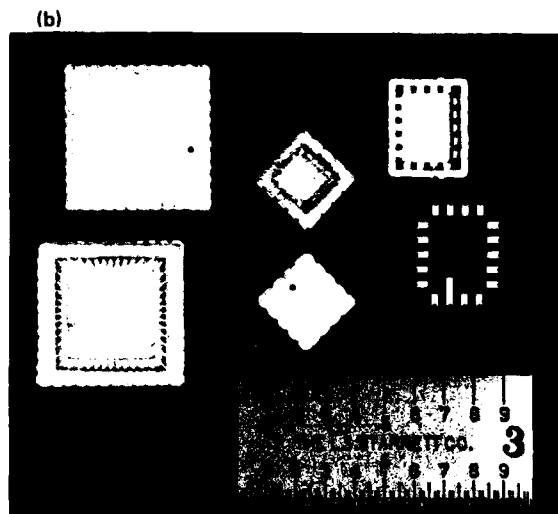
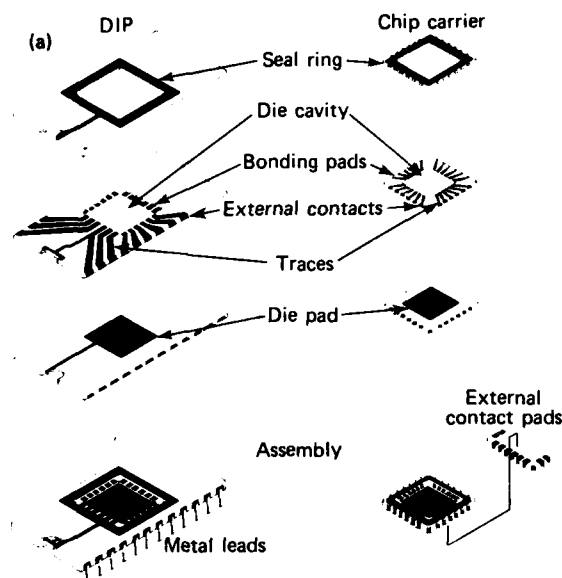


**Figure 2** — Ceramic chip carrier. (a) Comparison of structure with that of dual in-line package. (b) Examples of carriers used in APL programs.

lidding. It is also possible, by using a special ceramic lid, to make an entirely nonmagnetic package with the ceramic chip carrier.

The ceramic chip carrier as a direct replacement for the conventional, dual-in-line package (DIP) offers at least four distinct advantages:

1. In the larger ceramic chip carriers (i.e., 48 to 132 leads and more), there is considerable space savings over the DIP format with an

equivalent lead count. Board area savings factors between 3 and 5 are routinely achievable.<sup>4</sup> The packaging density can approach that of a conventional hybrid under certain circumstances while offering increased reliability, faster assembly, and greater ease of circuit repair.

2. It has a much lower profile than that of the standard DIP and of even most hybrids, thus affording a height savings factor of 2 to 4.
3. It has a shorter signal path length than the equivalent DIP (with the same number of input and output leads), resulting in less lead inductance and greater frequency response, typically by a factor of 2.<sup>5</sup>
4. It is compatible with other surface-mounted components such as chip resistors and capacitors. It needs no through-board hole preparation and is easily attached by a simple reflow operation using hot plates, belt furnaces, infrared ovens, or condensation reflow soldering (vapor phase soldering). It is particularly amenable to vapor phase soldering where the high ratio of pad area to weight (especially with the large carriers) makes it ideally suited for double-sided board applications (i.e., where the surface tension, even though reduced in the fluorocarbon vapor blanket, of the molten solder on the previously soldered bottom side of the board holds the components on while the top side is being reflowed). Similarly, it is easily removed and replaced, with a minimum of tooling.

### Chip Carrier Assembly and Testing

The placement of chips (dies) into ceramic chip carriers comprises three basic assembly operations (die attachment, wire bonding, and lid sealing) in addition to various inspections, quality control verifications, and electrical and environmental testing. The die is attached by means of epoxy or eutectic die bonding. Typical epoxies include Ablefilm 517 for nonconductive attachments and Ablefilm 36-2 silver-filled epoxy where electrical contact to the bottom of the integrated circuit chip is necessary. Eutectic die bonding with gold-silicon (94 % gold and 6% silicon by weight) and with gold-tin (80% gold and 20% tin by weight) solder alloy preforms has been performed routinely using standard hybrid die attachment procedures.

Integrated circuits in ceramic chip carriers can be wire bonded using thermosonic gold ball bonding, aluminum ultrasonic wedge bonding, and gold thermal compression bonding. Wire bonding chips in ceramic chip carriers can present problems, depending on the rel-

ative ratios of chip area to carrier internal cavity area and on chip height to carrier internal cavity height. Because carrier size is determined by the number of required input/output pins rather than strictly by chip area, small chips in large carriers (when many pins are needed) can suffer wire sagging and kinking because of the long runout and the low loop height necessitated by shallow cavities and thicker chips (especially with circuits from the 125 mm thick wafers used on most very-large-scale integrated circuits). Chips that completely fill the carrier cavity also pose similar problems. The distance from the chip bonding pad to the carrier bonding pad is very short, and there is not enough room to form the traditional loop. Figure 3 shows an example of a properly wire bonded die in a chip carrier cavity.

Ceramic chip carriers have been lidded using a solder sealing system after a 48 hour vacuum bake at 125°C to remove entrained moisture and volatiles. The lids typically are gold-plated Kovar with preattached gold-tin eutectic solder preforms. Lidding is typically carried out at 400°C with appropriate up and down temperature ramps. The flatness of the lid and the carrier seal ring appear to be the chief factors in determining if the hermetic seal is effective.

Once lidded, the assembly is subjected to a battery of electrical and environmental tests (constant acceleration, thermal cycling, thermal shock, etc.). For electrical testing prior to board assembly, contact to the chip corner is made using special sockets with spring contacts. A different socket is required for each size and style of carrier.

### Reflow Attachment and Reliability Testing

Solder reflow attachment has been performed using both paste solders and solder pot pretinning of the



Figure 3 — Chip and wire bonds in the die cavity of a ceramic chip carrier.

carrier. Paste solders (62% tin, 36% lead, and 2% silver by weight, with a mildly activated rosin flux vehicle) were applied to the substrate by hand with a fine wire probe. The solder assemblies were reflowed in air at  $205 \pm 5^\circ\text{C}$  without prewarming the assembly or drying the solder paste. When cooled, the assemblies were cleaned ultrasonically in AP20 for 20 min, followed by 5 min in absolute methanol and 5 min in boiling acetone. After being dried with nitrogen gas, the assemblies were inspected for joint appearance, solder balls, and the complete removal of flux residues around and beneath the carrier. Inspection techniques ranged from optical microscopy using both conventional and transparent substrates<sup>1</sup> to advance materials analysis techniques<sup>2</sup> such as energy dispersive X ray, scanning Auger microprobe, and secondary ion mass spectrometry. Solder ball formation has been noted with all paste solders, even when the pastes are predried.

Solder pot pretinning has proven successful and is preferred because of its ease of use and elimination of solder balls. Joint appearance and performance (strong and low resistance) are excellent when the ceramic chip carriers and the substrates are fluxed separately, floated on a solder bath, fluxed lightly, joined, and reflowed. (Large substrates and thick-film multiconductor-level substrates are tinned by hand using the appropriate wire solder and a small iron.) Soon vapor phase soldering techniques will be used to shorten assembly time, improve throughput, and facilitate double-sided board configurations.

Reliability tests include stabilization bake, thermal shock, temperature cycling, and vibration or centrifuge (depending on the size of the system module). Typical thermal shock testing consists of immersing the substrate/carrier combination in hot ( $100^\circ\text{C}$ ) fluorocarbon liquid (FC43) for a minimum of 1 min, followed by a rapid transfer ( $< 5$  s) to a cold ( $0^\circ\text{C}$ ) FC43 bath for 1 min, followed by a return to high temperature. This cycle is repeated 10 times. The stabilization bake test is usually 48 hours at  $125^\circ\text{C}$  for ceramic substrate systems and at  $100^\circ\text{C}$  for printed wire boards. Temperature cycling runs are from  $-55$  to  $+125^\circ\text{C}$  (typically 10 times) with 6 min excursions and 30 min holds at the extremes. Again, less extreme limits ( $-25$  to  $+100^\circ\text{C}$ ) are used for printed wire boards. Centrifuge and vibration testing can include accelerations

to 20,000 g (centrifuge) and both sinusoidal and random vibrations at shake frequencies from 10 to 2000 Hz with amplitudes up to 21 g.

Assemblies of carriers and printed wire boards and of carriers and ceramic circuit boards (thin film and thick film) have routinely survived the usual qualification tests outlined above. The most stringent test is thermal cycling as in the work of Settle.<sup>6</sup> Ceramic chip carriers on printed wire boards have survived several hundred thermal cycles. In ceramic substrate combinations, they have exhibited even greater reliability because of the much closer match in thermal expansion coefficients. Other factors influencing reliability include carrier height above the substrate (125 to 150  $\mu\text{m}$  appears to be optimal), ductility of the solder alloy, and range of amplitude of the thermal cycle. Large carriers (40 pins or more) in general fail after fewer accumulated temperature cycles than do smaller carriers.

## ACKNOWLEDGMENTS

The authors acknowledge all personnel who were involved in the chip carrier program. The efforts of B. R. Platte and G. S. Belt are especially appreciated.

## REFERENCES

- <sup>1</sup> H. K. Charles, Jr., and B. M. Romenesko, "The Reflow Attachment and Reliability Testing of Ceramic Chip Carriers," in *Proc. 1981 International Reliability Physics Symposium*, Orlando, Fla., p. 93 (7-9 Apr 1981).
- <sup>2</sup> H. K. Charles, Jr., and B. M. Romenesko, "Ceramic Chip Carrier Soldering, Cleaning and Reliability," in *Proc. 32nd Electronic Components Conf.*, San Diego, Calif., p. 369 (10-12 May 1982).
- <sup>3</sup> B. M. Hargis and D. J. Westervelt, "High Lead Count Packaging and Interconnect Alternatives," *Electron. Packag. Prod.* (Sep 1981).
- <sup>4</sup> J. W. Balde and D. I. Amey, "Ceramic Chip Carriers Are Easy to Assemble and Disassemble," *Electron. Des. News*, 120 (Sep 1978).
- <sup>5</sup> S. Acello, "Mini-Pak - A Cost Effective Leadless Flat Pack," in *Proc. Technical Program of the National Electronic Packaging and Production Conf.* (1977).
- <sup>6</sup> R. E. Settle, Jr., "A New Family of Microelectronic Packages for Avionics," *Solid State Tech.*, 54 (Jun 1978).

---

This work was supported by Independent R&D.

# NONDESTRUCTIVE PULL TESTING OF HYBRID MICROELECTRONICS

H. K. Charles, Jr., G. D. Wagner, and B. M. Romenesko

*The nondestructive pull testing of wire bonds in highly reliable microelectronic devices such as hybrids can be used to eliminate weak, poorly made wire bonds. Because each wire in the hybrid is actually pulled, using a miniature hook, to some predetermined limit (which ensures that the bonds are strong enough but that they will not be damaged during the test), many variables must be considered before such a test can be introduced routinely into the hybrid production process.*

## BACKGROUND

An extensive qualification program was undertaken to introduce nondestructive pull testing (NDPT) into the hybrid microelectronics production process. NDPT was made necessary by the occasional weak wire bond (primarily ball lifts) that appeared in otherwise strong hybrid wire bond destructive pull populations. A typical pull strength distribution for representative hybrids with thin-film gold substrate metallization is shown in Fig. 1. The weak bonds (occurring at a frequency of 1 in every 100 to 200 bonds) result from random causes such as bonding pad debris, surface metallization, wire defects, improper ball formation, ball-pad misalignment, etc. Modern hybrids usually have more than 100 bonds each; therefore, the probability of a weak bond and a resultant hybrid failure could be quite high. The implementation of a controlled, repeatable NDPT has only recently been made possible by the use of a microprocessor-based wire bond pull tester. One such instrument is the Unitek Micro Pull IV (Fig. 2). Once manually positioned over the wire to be pulled, the instrument automatically performs either a destructive or a nondestructive wire bond pull test, displays the results (or the NDPT limit) on a digital panel meter, and outputs the data to a Hewlett Packard 97S calculator, which processes the data. The instrument automatically detects NDPT wire bond failures (i.e., failures before the pull force reaches the preset limit) that occur during the test, as well as excessive wire bond loop heights, and records them.

## DISCUSSION

### NDPT Rationale and Limits

The NDPT is designed to remove weak, poorly made wire bonds with pull strengths below a predeter-

mined level at the time the test is performed. It does not ensure against later bond strength degradation resulting from aluminum-gold intermetallic formation<sup>1</sup> and subsequent voiding; fatigue produced by vibration, temperature, or power cycling<sup>2</sup>; and mechanical damage caused by improper handling. The main difficulty with the test is to establish a pull force limit that will determine if the bonds are strong enough but that will not cause metallurgical damage during the test. In order to minimize that possibility, no part of the wire loop ball or heel must be stressed beyond its elastic limit.<sup>2</sup> Because bonding wires are of many compositions, hardnesses, and elongations and because wire bond strength (and hence its elastic limit) is affected by bond geometry, the method of bonding,<sup>3</sup> and the placement of the pulling hook, different NDPT criteria have to be established for each system.

The pull limit setting can be determined statistically using the mean ( $\bar{X}$ ) and standard deviation ( $\sigma$ ) of a representative destructive pull test distribution. The normally distributed destructive pull control limit of  $\bar{X} - 3\sigma$  ensures that only 1 bond (normally distributed) in

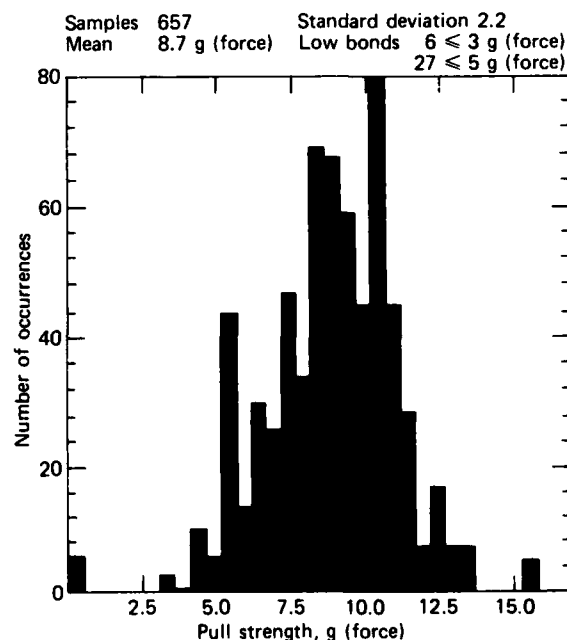


Figure 1 — Histogram of post-burn-in wire bond pulls for hybrids with gold substrate metallization (before the introduction of NDPT).

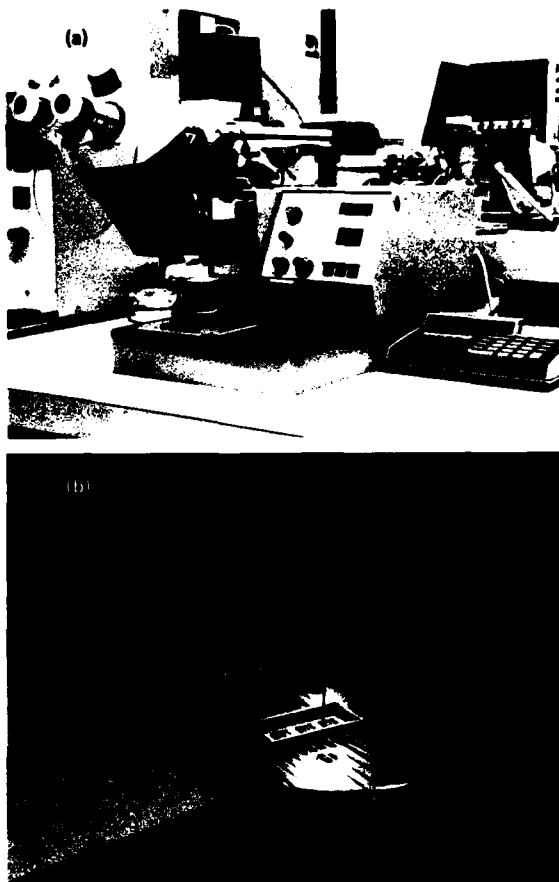


Figure 2 — (a) Unitek Micro Pull IV wire bond pull tester and HP 97S Calculator Readout System. (b) Close-up view of beam, rigid hook, horizontal platform, and hybrid under test.

740 will have a pull strength below that force. Typical NDPT limits are set at 90% of that value,<sup>4</sup> ensuring that no bond within the normal distribution is stressed past its elastic limit but that bonds with low, nonnormal, or bimodal pull strengths are detected. Only bonds that lie in the interval between  $(\bar{X} - 3\sigma)$  and  $0.9(\bar{X} - 3\sigma)$  may be stressed to some degree above their elastic limits. The number of bonds that actually lie in this interval depends on the relationship of  $\bar{X}$  and  $\sigma$ . For example, if  $\sigma = 0.25\bar{X}$ , only 1 bond in approximately 2600 lies within this range; if  $\sigma = 0.15\bar{X}$ , the number increases to 1 in approximately 1000. Typical controlled-geometry, destructive bond pull populations have standard deviations within those limits. If the standard deviations drop below  $0.15\bar{X}$ , an NDPT criterion limit of  $0.9(\bar{X} - 4\sigma)$  is recommended.<sup>5</sup> Unfortunately, the geometric influence on hybrid wire bond pull populations is not well controlled during the hybrid design phase, resulting in large standard deviations because of

various bond types and lengths, even though all the bonds are strong. This effect has been discussed elsewhere.<sup>6</sup> A criterion based on a percentage of the lowest acceptable bond strength (e.g., 50% of a 3 g (force) minimum) for the 25.4  $\mu\text{m}$  diameter gold wire seems more realistic, especially for a hybrid with a diversity of bond types. APL has adopted a 1.5 g (force) NDPT limit following a 24 h thermal aging at 125°C.

### Qualification Program

Before the introduction of NDPT into the hybrid production line, a qualification program was conducted whose aim was not only to get NDPT on line as soon as possible for the current hybrid-building program but also to establish criteria and guidelines for the application of NDPT to all future hybrid designs. The basic program involved four phases.

Phase I consisted of a controlled evaluation of the NDPT procedure on bare metallized substrates (substrate-to-substrate bonds). The test sequence was designed to evaluate several factors, including operation of the NDPT machine, the various pull criteria (e.g., 2.0 g (force) with no bake versus 1.5 g (force) with a 24 h thermal aging at 125°C in vacuum), and the influence of NDPT on destructive pull strengths before and after burn-in. Other tests involved the repeated purposeful stressing of wire bonds at higher limits to determine the maximum range for the 25.4  $\mu\text{m}$  diameter gold wire, thermosonically bonded hybrid wiring system.

Phase II was a repeat of Phase I evaluations for chip-to-substrate bonds.

Phase III was an NDPT evaluation of representative hybrids from the current line. Its goal was to screen empirically all the types of hybrids for NDPT suitability. Particular concern had arisen over package-pin-to-substrate bonds; they have an extremely poor geometry for placement of the NDPT rigid hook. Because most of them were bonded redundantly, the need for NDPT was reduced, and in most cases only one bond was finally subjected to the screening. In conjunction with the empirical testing, all existing circuit layouts were screened for NDPT suitability on the basis of minimum geometric spacing. The initial criterion was two hook lengths plus a 50% safety margin or approximately 0.51 mm (20 mils). This criterion can be flexible, depending on the specific design, but, in general, it is realistic, especially considering the results of Phase IV.

Phase IV involved the creation of special substrates with controlled-geometry bonding areas. Those substrates were used to determine the exact NDPT geometric limits and provided the needed inputs for future designs.

## RESULTS AND SUMMARY

Following the evaluations, it was concluded that NDPT could be conducted successfully on most bonds in our hybrid line except, perhaps, for a few hybrids and chip carriers<sup>7</sup> whose low lid heights caused a possible shorting condition. The tests confirmed that destructive bond pull strength was *not* influenced by NDPT, at least at the 1.5 to 2.0 g (force) limit. To date, NDPT has been performed on 100,000 bonds. Of those, 520 bonds have failed and have been reworked successfully. NDPT has done much to eliminate the occasional maverick bond that may be encountered in the hybrid wire bond pull distributions (e.g., Fig. 1). Figure 3 presents a histogram of hybrid bond pulls with gold metallized substrates after the introduction of NDPT.

## ACKNOWLEDGMENTS

The authors wish to acknowledge the efforts of all personnel who participated in the NDPT program. In particular, we sincerely appreciate the dedication of K. J. Mach who bonded most, if not all, of the samples and circuits considered in this study, and D. P. Glock who, with the exception of the bonds pulled by the authors, has pulled the tens of thousands of bonds described.

## BACKGROUND

An extensive qualification program was undertaken to introduce nondestructive pull testing (NDPT)

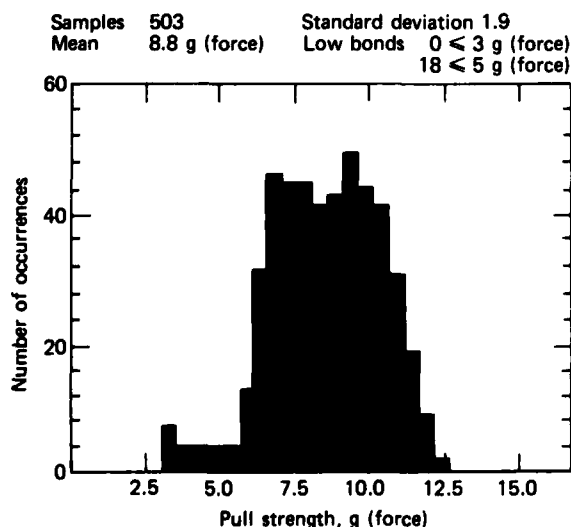


Figure 3 — Histogram of post-burn-in wire bond pulls for hybrids with gold substrate metallization (after the introduction of NDPT).

into the hybrid microelectronics production process. NDPT was made necessary by the occasional weak wire bond (primarily ball lifts) that appeared in otherwise strong hybrid wire bond destructive pull populations. A typical pull strength distribution for representative hybrids with thin-film gold substrate metallization is shown in Fig. 1. The weak bonds (occurring at a frequency of 1 in every 100 to 200 bonds) result from random causes such as bonding pad debris, surface metallization, wire defects, improper ball formation, ball-pad misalignment, etc. Modern hybrids usually have more than 100 bonds each; therefore, the probability of a weak bond and a resultant hybrid failure could be quite high. The implementation of a controlled, repeatable NDPT has only recently been made possible by the use of a microprocessor-based wire bond pull tester. One such instrument is the Unitek Micro Pull IV (Fig. 2). Once manually positioned over the wire to be pulled, the instrument automatically performs either a destructive or a nondestructive wire bond pull test, displays the results (or the NDPT limit) on a digital panel meter, and outputs the data to a Hewlett Packard 97S calculator, which processes the data. The instrument automatically detects NDPT wire bond failures (i.e., failures before the pull force reaches the preset limit) that occur during the test, as well as excessive wire bond loop heights, and records them.

## REFERENCES

- <sup>1</sup>H. K. Charles, Jr., B. M. Romenesko, G. D. Wagner, R. C. Benson, and O. M. Uy, "The Influence of Contamination on Aluminum-Gold Intermetallics," in *Proc. 20th IEEE Reliability Physics Symp.*, p. 128 (1982).
- <sup>2</sup>G. G. Harman, "Metallurgical Failure Modes of Wire Bonds," in *Proc. 12th IEEE Reliability Physics Symp.*, p. 131 (1974).
- <sup>3</sup>T. H. Ramsey, "Metallurgical Behavior of Gold Wire in Thermal Compression Bonding," *Solid State Tech.* 16, 43 (Oct 1973).
- <sup>4</sup>G. G. Harman, "A Metallurgical Basis for the Non-Destructive Wire-Bond Pull-Test," in *Proc. 12th IEEE Reliability Physics Symp.*, Las Vegas, p. 205 (1974).
- <sup>5</sup>*Standard Recommended Practice for Nondestructive Pull Testing of Wire Bonds*, ASTM Standard F458-78.
- <sup>6</sup>H. K. Charles, Jr., B. M. Romenesko, O. M. Uy, A. G. Bush, and R. von Briesen, "Hybrid Wire Bond Testing Variables Influencing Bond Strength and Reliability," *Int. J. Hybrid Microelectron.* 5, 260 (1982).
- <sup>7</sup>H. K. Charles, Jr., and B. M. Romenesko, "The Reflow Attachment and Reliability Testing of Ceramic Chip Carriers," in *Proc. 19th IEEE Reliability Physics Symp.*, p. 93 (1981).

This work was supported by Independent R&D.

# VEHICLE-FOLLOWER CONTROLLER DESIGNS FOR OFF-LINE AUTOMATED GUIDEWAY TRANSIT VEHICLES

H. Y. Chiu

*A state-constrained, vehicle-follower approach has been used successfully to design longitudinal controllers for vehicles operating off the main guideway of Automated Guideway Transit systems. These off-line operations include station entry, queue shift maneuvers, and station egress.*

## BACKGROUND

Much attention has been given to the use of Automated Guideway Transit (AGT) systems to improve public transit in congested urban areas. One AGT concept uses fully automated vehicles on dedicated guideways operating at short (about 3 s) headways. The vehicles leave the main guideway and enter stations to permit the boarding and departure of passengers. Such operations emphasize the problem of individual vehicle spacing and velocity control.

Vehicle-following (VF) is one approach to the vehicle control problem. It uses the states of a preceding vehicle to generate the velocity and spacing commands for the immediately trailing vehicle. APL has successfully implemented VF for regulating vehicles on the main guideway.<sup>1</sup> However, vehicle maneuvers that must be accomplished off the main guideway (off line) impose additional controller constraints. This article presents work that extends the APL VF controller design to off-line operations.

## DISCUSSION

There are three major types of off-line vehicle maneuvers: station entry, in-station queue shifting, and station egress. Station entry maneuvers involve diverting vehicles from the main guideway onto a ramp leading into a station. The vehicles are then decelerated from main guideway speeds to stop at a predetermined location in the station. Once stopped, the vehicle may be required to make one or several shifts to positions in various station queues. Eventually, it must be reinserted into the main guideway by a station egress maneuver.

To handle the off-line maneuvers, two controller designs were developed. Both station entry and queue shifting maneuvers require a high degree of stopping accuracy because of station door-alignment specifications and size constraints. These constraints necessitate a precision stop controller. Stopping accuracy is not a con-

cern for the station egress maneuver but, because of the finite length of the egress ramp, safety must be ensured when the vehicle reenters the main guideway. This problem presents a need for a station egress controller.

## Precision Stop Controller

An ideal maneuver for station entry is to decelerate at service jerk and acceleration limits from the main guideway speed and come to rest at a desired station location with a high degree of accuracy (typically  $\pm 15$  cm). A straightforward application of the APL VF controller to station entry proved unsatisfactory because the finite bandwidth of the vehicle plant produces unacceptable stopping errors and undesirable acceleration maneuver behavior. A precision stop controller design<sup>2</sup> was developed to correct these problems.

The precision stop controller generates an acceleration command to the station vehicles on the basis of the following error,  $e$ , calculation:

$$e = x_{\text{target}} - x - S(a, v),$$

where  $a$ ,  $v$ , and  $x$  are the station vehicle's acceleration, velocity, and position, respectively;  $x_{\text{target}}$  is the target stopping location; and  $S(a, v)$  is a kinematic stopping distance. When  $e > 0$  (usually during the final phase of the station entry maneuver), a linear regulator scheme is used to provide a smooth deceleration profile to the stopping point. The poles of the linear regulator were chosen to give a sufficiently quick and damped response.

The precision stop controller can also be used for shifting vehicles from one station position to another by specifying the appropriate  $x_{\text{target}}$ .

## Station Egress Controller

In a nominal station egress situation, a vehicle initially is at rest at the beginning of the egress ramp. An appropriate vehicle on the main guideway is designated the lead vehicle. The station vehicle accelerates at service limits and attains an operational spacing behind the lead vehicle when the main guideway speed is reached. A critical requirement for any station egress controller is to prevent the station vehicle from entering the main guideway ahead of the lead vehicle, despite any unpredicted maneuvers of the lead vehicle.

For headways greater than 3 s and egress ramp lengths greater than the distance required to accelerate to main guideway speeds at service acceleration and jerk limits, the APL VF controller was found to be satisfactory. However, for shorter headways and/or shorter egress ramp lengths, the controller must be modified to ensure safe main guideway entry of the vehicle.<sup>3</sup>

The station egress controller developed for short headways includes an egress initiator and an egress assurance controller. The egress initiator attempts to minimize the time to achieve a nominal spacing behind the

lead vehicle. At the same time, the egress assurance controller monitors the amount of egress ramp remaining and prevents the vehicle from entering the main guideway ahead of the lead vehicle. If necessary, the controller stops the vehicle on the egress ramp to allow the lead vehicle to pass.

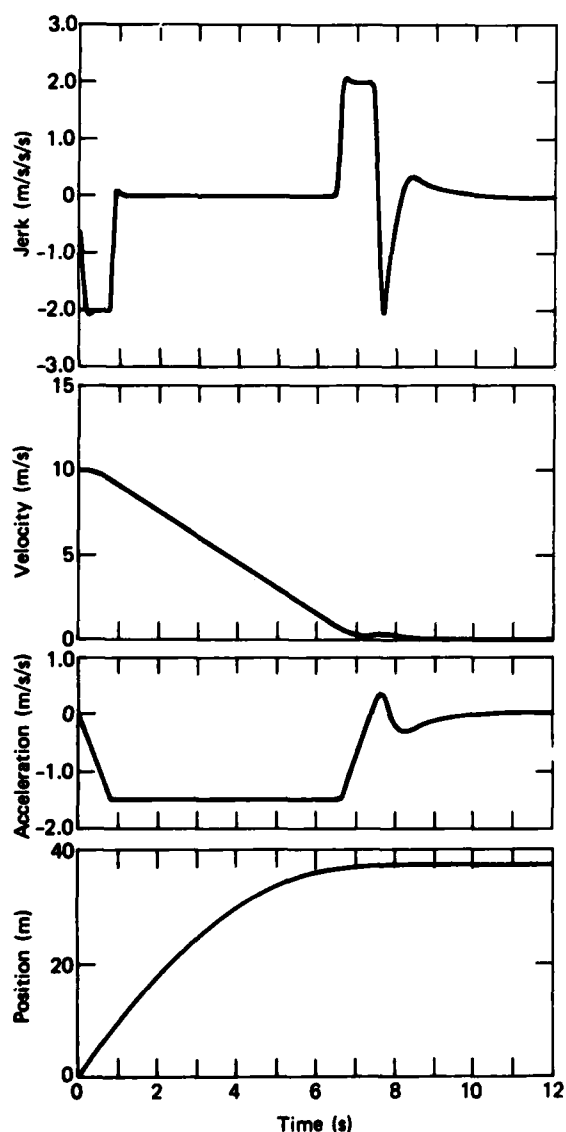


Figure 1 — Station stop from main line velocity of 10 m/s.

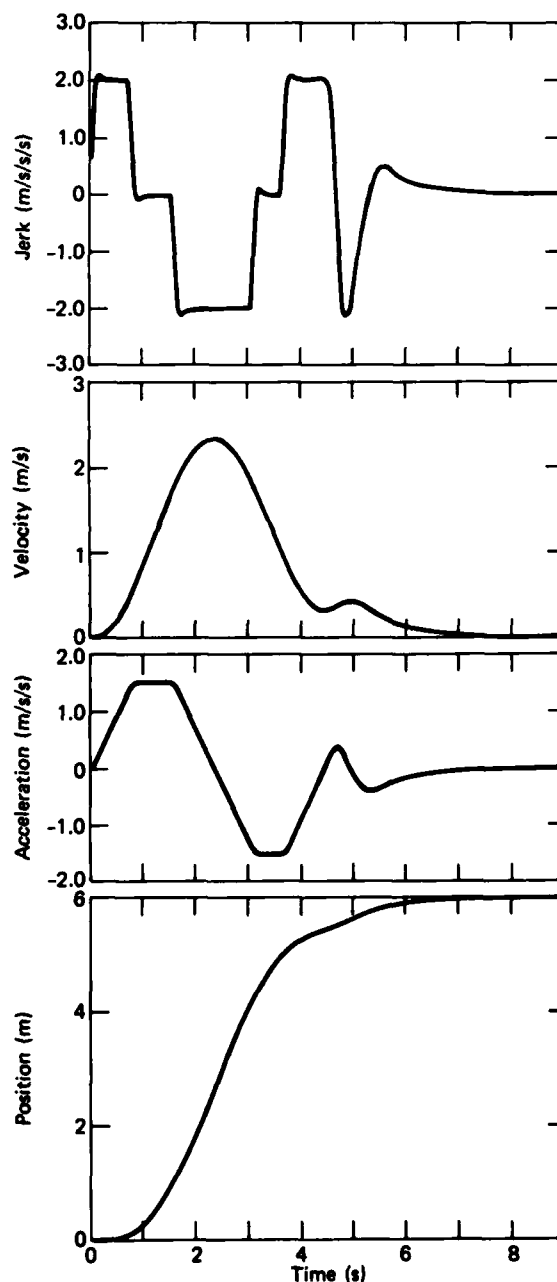


Figure 2 — Station queue shift maneuver, one berth shift (6 m).

## RESULTS

A digital simulation of the precision stop controller was constructed. For continuous state data, successful station entry maneuvers were accomplished from main guideway speeds as great as 10 m/s. Stopping errors were less than 1 cm. Typical vehicle responses for a station entry are shown in Fig. 1.

The introduction of sampling and delays into the simulation indicated that small sampling intervals were necessary to maintain a smooth tapering deceleration profile. Sampling rates and delays on the order of 0.02 s were the maximum tolerable levels to produce stopping errors of less than  $\pm 15$  cm and still give satisfactory deceleration responses.

Queue shift maneuvers were also investigated with the precision stop controller simulation. The response of a vehicle shifting from rest to the next queue berth (a berth length is 6 m) is shown in Fig. 2. Acceptable stopping errors and deceleration profiles again were achieved.

Another digital simulation was constructed for the station egress controller. The response of a vehicle in a nominal station egress situation is shown in Fig. 3 for an assumed operating headway of 0.5 s and an egress ramp length of 65 m. The vehicle is seen to merge smoothly behind a constant-speed lead vehicle. Other scenarios involving maneuvering lead vehicles and much shorter egress ramps also give satisfactory responses with the station egress controller.

## REFERENCES

- <sup>1</sup> A. J. Pue, *A State-Constrained Approach to Vehicle-Follower Control for Short-Headway AGT Systems*, JHU/APL TPR 038 (Aug 1977).
- <sup>2</sup> H. Y. Chiu, *A Vehicle-Follower Precision Stop Controller Design Using the State-Constrained Approach*, JHU/APL BTT-056-81 (31 Aug 1981).
- <sup>3</sup> A. J. Pue, H. Y. Chiu, and S. J. Brown, Jr., *Operational Concepts and Implementation Techniques for Vehicle-Follower Control of AGT Systems*, JHU/APL TPR 041 (Aug 1979).

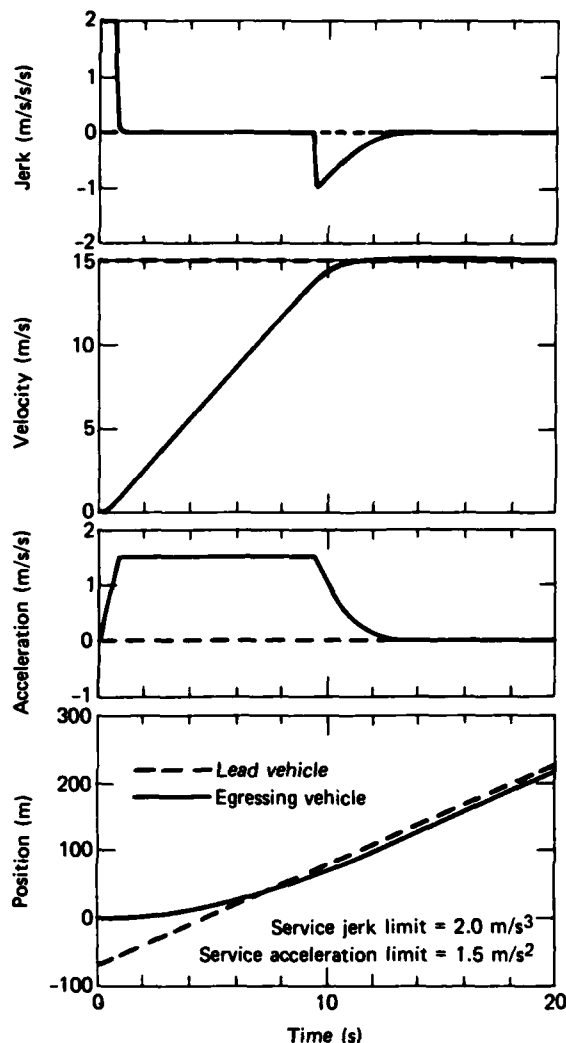


Figure 3 — Station egress for an assumed headway of 0.5 s, nominal case.

This work was supported by the Urban Mass Transit Administration.

# CONTROL SYSTEM FOR A MAGNETICALLY SUSPENDED TRANSIT VEHICLE

S. J. Brown

*A design evaluation and a simulation of a magnetic levitation and thrust control system for Automated Guideway Transit vehicles has been performed. The analysis have suggested two design modifications, while the basic principles of the control approach have essentially been verified.*

## BACKGROUND

Magnetic levitation and propulsion (Maglev) technology has been considered for application to urban Automated Guideway Transit systems for a number of years. The projected advantages of the technology include propulsion and braking independent of friction, low noise, improved reliability, improved ride quality, and lower maintenance costs. The Boeing Aerospace Co. has undertaken a research and development effort under Urban Mass Transportation Administration (UMTA) sponsorship to establish the viability of the Maglev concept for urban transit. One Maglev concept, initially developed by the Rohr Corp.,<sup>1</sup> uses linear induction motors (LIM's) in a combined lift and propulsion system for low speed (40 mph) vehicles.

As part of a continuing program to investigate automated transit control systems for UMTA, APL was asked to perform an independent evaluation of the control system design for a suspended monorail vehicle configuration, based on a previous Boeing controller design for a bottom-supported vehicle configuration.<sup>2</sup>

## DISCUSSION

### The Maglev System

The components of a top-suspended Maglev system are shown in Fig. 1. The vehicle consists of a propulsion and levitation system carriage and a passenger-carrying cabin suspended by the carriage through a mechanical, ride-smoothing, and thrust-coupling secondary suspension system designed as part of this study.

Three-phase alternating current passes through two sets of LIM primary windings located in a fore-aft configuration on the top of the carriage. The current produces a magnetic field that reacts with the LIM secondary built into the bottom of the guideway (Fig. 1) to

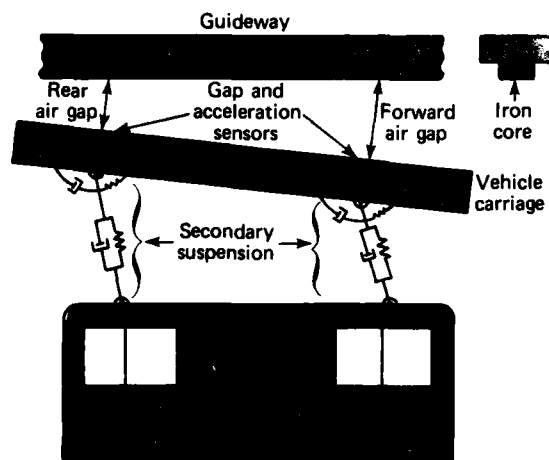


Figure 1 — The Maglev transit system.

generate lift and thrust and to provide pitch control through different fore-aft lift forces. (Mechanical guideway support is provided for startup and emergency conditions.)

The attractive magnetic levitation force,  $L$ , induced on the carriage may be approximated by

$$L = K_L \frac{\sum I_i^2}{g^2} \quad i = 1, 2, 3, \quad (1)$$

where the  $I_i$ 's are the instantaneous three-phase currents,  $g$  is the air gap between the motor primary and secondary (nominally 1/2 in.), and  $K_L$  is the design-dependent constant of proportionality.<sup>2,3</sup> The propulsive thrust induced on the carriage may be approximated by

$$T = (K_1 + K_2 g) (\omega - K_3 u) \quad (2)$$

where  $K_1$ ,  $K_2$ , and  $K_3$  are motor design coefficients,  $\omega$  is the excitation frequency of the applied motor current (all three phases), and  $u$  is the speed of the carriage along the guideway. Lift and thrust forces acting on the carriage are regulated (Eqs. 1 and 2) to match vehicle weight and desired thrust by varying the input voltage (and thus the currents,  $I_i$ ) and frequency of the three-phase excitation to the motor primaries. For steady-state cruise conditions,  $\omega$  is set equal to  $K_3 u_c$ , where  $u_c$

is the desired vehicle speed. During acceleration and deceleration,  $\omega$  is gradually varied to provide a smooth ride.

### Control System Concept

The major control system problem for an attractive Maglev system is the maintenance of the nominal fraction-of-an-inch air gap,  $g$ , between the carriage and the guideway, a problem made difficult because Eq. 1 represents an unstable equilibrium with respect to the air gap when lift equals vehicle weight. The control system concept proposed by previous investigators<sup>1,2</sup> is shown in Fig. 2. The control system components, described in detail in Ref. 4, consist of an analog lift servo (ALS), a digital control unit (DCU), and a speed command profiler. The ALS sends lift force commands to the front and rear motors in response to a commanded gap; it also sends signals obtained from gap and vertical-acceleration sensors located on the top surface of the vehicle carriage (Figs. 1 and 2). This control element was refined from previous designs by adapting it to a suspended vehicle configuration and by adding a pitch error integrator to eliminate carriage pitch biases during vehicle acceleration. The design is based on the ideal control path shown in Fig. 2 and was developed using classic control techniques.

The lift force commands generated by the analog lift servo are sent to the DCU, which is, from a control system point of view, a nonlinear motor cancellation compensator. The DCU generates three-phase motor voltage signals (based on the lift force commands) at an

excitation frequency determined by the acceleration and jerk limiting speed control profiler. When applied to the motor through solid-state inverters, the voltage commands generated by the DCU are intended to produce actual (rms) motor lift forces (Eq. 1) equal to the lift force commands sent to the DCU by the ALS. The lift and thrust obtained from the LIM's also depend on the actual vehicle speed and air gaps, as indicated by the feedback of those parameters in Fig. 2. Relatively high frequency (about 200 Hz bandwidth) gap sensors thus are required for proper DCU compensator operation.

### Design Evaluation

A computer simulation of the Maglev system, including detailed models of the secondary suspension, ALS, DCU, and three-phase excited LIM's, was developed as part of the evaluation effort. Initial runs showed unstable system response to a step change in the commanded air gap (Fig. 2), as was indicated by the vertical acceleration responses of the carriage and cabin (Fig. 3). The effects of the secondary suspension are evidenced by the difference in response of the two bodies. The instability, which was not present when the simulation was exercised using an option that represented the ideal control path in Fig. 2, was traced to the absence of a necessary gap sensor derivative term in the original DCU logic. Inclusion of this term in a modified DCU design resulted in a stable response (Fig. 4).

The simulation was also exercised to evaluate controller performance during pitch disturbances and speed change commands over a 0 to 40 mph operating

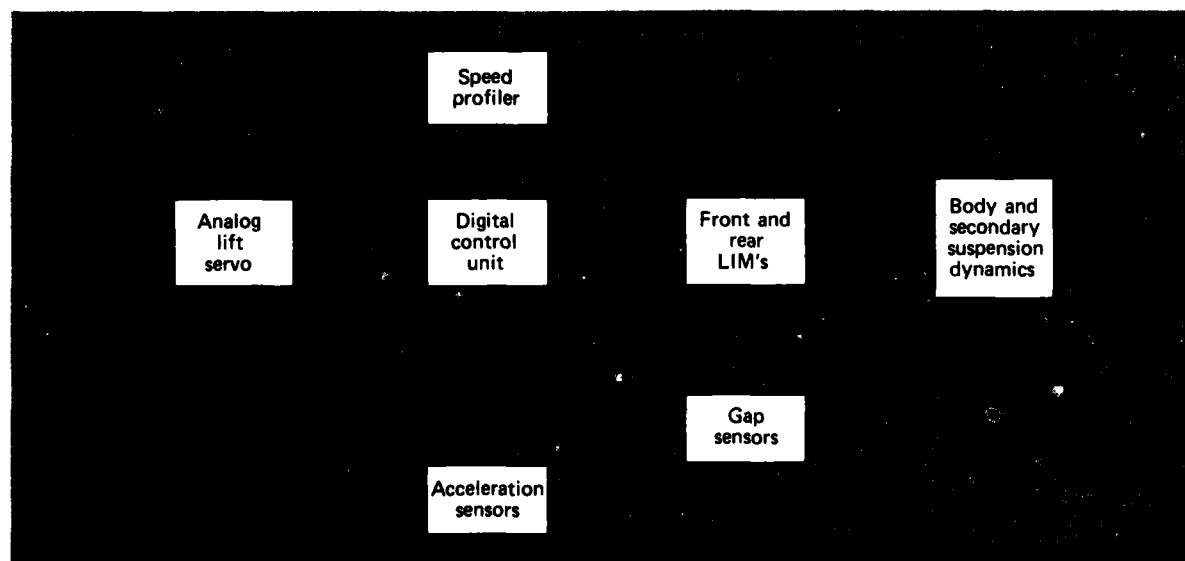


Figure 2 — The control system for Maglev.

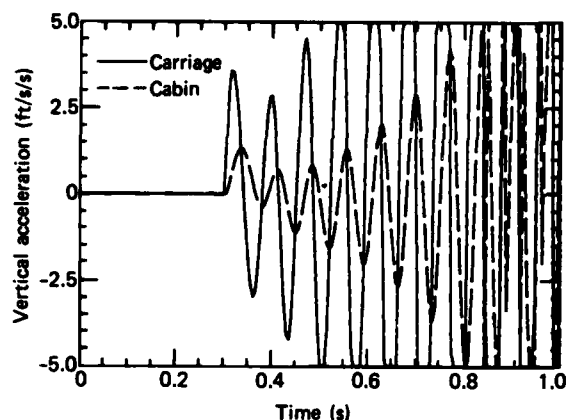


Figure 3 — Vehicle response to a step change in the commanded air gap (original DCU design).

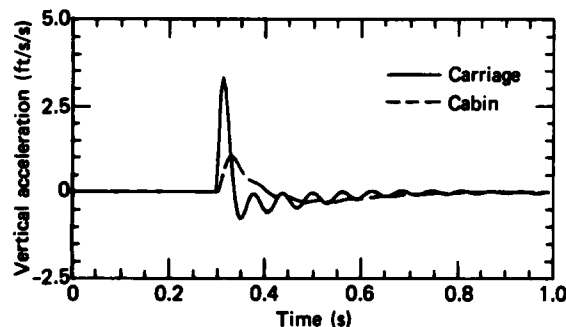


Figure 4 — Vehicle response to a step change in the commanded air gap (modified DCU design).

range. Satisfactory results were obtained using the modified DCU design. Finally, a limited evaluation of such factors as wind gusts on the vehicle, gap sensor errors, and parameter mismatches between the DCU's and the actual LIM's was performed. Satisfactory results were obtained using the modified DCU design, although any parameter mismatch between the DCU and physical reality tends to amplify periodic disturbances at the motor excitation frequency (Figs. 3 and 4). The results of the analysis, along with suggested design modifications, have been provided to Boeing for use in their ongoing Maglev developmental efforts.

## REFERENCES

- <sup>1</sup>J. A. Ross, "ROMAG Transportation System," in *Proc. IEEE* 61, pp. 617-620 (May 1973).
- <sup>2</sup>R. G. Rule and R. G. Gilliland, "Combined Magnetic Levitation and Propulsion: The Mag-Transit Concept," *IEEE Trans. Veh. Tech.* VT-29 (Feb 1980).
- <sup>3</sup>E. R. Laithwaite, *Induction Machines for Special Purposes*, Newnes, London (1966).
- <sup>4</sup>S. J. Brown, *Analysis and Simulation of the Boeing Mag-Transit Control System*, JHU/APL TPR 046 (to be published).

This work was supported by the Urban Mass Transportation Administration.

## **FUNDAMENTAL RESEARCH**

## INTRODUCTION

Fundamental research has been firmly established at APL for many years as one of the Laboratory's principal missions, which include the application of advanced science and technology to the enhancement of the security of the United States and the pursuit of basic research to which the Laboratory's facilities can make an especially favorable contribution. The incorporation of basic research into the Laboratory's mission recognizes that such research will play a vital role in future technological achievements and that it is needed to avoid institutional obsolescence.

Much of the basic research conducted at APL is done in the Research Center, which was formally established in 1947. Its initial objectives, still valid today, were to establish APL as a contributor to scientific knowledge, to develop and provide fundamental understanding basic to fields of present and potential interest to the Laboratory, and to enhance the professional competence of the staff by serving as a doorway to science. Since its inception, the Research Center has spawned new programs that are now carried out in other units of the Laboratory. Most notable are the Space Department and the Biomedical Research Program.

Today, the Milton S. Eisenhower Research Center is comprised of 56 staff members organized into eight groups. Research is reported in the professional scientific literature; typically, 60 papers are published each year. The articles in this section describe some recent accomplishments in basic research by staff members of the Research Center and of other Laboratory units.

The first article describes a family of organic semiconductors for which the phenomenon of optical switching has been observed. Next, a report is presented on the development of a simplified flame theory—an outgrowth of the Laboratory's long-standing interest in combustion problems. The third article deals with the discovery of a new class of low-energy electron diffraction patterns that have been shown to be sensitive to adsorbed gases and surface-layer displacement. Then an article is presented on the optical monitoring of energy-transfer processes accompanying the pulsed laser excitation of photosensitive dyes in condensed media. Finally, the structure of amorphous metallic alloys is discussed from the point of view of their magnetic hyperfine fields.

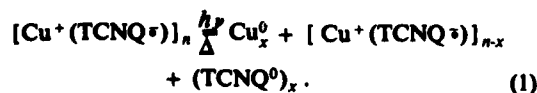
# OPTICAL SWITCHING IN SEMICONDUCTOR ORGANIC THIN FILMS

R. S. Potember, T. O. Poehler, and R. C. Benson

*A family of organic semiconductors that display unique optical and electronic properties has been reported. Preliminary studies indicate that this class of organic semiconductor may be superior to inorganic materials presently used as optical storage systems or as optically controlled solid-state devices for applications in optical communications or computers. These devices are much easier to fabricate, more reproducible in their electrical and optical behavior, and less sensitive to changes in ambient temperature and moisture than are devices based on conventional materials. An experimental research program has been undertaken to obtain a detailed understanding of the mechanism of conduction and switching in this class of organometallic semiconductor.*

## BACKGROUND

Stable and reproducible field-induced switching between two stable resistance states in polycrystalline organometallic semiconducting films has been reported.<sup>1-3</sup> The effects have been observed in films of copper or silver complexed with the electron acceptors tetracyanoethylene (TCNE), tetracyanonaphthoquinodimethane (TNAP), tetracyanoquinodimethane (TCNQ), and other derivatives of TCNQ. The switching in those materials is reversible and fast, with switching times of less than 5 ns observable in electrical switching experiments. On the basis of a series of experiments conducted to interpret the nature of the electrical switching and memory effects, it has been postulated that a phase containing a complex salt involving neutral TCNQ (TNCQ<sup>0</sup>) is formed as a result of a field-induced redox reaction. The film formed initially by the reaction of the metallic substrate and a TCNQ<sup>0</sup>/CH<sub>3</sub>CN solution was found to be Cu<sup>+</sup>TCNQ<sup>-</sup>, and it appears that the effect of the applied field is to induce the formation of a complex salt containing at least some neutral TCNQ:



Various diagnostic techniques, including infrared, Auger, x-ray, photoelectron, and Raman spectroscopy, have been applied to specimens from the CuTCNQ family to validate the mechanism shown in Eq. 1.<sup>4</sup> In addition, the methods have allowed one to estimate that after switching from the high resistance to the low resistance states, TCNQ is present in the film up to

30 molecular percent.<sup>5</sup> While the electric fields used to induce this reversible topotactic redox reaction in the copper and silver TCNQ family have so far been limited to DC, pulsed, and AC fields, with frequencies up to approximately 500 MHz, it is obvious that higher frequency electric fields, including those at optical frequencies, should also be effective in inducing such a redox reaction.

## DISCUSSION

The effects of electric fields at optical frequencies on thin organometallic films in this family of organic semiconductors have been investigated recently. Switching between the two stable phases described in Eq. 1 has been observed as a result of exposure to optical beams. These observations of switching have been made by both Raman spectroscopy and by direct observation of the electrical properties of the organometallic films.

Semiconducting charge-transfer salts, such as CuTCNQ, are grown as highly polycrystalline films directly on the metallic substrates by reacting neutral TCNQ in acetonitrile solution with copper metal, as described previously.<sup>1</sup> For electrical measurements, a top metal electrode of aluminum or chromium was evaporated or sputtered directly on the organic film, and contacts were made to the top metal electrode and the underlying metallic substrate. For the optical and electro-optical experiments reported in this article, the top metal electrode was either omitted or prepared with a thickness that permitted partial transmission of optical radiation.

Depending on the specific material involved, the field strengths required to cause switching transitions vary between  $2 \times 10^3$  and  $2 \times 10^4$  V/cm. Fields of this magnitude are easily obtained near focus in many laser beams of moderate power. CuTCNQ and AgTCNQ specimens have been irradiated with the 488 and 458 nm lines from an argon ion laser, and the effects have been observed both by Raman spectroscopy and by electrical measurements made on specimens of the conventional two-terminal switching geometry.

Measurements have been reported on the Raman spectra of TCNQ and of a number of simple TCNQ salts.<sup>6-11</sup> Strong Raman bands are observed in those materials (Fig. 1) for both TCNQ and a CuTCNQ film.

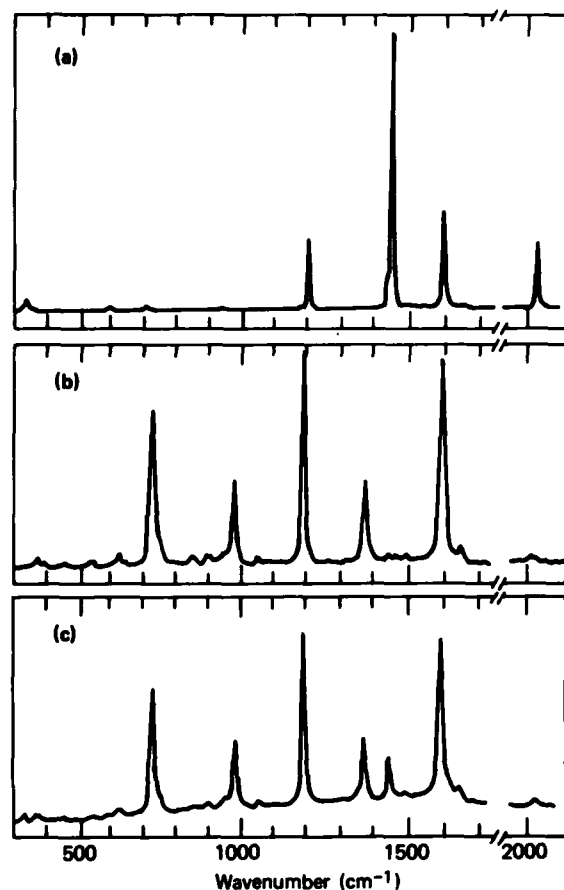


**Figure 1** — Raman bands. (a) Neutral TCNQ, (b) CuTCNQ film, and (c) CuTCNQ film after exposure to argon laser.

Some Raman modes are strongly affected by the electronic structure of the TCNQ. For example, the TCNQ carbon-carbon stretch mode shows a frequency shift from approximately  $1375\text{ cm}^{-1}$  for the fully charged transfer species to  $1451\text{ cm}^{-1}$  for the neutral species. It is apparent from the Raman spectrum of the CuTCNQ film (Fig. 1b) that the film contains essentially no neutral TCNQ. The spectrum was observed using an incident beam intensity that does not perturb the equilibrium state of the film. However, if the incident beam intensity is increased above a certain value, the Raman spectrum of the CuTCNQ film changes dramatically. A typical spectrum is shown in Fig. 1c. It is apparent that the system now contains a substantial quantity of neutral TCNQ, as evidenced by the appearance of the characteristic strong band at  $1450\text{ cm}^{-1}$ . Because this effect depends directly on field strength, the actual power required to cause the switching between the two states depends on the beam size at the film surface in the case of optical excitation. For the particular

case illustrated in Fig. 1c, the irradiance required to cause optical switching was approximately  $600\text{ W/cm}^2$ .

Large changes in the Raman spectrum of an irradiated film can be observed without any apparent change in the macroscopic properties of the film in the visible region. However, with intensified radiation, lines or patterns can be observed being generated at the surface of the film. The patterns are optically visible as a result of the formation of macroscopic regions of neutral TCNQ. Millisecond exposures to a modulated laser beam swept across the film surface are sufficient to write this type of line.

These optical effects can be observed in many copper and silver TCNQ derivatives, which were reported previously for the electrical switching. As in the case of low-frequency electric fields, details of the changes between stable states of the films vary according to the materials. For example, changes in the Raman spectrum of AgTCNQ are observed at lower optical field strengths than for CuTCNQ. Another major difference is the appearance of a broad feature in the  $1050$  to  $1800\text{ cm}^{-1}$  region of the Raman spectrum of AgTCNQ at laser powers well above those required for switching. That signal was not observed under similar conditions for CuTCNQ or for neutral TCNQ.

Changes in the electrical resistance induced by optical fields also were measured in several films. A conventional AgTCNQ switching structure with a partially transparent aluminum top metal electrode was subjected to laser radiation at  $488\text{ nm}$ , and the changes in the electrical resistance were measured. The film was biased with a DC electric field of approximately  $5\text{ V}$  across the aluminum/AgTCNQ/silver structure; the AgTCNQ film thickness was approximately  $5\text{ }\mu\text{m}$ . The DC field was adjusted so that the film remained in the high resistance state just below the threshold for electrical switching. Application of the argon laser beam induced the film to change state rapidly to the low resistance state. Rapid cycling of the optical beam caused the device to respond by switching rapidly between the high and low resistance states. When the optical beam was removed and the electrical bias was reduced to zero, the film returned to its equilibrium high resistance state. It is apparent that the irradiation of these films by optical fields can cause transitions that are observable by optical and electrical techniques.

## SUMMARY

It has been demonstrated that a laser beam can be used to induce both bistable optical and optoelectronic switching in organic charge-transfer complexes. Furthermore, it has been shown that by choosing the

appropriate donor-acceptor complex or by varying the applied electric field intensity, it is possible to produce both threshold and either permanent or erasable memory functions. The unique properties of these films may be used to construct optically controlled solid-state devices with potential applications in communications or data storage systems.

## REFERENCES

- <sup>1</sup> R. S. Potember, T. O. Poehler, and D. O. Cowan, *Appl. Phys. Lett.* **34**, 405 (1979).
- <sup>2</sup> R. S. Potember, T. O. Poehler, A. Rappa, D. O. Cowan, and A. N. Bloch, *J. Am. Chem. Soc.* **102**, 3659 (1980).
- <sup>3</sup> R. S. Potember, T. O. Poehler, D. O. Cowan, and A. N. Bloch, in *Proc. NATO Conference on Chemistry and Physics of One-Dimensional Materials*, L. Alcácer, ed., D. Reidel Publishing Co., Boston, pp. 419-428 (1980).

- <sup>4</sup> R. S. Potember, T. O. Poehler, D. O. Cowan, A. N. Bloch, P. Brant, and F. L. Carter, *Chemica Scripta* **17**, 219 (1981).
- <sup>5</sup> R. S. Potember, T. O. Poehler, P. Brant, and R. C. Benson (unpublished results).
- <sup>6</sup> T. Takenaka, *Spectrochim. Acta* **27A**, 1735 (1971).
- <sup>7</sup> A. Girlando and C. Pecile, *Spectrochim. Acta* **29A**, 1859 (1973).
- <sup>8</sup> R. Bozio, A. Girlando, and C. Pecile, *J. Chem. Soc. Faraday Trans. 2* **71**, 1237 (1975).
- <sup>9</sup> C. Chi and E. R. Nixon, *Spectrochim. Acta* **31A**, 1739 (1975).
- <sup>10</sup> D. L. Jeanmaire and R. P. VanDuyne, *J. Am. Chem. Soc.* **98**, 4029 (1976).
- <sup>11</sup> M. S. Khatkale and J. P. Devlin, *J. Chem. Phys.* **70**, 1851 (1979).

This work was supported by the Office of Naval Research, the Defense Advanced Research Projects Agency, and NAVSEASYSOM.

## A SIMPLE MODEL FOR FLAMES WITH COMPLEX CHEMISTRY

R. M. Fristrom

*This report describes the development of a flame theory that combines reliable predictions of the propagation rate and structure of premixed laminar flames with a simplicity that may allow its use as an engineering tool for the modeling of engines and other complex combustion systems. The work is an outgrowth of the long-term interest the Laboratory has had in combustion problems.*

### BACKGROUND

Combustion is clearly a key ingredient in the propulsion systems required for the guided missile program at APL. A strong intramural program in propulsion was instituted and was actively supported by the Research Center. Early studies resulted in the successful detection of radicals for the first time by mass spectrometry by S. Foner and R. Hudson and the rocket instability theories of F. McClure, R. W. Hart, and J. Bird. In the Propulsion Group, significant contributions were made by W. H. Avery, W. G. Berl,

N. deHaas, D. Dembrow, P. Breisacher, R. Edmonson, S. Favin, G. Fristrom, R. Fristrom, E. Gayhart, P. Rosen, W. Wilson, and R. Walker. The companion engineering program was carried out by F. Billig, G. Dugger, E. Franklin, R. Froelich, I. Faro, F. Hill, M. Hill, H. L. Olsen, R. Ray, J. Ray, J. Walker, W. Shippen, J. Hardgrave, and their associates. This was the backbone of the successful program that produced Terrier, Talos, and the T-Section missiles. On the fundamental research side, the results were equally impressive. A result of that long-term program has been several hundred papers on the fundamental aspects of combustion, the *Ramjet Technology* series published internally by APL, *Flame Structure* by Fristrom and Westenberg,<sup>1</sup> and over a dozen surveys of the state of the art. The success was due to continuity of effort and to dedication. The fundamental work was transferred to the Research Center on a reduced scale. Today, there is a renewed interest in combustion problems, and the Laboratory continues to make contributions in this area.

## DISCUSSION

The theory of premixed laminar flames was put on a rigorous basis by Hirshfelder et al.<sup>2</sup> The flame equations are derived from the conservation laws for mass and energy and the continuity relations describing the interaction of reaction, molecular diffusion, and convection for each chemical species. One equation is required for each species (reduced by the conservation constraints). Fortunately, the problem can be reduced to pseudo-one-dimensional form while still providing a quantitative description for many common laboratory flames. However, the problem is still formidable because several hundred species may be involved in common flame systems and the simultaneous, so-called "stiff" differential equations interact strongly. With modern computational capabilities, it is feasible to solve systems as complex as four-carbon hydrocarbon flames with air.<sup>3</sup> More complex chemistries such as those of interest in engineering practice are impractical because of computational requirements and the lack of suitable parameters for species rates and transport. The simplest engineering applications involve three-dimensional, time-dependent turbulent flow with complex mixtures. The solution of the latter type of problem requires thousands of calculations, severely limiting the use of the rigorous, fundamental approach. Simplified theories that reduce the chemistry to an overall global reaction have proven useful for aerodynamic simulations, but the chemical information is lost and the extrapolation of such empirical fits is suspect.

The new simplified model that has been developed is based on the insight provided by the past 30 years

of theoretical and experimental studies in combustion.<sup>1</sup> The one-dimensional flame equations are an overdetermined set of equations whose solution is a pseudo-Eigenvalue problem. This solution can be identified with the experimentally measured burning velocity, which theory indicates should be a unique function of the initial conditions. This is borne out experimentally, and one can think of a flame as a thin reaction sheet propagating normal to itself. The system is so strongly coupled that if it were possible to determine the reaction course for any reactant (fuel or oxidizer) under flame conditions, the rate would define the system burning velocity. This means that it is only necessary to solve one of the species continuity equations, providing one is interested principally in the burning velocity, as is often the case. In the past, the difficulty with this approach was that it involved the rate *under flame conditions*, which depends on the detailed behavior of other reactants as well as the temperature distribution. These conditions are not known *a priori*. However, sufficient auxiliary information can be derived to allow quantitatively significant estimates of the parameters. Thus, the new approach divides the flame into zones, each of which is dominated by a single or a few processes. Boundaries are chosen so that composition/temperature conditions can be estimated using simple reliable transport and thermodynamic computations. The primary reaction zone is confined to a narrow region (both in space and temperature) (Fig. 1) that can be suitably linearized using the boundary conditions. As a result, the problem is reduced from one of coupled, stiff, simultaneous differential equations to the solution of a set of simultaneous algebraic equations.

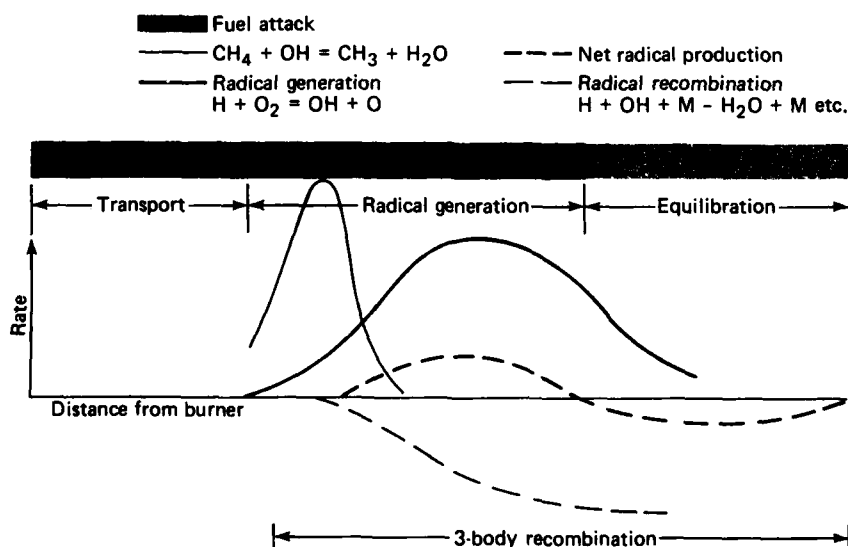


Figure 1 — The zones in a methane flame.

The remaining problem is the chemical one of establishing a reliable mechanism for one of the reactants. The flames of common interest involve reaction between fuel molecules composed of carbon, hydrogen, and oxygen with the oxygen of the air. The reactions of oxygen are of key importance for two reasons: (a) it is the common reactant in the flames, and (b) it is the principal source of the reactive atoms and radicals whose generation is required for the flame to propagate. The six parameters required to define the reaction zone are the oxygen concentration, the hydrogen atom concentration, the lower bound temperature ( $T_l$ ), the upper bound temperature ( $T_u$ ), the reaction zone thickness, and the burning velocity. The initial oxygen concentration can be obtained from a diffusion computation. The concentration of hydrogen (and oxygen) at the upper boundary can be obtained from a thermodynamic partial equilibrium computation.<sup>4</sup> The upper temperature boundary can be obtained from the balance among radical production, radical recombination, and radical flux. The reaction zone thickness can be obtained from the thermal conduction constraint at the lower boundary. The lower temperature boundary can be obtained from the maximal propagation constraint because a flame is the most rapid process that can connect the initial and final conditions. Peak concentrations of intermediate species can also be obtained using partial equilibrium, providing the mechanisms of formation and destruction are identified and the rates known.

The governing equations in the new model are all linear algebraic relations, and their solution has proven to be much less laborious than the rigorous approach. The results appear to be versatile and perhaps more reliable than the rigorous approach because most of the parameters are well known. By contrast, the rigorous approach requires the estimation of many transport and rate coefficients because they have not been measured or are poorly known.

It has been possible to predict the propagation velocity for the methane/air system as a function of composition (Fig. 2) and the stoichiometric normal hydrocarbon/air flames (Fig. 3). The results are in agreement with experimental studies and the rigorous computations.<sup>5</sup> It also has been possible to predict the detailed microstructure because composition and temperature in the primary zone are pure transport problems, temperature gradients and composition are linearized in the primary reaction zone, and temperature and composition in the equilibration region are computed from partial equilibrium relations. These results are most conveniently displayed as a temperature/composition plot (Fig. 4). To transform to a composition/distance plot, a temperature/distance relation-

- 1 Assumes maximal velocity only
- 2 Radicals limited by  $H + O_2 + M$ ,  $H + OH + M$ , and  $H + H + M$
- 3 Radicals limited by  $H + O_2 + M$ ,  $H + OH + M$ ,  $H + H + M$ , and  $CH_3 + O$
- 4 Radicals limited by  $H + O_2 + M$ ,  $H + OH + M$ ,  $H + H + M$ ,  $CH_3 + O$ ,  $H + CO + M$ , and  $H + CH_3 + M$

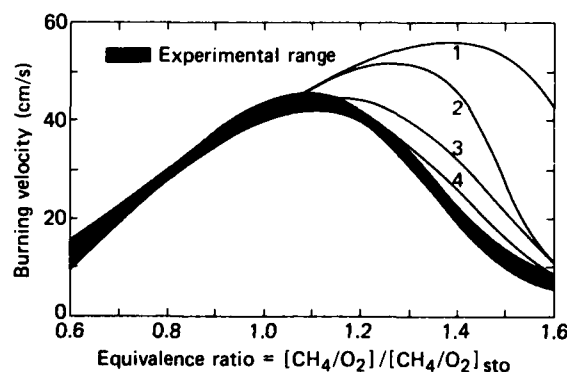


Figure 2 — Comparison of zonal theory computations with experimental results for the methane/air flame system (taken from Refs. 5 and 6).

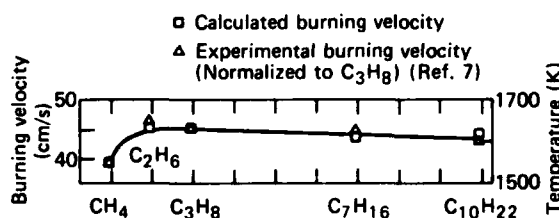


Figure 3 — Comparison of theoretical and experimental burning velocities of flames of normal hydrocarbons with air under stoichiometric conditions (taken from Ref. 5).

ship is required, which can be obtained from thermal conduction relationships in the transport zone, from the linear temperature gradient assumption in the primary reaction zone, and from reaction time computations in the equilibration zone. The resulting profiles have been compared with experimental measurements in one case, and good agreement has been found (Tables 1 and 2 and Fig. 4). The success of this approach suggests that it might be used as the initial guess in an iterative rigorous solution of the flame equations.

This solution to the flame equations requires no arbitrary parameters — only rate, transport, and thermodynamic information from the literature are used. Rate data have not been fitted, as is often done in so-called rigorous treatments. However, it should be pointed out that our choice of model and zone structure was made with full knowledge of the desired final re-

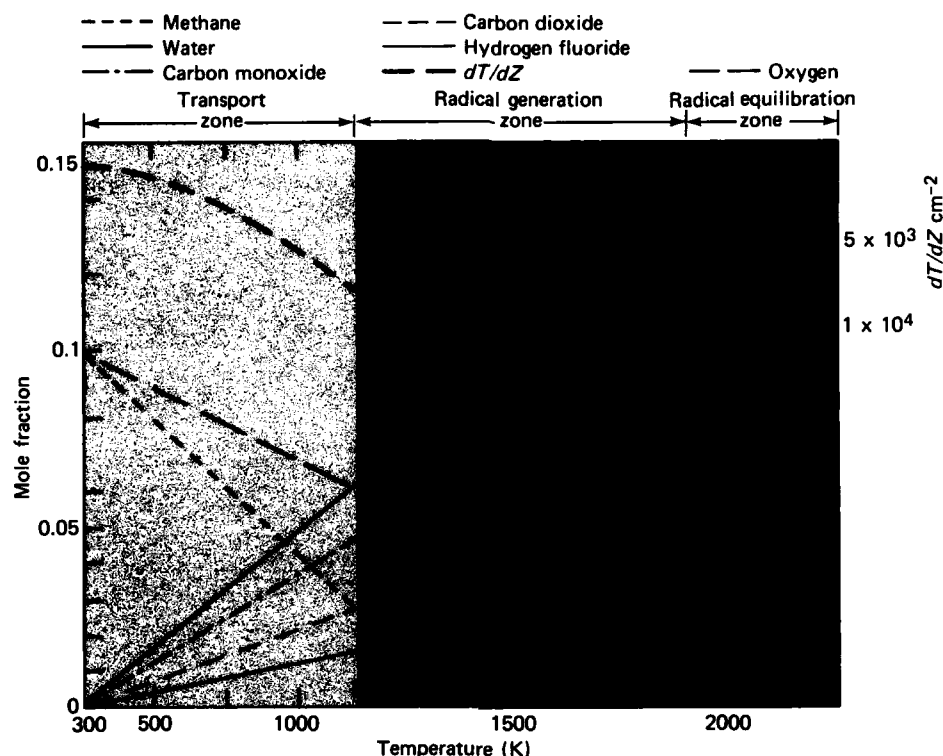


Figure 4 — Temperature/composition profile of a methane-argon-oxygen- $\text{CF}_3\text{Br}$  flame (taken from Ref. 5). The experimental points are from Ref. 8.

Table 1 — Comparison of experimental and calculated peak fuel intermediate concentrations (mole fractions). (10 parts  $\text{CH}_4$ , 20 parts  $\text{O}_2$ , 69 parts Ar, 1 part  $\text{CF}_3\text{Br}$ ; pressure 0.0528 atm).

	Calculated* 1200 K	Experimental† 1450 ± 50 K
$\text{CH}_4$	$1.25 \times 10^{-2}$	$2.5 \times 10^{-2}$
$\text{CH}_3$	$4 \times 10^{-3}$	$2.5 \times 10^{-3}$
$\text{OCH}_2$	$3 \times 10^{-4}$	$1 \times 10^{-3}$
$\text{HCO}$	$1.2 \times 10^{-4}$	$5 \times 10^{-5}$
$\text{CO}$	$5.5 \times 10^{-2}$	$6 \times 10^{-2}$
$\text{HO}_2$	$4 \times 10^{-7}$	Not reported

\*Reference 5.

†Reference 8.

sult. The quantitative agreement obtained, which is of the order expected from the probable errors in the parameters, should be construed as an indication that the approximations used in the model are proper.

The continuation of these studies will be directed toward the application of these ideas to more complex combustion systems with the hope that it will prove to be a useful tool for modeling studies.

Table 2 — Comparison of theoretical and experimental ole fractions at the hot boundary of the radical production zone.

	Theory* 1987 K	Experimental† 1950 K
H	$2.1 \times 10^{-2}$	$1.3 \times 10^{-2}$
O	$0.98 \times 10^{-3}$	$0.75 \times 10^{-2}$
F	$1.5 \times 10^{-5}$	Not reported
Br	$8.8 \times 10^{-3}$	$9 \times 10^{-3}$
OH	$0.9 \times 10^{-2}$	$1.3 \times 10^{-2}$
$\text{O}_2$	$2.4 \times 10^{-2}$	$3.5 \times 10^{-2}$
$\text{Br}_2$	$1 \times 10^{-8}$	Not reported
HF	$2.8 \times 10^{-2}$	$3 \times 10^{-2}$
HBr	$3.5 \times 10^{-4}$	$1 \times 10^{-4}$
CO	$5.9 \times 10^{-2}$	$4 \times 10^{-2}$
$\text{HO}_2$	$1 \times 10^{-7}$	Not reported
$\text{H}_2\text{O}$	$13 \times 10^{-2}$	$15 \times 10^{-2}$
$\text{CO}_2$	$6.1 \times 10^{-2}$	$6 \times 10^{-2}$

\*Reference 5.

†Reference 8.

## REFERENCES

- 1 R. M. Fristrom and A. A. Westenberg, *Flame Structure*, McGraw-Hill, New York (1965).
- 2 J. O. Hirschfelder, C. F. Curtis, and R. B. Bird, *Molecular Theory of Gases and Liquids*, John Wiley, New York (1954).

- <sup>3</sup>J. Warnatz, *Eighteenth Symposium on Combustion*, the Combustion Institute, Pittsburgh, p. 369 (1981).  
<sup>4</sup>R. M. Fristrom and S. Favin, "The Computation of Partial Equilibrium in Flames" (in preparation).  
<sup>5</sup>R. M. Fristrom, "Chemical Factors in the Inhibition and Extinction of CHO Flames," Meeting of the Western States Section of the Combustion Institute, Los Angeles (1980).  
<sup>6</sup>R. M. Fristrom, "Chemical Modeling of Combustion Systems," Plenary Lecture at the Meeting of the Eastern States Section of the Combustion Institute, Pittsburgh (1981).

<sup>7</sup>*Basic Considerations in the Combustion of Hydrocarbon Fuels with Air*, NACA 1300 (1959).

<sup>8</sup>J. Biordi, C. Lazzara, and J. Papp, *Fifteenth Symposium on Combustion*, the Combustion Institute, Pittsburgh, p. 917 (1975).

This work was supported by Independent R&D.

## DISCOVERY OF A NEW LOW-ENERGY ELECTRON DIFFRACTION PHENOMENON

C. B. Barger, A. N. Jette, and B. H. Nall

*A new low-energy electron diffraction phenomenon has been discovered and successfully explained. The experimental method, called current image diffraction, can be exploited to determine surface orientation and symmetry. The patterns have also been shown to be sensitive to adsorbed gases and surface-layer displacement. Theoretical considerations indicate that surface-layer displacement can be determined to 0.0005 nm, which is a factor of four better than the sensitivity of existing methods.*

### BACKGROUND

The study of processes occurring at solid surfaces is relevant to a wide variety of Department of Defense and civilian applications. For example, missiles traveling through the atmosphere are subjected to a number of complicated mechanisms leading to corrosion and ablation. Knowledge of gas/surface interactions is essential for the understanding of catalytic processes important to industry. A significant amount of effort, frequently using electrons as a probe, has been devoted to determining surface atom positions in order to obtain a detailed knowledge of these surface interactions.

Since the early days of the development of atomic theory and quantum mechanics when Davisson and Germer<sup>1</sup> performed the first electron diffraction experiment establishing the wave-particle duality of the elec-

tron, it has been known that crystals can act as a diffraction grating for electrons. After this pioneering work, interest in low-energy electron diffraction (LEED) waned because the stringent requirement for ultrahigh vacuum was not then attainable. With the advent of ultrahigh vacuum technology and surface preparation methods like ion bombardment in the early 1960's, LEED was revived as a surface tool. In a conventional LEED experiment, the crystal is irradiated with a stationary electron beam, and the backscattered electrons are displayed on a fluorescent screen. A typical LEED pattern is a symmetrical arrangement of spots whose geometry immediately determines surface structure and orientation and whose intensity, as measured by a Faraday cup or photometer, contains information on the surface unit cell when correlated with a theoretical calculation.

Recently, an interesting diffraction phenomenon was discovered in the specimen current image of single crystal metal surfaces.<sup>2</sup> In contrast to the conventional LEED configuration, the experimental method used to observe the new phenomenon, called current image diffraction (CID), uses a scanning electron beam that impacts the specimen at constantly changing azimuthal and polar angles. Consequently, in a CID pattern, changes in contrast are the result of variations in the total reflectivity of the crystal surface as a function of incident beam angle. The problem can be approached theoretically by calculating the sum of all the reflected beams giving rise to the LEED pattern.<sup>3</sup>

## DISCUSSION

Crystals of 99.999% purity were prepared by a mechanical polish and an electropolish before being mounted in the apparatus where they were subjected to annealing and further cleaning by bombardment of the surfaces with argon ions. The crystals were subjected to an analytical analysis by Auger spectroscopy and, in most cases, showed no detectable traces of impurities.

Figure 1 is a schematic of the apparatus. Low energy electrons ( $0 < E_p < 400$  eV) scan the surface of the sample. At each point on the crystal surface, the current adsorbed by the crystal is measured and displayed synchronously on a cathode ray tube; that is, the incident direction of the primary beam is varied by deflecting the beam in a raster, and the current to the sample is presented in a rastered display. Some of the resulting images from the (001) surface of aluminum (crystal planes are indexed by their Miller indices ( $h/k$ )) are shown in Fig. 2 where light areas correspond to regions of large sample current and dark areas to regions of high reflectivity of the incident electron

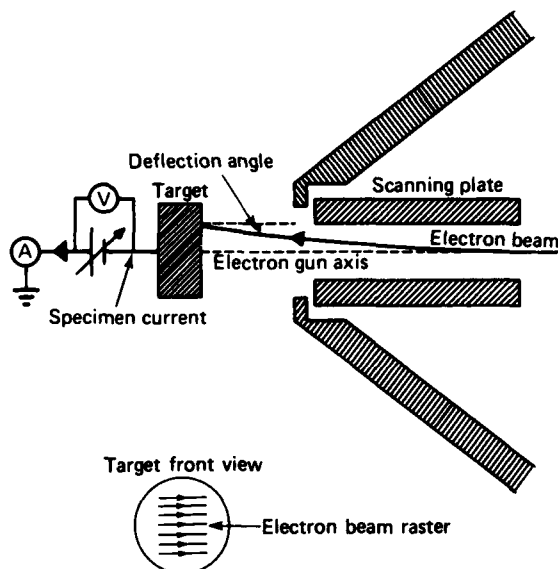


Figure 1 — Schematic diagram of the experimental apparatus.

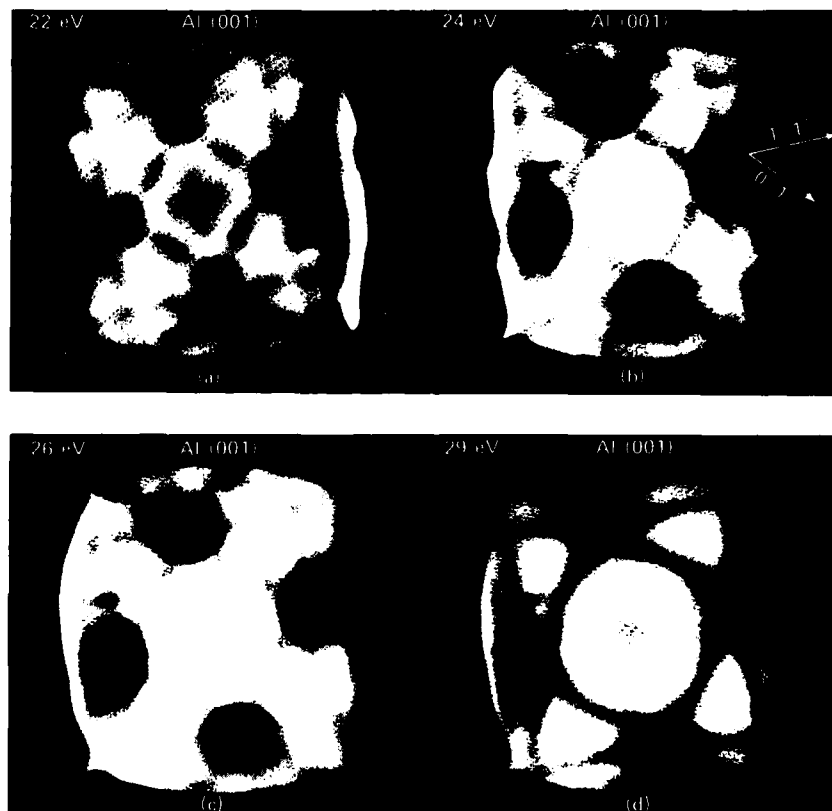


Figure 2 — CID patterns for the (001) face of aluminum. Primary beam energies are relative to the sample.

beam. The four-fold symmetry of this surface and its orientation are apparent in the patterns.

In Figs. 2a and 2b, the light lines, corresponding to regions of large sample current of absorbed electrons, result from channeling of the electrons into the crystal; in Figs. 2c and 2d, these lines become dark, indicating the high reflectivity of electrons. The changes are brought about by varying the energy of the incident electron beam by just a few volts and indicate the sensitivity of the patterns to the primary beam energy.

The line positions are predicted by Bragg scattering from specific atomic planes (Fig. 3). The incident beam of electrons, approximated by a plane wave, is incident on a parallel set of planes not necessarily parallel to the crystal surface. Whenever the extra distance traversed by the electron beam (given by  $2d \sin \theta$ ) is  $n\lambda$ , constructive interference occurs, resulting in strong scattering of the electrons. Here,  $d$  is the atomic plane separation,  $\theta$  is the Bragg angle (angle between the incident beam and the plane),  $\lambda$  is the wavelength of the incident electrons, and  $n$  is an integer.

As is apparent from Fig. 3, there is a cone of incident directions for the primary electron beam that can satisfy the Bragg condition for scattering from a particular atomic plane. The intersection of this cone with the Ewald sphere (whose radius is given by  $2\pi/\lambda$ ) estab-

lishes the conditions for Bragg diffraction. When the scattering occurs from planes parallel to the surface, the incident electrons satisfying the Bragg condition form a circle when projected onto the surface. If the scattering occurs from planes at right angles to the surface, the incident electrons satisfying the Bragg condition form a line when projected onto the crystal surface. If the planes are at an oblique angle to the surface, the projected circle on the surface plane appears elliptical. Because the incident polar angle of our apparatus is restricted to  $\pm 18^\circ$  by the scanning system, only small portions of these curves are imaged on the crystal surface in most cases.

The specific atomic planes that scatter the incident electron beam can thus be identified from the curvature and energy dependence of the lines, as in Fig. 2. When the images in Fig. 2 are compared with the simple Bragg theory, the atomic planes responsible for the four-fold lines are identified as the  $\{113\}$  set. Moreover, information on the size of the unit cell and the inner potential (the energy of conduction electrons relative to the closed-shell ion cores) can be derived from the energy dependence of these lines. Since the source of electrons in our apparatus is a heated tungsten filament, the incident electron beam has a distribution of energies approximately a half volt about the "incident energy." This fact is responsible for the broadened features in

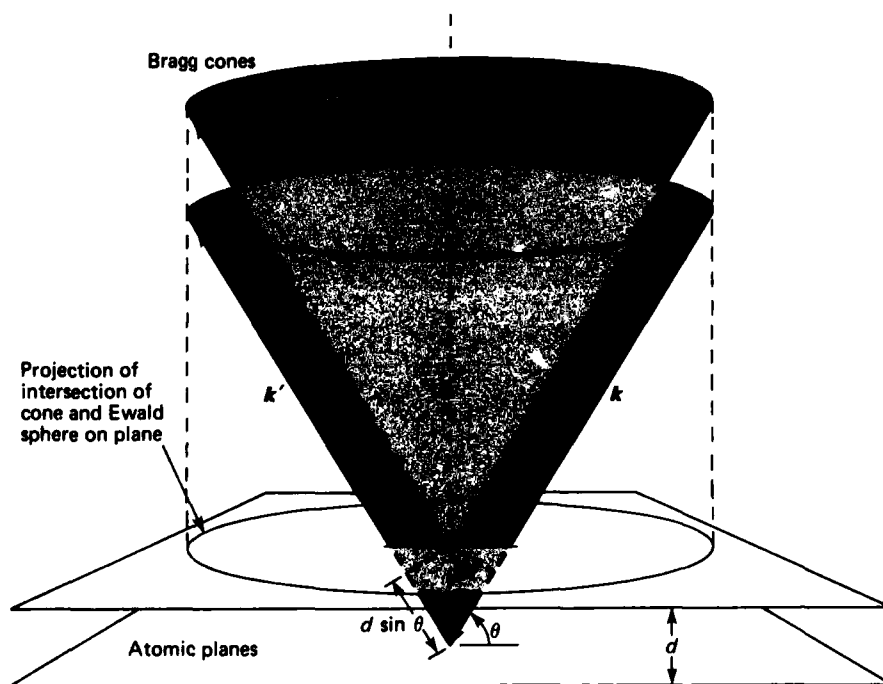


**Figure 3 —** Bragg scattering from atomic planes. The scalar form of the Bragg condition is  $2d \sin \theta = n\lambda$ . The wave vectors  $k$  and  $k'$  have magnitude  $2\pi/\lambda$ , which is also the radius of the Ewald sphere.

the experimental images and restricts our accuracy in determining the surface unit cell size,  $d$ . However, calculations indicate that if an energy monochromator is incorporated in our apparatus to reduce the breadth of energy distribution of the incident electron beam, the average planar separation of the layers parallel to the surface can be determined to 0.0005 nm, a factor of four better than with current methods.

The simple Bragg theory and diffraction patterns give the size and shape of the unit cell, but to obtain the contents of the unit cell and the bond distances between adsorbed atoms and the substrate, the reflectivity of the crystal surface caused by elastically scattered electrons must be computed as a function of angle of incidence and compared with the corresponding experimental CID patterns. The computations are quite complex and will only be described briefly.<sup>4</sup>

The dominant mechanism is the scattering of electrons by the ion cores. The phase shifts for scattering from a single ion core are first computed, and then the ion cores are arranged in the periodic array of the crystal and immersed in the constant complex optical potential. The complex potential is due to the electron gas of conduction electrons. The real part is the so-called inner potential of the metal and is roughly equal to the Fermi energy plus the work function. The imaginary part is due to inelastic collision with the electron gas. It is the imaginary component that is responsible for the attenuation of beam intensity within the crystal. The backscattered intensity of electrons is then calculated, including all multiple scattering events within an atomic layer of ion cores and all forward interlayer multiple scattering events between different layers. The relatively weak backscattering is then treated as a perturbation.

In this manner, the total reflectivity of the (001) surface of aluminum was computed as a function of azimuthal and polar angles. By means of computer imaging methods, the theoretical image of Fig. 4a was produced; it reproduces the general features of the experimental image in Fig. 4b at 161 eV.<sup>3</sup> It should be noted that theory neglects temperature effects and the width of the primary beam, thereby explaining the "smearing out" in the experimental picture of many of the sharp lines apparent in the theoretical image.

It is clear that much information can be extracted from CID patterns, and work is proceeding on developing the method further. For instance, it has been established that CID patterns are sensitive to adsorbed gases,<sup>5</sup> but much remains to be done. It is anticipated that the CID method will prove to be an important tool for surface analysis.

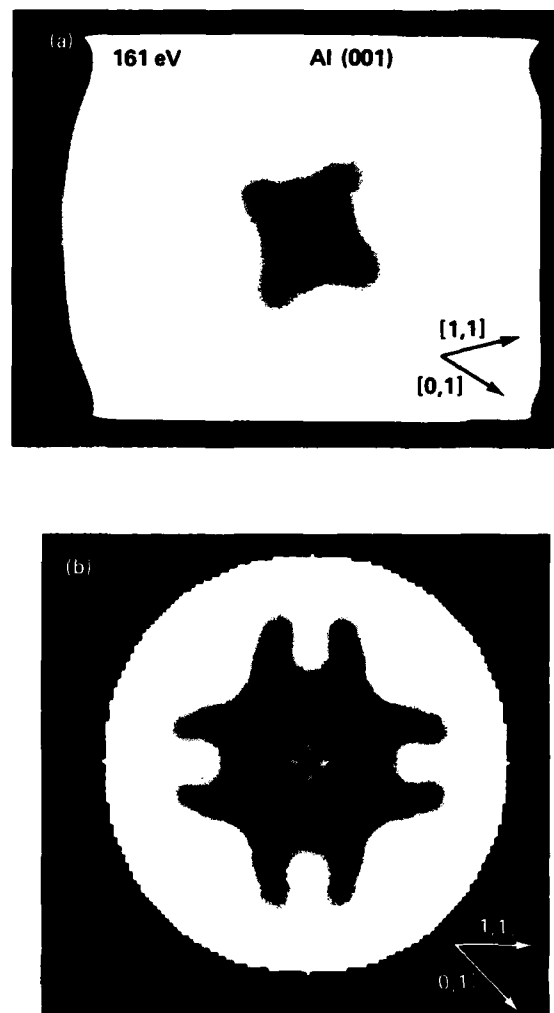


Figure 4 — Theoretical and experimental images of the (001) face of aluminum at 161 eV.

## REFERENCES

- <sup>1</sup> C. J. Davisson and L. H. Germer, "The Scattering of Electrons by a Nickel Crystal," *Phys. Rev. A* **29**, 908 (1927).
- <sup>2</sup> B. H. Nall, A. N. Jette, and C. B. Barger, "Diffraction Patterns in the Specimen-Current Image of a Single Crystal at Low Beam Energies," *Phys. Rev. Lett.* **48**, 882-885 (1982).
- <sup>3</sup> A. N. Jette, B. H. Nall, and C. B. Barger, "Current Image Diffraction Patterns of Metal Single Crystal Surfaces," *Phys. Rev. B* **27**, 708-714 (15 Jan 1983).
- <sup>4</sup> J. B. Pendry, *Low Energy Electron Diffraction*, Academic Press, New York (1974).
- <sup>5</sup> C. B. Barger, B. H. Nall, and A. N. Jette, "Oxygen Adsorption on the Aluminum (111) Surface by Low-Energy Current Image Diffraction: A New Approach," *Surf. Sci.* **120**, L483-L486 (1982).

This work was supported by Independent R&D.

# OPTICAL MONITORING OF ENERGY TRANSFER PROCESSES ACCOMPANYING PULSED LASER EXCITATION OF PHOTOSENSITIVE DYES IN CONDENSED MEDIA

J. G. Parker and W. D. Stanbro

*An electro-optical system of high sensitivity has been developed to monitor remotely the energy transfer processes accompanying pulsed laser excitation of photosensitive dyes in condensed media. This system, in combination with appropriate signal processing instrumentation, has provided a way to resolve the associated transient events both temporally and spectrally. Specifically, the system has been used to monitor simultaneously the deactivation rate of the dye triplet state by ambient dissolved molecular oxygen (which leads to the formation of singlet oxygen) as well as the subsequent quenching of the resultant singlet oxygen by the solvent. The unique identification of the singlet oxygen product is provided by recording its emission spectrum centered in a narrow range around 1.27  $\mu\text{m}$ .*

## BACKGROUND

Investigation of the nature and properties of singlet molecular oxygen formed in solution has become an extremely important area of photochemistry and photobiology,<sup>1</sup> encompassing a wide range of applications from bioluminescence to photochemotherapy. However, research in the past suffered from two main limitations: (a) an inability to correlate the transient behavior of the dye triplet state with that of the singlet oxygen product, and (b) the inadequacies of chemical indicators that are used to monitor singlet oxygen production, particularly problems with their solubility. The electro-optical techniques developed represent a substantially improved capability on both counts and are expected to be particularly useful in the investigation of photodamage in heterogeneous cellular systems. Remote optical monitoring has been used in two important cases, to be discussed in the following section; the first involves physical quenching only (i.e., no oxygen consumption), and the second is one in which oxygen is consumed.

## DISCUSSION

The experimental approach used in this research involves laser excitation of the dye from the ground singlet,  $S_0$ , to the first excited singlet,  $S_1$ , as indicated in Fig. 1. The dye triplet,  $T_1$ , is formed rapidly during the 10 ns duration of the laser pulse with subsequent gener-

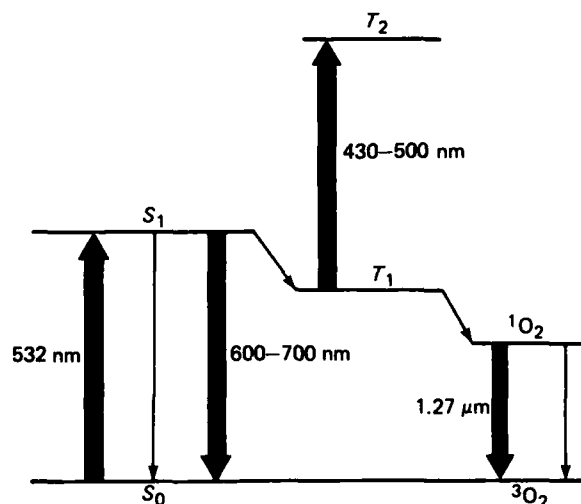
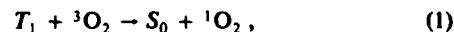
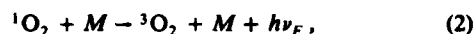


**Figure 1** — Laser excitation of singlet oxygen in solution. The dissolved dye molecule absorbs incident laser light at 532 nm and is elevated from ground singlet state,  $S_0$ , to excited singlet,  $S_1$ . Deactivation of  $S_1$  occurs mainly in two ways: (a) a direct return to  $S_0$  with emission of the energy difference in the form of visible light (fluorescence), and (b) an intramolecular process that converts  $S_1$  to the lowest triplet state,  $T_1$ . For photoactive dye molecules, route (b) is more probable than (a). Energy residing in  $T_1$  is then transferred to ground triplet state oxygen,  $^3O_2$ , in an intermolecular spin-conserving process whereby the oxygen is raised to the singlet molecular  $^1O_2$  state with the simultaneous transition  $T_1 \rightarrow S_0$ , mainly because solvent quenching of  $T_1$  is ineffective as a result of the absence of triplet ground states.

ation of singlet molecular oxygen,  $^1O_2$ , according to the intermolecular spin conserving interaction:



where  $^3O_2$  represents oxygen in its ground triplet electronic state. De-excitation of the  $^1O_2$  thus formed occurs mainly through collisional interaction with the solvent molecules. This interaction primarily involves conversion of the electronic energy of the  $^1O_2$  to vibrational energy of the solvent molecules. The vibrational energy is then rapidly converted to translational energy, i.e., heat. However, a few collisions of  $^1O_2$  with the solvent molecules,  $M$ , result in a radiative deactivation



where  $h\nu_E$  is the energy of the emitted photon. The frequency of the emitted radiation,  $\nu_E$ , corresponds to a wavelength of approximately  $1.27 \mu\text{m}$ , lying in the near infrared.

Detection of this infrared emission is accomplished by means of suitable optical filtering and lensing combined with the use of commercially available solid-state photodiodes. An overall schematic view of the experimental apparatus is shown in Fig. 2. Measurement of the transient dye triplet population,  $T_1$ , involves an active approach based on triplet-triplet absorption, i.e.,



where  $\nu_p$  is the probe-beam frequency corresponding to wavelength  $\lambda_p$ . This wavelength was selected to be in a region of the spectrum outside the region of strong singlet absorption in order to minimize effects associated with depletion of the dye ground state. Experimental details are shown on the left side of Fig. 2.

The first important application of this experimental system was to resolve an important controversy regarding the lifetime of  $^1\text{O}_2$  in protiated acetone as opposed to that for the deuterated species. Existing experimental data<sup>2</sup> indicated that the decay times in both solvents were the same, in contrast to the

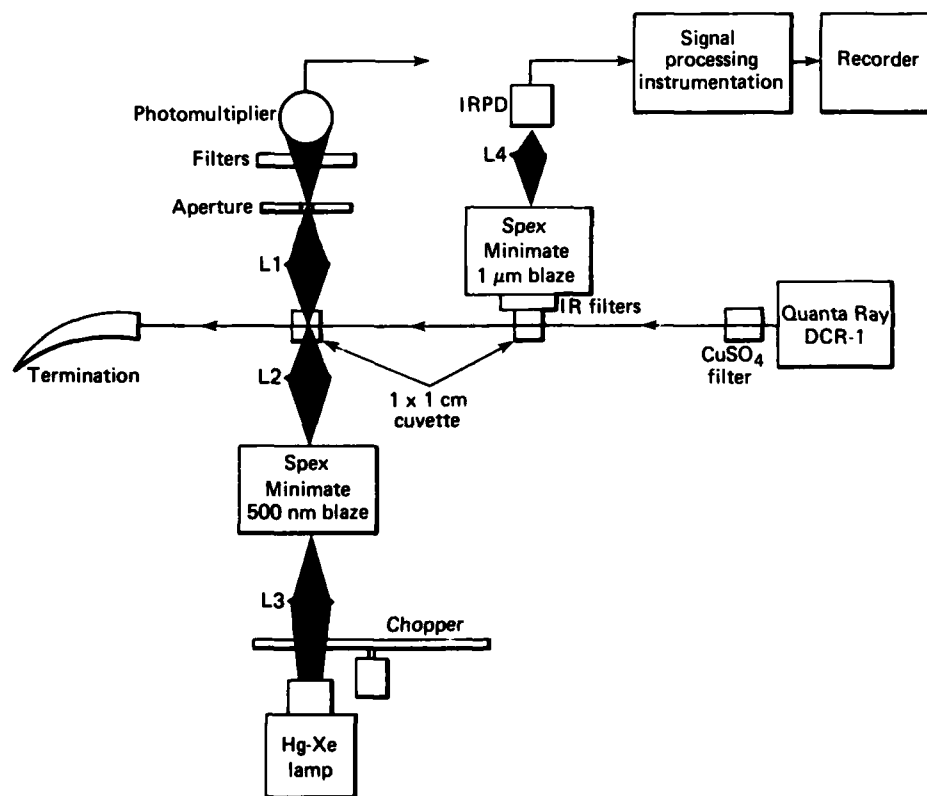


**Figure 2** — Two-channel optical system used to monitor singlet oxygen emission and dye triplet state concentration. Weak infrared radiation at  $1.27 \mu\text{m}$  emitted by the sample in the cuvette on the right side enters the spectrometer through infrared bandpass filters to eliminate scattered laser light. The signal emerging from the spectrometer is focused on the infrared photodiode (IRPD), and the resultant electrical signal is fed to signal processing instrumentation. The dye triplet state is monitored by the arrangement on the left side. The output of a high pressure Hg-Xe lamp is passed through a monochromator to yield the desired wavelength. The emerging beam is focused onto the sample in the left cuvette and finally through an aperture and suitable optical filters into a photomultiplier tube. The wavelength of the analyzing beam is selected so that negligible absorption resulting from the dye singlet takes place whereas absorption in the triplet state is large. The transient photomultiplier output corresponds to a decrease in transmitted light resulting from excitation of the absorbing triplet state.

usual experience in which the effect of deuteration is to decrease substantially the rate of solvent quenching. However, the singular behavior of acetone in this regard was predicted on the basis of a widely accepted theory<sup>3</sup>; as a matter of fact, agreement in this particular case was taken to provide key support for this theory. An important limitation was that the data had been obtained through the use of chemical indicators that were known in other instances to cause difficulties in data analysis and interpretation. Highlighting this difficulty, recent experimental data<sup>4</sup> in which the relative quenching rates were measured using an improved technique that required less indicator concentration suggested that the quenching rate in deuterated acetone was substantially smaller.

The controversy was resolved by measurements carried out using the optical monitoring system described above,<sup>5</sup> which permitted absolute quenching rates to be determined. Analysis of the resulting data yielded a time constant of 65  $\mu$ s for acetone and 840  $\mu$ s for the deuterated sample. In addition, the spectral variation of the emission was determined (Fig. 3), clearly establishing the emitting source as  $^1\text{O}_2$ . This result has been confirmed independently by other investigators<sup>6,7</sup> using similar techniques.

In the case of acetone, deactivation processes involving  $^1\text{O}_2$  were entirely physical; i.e., the ultimate fate of the electronic energy was conversion to heat. However, in certain cases the energy characterizing the formation of  $^1\text{O}_2$  (i.e., 1 eV) is sufficient to bring about chemical reaction in cases where the ground electronic

state,  $^3\text{O}_2$ , is essentially inert. The disappearance of free oxygen thus would tend to reduce  $^1\text{O}_2$  emission significantly, rendering this mode of monitoring ineffective. On the other hand, a reduction in ambient oxygen concentration tends to increase the triplet lifetime because solvent quenching is relatively ineffective.

An example of this behavior was encountered in a series of measurements of the triplet decay time of free base hematoporphyrin in a cell growth medium containing 10% fetal calf serum.<sup>8</sup> A medium of this type can be loosely considered to represent a "typical" physiological environment. The measurements exhibited a steady increase in the triplet decay time with increasing exposure to the incident laser radiation, from an initial value of several microseconds (characteristic of an aqueous environment) to times ultimately approaching 1 ms. Interpretation of these results leads to the conclusion that, in the proximity of the dye molecules, after  $^3\text{O}_2$  is excited to the  $^1\text{O}_2$  state, it is consumed through chemical reaction at a rate faster than it can be resupplied through diffusion, ultimately leading to anaerobic conditions and thus increased triplet lifetimes.

This conclusion suggests that oxygen depletion may be an important factor in photosensitization processes in biological systems, particularly in regard to dosimetry.

## REFERENCES

1. F. Wilkinson and J. G. Brummer, "Rate Constants for the Decay and Reactions of the Lowest Electronically Excited Singlet State of Molecular Oxygen in Solution," *J. Phys. Chem. Ref. Data* **10**(4), 809-999 (1981).
2. D. R. Kearns, *Singlet Oxygen*, Vol. 40 of Organic Chemistry Series, H. H. Wassermann and R. W. Murray, eds., Academic Press, New York, pp. 115-137 (1979).
3. P. B. Merkel and D. R. Kearns, "Radiationless Decay of Singlet Molecular Oxygen in Solution. An Experiment to Theoretical Study of Electronic-to-Vibrational Energy Transfer," *J. Am. Chem. Soc.* **94**, 7244-7253 (1972).
4. P. R. Ogilby and C. S. Foote, "Chemistry of Singlet Oxygen. 34. Unexpected Deuterium Isotope Effects on the Lifetime of Singlet Molecular Oxygen ( $^1\Delta_g$ )," *J. Am. Chem. Soc.* **103**, 1219-1221 (1981).
5. J. G. Parker and W. D. Stanbro, "Optical Determination of the Collisional Lifetime of Singlet Molecular Oxygen [ $\text{O}_2(^1\Delta_g)$ ] in Acetone and Deuterated Acetone," *J. Am. Chem. Soc.* **104**, 2067-2069 (1982).
6. J. R. Hurst, J. D. McDonald, and G. B. Schuster, "Lifetime of Singlet Oxygen in Solution Directly Determined by Laser Spectroscopy," *J. Am. Chem. Soc.* **104**, 2065-2067 (1982).
7. P. R. Ogilby and C. S. Foote, "Chemistry of Singlet Oxygen. 36. Singlet Molecular Oxygen ( $^1\Delta_g$ ) Luminescence in Solution Following Pulsed Laser Excitation," *J. Am. Chem. Soc.* **104**, 2069-2071 (1982).
8. J. G. Parker and W. D. Stanbro, "Energy Transfer Processes Accompanying Laser Excitation of Hematoporphyrin in Various Solvents," *Johns Hopkins APL Tech. Dig.* **2**, 196-199 (1981).

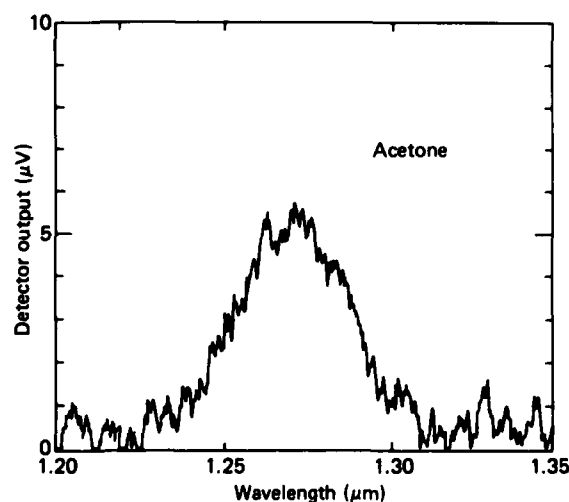


Figure 3 — The spectral variation of singlet oxygen emission for a sample containing free-base hematoporphyrin in acetone. A germanium photodiode was used in conjunction with an amplifier coupled to a boxcar integrator. The output was documented by means of a strip-chart recorder.

This work was supported by Indirectly Funded R&D.

# THE STRUCTURE OF AMORPHOUS IRON-BORON ALLOYS FROM THE ANALYSIS OF MAGNETIC HYPERFINE FIELDS

N.A. Blum and K. Moorjani

*Amorphous metallic alloys are of considerable current interest because of their useful, and in many cases unique, combination of mechanical, electrical, and magnetic qualities. Mössbauer spectroscopy together with other experimental and theoretical methods were used to analyze the microscopic structure and magnetic properties of several prototypical binary alloys containing iron and boron. This information is important for predicting the behavior and suggesting the composition of new amorphous alloys that possess useful technological characteristics.*

## BACKGROUND

Research on amorphous metallic alloys has shown that this new class of material is endowed with unusual and potentially useful metallurgical, mechanical, and magnetic properties, ranging from substitutes for scarce and strategic materials to novel applications in electromagnetic machinery and electronic devices. The key to fabricating these materials lies in their rapid solidification, either from the melt at a cooling rate greater than about  $10^5$  deg/s or from the vapor phase, where solidification is virtually instantaneous. The possibility of tailoring the structure and composition, and hence the behavior, of these amorphous alloys offers an enormous advantage over stoichiometric crystalline solids. The details of such tailoring depend crucially on a number of fundamental concepts, such as the nature of bonding and the degree of local atomic order; these, in turn, affect the electronic band structure and therefore the physical properties.

The work described here deals with understanding disorder-induced changes in the structural and magnetic characteristics of amorphous alloys. Theoretical modeling has included the evolution and behavior of ferromagnetism in disordered binary alloys and the changes in the magnetic ground state when competing exchange interactions are present.<sup>1</sup> The alloys studied experimentally were binary iron-boron films prepared by argon-ion sputtering from mixtures of the elements or from mixtures of the elements with the simple stoichiometric compounds FeB and Fe<sub>2</sub>B. The alloys, in the form of thin (1 to 5  $\mu$ m thick) films, were examined by x-ray diffraction, secondary-ion mass spectrometry (SIMS), magnetic resonance, and Mössbauer spectroscopy. While all the experimental techniques are important and complement one another in elucidating

an understanding of the physical behavior of the alloys, we will deal primarily with the results of the Mössbauer spectroscopy work that explains their atomic structure.

## DISCUSSION

Since the chemical orderings in crystalline FeB, Fe<sub>2</sub>B, and Fe<sub>3</sub>B differ from one another, as do their Mössbauer spectra, we chose initially to investigate the effects of disorder in amorphous Fe<sub>x</sub>B<sub>100-x</sub> around the concentration ranges of the stoichiometric compounds. Earlier studies of the melt-quenched alloys in the concentration range of  $x$  between 72 and 86 showed that the chemical short-range order for  $x \approx 75$  is similar to that in crystalline Fe<sub>3</sub>B. Details of sample preparation, characterization, and Mössbauer techniques are presented in Refs. 2 and 3.

Samples prepared by sputtering Fe<sub>2</sub>B were shown by SIMS to be homogeneous to better than 0.5% and to have a composition very close to that of Fe<sub>71</sub>B<sub>29</sub>. A comparison of the room-temperature Mössbauer spectrum of one sample and the spectrum of Fe<sub>2</sub>B powder is shown in Figs. 1a and 1b. Qualitatively, the spectra are similar except for three prominent features that characterize the Mössbauer spectra of nearly all the ferromagnetic amorphous films: (a) the six spectral lines are greatly broadened in the amorphous alloy, (b) the intensities of the second and fifth lines of the amorphous film are quite different from those of the crystalline powder, and (c) the amorphous film spectrum is noticeably asymmetric. The broadened lines reflect a distribution of hyperfine fields, and the line intensity ratios indicate that the iron magnetic moments in the amorphous alloy lie close to the plane of the substrate. In the (randomly oriented) powder, the line intensities are close to the theoretical ratio (3:2:1). One can fit the spectrum according to a model in which the magnetic hyperfine field is described by a distribution  $P(H)$ , as distinct from a fixed value of  $H$  for the stoichiometric compounds. Figure 1c shows the hyperfine magnetic field distribution for the amorphous alloy, a-Fe<sub>71</sub>B<sub>29</sub>; the vertical lines index the (discrete) values of the hyperfine field for ferromagnetic iron and for the three compounds of Fe and B.

The room temperature Mössbauer spectra of a-Fe<sub>71</sub>B<sub>29</sub> are not greatly different from those of its crystalline near-counterpart, Fe<sub>2</sub>B, and are similar to those for melt-quenched Fe<sub>71</sub>B<sub>29</sub>. The hyperfine field

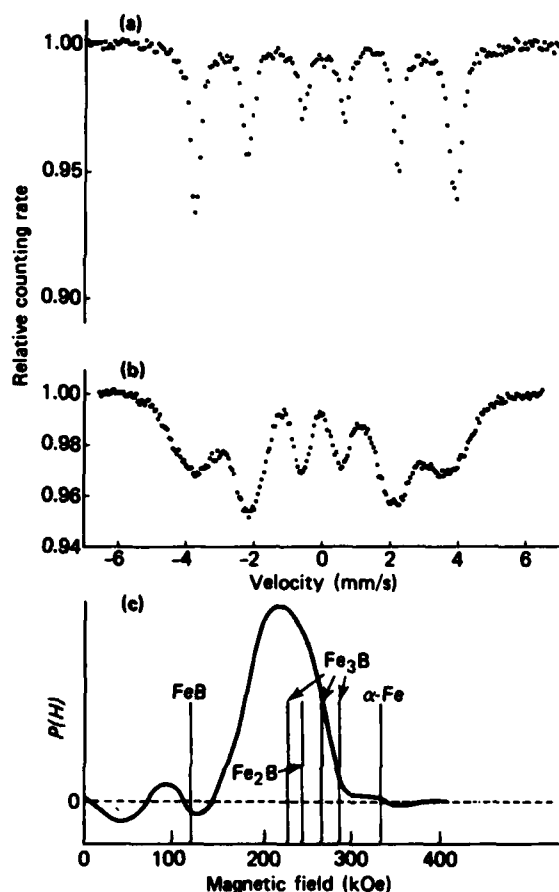


Figure 1 — Comparison of spectra of (a)  $\text{Fe}_2\text{B}$  polycrystalline powder and (b)  $\text{a-Fe}_{71}\text{B}_{29}$  sputtered film, both at room temperature. (c)  $P(H)$ , hyperfine magnetic field distribution of spectrum (b).  $1 \text{ mm/s} = 4.8 \times 10^{-8} \text{ eV}$ .

distribution, which depends on the configurations of neighboring magnetic atoms, is centered at a value near the  $\text{Fe}_2\text{B}$  hyperfine field and is rather symmetrically distributed about that value. This observation is in contrast to results with  $\text{a-FeB}$  (see below) and points toward the existence of a similar chemical short-range order in both crystalline and amorphous samples with a composition in the vicinity of  $\text{Fe}_2\text{B}$ .

Samples in a range around  $\text{Fe}_{50}\text{B}_{50}$  were prepared by sputtering  $\text{FeB}$  and  $\text{FeB}$  plus  $\text{B}$ . Uniform films were produced with compositions between  $\text{Fe}_{40}\text{B}_{60}$  and  $\text{Fe}_{53}\text{B}_{47}$ , as measured by SIMS. Figures 2a and 2b compare the room-temperature spectrum of  $\text{Fe}_{53}\text{B}_{47}$  with the spectrum of crystalline powder  $\text{FeB}$ . Unlike  $\text{Fe}_2\text{B}$ , where the amorphous sample spectrum is a broadened version of its crystalline counterpart,  $\text{a-Fe}_{53}\text{B}_{47}$  is quite different from crystalline  $\text{FeB}$ . In this case, the  $P(H)$  distribution is characterized by two

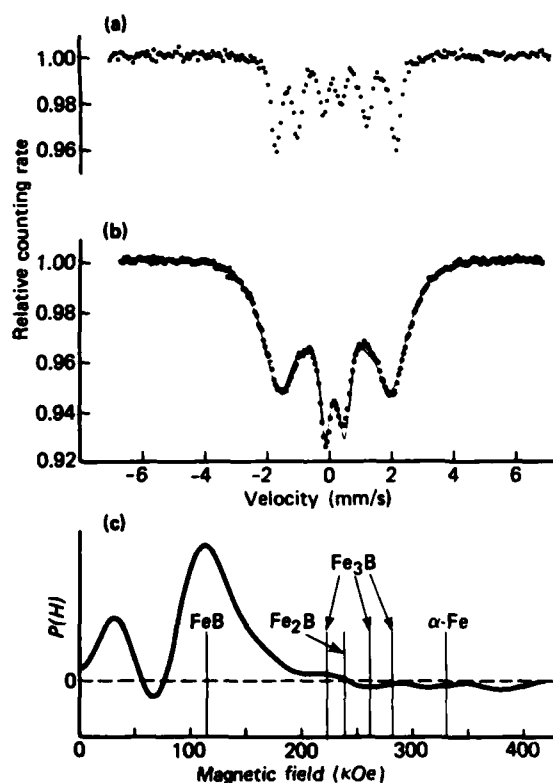


Figure 2 — Comparison of spectra of (a)  $\text{FeB}$  polycrystalline powder and (b)  $\text{a-Fe}_{53}\text{B}_{47}$  sputtered film, both at room temperature. (c)  $P(H)$ , hyperfine magnetic field distribution of spectrum (b).  $1 \text{ mm/s} = 4.8 \times 10^{-8} \text{ eV}$ .

peaks: one at around 40 kOe and another near 120 kOe (Fig. 2c). The lower field peak can be shown to represent  $\text{Fe}$  atoms in a nonmagnetic environment, while the higher field peak corresponds to  $\text{Fe}$  atoms in a ferromagnetic state.

The  $\text{Fe}$  atoms in crystalline  $\text{FeB}$  experience a unique environment with a saturation (i.e., low temperature) magnetic hyperfine field of 131 kOe; in order to explain the observed distribution of magnetic hyperfine fields in the amorphous  $\text{Fe}_{53}\text{B}_{47}$  alloy, one must conclude that a large number of  $\text{Fe}$  atom environments are significantly different from those in crystalline  $\text{FeB}$ . This result is in contrast to the interpretation of experiments on  $\text{a-Fe}_{71}\text{B}_{29}$  or on liquid-quenched alloys with compositions in the vicinity of  $\text{Fe}_{75}\text{B}_{25}$ , where the local chemical order is believed to be similar to  $\text{Fe}_2\text{B}$  or  $\text{Fe}_3\text{B}$ . Experiments were also performed at temperatures other than room temperature (from 10 to 600 K) and in external magnetic fields up to 80 kOe in order to elucidate the nature of the non-magnetic  $\text{Fe}$  sites.<sup>4</sup>

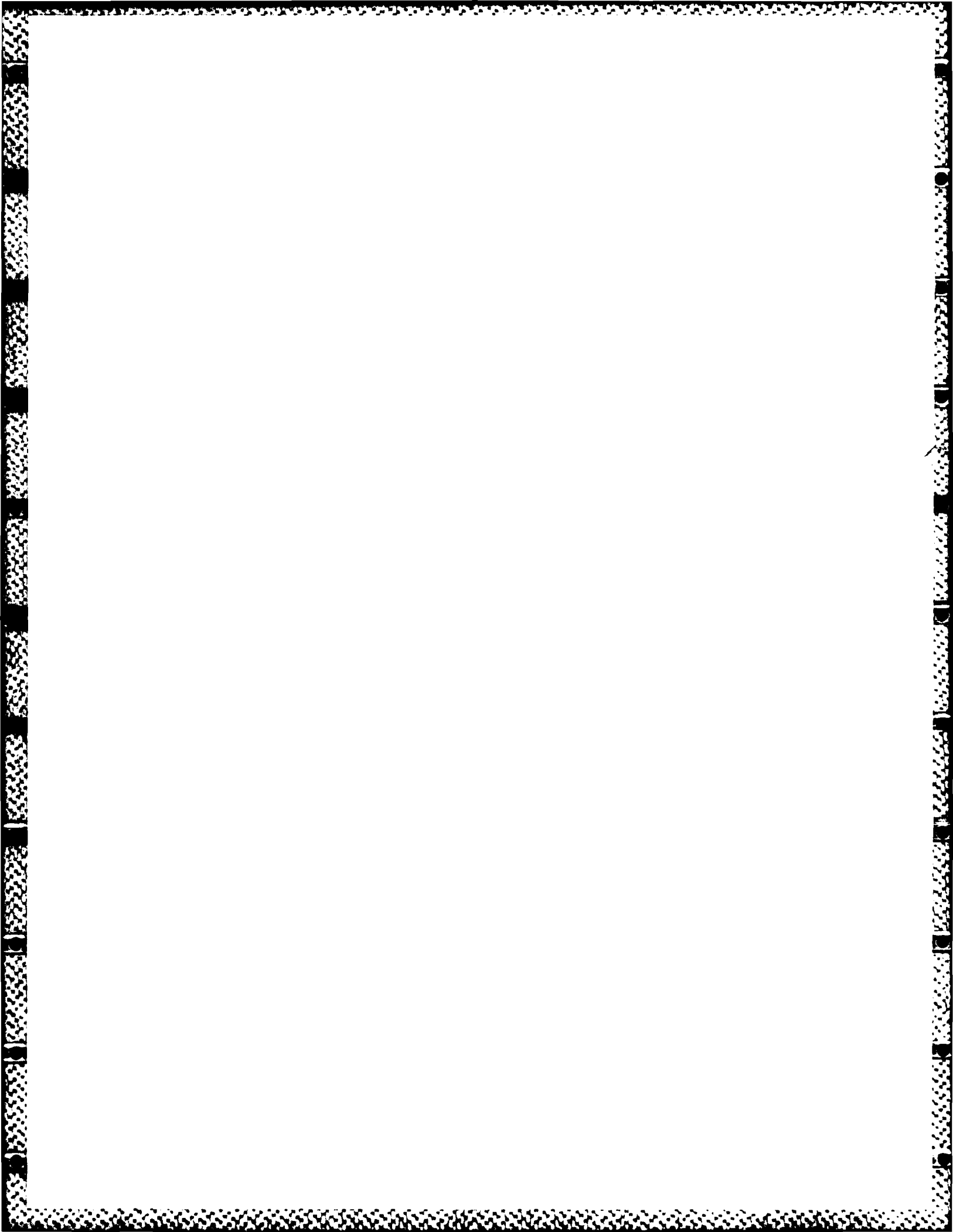
In addition to yielding relevant magnetic parameters for the alloys, Mössbauer studies have thrown light on their structure. Although the chemical short-range order in metallic glasses has been demonstrated to be similar to that in corresponding crystalline alloys, our results indicate this to be true only for iron concentrations greater than about 70 atomic percent. For alloys near 50% Fe, the chemical short-range order is significantly different from that in crystalline FeB for about 30% of the Fe sites. Such alloys also possess a magnetic ground state that is different from the ferromagnetic state of crystalline FeB.<sup>4</sup> An understanding of the modifications of chemical and magnetic short-range order would be extremely valuable for tailoring the various useful properties of these materials.

## REFERENCES

- <sup>1</sup>K. Moorjani, S. K. Ghatak, K. V. Rao, B. Kramer, and H. S. Chen, "Spin Glass — Paramagnetic Phase Boundary in Amorphous Magnetic Alloys," *J. Phys. Paris Colloquia C8*, 718 (1980).
- <sup>2</sup>N. A. Blum, K. Moorjani, T. O. Poehler, and F. G. Satkiewicz, "Hyperfine Field Distributions in Ferromagnetic Amorphous Fe<sub>x</sub>B<sub>1-x</sub> Thin Films," *J. Appl. Phys.* **52**, 1808 (1981).
- <sup>3</sup>N. A. Blum, K. Moorjani, T. O. Poehler, and F. G. Satkiewicz, "Mössbauer Investigation of Sputtered Ferromagnetic Amorphous Fe<sub>x</sub>B<sub>100-x</sub> Films," *J. Appl. Phys.* **53**, 2074 (1982).
- <sup>4</sup>N. A. Blum, "Mössbauer Study of Magnetism in an Amorphous Fe<sub>40</sub>B<sub>60</sub> Sputtered Film," *J. Appl. Phys.* **53**, 7747 (1982).

---

This work was supported by the U.S. Army Research Office and Independent R&D.



## PATENTS

## PATENTS ACTIVITIES

The APL Patents Office is responsible for ensuring compliance with contract and grant requirements relative to patent and data rights, as imposed by the various governmental agencies that sponsor work at the Laboratory. In addition to preparing formal disclosures of inventions for the appropriate sponsors, the Patents Office prepares and prosecutes patent applications on behalf of both the University and the Department of the Navy.

The following lists indicate the invention disclosures submitted to sponsors, the patent applications prepared and filed in the United States Patent Office, and the previously filed applications that were successfully prosecuted to issuance as patents, during fiscal year 1982.

## INVENTION DISCLOSURES

- W. E. Allen—*Liquid Crystal Solar Cell Panel Output Current Control*
- C. B. Barger, B. H. Nall, and A. N. Jette—*Method for Detecting Adsorption on a Metal Surface by Low-Energy Current Image Diffraction*
- F. R. Castella—*Automatic False Track Classification in ADT and IADT Radar Systems*
- J. G. Chubbuck and M. Epstein—*X-Ray Readable Implantable Pressure Sensor*
- S. A. Cohen—*Hybrid Frequency Hopping-Direct Sequence Low Probability Of Intercept Radar*
- C. Feldman and F. G. Satkiewicz—*Antimony Doping in Vacuum Deposited Thin Film Silicon Photovoltaic Cells*
- S. N. Foner and R. L. Hudson—*Internal Energy Transfer in Molecule-Surface Collisions*
- J. A. Frantz and R. T. Cusick—*Photic Arc-Fault Sensor*
- A. B. Fraser—*Vertical Water Sampling Array*
- J. G. Frink—*Extensible Computer Network System*
- W. H. Guier, W. Schneider, and R. S. Carlson—*Computer Controlled Closed Loop Block Pressure Control System*
- J. E. Hanson and J. W. Gilbert—*Radome Induced Coupling Avoidance for Missile Guidance*
- B. F. Hochheimer—*Fundus Camera Adapter*
- D. A. Hurd, T. D. Taylor, A. J. Klaunberg, and F. Jurgens—*Use of Vinyl-Coated Polyurethane Foam Surface to Reduce Hydrodynamic Drag*
- E. P. Irzinski—*A Coaxial Waveguide Commutator Feed for a Scanning Circular Phased Array Antenna*
- C. A. Keller—*Non-Contact Means for Detecting Water Surface Structure*
- C. A. Keller—*Wiperless Optical High Speed Signal Transmitter*
- D. A. Kitchin—*Synchronous Clock Stopper for Microprocessor Operated in a Power-Limited Environment*
- H. B. Land and R. T. Cusick—*Pressure Arc Fault Sensor*
- S. C. Ling—*A Non-Fouling Fast-Response Conductivity Probe*

- D. L. Mitchell and R. E. Bateman—*Test Set for SRN-19 Navigation Receiver*
- R. C. Moore and R. E. Hicks—*Low Power to IC Event Counter*
- J. C. Murphy and L. C. Aamodt—*Photo Thermal Imaging*
- J. G. Parker and W. D. Stanbro—*Electro-Optical Device for in vivo Monitoring of Instantaneous Singlet Oxygen Concentration Produced During the Treatment of Cancer by Means of Photochemotherapy*
- T. O. Poehler—*Carbon Dioxide Sensing for Life Support Systems*
- F. J. Porter—*A Solar Array Powered Power System Using Solar Array Shadowing to Limit Battery Overcharge*
- D. W. Rabenhorst—*Hub Lamina for Spin Test Apparatus*
- B. A. Raff—*Oceanographic Data Acquisition and Analysis Recorder*
- M. E. Schmid, R. L. Trapp, and A. E. Davidoff—*Pseudo-Random Sequence for Bus Arbitration*
- W. Schneider—*Method of Rate Extraction from a Pulse-Width Modulation Driven Permanent Magnet Motor*
- D. M. Silver and N. DeHaas—*Internal Suspension for Cryogenic Tanks*
- M. M. Soukup—*Multiple Target Doppler Simulator*
- R. W. Spangler and W. I. Sternberger—*Constant Operating Temperature Thermistor Anemometer I*
- W. I. Sternberger and R. W. Spangler—*Constant Overheat Temperature Thermistor Anemometer II*
- R. R. Talbott—*Microprocessor Probe*
- R. L. Trapp—*Improved Coherent-on-Receive Radar Processing with Dynamic Transversal Filters*
- W. E. Tye, Sr.—*Inductor Fabrication Using Nylon Threaded Material as a Form*
- R. Von Briesen and C. S. Leffel—*Cryogenic Condensable Material Transfer Device*
- T. M. Walter and R. S. Strider—*Fabrication Technique for Dichroic Antenna Elements*
- J. J. Wozniak—*Sutureless Vascular Anastomosis System*

## PATENT APPLICATIONS

- W. H. Avery—*Methanol Production by OTEC*
- W. H. Avery—*Open Cycle OTEC Plant*
- R. E. Fischell, G. H. Fountain and C. M. Blackburn—*Self-Injurious Behavior Inhibiting System (SIBIS)*
- R. E. Fischell—*Intracorporeal and/or Extracorporeal Biomedical Device Systems Having Two or More Modules*
- R. E. Fischell—*Manually Actuated Hydraulic Sphincter*
- R. E. Fischell—*Refillable Medication Infusion Apparatus*
- R. W. Flower—*A Method and Apparatus for the Continuous Monitoring of Hemoglobin Saturation in the Blood of Premature Infants*
- S. E. Grenleski, J. L. Keirsey, L. A. Dale, and C. E. Stevens—*Multi-Port Dump Combustor*
- J. C. Murphy and L. C. Aamodt—*Optical Beam Deflection Thermal Imaging*
- J. G. Parker and W. D. Stanbro—*Electro-Optical Device for Monitoring Instantaneous Singlet Oxygen Concentration Produced During the Treatment of Cancer by Means of Photochemotherapy*
- R. S. Potember, T. O. Poehler, and D. O. Cowan—*Method of Fabricating a Current Controlled Bistable Electrical Organic Thin Film Switching Device*

R. J. Prengaman, R. E. Thurber, J. Phipps, R. I. Greenberg, W. L. Horn, J. F. Jaworski, and G. W. Riffle—*Retrospective Data Filter*

T. R. Small—*Vibration Dissipation Mount for Motors or the Like*

G. M. Starken, R. R. Talbott, J. R. Doza, G. A. Smoot, and A. C. Prewitt—*Method and Apparatus for Enhancing Recorded Acoustic Signals*

D. J. Thomas and J. J. Poetker—*Aimpoint Processor for Quantizing Target Data*

W. O. Wilkinson and D. W. Rabenhorst—*High Speed Imaging Television System*

J. J. Wozniak—*Sutureless Vascular Anastomosis Means and Method*

## PATENTS ISSUED

R. E. Fischell—*Recorder with Patient Alarm and Service Request Systems Suitable for Use with Automatic Implantable Defibrillator*, No. 3, 295,474

C. Philippides—*Clock Invariant Synchronization for Random Binary Sequences*, No. 4,293,949

R. H. Lapp—*Pivotal Support with Independent Adjusting Elements and Locking Means*, No. 4,298,949

C. Feldman, H. K. Charles, and F. G. Satkiewicz—*Thin-Film Silicon Solar Cell with Metal Boride Bottom Electrode*, No. 4,313,254

A. Kossiakoff—*Graphical Automatic Programming*, No. 4,315,315

C. A. Keller—*Linear Response Capacitance Wave Height Measuring System*, No. 4,319,484

R. W. Blevins, J. L. Keirse, and W. B. Shippen—*Thrust Augmented Rocket*, No. 4,327,885

A. J. Bell, A. S. Polk, L. Cronvich, and E. J. Hardgrave—*Integral Rocket Ramjet Missile*, No. 4,327,886

A. J. Pue—*Optimal Vehicle Following Control System*, No. 4,335,432

R. H. Bauer and M. Heidkamp—*Method for Correcting Navigation Errors Due to Water Currents*, No. 4,335,433

J. F. Kincaid—*Bonding Agent for HMX (Cyclotetramethylene-tetranitramine)*, No. 4,350,542

## **PUBLICATIONS AND PRESENTATIONS**

## PUBLICATIONS

- L. C. Aamodt and J. C. Murphy, "Effect of 3-D Heat Flow near Edges in Photothermal Measurements," *Appl. Opt.* **21**, 111-115 (1982).
- F. J. Adrian, "Interstack Spin-Orbit Coupling and ESR Line Broadening in Tetrathiafulvalenium Tetracyanoquinodimethanide (TTF-TCNQ)," *Phys. Rev. B* **26**, 2682-2685 (1982).
- S. I. Akasofu and D. N. Covey (Univ. Alaska) and C.-I. Meng (APL), "Dependence of the Geometry of the Region of Open Field Lines on the Interplanetary Magnetic Field," *Planet. Space Sci.* **29**, 803-807 (1981).
- J. R. Apel, "Spaceborne Synthetic Aperture Radar for Oceanography: A Book Review," *Johns Hopkins APL Tech. Dig.* **2**, 330 (1981).
- W. H. Avery, "The Talos Booster Rockets," *Johns Hopkins APL Tech. Dig.* **3**, 135-137 (1982).
- C. B. Barger and R. B. Givens, "A Signature in the Current during Early Events in the Pitting Corrosion of Aluminum," *J. Electrochem. Soc.* **129**, 340-341 (1982).
- C. B. Barger and B. H. Nall, "An Electron Energy Loss Study of Aluminum Single Crystals Exposed to Carbon Monoxide," *Surf. Sci.* **119**, L319-L325 (1982).
- C. B. Barger, B. H. Nall, and A. N. Jette, "Oxygen Adsorption on the Aluminum (111) Surface by Low-Energy Current Image Diffraction: A New Approach," *Surf. Sci.* **120**, L483-L486 (1982).
- W. G. Bath, "Terrier/Tartar: Integration and Automation of Navy Shipboard Surveillance Sensors," *Johns Hopkins APL Tech. Dig.* **2**, 261-267 (1981).
- W. G. Bath (APL) and V. D. Vandelinde (JHU), "Robust Memoryless Quantization for Minimum Signal Distortion," *IEEE Trans. Inf. Theory* **IT-28**, 296-306 (1982).
- C. W. Bauschlicher, Jr. (NASA), D. M. Silver (APL), and D. R. Yarkony (JHU), "Multiconfiguration Self-Consistent-Field Wavefunction for Excited States," in *Proc. The Unitary Group Workshop 1979*, Springer-Verlag, New York, pp. 136-142 (1981).
- W. G. Berl, "Annotated Bumblebee Initial Report," *Johns Hopkins APL Tech. Dig.* **3**, 176-179 (1982).
- T. R. Bertzer, "Terrier/Tartar: New Threat Upgrade Program," *Johns Hopkins APL Tech. Dig.* **2**, 276-282 (1981).
- F. S. Billig, R. E. Lee, and P. J. Waltrup, "Instrumentation for Supersonic Combustion Research," in *Proc. 1981 JANNAF Propulsion Meeting*, JHU/APL CPIA Pub. 340 II, pp. 67-100 (1981).
- J. F. Bird, "Kinetic Torque and Dynamic Behavior in a Magnetic Levitation Device," *J. Appl. Phys.* **53**, 1326-1333 (1982).
- B. I. Blum, "A Methodology for Information System Production," in *Proc. 26th Annual Meeting, Society for General Systems Research on Systems Methodology* (5-9 Jan 1982).
- B. I. Blum, "An Approach to Computer Maintained Software Documentation," in *Proc. NBS/FIPS Software Documentation Workshop* (3 Mar 1982).
- B. I. Blum "A Tool for Developing Information Systems," in *Automated Tools for Information System Design and Development*, H. H. Schneider and A. I. Wasserman, eds., North Holland Pub. Co. (1982).
- B. I. Blum, "Generating MUMPS Programs with TEDIUM," *MUMPS Users Group Q.* **XI**, p. 1 (1981).
- B. I. Blum, "Hospital Information Systems: User Perspectives and Orientation," in *Proc. 5th Annual Symp. on Computer Applications in Medical Care*, p. 790 (1981).
- B. I. Blum, "MUMPS, TEDIUM and Productivity," in *Proc. MEDCOMP '82—First IEEE Computer Society International Conf. on Medical Computer Science/ Computational Medicine*, pp. 200-209 (Sep 1982).
- B. I. Blum, "Review of the Established Benefits of Automated Information Systems in Patient Care," in *Applications of Computers in Medicine*, IEEE TH0095-0, pp. 1-7 (Mar 1982).
- N. A. Blum, K. Moorjani, T. O. Poehler, and F. G. Satkiewicz, "Mossbauer Investigation of Sputtered Ferromagnetic Amorphous Fe<sub>B<sub>100-x</sub></sub> Films," *J. Appl. Phys.* **53**, 2074-2076 (1982).
- J. Bohandy and B. F. Kim, "Fluorescence of Mg Porphin in Anthracene," *J. Chem. Phys.* **76**, 1180-1181 (1982).
- H. Bouver (APL) and R. E. Bargmann (Univ. Georgia), "Evaluation and Graphical Application of Probability Contours for the Bivariate Normal Distribution," in *Proc. Statistical Computing Section, American Statistical Association*, pp. 272-277 (1981).
- C. A. Boyles and G. W. Joice, "Comparison of Three Acoustic Transmission Loss Models with Experimental Data," *Johns Hopkins APL Tech. Dig.* **3**, 67-76 (1982).
- A. Brandt and D. A. Hurdin, "Simulation of Oceanographic Processes in the Hydrodynamics Research Laboratory," *Johns Hopkins APL Tech. Dig.* **3**, 43-48 (1982).
- C. R. Brown and C. F. Meyer, "The Talos Continuous-Rod Warhead," *Johns Hopkins APL Tech. Dig.* **3**, 157-159 (1982).
- P. F. Bythrow and T. A. Potemera (APL) and R. A. Hoffman (NASA/Goddard), "Observations of Field-Aligned Currents, Particles, and Plasma Drift in the Polar Cusps Near Solstice," *J. Geophys. Res.* **87**, 5131-5139 (1982).
- J. F. Carbary, P. F. Bythrow, and D. G. Mitchell, "The Spokes in Saturn's Rings: A New Approach," *Geophys. Res. Lett.* **9**, 420-422 (1982).
- J. F. Carbary and S. M. Krimigis, "Charged Particle Periodicity in the Saturnian Magnetosphere," *Geophys. Res. Lett.* **9**, 1073-1076 (1982).
- J. R. Champion, F. F. Mobley, and A. C. Sadilek, "A Low Susceptibility Proof Mass for the Nova Satellite," *IEEE Trans. Magn.* **MAG-17**, 3382-3384 (1981).
- H. K. Charles, Jr., B. M. Romenesko, G. D. Wagner, R. C. Benson, and O. M. Uy, "Influence of Contamination on Aluminum-Gold Intermetallics," in *Proc. 1982 Reliability Physics Symp.* **126**, pp. 128-139 (1982).
- L. J. Crawford, D. P. Vasholz, J. W. Giles, Jr., and C. J. Gundersdorf, "Evolution of a Vertically Distributed Passive Scalar in the Seasonal Thermocline," *Johns Hopkins APL Tech. Dig.* **3**, 36-41 (1982).
- L. L. Cronvich, "Talos Aerodynamics," *Johns Hopkins APL Tech. Dig.* **3**, 138-141 (1982).
- E. P. Cunningham, "Estimating the Probability of Crashing for a Terrain-Following Missile," *J. Guid. Control* **5**, 86-91 (1982).
- F. A. Dean, "The Talos Missile," *Johns Hopkins APL Tech. Dig.* **3**, 123-125 (1982).
- R. B. Decker (APL), M. E. Pesses (Univ. Maryland), and T. P. Armstrong (Univ. Kansas), "On the Acceleration of Thermal Coronal Ions by Flare Induced Shock Waves," in *Proc. 17th International Conf. on Cosmic Rays* (1981).
- B. D. Dobbins and G. W. Luke, "From Kamikaze to Aegis: An Introduction," *Johns Hopkins APL Tech. Dig.* **2**, 233-236 (1981).
- H. W. Dodson, E. R. Hedeman, and E. C. Roelof, "Large Scale Solar Magnetic Fields at the Site of Flares, the Great-

- ness of Flares, and Solar-Terrestrial Disturbances," *Geophys. Res. Lett.* **9**, 199-202 (1982).
- L. W. Ehrlich, "An Ad-Hoc SOR Method," in *Elliptic Problem Solvers*, M. H. Schultz, ed., Academic Press, New York; also published in *J. Comput. Phys.* **44**, 31-45 (1981).
- D. H. Fairfield (NASA/Goddard), E. W. Hones, Jr. (Univ. California), and C.-I. Meng (APL), "Multiple Crossings of a Very Thin Plasma Sheet in the Earth's Magnetotail," *J. Geophys. Res.* **86**, 11189-11200 (1981).
- R. S. Farris and R. J. Hunt, "Battle Group Operations: Air Defense Analysis," *Johns Hopkins APL Tech. Dig.* **2**, 302-307 (1981).
- M. R. Feinstein and R. A. Farrell, "Trial Functions in Variational Approximations to Long-Wavelength Scattering," *J. Opt. Soc. Am.* **72**, 223-231 (1982).
- C. Feldman, "Seventh International Symposium on Boron, Borides, and Related Compounds: A Trip Report," *Johns Hopkins APL Tech. Dig.* **2**, 222-223 (1981).
- C. Feldman, F. G. Satkiewicz, and N. A. Blum, "Vacuum Deposited Polycrystalline Silicon Solar Cells on Foreign Substrates," *Thin Solid Films* **90**, 461-471 (1982).
- C. Feldman, F. G. Satkiewicz, and G. Jones, "Preparation and Electrical Properties of Stoichiometric  $TiB_2$  Thin Films," *J. Less-Common Met.* **79**, 221-225 (1981).
- R. E. Fischell, W. E. Radford, and J. R. Champion, "A Computerized Implantable Medication System," in *Proc. 14th IEEE Southeastern Symp. on System Theory*, pp. 30-33 (15 Apr 1982).
- J. D. Flanagan and G. W. Luke, "Aegis: Newest Line of Navy Defense," *Johns Hopkins APL Tech. Dig.* **2**, 237-242 (1981).
- J. D. Flanagan and W. N. Sweet, "Aegis: Advanced Surface Missile System," *Johns Hopkins APL Tech. Dig.* **2**, 243-245 (1981).
- R. W. Flower, "The Role of Oxygen in the Retinopathy of Prematurity," *Johns Hopkins APL Tech. Dig.* **2**, 143-152 (1981).
- R. W. Flower (APL), A. E. Maumenee (JHMI), and E. A. Michelson (APL), "Long Term Continuous Monitoring of Intraocular Pressure in Conscious Primates," *Ophthalmic Res.* **14**, 98-106 (1982).
- D. W. Fox and V. G. Sigillito, "Bounds for Eigenfrequencies of a Plate with an Elastically Attached Reinforcing Rib," *Int. J. Solids Structures* **18**, 235-247 (1982).
- J. D. Franson, "Extension of the Einstein-Podolsky-Rosen Paradox and Bell's Theorem," *Phys. Rev. D* **26**, 787-800 (1982).
- E. A. Frekko, "Terrier/Tartar: Demonstration of AN/SYS-1 Integrated Automatic Detection and Tracking System," *Johns Hopkins APL Tech. Dig.* **2**, 268-275 (1981).
- M. H. Friedman, F. F. Mark, O. J. Deters, and C. B. Barger (APL) and G. M. Hutchins (JHMI), "Geometric Factors and Atherogenesis in Human Arteries," in *Proc. 35th Conf. on Engineering in Medicine and Biology* **24**, p. 125 (Sep 1982).
- J. B. Garrison, W. L. Ebert, R. E. Jenkins, S. M. Yionoulis, P. Malcom, and G. A. Heyler (APL) and A. A. Shoukas, W. L. Maughan, and K. Sagawa (JHMI), "Measurement of Three-Dimensional Positions and Motions of Large Numbers of Spherical Radiopaque Markers from Biplane Cineradiograms," *Comput. Biomed. Res.* **15**, 76-96 (1982).
- W. Garten, Jr., and F. A. Dean, "Evolution of the Talos Missile," *Johns Hopkins APL Tech. Dig.* **3**, 117-122 (1982).
- R. F. Gasparovic, K. Peacock, and L. D. Tubbs, "Airborne Radiometric Measurements of Sea Surface Temperature," *Johns Hopkins APL Tech. Dig.* **3**, 4-11 (1982).
- J. F. George and D. Richards, "Model Basin Tests of Ocean Wave Responses for a 40 MW OTEC Pilot Plant," *J. Solar Energy Eng.* **104**, 46-51 (1982).
- R. E. Gibson, "Richard Brandon Kershner," *Johns Hopkins APL Tech. Dig.* **3**, 97-101 (1982).
- R. E. Gold, H. W. Dodson-Prince, E. R. Hedeman, and E. C. Roelof, "The Influence of Solar Active Region Evolution on Solar Wind Streams, Coronal Hole Boundaries and Geomagnetic Storms," in *Proc. 17th International Conf. on Cosmic Rays* (1981).
- A. D. Goldfinger, R. C. Beal, and D. G. Tilly, "Optimal Spatial Filtering and Transfer Function for SAR Ocean Wave Spectra," in *Proc. 15th International Symp. on Remote Sensing of Environment*, Ann Arbor, Mich., pp. 291-297 (1981).
- J. Goldhirsh, "Ice Depolarization of the COMSTAR Beacon at 28.56 GHz during Low Fades and Correlation with Radar Backscatter," *IEEE Trans. Antennas Propag.* **AP-30**, 183-190 (1982).
- J. Goldhirsh, "Slant Path Fade and Rain-Rate Statistics Associated with the COMSTAR Beacon at 28.56 GHz for Wallops Island, Virginia over a Three-Year Period," *IEEE Trans. Antennas Propag.* **AP-30**, 191-198 (1982).
- J. Goldhirsh (APL) and E. J. Walsh (NASA/Wallops), "Rain Measurements from Space Using a Modified SEASAT-Type Radar Altimeter," *IEEE Trans. Antennas Propag.* **AP-30**, 726-733 (1982).
- W. H. Goss, "Talos in Retrospect," *Johns Hopkins APL Tech. Dig.* **3**, 116 (1982).
- B. L. Gotwols and G. B. Irani, "Charge-Coupled Device Camera System for Remotely Measuring the Dynamics of Ocean Waves," *Appl. Opt.* **21**, 851-860 (1982).
- B. L. Gotwols and G. B. Irani, "Optical Measurement of the Phase Velocity of Ocean Waves during the 1978 Wave Dynamics Experiment," *Johns Hopkins APL Tech. Dig.* **2**, 56-62 (1981).
- D. D. A. Gray, "The Talos Shipboard Test Program," *Johns Hopkins APL Tech. Dig.* **3**, 167-169 (1982).
- R. A. Greenwald, "Recent Advances in Magnetosphere-Ionosphere Coupling," *Rev. Geophys. Space Phys.* **20**, 577-588 (1982).
- R. W. Greenwald and A. D. M. Walker (APL), and M. Candidi (IPS/CNR), "Use of Hydromagnetic Waves to Map Geomagnetic Field Lines," *J. Geophys. Res.* **86**, 11251-11257 (1981).
- J. Gulick, W. C. Hyatt, and O. M. Martin, Jr., "The Talos Guidance System," *Johns Hopkins APL Tech. Dig.* **3**, 142-153 (1982).
- L. W. Hall, Jr., and D. T. Burton (APL) and L. H. Liden (JHU), "Power Plant Chlorination Effects on Estuarine and Marine Organisms," *CRC Crit. Rev. Toxicol.* **10**, 27-47 (1982).
- D. C. Hamilton and G. Gloeckler (Univ. Maryland), S. M. Krimigis (APL), and L. J. Lanzerotti (Bell Labs), "Composition of Nonthermal Ions in the Jovian Magnetosphere," *J. Geophys. Res.* **86**, 8301-8342 (1981).
- S. Hess (Univ. Erlangen-Nürnberg) and L. Monchick (APL), "Diffusion Controlled Reactions of Gases with Surfaces and State Dependent Reactivity," *J. Chem. Phys.* **77**, 307-313 (1982).
- M. L. Hill, "World Endurance Record for Radio-Controlled Aeromodels," *Johns Hopkins APL Tech. Dig.* **3**, 81-89 (1982).
- R. S. Hirsch, T. D. Taylor, M. Nadworny, and J. Kerr, "Techniques for Efficient Implementation of Pseudo-Spectral Methods and Comparison with Finite Difference Solutions of the Navier-Stokes Equations," in *Proc. 8th International Conf. on Numerical Methods in Fluid Mechanics*, Aachen, FRG (Jun 1982).
- B. F. Hochheimer, "Second Harmonic Light Generation in the Rabbit Cornea," *Appl. Opt.* **21**, 14-18 (1982).

- R. Holzworth (Aerospace Corp.), J. Wygant and F. Mozer (Univ. California), C. Gonzales (Arecibo Observatory), R. Greenwald (APL), M. Blac (CNET/CRPE), J. Vickrey (SRI), and A. Kishi (Aerospace Corp.), "Global Ionospheric Electric Field Measurements in April 1978," *J. Geophys. Res.* **86**, 6859-6868 (1981).
- L. W. Hunter, "Transient Thermal Expansion of Solids during Inert Heating, Phase Change, and Surface Gasification," *J. Heat Transfer* **103**, 601-602 (1982).
- L. W. Hunter and S. Favin, "Fire Resistance of Penetrated Walls," *Fire Tech.* **17**, 285-291 (1981).
- T. Iijima (Univ. Tokyo) and T. A. Potemra (APL), "The Relationship between Interplanetary Quantities and Birkeland Current Densities," *Geophys. Res. Lett.* **9**, 442-445 (1982).
- G. B. Irani and B. L. Gotwols, "WAVDYN: Measurements of the Independence of Ocean Wind Waves," *Johns Hopkins APL Tech. Dig.* **3**, 49-58 (1982).
- E. P. Irzinski, "APL Contributions to Aegis," *Johns Hopkins APL Tech. Dig.* **2**, 250-255 (1981).
- S. Ismail and C.-I. Meng, "A Classification of Polar Cap Auroral Arcs," *Planet. Space Sci.* **30**, 319-330 (1982).
- A. N. Jette and F. J. Adrian (APL) and J. M. Spaeth (Univ.-GH-Paderborn), "Contributions of Hydrogen Zero-Point Vibration to Fluorine Transferred Hyperfine Constants Nearest Neighbour to the  $H^2$  Centre in  $CaF_3$ ," *J. Geophys. C: Solid State Phys.* **30**, L345-L348 (1982).
- S. A. Kahn, S. G. Tolchin, R. L. Stewart, G. P. Gayle, and E. S. Bergan, "Design and Implementation of a Fiber Optic Contention Bus Network," in *Proc. 15th Hawaii International Conf. on System Sciences*, pp. 430-434 (1982).
- S. M. Kane (JHU), W. F. Barron (Oak Ridge Natl. Lab.), F. C. Paddison (APL), and P. Kroll (JHU), "GRITS - A Computer Program for Economic Evaluation of Geothermal Energy," *ASHRAE Trans.* **88**, 1323-1336 (1982).
- R. B. Kershner, "Where Have All the Underruns Gone?" *Johns Hopkins APL Tech. Dig.* **2**, 327-329 (1981).
- H. W. Ko, J. A. Giannini, and P. A. Herchenroeder, "Oceanographic ELF Electromagnetic Investigations at APL," *Johns Hopkins APL Tech. Dig.* **3**, 59-66 (1982).
- S. Koslov, "Combat Casualty Care: Can Technology Help?" *Johns Hopkins APL Tech. Dig.* **3**, 189-206 (1982).
- J. A. Krill, R. H. Andreo, and R. A. Farrell, "A Computational Alternative for Variational Expressions that Involve Dyadic Green Functions," *IEEE Trans. Antennas Propag.* **AP-30**, 1003-1005 (1982).
- S. M. Krimigis, "A Post-Voyager View of Saturn's Environment," *Johns Hopkins APL Tech. Dig.* **3**, 180-188 (1982).
- S. M. Krimigis, "Planetary Magnetospheres: The *in Situ* Astrophysical Laboratories," in *Proc. 17th International Conf. on Cosmic Rays* (1981).
- S. M. Krimigis, "Voyager Encounters with Jupiter's Magnetosphere: Results of the Low Energy Charged Particle (LECP) Experiment," in *Compendium in Astronomy*, E. G. Mariopoulos et al., eds, D. Reidel Pub. Co., New York, pp. 191-200 (1982).
- S. M. Krimigis (APL) and T. P. Armstrong (Univ. Kansas), "Two-Component Proton Spectra in the Inner Saturnian Magnetosphere," *Geophys. Res. Lett.* **9**, 1143-1146 (1982).
- S. M. Krimigis (APL), T. P. Armstrong (Univ. Kansas), W. I. Axford (Max-Planck Inst. Aeronomy), C. O. Bostrom (APL), G. Gloeckler (Univ. Maryland), E. P. Keath (APL), L. J. Lanzerotti (Bell Labs), J. F. Carbary (APL), D. C. Hamilton (Univ. Maryland), and E. C. Roelof (APL), "Low-Energy Hot Plasma and Particles in Saturn's Magnetosphere," *Science* **215**, 571-577 (1982).
- J. R. Kuttler, "Bounds for Stekloff Eigenvalues," *SIAM J. Numer. Anal.* **19**, 121-125 (1982).
- J. R. Kuttler and V. G. Sigillito, "Upper and Lower Bounds for Frequencies of Trapezoidal and Triangular Plates," *J. Sound Vib.* **78**, 585-590 (1981).
- B. W. Kuvshinov, "U.S. USSR Cooperative Agreement on Housing and Other Construction: Building Fire Safety," *Johns Hopkins APL Tech. Dig.* **3**, 90-96 (1982).
- K. Lerstrup and D. Talham (JHU), A. N. Bloch (Exxon Co.), T. O. Poehler (APL), and D. O. Cowan (JHU), "Dibenzotetratellurafulvalene (DBTTeF)," *J. Chem. Soc. Chem. Commun.*, 336-337 (1982).
- A. T. Y. Lui and S. M. Krimigis, "Several Features of the Earthward and Tailward Streaming of Energetic Protons (0.29-0.5 MeV) in the Earth's Plasma Sheet," *J. Geophys. Res.* **86**, 11173-11188 (1981).
- A. T. Y. Lui and S. M. Krimigis (APL) and T. P. Armstrong (Univ. Kansas), "Association between Magnetic Field Fluctuations and Energetic Particle Bursts in the Earth's Magnetotail," *J. Geophys. Res.* **87**, 8315-8320 (1982).
- A. T. Y. Lui, C.-I. Meng, and S. Ismail, "Large Amplitude Undulations on the Equatorward Boundary of the Diffuse Aurora," *J. Geophys. Res.* **87**, 2385-2400 (1982).
- S. A. Mack, D. C. Wenstrand, J. Calman, and R. C. Burkhardt, "Characteristics of Thermal Microstructure in the Ocean," *Johns Hopkins APL Tech. Dig.* **3**, 28-35 (1982).
- C. G. MacLennan and L. J. Lanzerotti (Bell Labs), S. M. Krimigis (APL), and R. P. Lepping and N. F. Ness (NASA), "Effects of Titan on Trapped Particles in Saturn's Magnetosphere," *J. Geophys. Res.* **87**, 1411-1418 (1982).
- T. S. Margulies (APL) and W. H. Schwartz (JHU), "Viscothermal Theory of Sound Wave Propagation in Chemically Reacting Mixtures of Nondiffusive Fluids," *J. Chem. Phys.* **77**, 1005-1016 (1982).
- T. Martinsen and L. J. Pace (Northwestern Univ.), T. E. Phillips (APL), and B. M. Hoffman and J. A. Ibers (Northwestern Univ.), "(Tetrabenzoporphyrinato) Nickel (II) Iodide, A Doubly Mixed Valence Molecular Conductor," *J. Am. Chem. Soc.* **104**, 83-91 (1982).
- R. L. McCally and R. A. Farrell, "Structural Implications of Small-Angle Light Scattering from Cornea," *Exp. Eye Res.* **34**, 99-113 (1982).
- R. L. McCally and R. A. Farrell, "Structural Implications of the Small Angle Light Scattering (SALS) and Birefringence Properties of the Cornea," abstract in *Bull. Am. Phys. Soc.* **26**, 245 (1981).
- W. B. McCloskey, Jr., "The New Fisherman," *Johns Hopkins APL Tech. Dig.* **2**, 74-83 (1981).
- C.-I. Meng, "Latitudinal Variation of the Polar Cusp during a Geomagnetic Storm," *Geophys. Res. Lett.* **9**, 60-63 (1982).
- W. E. Meyer and R. W. Anderson, "Operational Lessons Learned," *Johns Hopkins APL Tech. Dig.* **3**, 170 (1982).
- J. T. Miller, Jr., and E. W. G. David, "Battle Group Operations: Gridlock Demonstration," *Johns Hopkins APL Tech. Dig.* **2**, 314-320 (1981).
- F. M. Mmonaldo (APL) and R. S. Kasevich (Raytheon Co.), "Optical Determination of Short-Wave Modulation by Long Ocean Gravity Waves," *IEEE Trans. Geosci. Remote Sensing* **GE-20**, 254-259 (1982).
- J. M. Morris, "On Worst Case Interference for *M*-ary Signaling with Correlation Receivers," *IEEE Trans. Inf. Theory* **IT-28**, 74-83 (1982).
- B. H. Nall, A. N. Jette, and C. B. Barger, "Diffraction Patterns in the Specimen Current Image of a Single Crystal at Low Beam Energies," *Phys. Rev. Lett.* **48**, 882-885 (1982).

- R. R. Newton, "An Analysis of the Solar Observations of Regiomontanus and Walther," *Q. J. R. Astron. Soc.* **23**, 67-93 (1982).
- R. R. Newton, "Astronomy, Astrology, Ptolemy, and Us," *Johns Hopkins APL Tech. Dig.* **3**, 77-80 (1982).
- J. H. Nonnast and T. P. Armstrong (Univ. Kansas) and J. W. Kohl (APL), "A Study of Solar Flare Soft X Rays and Their Relation to Particle Events Observed with IMP 8," *J. Geophys. Res.* **87**, 4327-4337 (1982).
- V. O'Brien, "Conformal Mappings for Internal Viscous Flow Problems," *J. Comput. Phys.* **44**, 220-226 (1981).
- V. O'Brien, "Permeable Wall Effects on Poiseuille Flows," in *Proc. ASCE (EMD)* **107**, pp. 119-121 (1981).
- M. E. Oliver, "Terrier/Tartar: Pacing the Threat," *Johns Hopkins APL Tech. Dig.* **2**, 256-260 (1981).
- M. E. Oliver and W. N. Sweet, "Standard Missile: The Common Denominator," *Johns Hopkins APL Tech. Dig.* **2**, 283-288 (1981).
- F. C. Paddison, "The Talos Control System," *Johns Hopkins APL Tech. Dig.* **3**, 154-156 (1982).
- P. P. Pandolfini, G. L. Dugger, and J. A. Funk, "Test Results for the APL/JHU Folded-Tube Aluminum Condenser," *J. Energy* **5**, 394-400 (1981).
- H.-P. Pao, R. Y. Lai, and C. E. Schemm, "Vortex Trails in Stratified Fluids," *Johns Hopkins APL Tech. Dig.* **3**, 12-18 (1982).
- J. G. Parker and W. D. Stanbro, "Optical Determination of the Collisional Lifetime of Singlet Molecular Oxygen [ $O_2(^1\Delta_g)$ ] in Acetone and Deuterated Acetone," *J. Am. Chem. Soc.* **104**, 2067-2069 (1982).
- K. Peacock, R. F. Gasparovic, and L. D. Tubbs, "High Precision Radiometric Temperature Measurements of the Ocean Surface," in *Proc. 15th International Symp. on Remote Sensing of Environment*, pp. 793-802 (1981).
- R. Peyret (Univ. Nice) and T. D. Taylor (APL), *Computational Methods for Fluid Flow*, W. Beiglböck et al., eds., Springer-Verlag, Berlin (1982).
- C. C. Phillips, "Aegis: Advanced Multi-Function Array Radar," *Johns Hopkins APL Tech. Dig.* **2**, 246-249 (1981).
- C. C. Phillips, "Battle Group Operations: War at Sea," *Johns Hopkins APL Tech. Dig.* **2**, 299-301 (1981).
- C. C. Phillips and E. C. Prettyman, "Battle Group Operations: Anti-air Warfare Coordination," *Johns Hopkins APL Tech. Dig.* **2**, 308-313 (1981).
- T. E. Phillips, K. Moorjani, J. C. Murphy, and T. O. Poehler, "TiO<sub>2</sub>-VO<sub>2</sub> Alloys: Reduced Bandgap Effects in the Photoelectrolysis of Water," in *Proc. Symp. on Photoelectrochemical Processes and Measurement Techniques for Photoelectrochemical Solar Cells*, **82-3**, pp. 673-680 (1982).
- T. E. Phillips, K. Moorjani, J. C. Murphy, and T. O. Poehler, "TiO-VO Alloys - Reduced Bandgap Effects in the Photoelectrolysis of Water," *J. Electrochem. Soc.* **129**, 1210-1215 (1982).
- V. L. Pisacane, J. C. Ray, and J. L. MacArthur (APL) and S. E. Bergeson-Willis (NASA/Goddard), "Description of the Dedicated Gravitational Satellite Mission (GRAVSAT)," *IEEE Trans. Geosci. Remote Sensing GE-20*, 315-321 (1982).
- V. L. Pisacane and S. M. Yionoulis, "Tracking Requirements for the Dedicated Gravitational Satellite (GRAVSAT) Mission," in *Proc. XXXII Congress, International Astronautical Federation* (1981).
- T. O. Poehler, "Infrared Extinction in Organic Compounds and Polymers," in *Proc. 1979 Chemical Systems Laboratory Conf. on Obscuration and Aerosol Research*, ARCSL-CR-81023, R. H. Kohl & Assoc., pp. 401-412 (1982).
- R. S. Potember et al., *Reversible Field Induced Switching in Copper and Silver Radical-Ion Salts*, Naval Res. Lab. Report 4662, Washington (1981).
- R. S. Potember and T. O. Poehler, "Electrical Switching and Memory Phenomena in Semiconducting Organic Thin Films," in *Proc. Symp. on Polymer Materials for Electronic Applications*, E. D. Feit and C. Wilkins, Jr., eds., American Chemical Soc. Symp. Series No. 184 (1982).
- R. S. Potember, T. O. Poehler, and R. C. Benson, "Optical Switching in Semiconductor Organic Thin Films," *Appl. Phys. Lett.* **4**, 548-550 (1982).
- R. S. Potember and T. O. Poehler (APL), A. Rappa and D. O. Cowan (JHU), and A. N. Bloch (Exxon Co.), "A Current-Controlled Electrically Switched Memory State in Silver and Copper-TCNQF<sub>4</sub> Radical-Ion Salts," *Synth. Met.* **4**, 371-380 (1982).
- E. M. Poulter and E. Nielsen (Max-Planck Inst. Aeronomy) and T. A. Potemra (APL), "Field-Aligned Currents Associated with Pc5 Pulsations: STARE and TRIAD Observations," *J. Geophys. Res.* **87**, 2331-2336 (1982).
- W. R. Powell, "Alternate Expressions for the Average Output Power of a Wind Machine," *Solar Energy* **28**, 551-552 (1982).
- A. J. Pue, "Macroscopic Traffic Models for Vehicle-Follower Automated Transportation Systems," *Transp. Res.* **16B**, 125-142 (1982).
- D. W. Rabenhorst, "The All-Mechanical Electric Car," *Phys. Technol.* **13**, 98-105 (1982).
- J. C. Ray and R. E. Jenkins (APL), D. B. DeBra and R. A. Van Patten (Stanford Univ.) and J. L. Junkins (VPI&SU), "Attitude and Translation Control of a Low-Altitude GRAVSAT," in *Proc. AIAA/AAS Astrodynamics Conf.*, AIAA-82-1416 (1982).
- D. Richards and J. F. George (APL) and J. S. Seward (Seward Assoc.), "Design of 40-MW Grazing and Moored OTEC Pilot/Demonstration Plants," *J. Energy* **5**, 224-230 (1982).
- D. Richards and L. L. Perini, "An OTEC Pilot Plant Heat Engine," *J. Energy Resources Tech.* **103**, 172-179 (1981).
- R. M. Robinson and R. R. Vondrak (SRI International) and T. A. Potemra (APL), "Electrodynamic Properties of the Evening Sector Ionosphere within the Region 2 Field-Aligned Current Sheet," *J. Geophys. Res.* **87**, 731-741 (1982).
- E. C. Roelof, R. B. Decker, and S. M. Krimigis (APL), D. Venkatesan (Univ. Calgary), and A. J. Laxarus (MIT), "Galactic Cosmic Ray Gradients, Field-Aligned and Latitudinal, Among Voyagers 1/2 and IMP 8," in *Proc. 17th International Conf. on Cosmic Rays* (1981).
- M. W. Roth, "The Separation of Oceanic Temperature Fine-structure and Internal Motion," *Johns Hopkins APL Tech. Dig.* **3**, 19-27 (1982).
- L. J. Rueger, "Characteristics of the NASA Research Hydrogen Maser," *J. Inst. Electron. Telecommun. Eng.* **27**, 493-500 (1981).
- T. R. Sanderson, R. Reinhard, and K. P. Wenzel (ESA) and G. G. Mitchell and E. C. Roelof (APL), "ISEE-3/IMP-8 Observations of Simultaneous Upstream Proton Events," in *Proc. 17th International Conf. on Cosmic Rays* (1981).
- E. T. Sarris (Univ. Thrace) and S. M. Krimigis (APL), "Evidence for Solar Magnetic Loops Beyond 1 AU," *Geophys. Res. Lett.* **9**, 167-170 (1982).
- J. A. Schetz, F. S. Billig, and S. Favin, "Flowfield Analysis of a Scramjet Combustor with a Coaxial Fuel Jet," *AIAA J.* **20**, 1268-1274 (1982).
- J. A. Schetz, F. S. Billig, and S. Favin, "Scramjet Combustor Wall Boundary Layer Analysis," in *Proc. AIAA SAE ASME 17th Joint Propulsion Conf.*, pp. 1-10 (1981).
- M. E. Schmid, R. L. Trapp, and A. E. Davidoff (APL) and C. M. Masson (JHU), "Upset Exposure by Means of Abstraction Verification," in *Proc. FTCS 12th Annual International Symp. Fault-Tolerant Computing* (1982).

- D. P. Serpico, "Combat Systems Evaluation Laboratory," *Johns Hopkins APL Tech. Dig.* 2, 321-326 (1981).
- W. B. Shippen, W. G. Berl, W. Garten, Jr., and E. J. Hardgrave, Jr., "The Talos Propulsion System," *Johns Hopkins APL Tech. Dig.* 3, 126-134 (1982).
- D. W. Simborg and Q. E. Whiting-O'Keefe (Univ. California/S.F.) and S. G. Tolchin (APL), "Early Experience with the First Use of a Local Area Communications Network Technology in a Hospital," in *Proc. American Medical Informatics Assoc. Congress* (1982).
- G. L. Smith, "Guest Editor's Introduction," *Johns Hopkins APL Tech. Dig.* 3, 2-3 (1982).
- W. D. Stanbro and M. J. Lenkevich, "Slowly Dechlorinated Organic Chloramine," *Science* 215, 967-968 (1982).
- J. Stricker and J. G. Parker, "Experimental Investigation of Electrical Breakdown in Nitrogen and Oxygen Induced by Focused Laser Radiation at 1.064  $\mu\text{m}$ ," *J. Appl. Phys.* 53, 851-855 (1982).
- H. Sulzbacher (Univ. Münster), W. Baumjohann and T. A. Potemra (APL), E. Nielsen (Max-Planck Inst.), and G. Gustafsson (Kiruna Geophysical Inst.), "Observations of Ionospheric and Field-Aligned Currents in the Late Afternoon Sector with Triad and the Scandinavian Magnetometer Array," *J. Geophys.* 51, 55-65 (1982).
- T. D. Taylor, "Recent Advances in Pseudo-Spectral Methods," in *Proc. ICASE Symp. on Spectral Methods*, NASA/Langley (1982).
- T. D. Taylor and R. S. Hirsch, "Implementation of Pseudo-Spectral Calculations on a Large Array Processor," in *Proc. EUROMECH Conf. No. 159—Spectral Methods in Computational Fluid Mechanics* (1982).
- D. L. Thayer, L. Scheer, and B. E. Tossman, "A Triaxial Coil Receiver System for the Study of Subsurface Electromagnetic Propagation," *IEEE J. Oceanic Eng.* OE-7, 75-82 (1982).
- M. E. Thomas (APL) and R. J. Nordstrom (Batelle), "The  $\text{N}_2$ -Broadened Water Vapor Absorption Line Shape and Infrared Continuum Absorption—I. Theoretical Development," *J. Quant. Spectrosc. Radiat. Transfer* 28, 81-101 (1982).
- M. E. Thomas (APL) and R. J. Nordstrom (Batelle), "The  $\text{N}_2$ -Broadened Water Vapor Absorption Line Shape and Infrared Continuum Absorption—II. Implementation of the Line Shape," *J. Quant. Spectrosc. Radiat. Transfer* 28, 103-112 (1982).
- J. E. Tillman (APL), A. Poosti (Atomic Energy Organization, Iran), S. Rossello (Canastota), and A. Eckert (Dames & Moore), "Structural Evolution of Sanandaj-Sirjan Ranges near Esfahan, Iran," *Am. Assoc. Pet. Geol. Bull.* 65, 674-687 (1981).
- S. G. Tolchin, E. S. Bergan, S. A. Kahn, and R. L. Stewart (APL) and D. W. Simborg, M. G. Chadwick, and Q. E. Whiting-O'Keefe (Univ. California/S.F.), "Progress and Experience in the Implementation of a Hospital Local Area Network at UCSF," in *Proc. MED—COMP '82—First IEEE Computer Society International Conf. on Medical Computer Science Computational Medicine*, pp. 291-298 (1982).
- S. G. Tolchin, R. L. Stewart, S. A. Kahn, E. S. Bergan, and G. P. Gafke (APL) and D. W. Simborg, M. G. Chadwick, and Q. E. Whiting-O'Keefe (Univ. California/S.F.), "A Prototype Generalized Network Technology for Hospitals," *J. Med. Syst.* 6, 359-375 (1982).
- S. G. Tolchin, R. L. Stewart, S. A. Kahn, G. P. Gafke, E. S. Bergan (APL) and D. W. Simborg, M. G. Chadwick, and Q. E. Whiting-O'Keefe (Univ. California/S.F.), "A Prototype Generalized Network Technology for Hospitals: Initial Implementation," in *Proc. 15th Hawaii International Conf. on System Sciences*, pp. 591-600 (1982).
- R. B. Torbert, C. A. Cattell, and F. S. Mozer (Univ. California) and C.-I. Meng (APL), "The Boundary of the Polar Cap and Its Relation to Electric Fields, Field-Aligned Currents, and Auroral Particle Precipitation," in *Physics of Auroral Arc Formation*, AGU Monograph 25, S.-I. Akasofu and J. R. Kan, eds., pp. 143-153 (1981).
- D. J. Webb and S. M. Bhagat (Univ. Maryland) and K. Moorjani, T. O. Poehler, and F. G. Satkiewicz (APL), "Spin Glass Behavior and Non-Ergodicity in Amorphous Iron-Boron Alloys," *Solid State Commun.* 43, 239-242 (1982).
- R. W. Witte and R. L. McDonald, "Standard Missile: Guidance System Development," *Johns Hopkins APL Tech. Dig.* 2, 289-298 (1981).
- S. Wilson (Univ. Oxford) and D. M. Silver (APL), "Diagrammatic Perturbation Theory: An Application to the LiH and FH Molecules Using a Universal Even-Tempered Basis Set," *J. Chem. Phys.* 77, 3674-3675 (1982).
- L. J. Zanetti and T. A. Potemra, "Correlated Birkeland Current Signatures from the TRIAD and MAGSAT Magnetic Field Data," *Geophys. Res. Lett.* 9, 349-352 (1982).
- L. J. Zanetti and T. A. Potemra (APL), J. P. Doering and J. S. Lee (JHU), J. F. Fennell (Aerospace Corp.), and R. A. Hoffman (NASA/Goddard), "Interplanetary Magnetic Field Control of High-Latitude Activity on July 29, 1977," *J. Geophys. Res.* 87, 5963-5975 (1982).
- L. J. Zanetti and T. A. Potemra (APL) and M. Sugiura (NASA/Goddard), "Evaluation of High Latitude Disturbances with MAGSAT (The Importance of the MAGSAT Geomagnetic Field Model)," *Geophys. Res. Lett.* 9, 365-368 (1982).
- R. D. Zwickl (Univ. California), S. M. Krimigis, J. F. Carbary, and E. P. Keath (APL), T. P. Armstrong (Univ. Kansas), and D. C. Hamilton and G. Gloeckler (Univ. Maryland), "Energetic Particle Events ( $\geq 30$  keV) of Jovian Origin Observed by Voyager 1 and 2 in Interplanetary Space," *J. Geophys. Res.* 86, 8125-8140 (1981).
- R. D. Zwickl and E. C. Roelof, "Interplanetary Propagation of  $< 1$ -MeV Protons in Nonimpulsive Energetic Particle Events," *J. Geophys. Res.* 86, 5449-5471 (1981).

## PRESENTATIONS

- R. H. Andreo, "Discrete Methods and Schwinger Variational Principles for Random Scattering: The Coherent Field for Scattering," 1982 CSL Scientific Conf. on Obscuration and Aerosol Research, Aberdeen Proving Ground, Md. (26 Jun 1982).
- R. H. Andreo, "Variational Methods for Wave Scattering from Random Systems," Wave Optics Lecture Series at NBS, Gaithersburg, Md. (23 Sep 1981).
- J. R. Apel, "Solitons and Pirates in the Sulu Sea," JHU/APL Colloq. (12 Feb 1982).
- C. B. Barger, A. N. Jette, and B. H. Nall, "Diffraction Patterns in the Specimen Current Images of Single Crystals for Low-Energy Electrons," Milton S. Eisenhower Research Center Seminar, APL (2 Mar 1982).
- C. B. Barger, R. L. McCally, W. R. Green, and R. A. Farrell, "Stromal Damage from Corneal Exposure to Infrared Radiation," Spring Meeting, Association for Research in Vision and Ophthalmology, Sarasota (2-7 May 1982).
- R. C. Benson, "Laser-Induced Decomposition of Sodium Azide," American Physical Society Conf., Pacific Grove, Calif. (Aug 1982).

- N. A. Blum, "Mössbauer Study of Magnetism in an Amorphous  $\text{Fe}_{40}\text{B}_{60}$  Sputtered Film," 3rd Joint International Magnetism and Magnetic Materials Conf., Montreal (Jul 1982).
- N. A. Blum, K. Moorjani, T. O. Poehler, and F. G. Satkiewicz, "Mössbauer Investigation of Sputtered Ferromagnetic Amorphous  $\text{Fe}_{100-x}\text{B}_x$  Alloys," Magnetism and Magnetic Materials Meeting, Atlanta (10-13 Nov 1981).
- J. F. Carbary, S. M. Krimigis, and E. P. Keath, "Anisotropies in the Jovian Magnetosphere," Conf. on the Physics of the Jovian and Saturnian Magnetospheres, APL (22-24 Oct 1981).
- G. L. Dugger, D. Richards, F. C. Paddison, L. L. Perini, and W. H. Avery (APL) and P. J. Ritzcovan (DOE), "Alternative Ocean Energy Products and Hybrid Geothermal-OTEC Plants," AIAA 2nd Terrestrial Energy Systems Conf., Colorado Springs (1-3 Dec 1981).
- L. W. Ehrlich, "The Ad Hoc SOR Method - A Closer Look," 40th National SIAM Meeting, Stanford Univ. (23 Jul 1982).
- R. A. Farrell, R. H. Andreo, and R. L. McCally, "Calculated Small Angle Light Scattering Patterns: Wavy Lamella Model," Army Research Office, Raleigh (9 Mar 1982) and American Physical Society, Dallas (11 Mar 1982).
- C. Feldman, "Antimony Doping in Vacuum Deposited Thin Film Silicon Photovoltaic Cells," 4th European Communities Photovoltaic Solar Energy Conf., Stresa, Italy (10-14 May 1982).
- R. E. Fischell, W. E. Radford, and J. R. Champion, "A Computerized Implantable Medication System," 14th Southeastern Symp. on System Theory, Virginia Polytechnic Inst. and State Univ., Blacksburg (15 Apr 1982).
- J. W. Follin, Jr., "A New Theory of the Formation and Evolution of the Solar System," JHU/APL Colloq. (28 May 1982).
- M. H. Friedman, "Geometric Risk Factors for Arteriosclerosis," JHU/APL Colloq. (8 Jan 1982).
- M. H. Friedman, O. J. Deters, F. F. Mark, C. B. Barger, and G. M. Hutchins, "Geometric Effects on the Hemodynamic Environment of the Arterial Wall: A Basis for Geometric Risk Factors," Symp. on Fluid Dynamics as a Localizing Factor for Atherosclerosis, Heidelberg (19-20 Jun 1982).
- J. A. Giannini and D. L. Thayer, "Propagation Measurements from a Calibrated Source in the Ocean," International Union of Radio Science, Boulder, Colo. (13-15 Jan 1982).
- J. S. Hansen, D. A. Bowser, and H. W. Ko (APL), D. Brenner (Rockwell International), and F. Richer and J. Beatty (Univ. California/L.A.), "Adaptive Noise Cancellation in Neuro-magnetic Measurements," 4th International Workshop on Biomagnetism, Rome (14-16 Sep 1982).
- R. E. Kemelhor and W. R. Mentzer, "Intelligence Data and Test and Evaluation Examples of a Necessary Relationship," 48th Symp., Military Operations Research Soc., Naval Postgraduate School, Monterey, Calif. (3 Dec 1981).
- R. J. Klauda (APL) and D. S. Vaughan (Oak Ridge National Lab.), "An Introduction and Perspective on the Hudson River Power Plant Case," American Fisheries Soc. Meeting, Hilton Head, S.C. (25 Sep 1982).
- H. W. Ko, J. W. Sari, and J. W. Follin, Jr., "Anomalous Propagation and Radar Coverage," 2nd Tactical Air Surveillance and Control Conf., Griffiss AFB, N.Y. (2-5 Nov 1981).
- J. A. Krill, J. F. Bird, and R. A. Farrell, "Trial Functions for Variational Calculations," 1982 CSL Scientific Conf. on Obscuration and Aerosol Research, Aberdeen Proving Ground, Md. (26 Jun 1982).
- S. Krimigis, "The Magnetosphere and Radiation Belts of Saturn: Results from the Voyager Encounters," JHU/APL Colloq. (2 Oct 1981).
- S. M. Krimigis (APL), T. P. Armstrong (Univ. Kansas), W. I. Axford (Max-Planck Inst. Aeronomy), C. O. Bostrom (APL), G. Gloeckler (Univ. Maryland), E. P. Keath (APL), L. J. Lanzerotti (Bell Labs), J. F. Carbary (APL), D. C. Hamilton (Univ. Maryland), and E. C. Roelof (APL), "Hot Plasma Torus in the Magnetosphere of Saturn," Conf. on the Physics of the Jovian and Saturnian Magnetospheres, APL (22-24 Oct 1981).
- E. G. LeDet (APL) and C. S. Ih (Univ. Delaware), "Acoustical Holographic Scanner," 12th International Symp. on Acoustical Imaging, London (19-22 Jul 1982).
- C. S. Leffel and C. A. Wingate, "Stirling Cycle Cryogenic Refrigerators for Satellite Gamma Ray Experiment," 8th DARPA Strategic Space Symp., Naval Postgraduate School, Monterey, Calif. (22-25 Jun 1982).
- R. Manley and J. Bluestein (Mitre Corp.) and E. J. Francis (APL), "An Estimate of OTEC Costs, Market Potential, and Proof-of-Concept Vessel Financing," AIAA 2nd Terrestrial Energy Systems Conf., Colorado Springs (1-3 Dec 1981).
- R. L. McCally, "Corneal Structure and Light Scattering," Stanford Univ. School of Medicine (20 Jul 1982).
- R. L. McCally and R. A. Farrell, "Corneal Light Scattering Calculations Based on Electron Micrographs," Spring Meeting, Association for Research in Vision and Ophthalmology, Sarasota (2-7 May 1982).
- K. Moorjani, "Frustration, Spin Glasses and Non-Ergodicity," Solid State Laboratory Seminar, Univ. Bordeaux (6 Jul 1982).
- J. C. Murphy, "Photothermal Imaging Applied to Materials Characterization," Workshop on Nondestructive Microstructure Characterization, DARPA 1982 Materials Research Council Meeting, La Jolla, Calif. (6-7 Jul 1982).
- J. C. Murphy and L. C. Aamodt, "Nondestructive Evaluation of Defects in Materials Using Photothermal Imaging," 1982 Meeting, American Society for Nondestructive Testing, Boston (23 Mar 1982).
- J. C. Murphy and L. C. Aamodt, "Photothermal Imaging," 182nd Meeting, American Chemical Society, New York (Aug 1981).
- V. O'Brien, "Classifying 2-D Separation," 9th U.S. National Congress of Applied Mechanics, Cornell Univ. (23 Jun 1982).
- V. O'Brien, "Pulsatile Blood Flow," Bioengineering Seminar, The Johns Hopkins Univ., Baltimore (19 Oct 1981).
- V. O'Brien, "Scattering from Random Systems," Physics Department Colloq., Catholic Univ., Washington, (29 Oct 1981).
- V. O'Brien, O. J. Deters, F. F. Mark, and L. W. Ehrlich (APL) and K. Sagawa and G. M. Hutchins (JHMI), "Flow Fields near Arterial Ring Occlusions," Fluid Mechanics and Biomedical Engineering Seminar, The Johns Hopkins Univ., Baltimore (18 Sep 1981).
- J. G. Parker, "Energy Transfer Processes Accompanying Laser Excitation of Hematoporphyrin in Various Solvents," Chemistry Dept. Colloq., Howard Univ. (16 Apr 1982).
- J. G. Parker, "Optical Monitoring of Energy Transfer Processes Accompanying Pulsed Laser Excitation of Hematoporphyrin in Solution," Gordon Research Conf. on Lasers in Medicine and Biology, Meriden, N.H. (29 Jun 1982).
- J. G. Parker, "Energy Transfer Processes Involving Hematoporphyrin in Various Solvents," ONR-Sponsored Conf. on Laser-Induced Processes in Biological Molecules, Stanford Univ. (6-9 Jul 1982).
- T. E. Phillips, K. Moorjani, J. Murphy, and T. O. Poehler, " $\text{TiO}_2$ - $\text{VO}_2$  Reduced Bandgap Effects in the Photoelectroly-

- sis of  $H_2O$ ," Electromechanical Soc. Meeting, Denver (14 Oct 1981).
- R. S. Potember, "Optical and Electrical Switching in Semiconductor Organic Thin Films," Colloq., Allied Chemical Co., Morristown, N.J. (12 May 1982).
- R. S. Potember, "Optical Phase Transitions in Organic Semiconductors," Conf. on Nonlinear Optical Materials for Laser Protection, La Jolla, Calif. (22 Jul 1982).
- R. S. Potember, "Optical Switching in Semiconducting Organic Thin Films," Gordon Conf., Wolfeboro, N. H. (18 Aug 1982); also presented at IUPAC, Univ. Massachusetts, Amherst (16 Jul 1982).
- R. S. Potember and T. E. Phillips, "Thin Films Transition Materials Development," Technical Review, F7U5, Cornell Univ. (Aug 1982).
- R. S. Potember and T. O. Poehler, "Electrical Switching and Memory Phenomena in Semiconducting Organic Thin Films," Colloq., Northwestern Univ. (17 Dec 1981).
- F. G. Satkiewicz, "Relative Yields of Positive Ions Sputtered from Several Silicides," 30th Conf. on Mass Spectrometry and Allied Topics, Honolulu (Jun 1982).
- V. G. Sigillito, "Bounds for Eigenvalues of Membranes, Waveguides, and Plates," 40th National SIAM Meeting, Stanford Univ. (22 Jul 1982).
- V. G. Sigillito, "Explicit *a Priori* Inequalities in Eigenvalue Estimation," Colloq., Dept. of Mathematics, Univ. Maryland, Catonsville (11 Dec 1981).
- J. T. Stadter, "An Approximate Method for Predicting Rain Erosion of Slip-Cast Fused Silica Radomes," 16th Symp. on Electromagnetic Windows, Georgia Inst. of Tech. (11 Jun 1982).
- B. Walker, "Writing Audio-Visuals," Baltimore Writers' Alliance, Notre Dame College, Baltimore (14 Oct 1981).
- P. J. Waltrup, F. S. Billig, and R. D. Stockbridge, "Engine Sizing and Integration Requirements for Hypersonic Airbreathing Missile Applications," 58th PEP (AGARD) Symp. on Ramjets and Ramrockets in Military Applications, London (26-29 Oct 1981).

The following papers were presented at the 4th Scientific Assembly of IAGA, Edinburgh (3-15 Aug 1981):

- R. Fujii, T. Iijima, and T. A. Potemra, "Seasonal Dependence of Large-Scale Birkeland Currents";
- R. A. Greenwald, A. D. M. Walker, and M. Candidi, "Use of Hydromagnetic Waves to Map Geomagnetic Field Lines";
- T. Iijima and T. A. Potemra, "On the Relationship Between Interplanetary Quantities and Birkeland Current Amplitudes";
- T. A. Potemra, "Fridtjof Nansen: Principal Investigator for the Fram Expedition—An Early IMS Program (1893-1896)";
- A. D. M. Walker, R. A. Greenwald, A. Korth, G. Kremser, G. Haerendel, and M. Candidi, "GEOS 2 and STARE Observations of Pc5 Pulsations Associated With the Drift Mirror Instability";
- L. J. Zanetti, T. A. Potemra, and M. Sugiura, "Preliminary Evaluation of Distant Magnetic Field Disturbances from

Birkeland Currents using MAGSAT Data";

- L. J. Zanetti and T. A. Potemra, "Asymmetric Polar Cap Currents Following a Major Magnetic Storm";
- M. Zi, E. Nielsen, and T. A. Potemra, "Field Aligned Currents Near the Dayside Convection Reversal."

The following papers were presented at the 48th Symp. of the Military Operations Research Society, Monterey, Calif. (1-3 Dec 1981):

- D. K. Pace, "Data Link Support for Battle Group Anti-Air Warfare Coordination (BGAAWC)";
- D. K. Pace, "An Overview of Naval AAW";
- J. Wang, "Naval AAW Analysis Procedures."

The following papers were presented at the National Radio Science Meeting, Boulder, Colo. (12-15 Jan 1982):

- J. A. Giannini and D. L. Thayer, "Propagation Measurements from a Calibrated Source in the Ocean";
- D. A. Bowser, J. W. Sari, and H. W. Ko, "Spectra of Geomagnetic Field Fluctuations from Ocean Surface Waves";
- D. A. Bowser, L. W. Hart, and J. W. Sari, "Vertical Coherence of Geomagnetic Noise Propagating through Seawater";
- J. W. Sari and D. A. Bowser, "Propagation of an ELF Transient Pulse in the Ocean";
- J. W. Sari, R. I. Joseph, and M. E. Thomas, "Electromagnetic Scattering from Random Conductivity Fluctuations";
- J. W. Sari, and R. I. Joseph, "Tropospheric Propagation of Radiation in an Inhomogeneous, Stratified Atmosphere";
- J. P. Skura, J. W. Sari, and H. W. Ko, "Application of the Parabolic Equation Method to Propagation in Inhomogeneous Refractive Layers."

The following papers were presented at the Army Research Office Workshop on Wave Propagation in Random Media, North Carolina State Univ., Raleigh (8 Mar 1982):

- R. H. Andreo, "Discrete Methods and Schwinger Variational Principles for Random Scattering";
- R. A. Farrell and J. A. Krill, "Trial Functions in Variational Calculations";
- R. A. Farrell, R. L. McCally, and R. H. Andreo, "Calculated Corneal SALS Patterns."

The following papers were presented at the Meeting, American Physical Society, Dallas (8-12 Mar 1982):

- R. A. Farrell, R. L. McCally, and R. H. Andreo, "Calculated Corneal SALS Patterns";
- A. N. Jette, F. J. Adrian, and J. M. Spaeth, "Contributions of Hydrogen Zero-Point Vibration to Fluorine Transferred Hyperfine Constants Nearest Neighbor to Trapped Interstitial Hydrogen Atoms in  $CaF_2$ ";
- B. H. Nall, C. B. Barger, and A. N. Jette, "Diffraction Patterns in the Specimen Current Images of a Single Crystal for Low-Energy Electrons."

## **AUTHOR INDEX**

## AUTHOR INDEX

### A

Arrow, A., 26

### B

Ball, R. E., 106  
Barger, C. B., 128, 174  
Benson, R. C., 34, 168  
Best, C. S., 112  
Blum, B. I., 140  
Blum, N. A., 181  
Bockstahler-Brandt, J. S., 110  
Brown, N. K., 55  
Brown, S. J., 162

### C

Carpenter, L. B., 52  
Champion, J. R., 137  
Chappell, R. G., 102  
Charles, H. K., Jr., 152, 156  
Chiu, H. Y., 159  
Cohn, R. F., 106  
Conn, D. W., 85  
Coolahan, J. E., 106  
Cronvich, L. L., 26

### D

D'Anna, S. A., 131  
Davidoff, A. E., 69  
Deters, O. J., 128  
Dunkelberger, G., 131

### E

Eisner, A., 88

### F

Fischell, R. E., 137  
Frantz, J. A., 67  
Fraser, A. B., 100, 112  
Friedman, M. H., 128  
Fristrom, R. M., 170

### G

Gafke, G. P., 67  
Guenther, R. R., 55

### H

Hagan, J. C., 85

Harris, R. B., III, 110  
Heffernan, K. J., 82  
Hicks, R. E., 152  
Hirst, L. W., 131  
Hocker, T. R., 62  
Hoshall, C. H., 34  
Hutchins, G. M., 128

### J

Jette, A. N., 174

### K

Karner, L. E., 112  
Kitchin, D. A., 112  
Ko, H. W., 72  
Kratz, D. B., 37  
Kues, H. A., 131

### L

Lee, R. P. H., 100, 112  
Levy, L. J., 40  
Loveless, J. H., 134

### M

Man, T. H., 121  
Mark, F. F., 128  
Masson, G. M., 69  
Mengel, E. E., 121  
Meyrick, C. W., 92  
Mobley, F. F., 82  
Moffett, J. B., 88  
Moorjani, K., 181

### N

Nall, B. H., 174  
Nelson, C. V., 102  
Newman, R. W., 34

### O

Ousborne, J. J., 118

### P

Paddison, F. C., 148  
Parker, J. G., 178  
Peck, L. D., 50  
Perini, L. L., 85  
Philippides, C., 17

Poehler, T. O., 168  
Potember, R. S., 168  
Potemra, T. A., 82  
Preziotti, G. R., 44

## R

Radford, W. E., 137  
Raff, B. E., 114  
Reichert, R. T., 19  
Riedel, F. W., 31  
Rodeffer, C. C., 37  
Romenesko, B. M., 152, 156  
Rouse, R. E., 14

## S

Sari, J. W., 72  
Saudek, C. D., 137  
Schmid, M. E., 69  
Schneider, W., 134  
Seamone, W., 134  
Skura, J. P., 72  
Stader, J. F., 55  
Stanbro, W. D., 178

Stone, A. M., 148  
Sunday, D. M., 67

## T

Taylor, T. D., 65  
Thompson, T., 92  
Trapp, R. L., 69  
Twigg, C. A., 121

## V

Vigliotti, V., 106

## W

Waeber, K. R., 85  
Wagner, G. D., 152, 156  
Waters, C. A., 75  
Woodford, B. W., 23  
Woodyard, J. C., 67

## Y

Yanek, S. P., 67

REPORT DOCUMENTATION PAGE		
1. REPORT NUMBER JHU/APL DST-10	2. GOVT ACCESSION NO AD-A139624	3. RECIPIENT'S CATALOG NUMBER
4. TITLE (and Subtitle) Developments in Science and Technology		5. TYPE OF REPORT & PERIOD COVERED Technical Memorandum Fiscal Year 1982
		6. PERFORMING ORG. REPORT NUMBER JHU/APL DST-10
7. AUTHOR(s) Various		8. CONTRACT OR GRANT NUMBER(s) N00024-83-C-5301
9. PERFORMING ORGANIZATION NAME & ADDRESS The Johns Hopkins University, Applied Physics Lab. Johns Hopkins Road Laurel, MD 20707		10. PROGRAM ELEMENT, PROJECT, TASK AREA & WORK UNIT NUMBERS Various
11. CONTROLLING OFFICE NAME & ADDRESS Naval Plant Representative Office Johns Hopkins Road Laurel, MD 20707		12. REPORT DATE Fiscal Year 1982
		13. NUMBER OF PAGES 200
14. MONITORING AGENCY NAME & ADDRESS Naval Plant Representative Office Johns Hopkins Road Laurel, MD 20707		15. SECURITY CLASS. (of this report) Unclassified
16. DISTRIBUTION STATEMENT (of this Report) Approved for public release; distribution unlimited.		15a. DECLASSIFICATION/DOWNGRADING SCHEDULE --
17. DISTRIBUTION STATEMENT (of the abstract entered in Block 20, if different from Report) --		
18. SUPPLEMENTARY NOTES --		
19. KEY WORDS (Continue on reverse side if necessary and identify by block number) See attached List		
20. ABSTRACT (Continue on reverse side if necessary and identify by block number) This report is a compilation of brief accounts of the Laboratory's significant accomplishments during fiscal year 1982. The following areas are covered: weapon systems development; naval warfare analysis; computer technology; space science and technology; ocean science and technology; biomedical science and engineering; energy, engineering, and civilian technology; and fundamental research.		

AD-A139 624

DEVELOPMENTS IN SCIENCE AND TECHNOLOGY(U) JOHNS HOPKINS  
UNIV LAUREL MD APPLIED PHYSICS LAB 1982 JHU/APL/DST-10  
N00024-83-C-5301

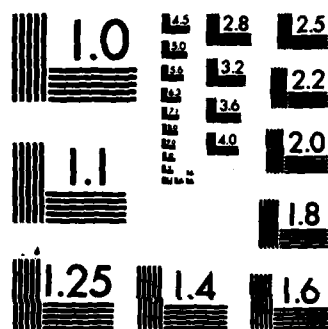
3/3

UNCLASSIFIED

F/G 14/2

NL





MICROCOPY RESOLUTION TEST CHART  
NATIONAL BUREAU OF STANDARDS-1963-A

1. Aid Control and Monitor System
2. Arteriosclerosis
3. Automated Guideway Transit Systems
4. Autopilot Aerodynamic Requirements
5. Autopilot Model
6. Ceramic Chip Carrier
7. Computer Fault Detectors
8. Corneal Studies
9. Electromagnetic Propagation Simulation
10. Electron Diffraction
11. Flame Chemistry
12. Geothermal Energy
13. Graphite Ablation
14. Handicapped Aids
15. Harpoon Model
16. Hospital Information System
17. Hydrodynamic Computational Facility
18. Implantable Medication System
19. Iron-Boron Alloys
20. Laplace Differential Equations
21. Laser Escitation of Dyes
22. Microelectronics Pull Testing
23. Microwave Corneal Effects
24. Ocean Heat Flux Measurements
25. Oceanographic Fluorometer
26. Oceanographic Measurements
27. Pershing II
28. Radar Environment Simulator
29. Radar Target Detection
30. Radioisotope Heater Unit
31. Robotic Arm
32. Satellite Missile Tracking
33. Search and Rescue Satellite
34. Semiconductor Optical Switching
35. Ship Classification
36. SMITE
- 37A. Standard Missile
- 37B. Switch-tube Modulator
38. Terrier Simulation
39. Towed Sensor Arrays
40. Trident II
41. UNITAS XXII Communications
42. VIKING Magnetometer
43. War Game Software

END

FILMED

5-84

DTIC